12-2009

COVALENT IMMOBILIZATION OF L1 NEURAL CELL ADHESION MOLECULE TO ACRYLATED TETRONICÂ® HYDROGELS FOR NEURAL REGENERATION

Rebecca Cribb
Clemson University, rebeccacribb@gmail.com

COVALENT IMMOBILIZATION OF L1 NEURAL CELL ADHESION MOLECULE TO ACRYLATED TETRONIC® HYDROGELS FOR NEURAL REGENERATION

A Dissertation
Presented to
the Graduate School of
Clemson University

In Partial Fulfillment
of the Requirements for the Degree
Doctor of Philosophy
Bioengineering

---

by
Rebecca Copeland Cribb
December 2009

Accepted by:
Dr. Ken Webb, Committee Chair
Dr. Karen J.L. Burg
Dr. Andrew Metters
Dr. Xuejun Wen

ABSTRACT

Spinal cord injuries cost the United States $20 billion per year, with an existing patient population of 256,000 growing by an estimated 12,000 each year. Current clinical therapies for spinal cord injury are limited to spinal immobilization and realignment via traction, surgery, administration of methylprednisolone sodium succinate (MPSS) within eight hours post-injury, and rehabilitation exercises. While these therapies are important and may minimize damage and restore limited function, there is a dire clinical need for treatments to address the growing population of chronically-injured patients.

Varying degrees of axonal regeneration and functional recovery following spinal cord injury have been achieved in animal models by transplantation of glial cells from the peripheral nervous system and olfactory region. The recent identification of bioactive soluble and adhesive molecules produced by glial cells provides the opportunity to deliver these stimuli through biomaterial-mediated approaches, such as controlled release, gene therapy, and recombinant protein immobilization. The long-term objective of this project is a biomimetic, multi-factorial approach utilizing grooved fibers to restore structure and provide guidance for regenerating axons coupled with bioactive adhesive molecule delivery via immobilization to a hydrogel within the fiber grooves and controlled release of neurotrophic factors from the hydrogel. The implant design can serve as a platform for both *in vitro* and *in vivo* analysis of combination therapies for different injured nerve populations.

The first part of this research focused on cloning and expression of a bioactive 140kDa fragment of L1 neural cell adhesion molecule. L1 is a particularly attractive

candidate for neural regeneration because it is critical for proper nervous system development and *in vitro* studies have demonstrated selectivity of neuron adhesion to L1 in the presence of astrocytes, which play a major role in nervous system inflammation. The second part of this research focused on the synthesis and purification of acrylated Tetronic macromers, and the development of Michael addition methods for hydrogel crosslinking and protein immobilization. In order to establish the feasibility of these hydrogels for neural regeneration, initial testing was conducted using NIH 3T3 fibroblasts and fibronectin because of the well-known RGD-dependent interaction. Results demonstrated that fibronectin encapsulation and surface-immobilization through acrylation of fibronectin positively influenced fibroblast spreading and proliferation. The last part of this research focused on evaluating neuronal cell line and primary neuron response to L1, evaluating cytocompatibility of T904-acrylate hydrogels with neural cells, and developing immobilization methods for L1. Results indicate that surface-immobilization of L1 to hydrogels may be the most promising method of bioactive cell adhesion molecule delivery for neural regeneration.

ACKNOWLEDGMENTS

I would like to acknowledge the Department of Bioengineering at Clemson University for the opportunity to pursue this dream and to experience both research and teaching assistant roles. I would first like to thank my advisor, Dr. Ken Webb, who took a chance on me despite my lack of research experience, and who has been a constant support and has greatly contributed to my academic and research development over the last several years. I would like to thank Dr. Webb and my committee members, Dr. Karen Burg, Dr. Andrew Metters, and Dr. Xuejun Wen, for their time, advice, guidance, and patience, all of which has improved my work. I would also like to thank Dr. Webb, Dr. Jiro Nagatomi, Dr. Delphine Dean, and Dr. Alexey Vertegel for the teaching guidance I received while teaching their classes, and I am appreciative of all the students I have taught because I have learned just as much from them.

I extend my gratitude to all those who have helped me over the years either by answering endless questions or by allowing me to use their labs, including Dr. Jeoung Soo Lee, Dr. Fuad Haddadin, Dr. Agneta Simionescu, Dr. Bruce Gao, Dr. Yonnie Wu, Dr. Ken Christensen, and Dr. Alex Kitaygorodskiy. A special thank you to Cassie Gregory, Tabitha Rosenbalm, Kirk Pirlo, and Andrew Sweeney for the extended discussions and assistance with neuron dissection and culture. I would like to express my appreciation for all the labmates I've had the pleasure to work with over the years, Kedar Datar, Sagar Joshi, Jai Kutty, Eunhee Cho, Nihar Shah, and Kris Sinclair. I would also like to encourage the new students in the lab whom I've had the pleasure of briefly working with, Jessica Bielawski, Atanu Sen, Jeremy Zhang, and Carlyn Sander.

Last, but certainly not least, I want to express my appreciation to my Lord and Savior, for without Him, nothing is possible. I am appreciative of all the people in my life who have been especially supportive of everything I try to do, regardless of how crazy it may seem. I would like to thank my family, especially my mom and dad and brother, for always believing in me. I would also like to thank my in-laws, because they have been genuinely supportive and excited about my endeavors. I would like to thank my extended music and church families and all of my friends. Finally, I want to express my greatest appreciation for my husband, Troy Cribb, whose encouragement and undying love and support have enabled me to capture a dream.

TABLE OF CONTENTS

Page

Table of Contents (Continued)

Page

Table of Contents (Continued)

Page

Table of Contents (Continued)

Page

LIST OF TABLES

LIST OF FIGURES

List of Figures (Continued)

Figure Page

List of Figures (Continued)

CHAPTER ONE

INTRODUCTION

Spinal cord injury requires continuous medical care as a result of the devastating physical and psychological consequences to the affected individual, including paralysis, respiratory deficiency, bladder and bowel dysfunction, loss of reproductive and sexual function, and ultimately, loss of personal independence. According to the National Spinal Cord Injury Statistical Center (NSCISC, Facts and Figures at a Glance, January 2008), approximately 12,000 new spinal cord injuries occur in the United States each year, in addition to an existing patient population of approximately 256,000. The average patient age at injury is 39.5 years, with life expectancies and lifetime medical costs ranging from approximately 20-40 years and $494,000 to $3,000,000, respectively. Spinal cord injuries typically occur during an individual's most productive years, resulting in a substantial economic burden to society, not only because of medical costs but also the ongoing disability support and lost productivity due to unemployment or reduced employment. A 1998 analysis estimated that spinal cord injuries cost the United States over $14.5 billion per year in direct medical costs and disability support, as well as an additional $5.5 billion per year in lost productivity, for an estimated total $20 billion per year. [1]

Current clinical therapies for spinal cord injury are limited to spinal immobilization and realignment via traction, surgery, administration of methylprednisolone sodium succinate (MPSS) within eight hours post-injury, and rehabilitation exercises. MPSS is thought to attenuate the secondary injury cascade and

improve functional recovery, and has been adopted as the standard of care since 1990 in most of North America. [2] Other experimental methods for treatment of acute injuries include decompression surgery and moderate hypothermia. [3] While these therapies are important and may minimize damage and restore limited function, there is a dire clinical need for treatments to address the growing population of chronically-injured patients.

Spinal cord injury and paralysis have been considered severe and irreversible conditions throughout much of scientific history, beginning with an account from an Egyptian papyrus roll manuscript as early as 1700 B.C. describing spinal cord injury accompanied by paralysis as "an ailment not to be treated." [4] Evidence of the first nerve graft in dogs resulting in limited degree of functional restoration was reported in France in the 1860s [5]; however, pioneering work by Spanish neuroanatomist and histologist Ramón y Cajal in the early 1900's provided evidence that nerve cells from the peripheral nervous system (PNS) have the capacity to repair themselves, but nerve cells from the adult central nervous system (CNS) display only an abortive sprouting attempt in response to injury. [6, 7] Cajal hypothesized that the differences in regenerative capacity were likely a result of the cellular environment that supports the nerve cells, and stated, "From this it may be inferred that if experimental neurology is some day to supply artificially the deficiencies in question it must accomplish these two objects: First, it must give to the sprouts by means of adequate alimentation a vigorous capacity for growth, and second, place in front of the disoriented nerve cones and in the thickness of white matter tracks, specific orienting substances." [8] Cajal believed the regenerative

capacity of the adult central nervous system could be enhanced through bioengineering efforts.

A number of mechanisms have been implicated in regenerative failure of the adult CNS following injury and are broadly classified into two categories: intrinsic barriers, or an inherent decline in growth capacity that occurs with neuronal cell maturation; and extrinsic barriers, or the non-permissive regenerative environment in the adult CNS following injury as compared to the permissive PNS and developing CNS environments. Proposed mechanisms of intrinsic regenerative failure include a decrease in the rate of retrograde transport of injury signals with increasing distance between axotomy site and cell body, delayed synthesis and diminished anterograde transport of cytoskeletal proteins required for growth cone and axon formation, a developmentally-regulated decrease in endogenous levels of neuronal cyclic adenosine monophosphate (cAMP) in mature neurons, and variable ability of different neuronal cell types to sustain expression of regeneration-associated genes. [9-12] Surviving neurons in the CNS generally do sprout axons in an attempt at regeneration; however, this attempt is quickly aborted upon encountering the hostile external environment. [13] Proposed mechanisms of extrinsic regenerative failure include delayed and incomplete clearance of axon and myelin debris; exposure to myelin-associated inhibitory glycoproteins that are not present during early stages of development; exposure to inhibitory chondroitin sulfate proteoglycans (CSPGs) present in reactive astrocytic glial scar tissue; the formation of cystic cavities; the loss of the structural organization of the mature CNS; and a lack of supporting neurotrophic

factors and growth-promoting adhesion ligands that are present during development. [9, 11, 12, 14]

Varying degrees of axonal regeneration and functional recovery following spinal cord injury have been achieved in animal models by transplantation of glial cells from the peripheral nervous system and olfactory region; however, major limitations of cell transplantation approaches include the time required to isolate, purify, genetically modify, and expand suitable autologous cells for transplantation and immune complications inherent to allographic or xenographic cell transplantation. Cell therapies for spinal cord repair do not necessarily address the disorganized structure of the injured CNS, and are plagued with additional challenges including limited cell survival and migration out of the lesion area following transplantation. Current approaches seek to address these challenges by incorporating cells within biomaterial-based scaffolds with channels to improve cell survival, limit migration, and also provide guidance for regenerating axons [15-17]; however, the recent identification of bioactive soluble and adhesive molecules produced by glial cells provides the opportunity to deliver these stimuli through biomaterial-mediated approaches, such as controlled release, gene therapy, and recombinant protein immobilization.

Synthetic degradable acellular biomaterial bridges with customizable properties and combinations of adhesive stimuli and growth factors offer the unique opportunity to tailor implants to the desired nerve populations that are to be regenerated, and also potentially open the door to readily available, large-scale production of “off-the-shelf” implants for patients with both CNS and PNS nerve injuries. [12, 18] The long-term

objective of this project is a biomimetic, multi-factorial approach utilizing grooved fibers to restore structure and provide guidance for regenerating axons coupled with bioactive adhesive molecule delivery via immobilization to a hydrogel within the fiber grooves and controlled release of neurotrophic factors from the hydrogel (Figure 1.1). The implant design can serve as a platform for both *in vitro* and *in vivo* analysis of combination therapies for different injured nerve populations.

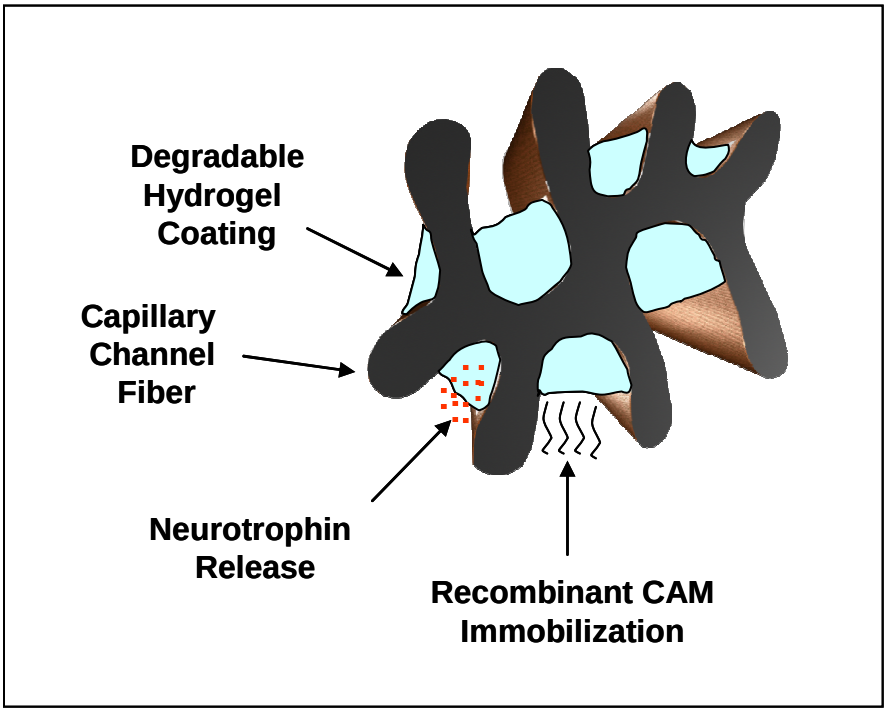

Figure 1.1 Proposed Implant Design

Neurotrophic factors are excellent promoters of neurite outgrowth on permissive substrates, but they are not sufficient for growth cone or cell adhesion to a biologically inert material; therefore, this research is focused on covalent immobilization of cell adhesion proteins to acrylated Tetronic® hydrogels with future plans of neurotrophin

incorporation to further enhance neural regeneration rates. The goals of this research were: (1) cloning and expression of a bioactive 140kDa fragment of L1 neural cell adhesion molecule, chosen for its critical role in proper nervous system development and because it has demonstrated selectivity of neuron adhesion in the presence of astrocytes, which play a major role in nervous system inflammation, (2) synthesis and purification of acrylated Tetronic macromers and the development of Michael addition methods for hydrogel crosslinking and protein immobilization, (3) evaluation of hydrogel cytocompatibility, immobilized protein bioactivity, and immobilization efficiency in terms of cell spreading and proliferation using NIH 3T3 fibroblasts and fibronectin because of the well-known RGD-dependent interaction, to demonstrate the feasibility of this system for neural repair, and (4) assessment of neuronal cell line and primary neuron response to L1, evaluation of the cytocompatibility of T904-acrylate hydrogels with neural cells, and development of immobilization methods for L1.

CHAPTER TWO

LITERATURE REVIEW

INTRODUCTION

This chapter begins by studying the mechanisms of regenerative failure in the adult CNS and investigating the differences in CNS and PNS anatomy, physiology, and response to injury in order to gain an understanding of the cues driving regeneration as well as factors contributing to the inhibition of regeneration. An understanding of these cues and factors is of crucial importance in developing therapies for functional neural regeneration (axonal regeneration with restoration of function). Current reported experimental approaches to regeneration and those that have made it to human clinical trials will also be discussed.

THE NERVOUS SYSTEM

General Anatomy/Physiology of Nervous Tissue

The human nervous system is classified into two main categories: the central nervous system (CNS), consisting of the brain and spinal cord; and the peripheral nervous system (PNS), consisting of twelve pairs of cranial nerves; thirty-one pairs of spinal nerves; and dorsal root ganglia, which are bundles of sensory nerve cell bodies with processes that branch into both the CNS and PNS. Both branches function as one actively conducting axon, which transmits information from the periphery to the CNS. Spinal nerves are connected to the spinal cord by two short roots: the dorsal root (toward the back), where sensory signals from dorsal root ganglia enter the grey matter of the

CNS; and the ventral root (toward the abdomen), where motor signals are transmitted from motor neuron cell bodies in the grey matter of the CNS to the periphery. The two roots join to form the spinal nerve just before the nerve leaves the vertebral column. [19] Figure 2.1 depicts a cross-section of the spinal cord and the position of the dorsal and ventral roots as they join to form a spinal nerve.

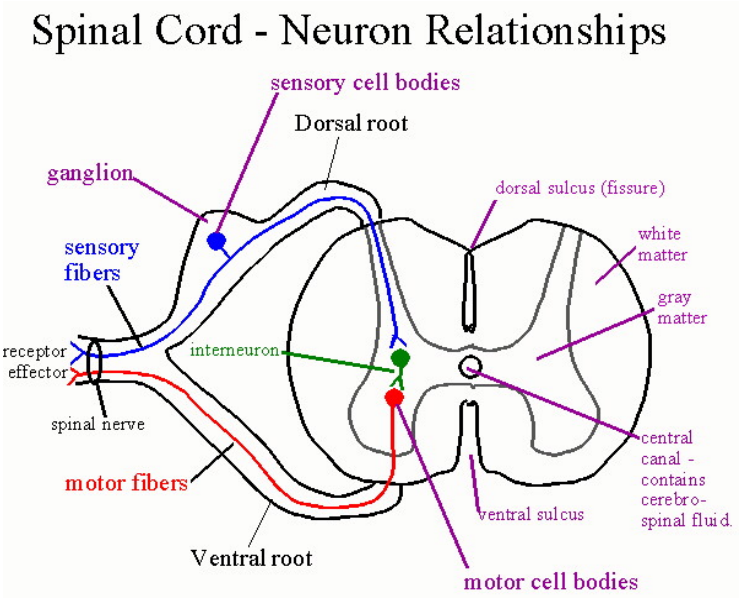

Figure 2.1 Cross-Section of the Spinal Cord
(http://webanatomy.net/anatomy/spinal_neurons.jpg)
Permission granted by Dr. Jim Swan, University of New Mexico

Cells of the Nervous System

The two main cell types in the human nervous system are neurons and neuroglia. Neurons are the main functional conducting units of the nervous system and are post-mitotic cells. They typically consist of a cell body, one axon, and one to several dendrites; however, dorsal root ganglia generally do not exhibit dendrites due to

bifurcation of their axon. Dendrites appear as branches of a tree or spikes and receive messages for the cell body. Axons may be long, short, single, or branched, and they transmit messages from the cell body to other neurons or target cells. Dendrites are most commonly observed in grey matter, where neural cell bodies are concentrated. The three classes of neurons include sensory (afferent) neurons, which transmit sensory information to the brain; motor (efferent) neurons, which have long axons and transmit information to the muscles and glands of the body; and interneurons, which provide connections between sensory and motor neurons, have short axons, only communicate within their immediate region, and are prevalent in grey matter of the spinal cord.

Neuroglia are nonconductive, mitotic cells and serve to support, nourish, and protect neurons by providing physical structure and insulation, supplying nutrients and oxygen, and destroying pathogens and removing necrotic neural tissue. Neuroglia in the CNS consist of oligodendrocytes, which myelinate axons [20]; astrocytes, which are fibroblast-like cells that secrete neurotrophic factors and are involved in signaling, energy metabolism, extracellular ion homeostasis, volume regulation, and neuroprotection [21]; and microglia, which are phagocytic, specialized macrophages of the CNS that normally maintain a resting phenotype. The brain and spinal cord are considered "immune privileged" because they are separated from the blood circulation by a series of endothelial cells known as the blood-brain barrier (BBB). The BBB prevents blood-borne immune cells such as lymphocytes, monocytes and neutrophils, as well as antibodies, from entering the CNS; therefore, microglia are thought to enable the CNS to mount a

prompt immune response to infectious or inflammatory stimuli despite the inability of blood-borne immune cells to cross the blood-brain barrier. [22]

Oligodendrocyte precursor cells (OPCs) are a newly recognized glial cell type of unknown function in the normal adult CNS; however, these cells have been shown to rapidly proliferate following injury in localized areas close to the site of damage, and their distribution in the developing CNS may point to a function in axonal guidance. [23] In addition, these cells appear to possess similar characteristics as neuronal and glial stem cells.

Schwann cells function as neuroglia in the PNS and may be divided into four classes in the mature nervous system: myelinating Schwann cells (MSCs), nonmyelinating Schwann cells (NMSCs), perisynaptic Schwann cells (PSCs), and satellite cells of peripheral dorsal root ganglia (DRG). [24] MSCs are the most well-characterized category and function similarly to oligodendrocytes in the CNS in that they wrap around large-diameter PNS axons to form the myelin sheath. The function of NMSCs is not as well-characterized but they wrap around several small-diameter unmyelinated sensory axons to form a Remak bundle, keeping individual axons separated by thin extensions of the Schwann cell body. The interaction of NMSCs with unmyelinated axons may play a key role in sensitivity to pain and other sensory stimuli. PSCs express similar proteins to MSCs and are important in development and maintenance of the neuromuscular junction. Little is known about the function of satellite cells except that they surround DRG cell bodies to form a discrete anatomical

unit. [25] Schwann cells appear to be able to switch their function by a change in gene expression. [26]

Peripheral Nerve Structure

Figure 2.2 depicts a cross-section of a peripheral nerve. Individual myelinated axons are surrounded by spirally-wrapped myelinating Schwann cells. The myelin sheath is called the neurilemma. [27] Myelinated nerves and Remak bundles of unmyelinated axons are individually-encased by endoneurium. The perineurium then binds bundles of endoneurium-encased axons together to form fascicles. Epineurium, a loose connective tissue layer, is the collagen-rich outer nerve covering forming a sheath around a bundle of fascicles. Fibroblasts secrete the type I collagen fibers and are located in the endoneurium. [28] Each peripheral nerve typically contains twice as many unmyelinated axons as myelinated axons. [19]

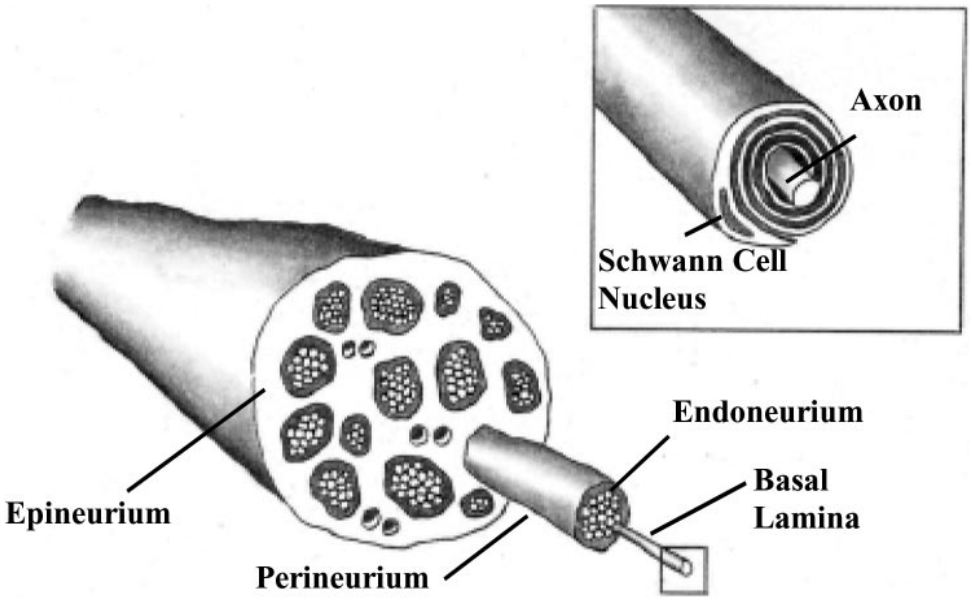

Figure 2.2 Peripheral Nerve Structure
(Reprinted from Schmidt and Leach 2003 [28])

The blood supply of peripheral nerves is composed of an intrinsic system of capillaries ensheathed along with axons within the perineurium, arterioles ensheathed within the epineurium [9], and an extrinsic system made up of vessels that penetrate the nerve from surrounding arteries and veins. [28] Figure 2.3 depicts a diagram of potential patterns of blood supply to the peripheral nerves. [29]

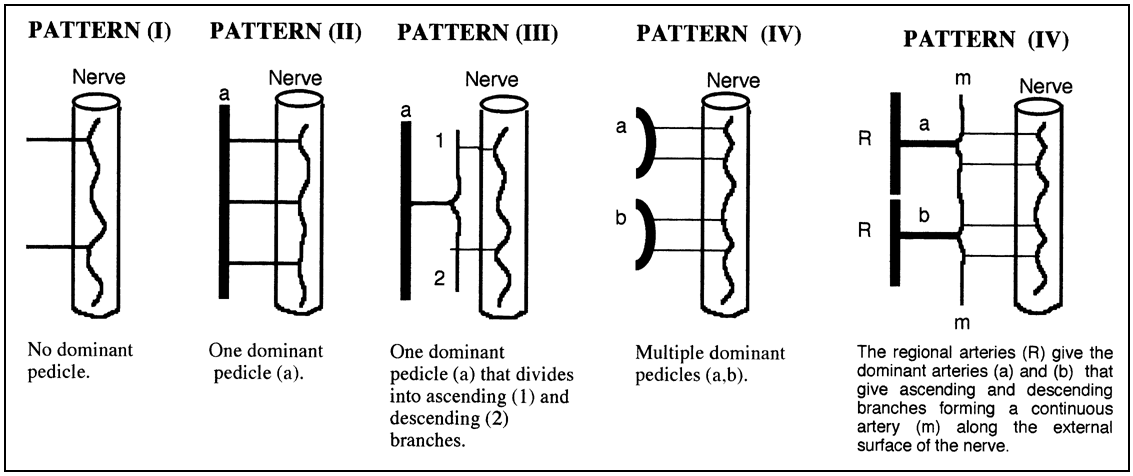

Figure 2.3 Peripheral Nerve Blood Supply Patterns
(Reprinted from el-Barrany et al. 1999 [29])

Spinal Cord Structure

The human spinal cord is highly organized and is divided into a central canal, remaining from embryonic development and containing cerebrospinal fluid (CSF); grey matter, the inner region consisting of unmyelinated cell bodies and short fibers; and white matter, the outer region consisting of myelinated long fibers in bundles called tracts. The grey-brown color of the grey matter results from the capillary blood vessels and neuronal cell bodies. The white matter appears white because of the high concentration of lipids in the myelin sheath surrounding the axons. Reflexes are also mediated in the spinal cord without going to the higher brain centers.

White matter axon tracts provide a route for signals to be transmitted up and down the spinal cord between the brain and spinal nerves. Knowledge of the functions of the different spinal cord tracts aids a neurologist in determining if an injury is complete or incomplete based on what type of sensory, motor, and reflex information the injured

patient has lost, as damage to white matter affects function at all levels below the neurological injury site. Complete lesions result in loss of all sensory and motor functions below the level of injury. Incomplete lesions result in retention of some sensory and motor functions, which can be used to diagnose which side of the spinal cord the injury has occurred. For example, the dorsal column medial lemniscus system transmits ipsilateral fine touch, proprioception, and vibration information to the brain. The lateral spinothalamic tract transmits contralateral pain and temperature sensations. The corticospinal tract is primarily responsible for skilled motor movements and injury results in ipsilateral paralysis. [19] One important consideration to take into account when developing therapies for spinal cord injury is that different axon tracts may respond differently to injury and therapeutic measures, and may have specific requirements for regeneration. [12]

Blood supply to the spinal cord is complex. [30] Briefly, arterial supply of the spinal cord is from the vertebral arteries and radicular arteries originating from the thoracic and abdominal aortae. Vertebral arteries supply upper cervical levels and branch into two posterior spinal arteries, which are located along the dorsal roots; and two anterior spinal arteries which fuse to form a single midline anterior spinal artery that runs the length of the spinal cord. Lower cervical levels are supplied by vertebral and radicular arteries but are generally dependent upon radicular arteries for survival. Figure 2.4 depicts the horizontal view of blood distribution from the posterior (dorsal) and anterior (ventral) arteries.

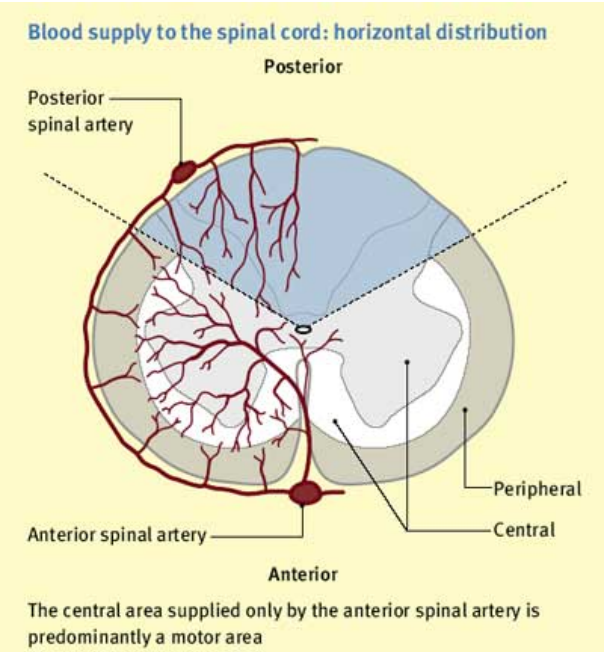

Figure 2.4 Horizontal View of Spinal Cord Blood Supply
(http://www.anaesthesiauk.com/images/spinal-cord4.jpg)
Reprinted with permission

The PNS-CNS Transitional Zone

The transitional zone consists of the thin dorsal and ventral roots that connect spinal nerves to the spinal cord. It is the location where CNS tissue is separated from PNS tissue by the glia limitans and the basal lamina of blood vessels. [31] On the CNS side of the glia limitans, nerves are surrounded mainly by astrocytic processes along with a small population of oligodendrocytes and microglia. On the PNS side of the glia limitans, nerves are ensheathed by endoneurial connective tissue consisting of Schwann cells, fibroblasts, and collagen. Lesioned dorsal root ganglia (DRG) axons that successfully regenerate the peripheral segment have been shown to stop upon reaching

the transitional zone [9], thus demonstrating the inhibitory nature of the CNS environment to regeneration.

PATHOPHYSIOLOGY OF CENTRAL NERVOUS SYSTEM INJURY

Spinal cord injuries are classified clinically according to their segmental level, as depicted in Figure 2.5; as complete or incomplete depending upon which sensory and motor functions are spared; and according to the mechanism leading to injury. [11] The human spinal cord is approximately 45 cm (1.5 ft) with 30 levels, and each spinal level in the spinal cord is around 1-2 cm. [14] Regeneration over even just one or two spinal levels can possibly result in significant improvements in function.

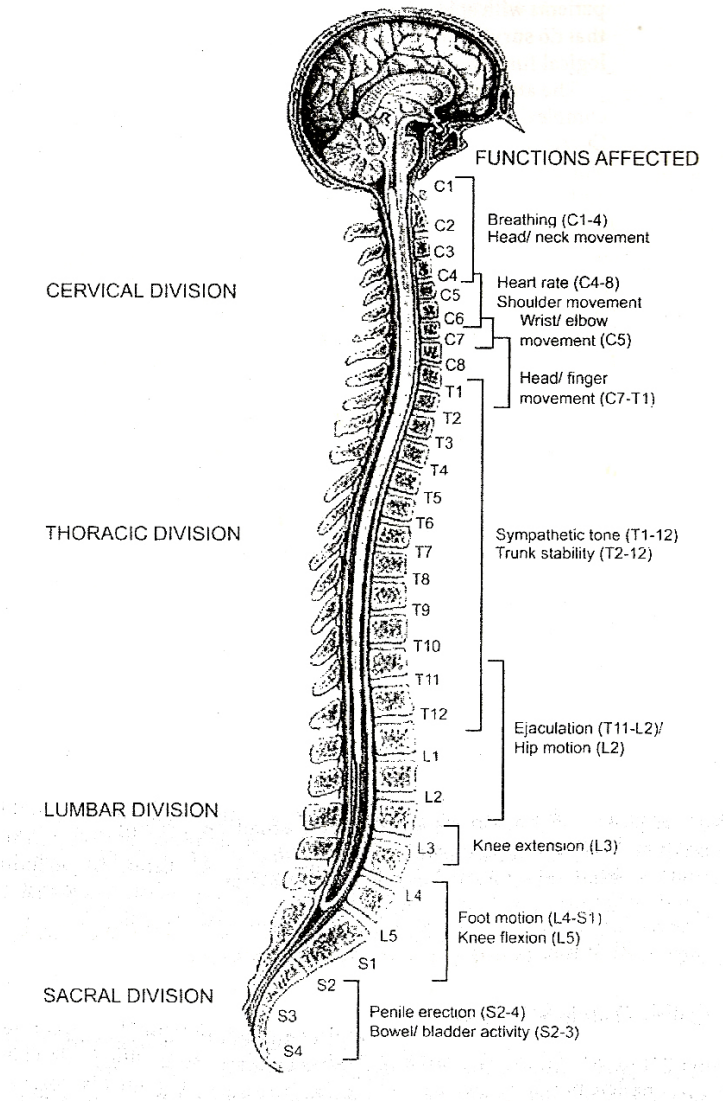

Figure 2.5 Spinal Levels and Effects of Injury
(Reprinted from Verma and Fawcett 2005 [14])

Because of clinical confusion as to the terminology associated with spinal cord injury levels, severity, and classification, the American Spinal Injury Association (ASIA) Impairment Scale (*www.asia-spinalinjury.org)* was developed with further classifications of complete and incomplete injuries, resulting in more consistent terminology being used to describe the findings in spinal cord injury around the world, depicted in Figure 2.6.

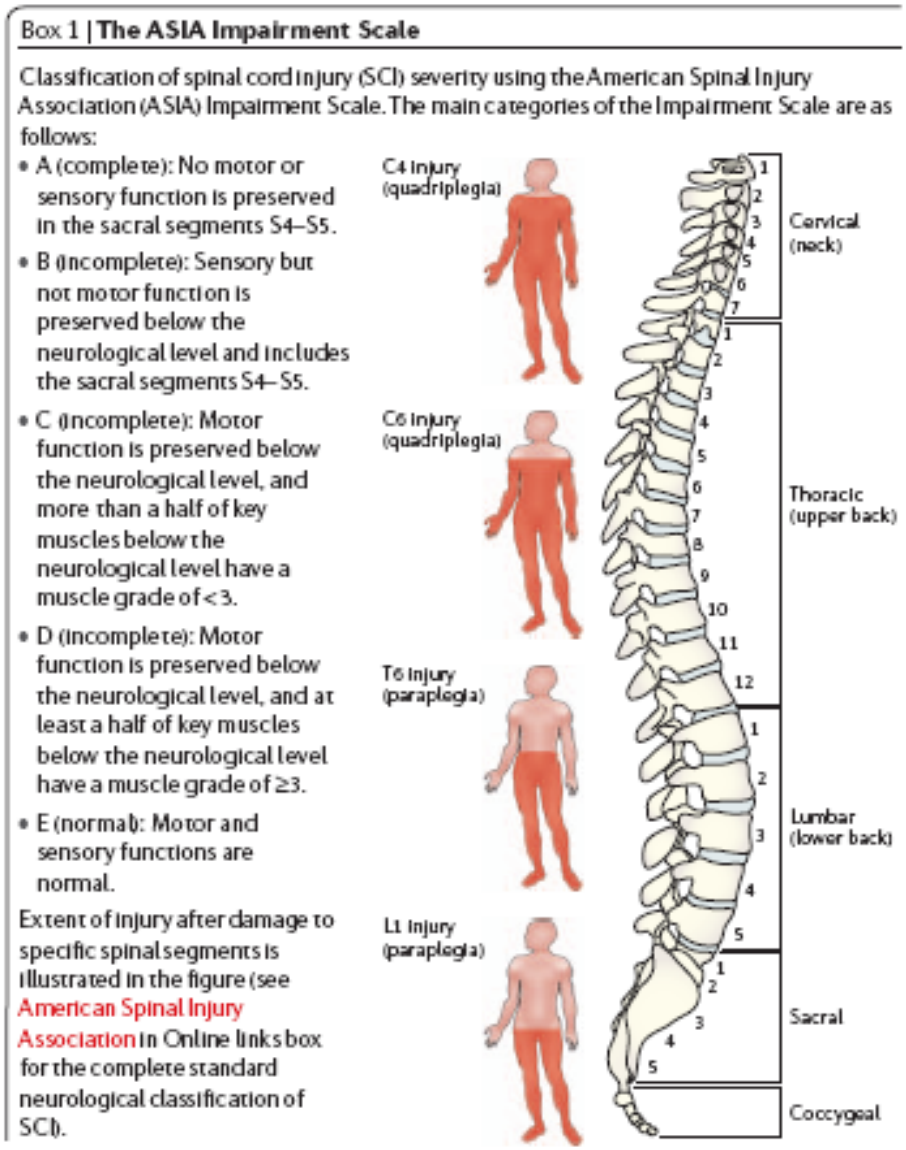

Figure 2.6 ASIA Impairment Scale
(Reprinted from Thuret et al. 2006 [32])

The ASIA Scale also includes other classifications of incomplete spinal cord injuries:

- Central cord syndrome often is associated with a cervical region injury leading to greater weakness in the upper limbs than in the lower limbs with sacral sensory sparing.
- Brown-Séquard syndrome often is associated with a hemisection lesion of the cord, causing a relatively greater ipsilateral proprioceptive and motor loss with contralateral loss of sensitivity to pain and temperature.
- Anterior cord syndrome often is associated with a lesion causing variable loss of motor function and sensitivity to pain and temperature, while proprioception is preserved.
- Conus medullaris syndrome is associated with injury to the sacral cord and lumbar nerve roots leading to areflexic bladder, bowel, and lower limbs, while the sacral segments occasionally may show preserved reflexes (e.g., bulbocavernosus and micturition reflexes).
- Cauda equina syndrome is due to injury to the lumbosacral nerve roots in the spinal canal leading to areflexic bladder, bowel, and lower limbs.

The spinal column normally experiences four forces: flexion, extension, rotation, and compression, and any combination of forces may lead to injury resulting in fractured vertebral bodies or dislocated vertebrae. These injuries result in concussion, contusion, or laceration of the spinal cord. Concussion produces no anatomical damage resulting in

transient loss of function. Both contusion and laceration injuries involve anatomical damage resulting in permanent deficits, [11].

This primary, mechanical disruption of tissue is quickly followed by a secondary injury cascade. Schwab and Bartholdi completed an extensive review of spinal cord injury and have described three main phases of the secondary injury cascade: the acute phase, the subacute phase, and the late phase. [11] The acute phase immediately follows injury and is characterized by hemorrhage, local ischemia, and edema followed by necrosis and inflammation. Hemorrhage begins in the highly vascularized gray matter adjacent to the central canal or anterior horns and spreads radially to the posterior horns and into white matter in a rostral and caudal direction. [33] The first signs of necrotic endothelial, neuronal and glial cells appear within the first hour following injury and peak within 6-12 hours of injury, along with necrosis of white matter axons. Local ischemia may result from posttraumatic hypotension or loss of autoregulation and results in predominantly anaerobic metabolism for the first 4 hours following injury followed by an increase in metabolic rate between 4 and 24 hours. Injury results in circumferential spreading of vasogenic edema into white matter caused by a disruption of the blood-brain barrier; this disruption results in increased vascular permeability which allows an abnormal accumulation of fluid in intercellular spaces of the spinal cord, which may result in compression and an abnormal electrolyte environment consisting of excess calcium and potassium followed by a chronic loss of potassium. Tissue damage may be exacerbated by compression of the swollen spinal cord tissue against the vertebrae causing an increase in ischemia. The altered electrolyte environment coupled with

oxygen free radical and lipid peroxidation reactions catalyzed by hemorrhage and the resultant ischemia, as well as release of the excitatory amino acids glutamate and aspartate, ultimately lead to necrotic cell death. Oxygen and glucose deprivation followed by reoxygenation may also induce apoptosis of neurons. [33] The inflammatory response begins within hours of injury and peaks within several days.

The subacute phase follows necrosis and is characterized by an ongoing inflammatory response resulting from reactive gliosis by microglia and astrocytes, as well as disruption of the blood-brain barrier which allows blood-borne immune cells from the periphery to infiltrate the spinal cord. Neuronal degeneration signals microglia to upregulate cell surface proteins such as major histocompatability complex II (MHC II) leading to transformation into macrophages, with markers being prominent by 3 days following injury; however, these markers decline sharply after 3 days and are not evident again until 18-20 days following dorsal root axotomy. [34] Reactive astrocytes begin proliferating within 2 days following injury and begin to accumulate at the lesion margins within 1 week, peaking at 14 days and still present at 28 days. Neutrophils infiltrate the lesion first, within 6-12 hours following injury with maximum infiltration occurring within 24 hours; however, neutrophils disappear from the lesion site at 3 days post-injury. Macrophage infiltration from the periphery follows neutrophil infilatration, and macrophages persist in the lesion site for weeks. Schwann cells, meningeal cells, and fibroblasts from the periphery also infiltrate the injured spinal cord. Meningeal cells proliferate following injury and migrate into the lesion to aid astrocytes in reestablishing the blood-brain barrier. [35] Demyelination begins within 24 hours and increases over

several days as Wallerian degeneration of distal axons progresses. Interestingly, an accurate neurological examination requires patients to be at least 72 hours post-injury, or in the subacute phase of injury. [2]

The late phase, also termed chronic injury, occurs weeks to months following injury and is characterized by well-defined cyst formation by two weeks, with some cysts containing fluid, followed by resolution of the inflammatory response with a disappearance of macrophages. In post-traumatic cystic cavitation, the size and severity of a CNS injury progress from a small area of direct trauma to a greatly enlarged secondary injury due to persistent inflammation. [36] Reactive astrocytes that migrate to the margin of the lesion site form the glial scar, which may also include reactive microglial cells. The glial scar serves to repair the blood-brain barrier and encapsulate the injury site in order to limit the inflammatory response and resulting cellular degeneration. [37] Ablation of reactive astrocytes adjacent to a forebrain stab injury in adult transgenic mice resulted in a failure of blood-brain barrier repair and a sustained increase in infiltration of immune cells from the periphery. [38] The BBB remains disrupted for up to 14 days following injury, with areas of greatest glial scarring corresponding to areas with the most extensive BBB disruption. [39] Lastly, late phase demyelination may continue to increase for a period of two weeks following injury, even in spared axon tracts. [11]

In summary, spinal cord injury results in cell death, both of neuronal cells and their supporting glial cell populations; destruction of the physical structure of axons and myelin resulting from Wallerian degeneration; progressive cystic cavitation and the

formation of glial scar tissue; and continued destruction of myelin relative to secondary injury or lack of remyelination resulting in a loss of conduction in spared axons.

REGENERATIVE FAILURE OF THE ADULT CENTRAL NERVOUS SYSTEM

A number of mechanisms have been implicated in regenerative failure of the adult CNS following injury and are broadly classified into two categories: intrinsic barriers, or an inherent decline in growth capacity that occurs with neuronal cell maturation; and extrinsic barriers, or the non-permissive regenerative environment in the adult CNS following injury as compared to the permissive PNS and developing CNS environments. Proposed mechanisms of intrinsic regenerative failure include a decrease in the rate of retrograde transport of injury signals with increasing distance between axotomy site and cell body, delayed synthesis and diminished anterograde transport of cytoskeletal proteins required for growth cone and axon formation, a developmentally-regulated decrease in endogenous levels of neuronal cyclic adenosine monophosphate (cAMP) in mature neurons, and variable ability of different neuronal cell types to sustain expression of regeneration-associated genes. [9-12] Surviving neurons in the CNS generally do sprout axons in an attempt at regeneration; however, this attempt is quickly aborted upon encountering the hostile external environment. [13] Proposed mechanisms of extrinsic regenerative failure include delayed and incomplete clearance of axon and myelin debris; exposure to myelin-associated inhibitory glycoproteins that are not present during early stages of development; exposure to inhibitory chondroitin sulfate proteoglycans (CSPGs) present in reactive astrocytic glial scar tissue; and a loss of the structural organization of

the mature CNS, the formation of cystic cavities, and a lack of supporting neurotrophic factors and growth-promoting adhesion ligands that are present during development.

Intrinsic Regenerative Failure

Embryonic neurons will grow axons when transplanted into the same environment that blocks adult axon regeneration, but adult neurons do not regenerate into embryonic environments [40, 41], suggesting intrinsic mechanisms for regenerative failure of mature neurons.

Failure of Upregulated Gene Expression and Transport

Injury signals are transported retrogradely from the site of injury to the cell body in the grey matter, and successful regeneration occurs only when the cell body is able to increase the rate of transport. Axotomy at more distal sites results in a marked decrease in retrograde transport, thus delaying changes in gene expression required for initiation of regeneration. [42] This also corresponds to observations that PNS regeneration rates are slower when lesions are far from the cell body. [27] The synthesis and anterograde transport of cytoskeletal proteins, such as actin, tubulin, and neurofilaments, is essential for the formation of growth cones and axons during development and regeneration. These cytoskeletal proteins are transported from the cell body to the growth cone by slow axonal transport, and successful regeneration occurs only when the cell body is able to increase the rate of transport. CNS neurons do not successfully upregulate gene expression and transport rates following injury [43, 44] as compared to the upregulation in gene expression demonstrated in the PNS following injury. [45]

In addition to mRNA translation and protein synthesis by the cell body, recent studies have shown that mRNAs are also transported from the cell body for local protein synthesis in developing and mature axons [46, 47], although it is unclear if adult CNS axons contain ribosomes. [48] Protein synthesis in developing axons may allow the distal axon to autonomously respond to guidance cues by rapidly changing its direction of outgrowth. Injury of mature axons triggers formation of a growth cone through locally synthesized proteins and proteolysis in the proximal axon, and locally synthesized proteins provide the retrogradely transported signaling complex that initiates the regenerative response. Neurotrophins may have the potential to enhance the localized protein synthesis of axons.

Reduced cAMP Levels

Myelin has been shown to inhibit regeneration from mature neurons; however, embryonic or neonatal neurons are capable of growth on myelin inhibitory molecules. Neuronal cyclic adenosine monophosphate (cAMP) is a cyclic nucleotide whose endogenous levels are dramatically higher in young neurons, suggesting that the switch from permissive to non-permissive growth on myelin during development is due to a developmentally regulated decrease in cAMP levels. [10] Lesion models of dorsal root ganglion neurons that project axons in both the PNS and CNS have shown that a conditioning lesion of the peripheral segment one to two weeks prior to a lesion of the central segment enables central processes to regenerate with no modification of the external environment. One theory regarding the conditioning lesion is that it allows CNS axons to overcome inhibition by myelin via a transient increase in cAMP, and that

elevation of cAMP is not only necessary but sufficient to promote regeneration. [49, 50] Spencer et al. “primed” postnatal CNS neurons overnight with neurotrophins and found that they were able to regenerate on inhibitory myelin substrates, and an increase in cAMP levels was able to mimic the effect of this neurotrophin “priming”; in fact, an increase in endogenous cAMP levels followed neurotrophin treatment. [50] *In vivo* injection, prior to injury, of cyclic AMP (cAMP) into DRG neurons resulted in regenerative sprouting of sensory axons following CNS lesion, with an elongated pattern of neurite outgrowth. [51] Protein kinase A (PKA) is a downstream effector of cAMP, and activation of PKA may phosphorylate Rho thus rendering it inactive. [52, 53] Figure 2.7 depicts a summary of signaling pathways related to myelin inhibitory molecules.

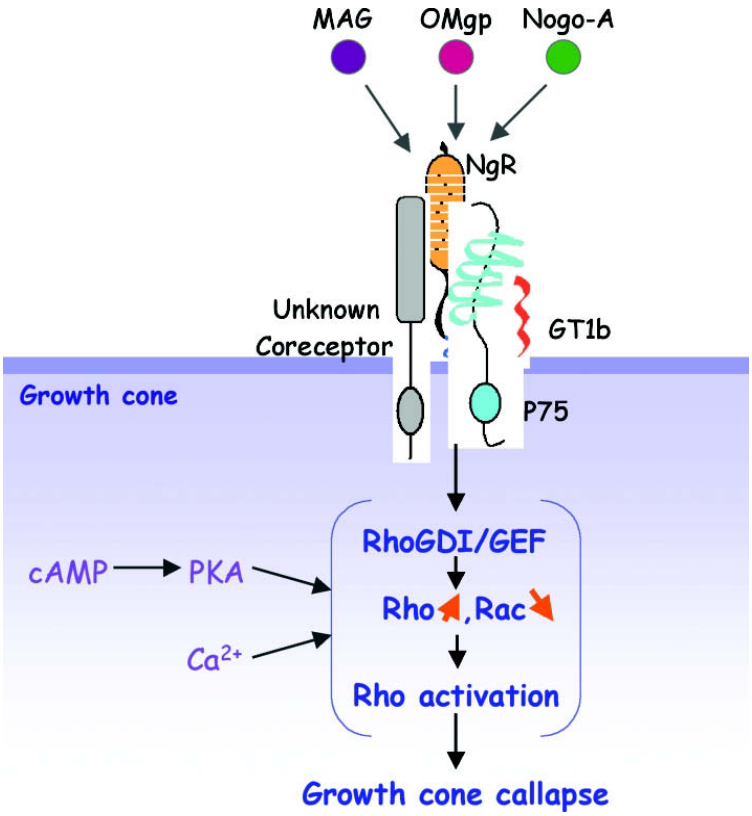

Figure 2.7 Signaling Pathways in Myelin-Related Growth Cone Collapse
(Reprinted from He et al. 2004 [52])

A conditioning lesion of DRG peripheral segments one to two weeks prior to a lesion of the central segment enables central processes to regenerate, suggesting that PNS injury activates a "growth program" that improves the inherent growth capacity of mature CNS neurons. [54] Growth-associated protein 43kDa (GAP-43) and cortical cytoskeleton-associated protein 23kDa (CAP-23) are proteins localized to the growth cone that influence axonal growth and synaptic plasticity. *In vivo* concomitant overexpression of both GAP-43 and CAP-23 has been shown to promote significant regeneration of central DRG axons into peripheral nerve implants in transgenic mice,

although not as extensive as the regeneration produced by a conditioning lesion. Also, overexpression of either protein alone failed to promote regeneration, demonstrating that each proteins is necessary, but not sufficient for regeneration. [55] The transient elevation in cAMP levels following a conditioning lesion may, in part, be responsible for the improvement in the mature CNS growth capacity, possibly mimicking that of embryonic or newborn neurons whose endogenous cAMP levels are higher. Obviously, a conditioning lesion made prior to spinal cord injury is useless clinically; however, Neumann et al. have demonstrated that conditioning lesions made at the time of spinal cord injury and again one week later promoted regeneration within and beyond the lesion site, perhaps by elevating cAMP levels or by accelerating retrograde and anterograde transport rates, thus enhancing and sustaining intrinsic growth capacity. [56]

Axonal type also affects regeneration as different axons have different intrinsic regeneration capabilities. Cerebellar Purkinje cells of the brain appear to have no regenerative response to axotomy; however, spinal motor neurons mount a robust regenerative response. [14] Dorsal root ganglia sensory axons regenerate vigorously into permissive environments. [48] Deumens et al. presented a detailed review of the sprouting responses of descending axon tracts in response to injury and descending axon tract-specific regenerative therapies. [12]

Extrinsic Regenerative Failure

Delayed and Incomplete Clearance of Axon and Myelin Debris

One drawback to the "immune-privilege" of the CNS is a delay in phagocytic clearance of degenerating axon and myelin debris, in part due to the delay in infiltration of blood-borne immune cells from the periphery and in fewer numbers than seen in the PNS; macrophages are rapidly recruited in large numbers to peripheral injury sites. [9] In addition, resident reactive microglia that transform into macrophages in the CNS abort their phagocytic response at 3 days post-injury. [34] Sensory axon and myelin debris are almost completely cleared from peripheral nerve roots by 30 days post-injury; however, axon and myelin debris in sensory axons of the spinal cord are still visible 90 days after injury. [34] Another factor contributing to differences in clearance is that Schwann cells in the PNS exhibit the unique ability to aid in phagocytosis following injury, being the primary contributors in the first two days. Myelinating Schwann cells in the distal nerve are induced to dedifferentiate into non-myelinating Schwann cells by axon and myelin debris and proliferate extensively. In the CNS, however, adult oligodendrocytes will either undergo apoptosis or enter a state of rest following injury. [57] Unlike Schwann cells in the PNS, oligodendrocytes do not participate in phagocytosis of axon and myelin debris in the CNS.

Inhibitory Molecules in the CNS

Interaction of regenerating CNS axons with inhibitory molecules results in two forms of stalled growth: growth cone collapse and formation of dystrophic endbulbs. Growth cone collapse occurs when mature regenerating axons encounter myelin debris

and oligodendrocytes following injury. Myelin inhibitors are only exposed after damage; adult sensory neurons implanted into degenerating white matter of the adult rat spinal cord extended long axons on the outer surface of undamaged myelin. [58] Myelin inhibitory molecules arrest normal growth cone progression, causing collapse and often retraction into a shrunken, quiescent growth cone. Growth cones form dystrophic endbulbs upon encountering the glial scar and it is thought that they are an aberrant growth cone that adult neurons form in order to survive in a hostile environment. These endbulbs have been shown to be highly active structures capable of returning to active growth states after extended periods of time with the appropriate stimuli. [39] Myelin inhibitors are early impediments to regeneration immediately following injury, before the formation of the glial scar.

Inhibitory myelin-associated proteins

Regeneration of injured axons recapitulates development to a certain extent; however, the regenerating axons are exposed to molecules not seen during early stages of development. Spinal cord lesions in embryos and newborns of higher vertebrates are capable of robust regeneration following injury; however, axons are no longer able to regenerate post-injury in embryonic chicken following myelin formation in the spinal cord, suggesting that oligodendrocytes and myelin play an important role in inhibition of CNS regeneration. [59] These myelin inhibitory molecules are thought to prevent aberrant sprouting of mature CNS neurons in order to prevent axon connection to inappropriate targets; however, following CNS injury, incomplete clearance of myelin debris results in growth cone collapse of regenerating axons. Some studies suggest that

myelin inhibitory molecules serve to orient neurite outgrowth in a parallel direction [60, 61] and *in vitro* studies demonstrated that disruption of axon tract geometry in relationship to myelin is sufficient to inhibit neurite outgrowth. [61]

The inhibitory molecules in myelin debris of the adult CNS include Nogo-A, -B, and -C; Nogo-66, a 66 amino acid sequence found in the extracellular domain of all three Nogo isoforms thought to be responsible for their inhibitory function; myelin-associated glycoprotein (MAG); and oligodendrocyte-myelin glycoprotein (OMgp). [13, 48, 62-64] Additional myelin inhibitory molecules include Semaphorin4D and versican, a chondroitin sulfate proteoglycan. [48] Nogo, MAG, and OMgp have been found to compete for binding to the same Nogo receptor, NgR, suggesting redundancy in their action. [65] The Nogo receptor NgR lacks an intracellular signaling domain and partners with the p75 neurotrophin receptor, the TROY receptor, and possibly other currently unknown receptors to activate Rho and its downstream target ROCK, which has demonstrated inhibitory influences on axon growth. [66, 67] Another intracellular component of Nogo signaling involves calcium-dependent cytoplasmic protein phosphorylation mechanisms; however, the role of calcium in myelin inhibition is not completely understood. [52, 68, 69]

Many groups of CNS axons are capable of regenerating into peripheral nerve grafts, suggesting that there are differences in CNS and PNS myelin and that CNS myelin is selectively inhibitory. For example, Nogo has been shown to be highly expressed by CNS oligodendrocytes but not by PNS Schwann cells. [70] In fact, regulated transgenic

expression of Nogo-A by PNS Schwann cells impaired axonal regeneration and functional recovery after sciatic nerve crush. [71]

Inhibition by the glial scar

An unfortunate complication of CNS injury occurs due to the secondary injury cascade when a small area of trauma progresses to a much larger cystic cavity that may be fluid-filled and is surrounded by glial scar tissue. In Chapter 3 of "CNS Regeneration", Fitch and Silver provide a review of the mechanisms by which glial cells contribute to CNS failure to regenerate. For many years, it was thought that the glial scar was simply a mechanical barrier to regeneration because axons will not traverse a purely fluid environment [72]; however, regeneration does not occur even in the absence of a fluid-filled cyst at the lesion site, suggesting that there are additional causes of inhibition by the glial scar. [9]

The glial scar is comprised of a lesion core populated by meningeal fibroblasts, vascular endothelial cells, and oligodendrocyte precursor cells (OPCs); and a surrounding area comprised of reactive astrocytes, OPCs, and microglia. [48] It has been demonstrated that neonatal astrocytes are supportive of axon growth *in vitro*, whereas mature reactive astrocytes are nonpermissive substrates for axon growth; typically dendrites but not axons form on reactive astrocyte substrates. [9] In response to injury, mature reactive astrocytes produce extracellular matrix components of the glial scar, including proteoglycans and tenascin, which may inhibit neurite outgrowth. The ECM of the glial scar also consists of hyaluronic acid, the most abundant ECM protein in the CNS.

Proteoglycans consist of a protein core with covalently attached polysaccharide chains termed glycosaminoglycans (GAGs) and are characterized by their GAG compositions as chondroitin sulfate, heparin sulfate, keratin sulfate, and dermatan sulfate. [9] Chondroitin sulfate proteoglycans (CSPGs) have been shown to be upregulated following injury; they persist in the extracellular matrix of the glial scar and inhibit neurite outgrowth. The hyalectan family of CSPGs includes neurocan, aggrecan, versican, brevican and these molecules share a common structure that includes an N-terminal hyaluronic acid binding site and a C-terminal with epidermal growth factor (EGF). [73] Other CSPGs include NG2, versican, [73] and biglycan, as well as other inhibitory molecules including ephs/ephrins and semaphorins. [48] Ephrins and semaphorins are primary axon guidance molecules that demarcate non-permissive regions of the developing CNS for certain classes of neurons. [23]

Neurocan is expressed by astrocytes and OPCs. Versican appears to only be expressed by immature oligodendrocytes (OPCs) in the adult CNS. Brevican is one of the most abundant CSPGs in the adult CNS and is expressed by astrocytes and mature oligodendrocytes and is present in myelin debris contained in the glial scar. NG2 is expressed by OPCs and may be expressed by reactive astrocytes following injury. Phosphacan expression is limited to neuronal tissues and is expressed by both astrocytes and OPCs. Deletion of ephs/ephrins in animals almost completely abolished reactive gliosis by astrocytes thus improving regeneration, and meningeal cells produce semaphorins as well as NG2. [48]

CSPGs may inhibit neuronal outgrowth through several mechanisms. Neurocan and phosphacan have high affinity for L1 and NCAM via the chondroitin sulfate sidechains, and binding may potentially inhibit homophilic interactions of these cell adhesion molecules, thus inhibiting regeneration. [73] CSPGs are also capable of binding to laminin, potentially masking its growth-promoting properties. An interesting feature of CSPGs in the glial scar is that they signal through the Rho/ROCK pathway, the same signaling pathway used by myelin inhibitory molecules. [74]

Loss of Organized Structure and Lack of Growth-Promoting Neurotrophic Factors and Adhesion Ligands

In humans, peripheral axons regenerate at a rate of approximately 2-5 mm/day following crush injury that leaves the endoneurial tube structure intact [27, 75]; however, transection injury without surgical intervention typically results in slower regeneration rates and lack of functional recovery, suggesting that PNS regeneration is highly dependent on the ensheathed nerve anatomy for guidance. Following degeneration of the PNS distal axons, Schwann cells remaining in the phagocytosed endoneurial tubes proliferate and align along the basement membrane of the endoneurial tube into linear arrays known as Bands of Büngner, providing a spatial scaffold for axon regeneration. In addition to their phagocytic activities following injury, Schwann cells also increase their synthesis of surface cell adhesion molecules (CAMs), such as NCAM, NgCAM, and L1; they secrete extracellular matrix (ECM) molecules such as collagen, laminin, fibronectin, and tenascin; and they produce and spatially present neurotrophic factors such as nerve growth factor (NGF), neurotrophin 4/5 (NT-4/5), brain-derived neurotrophic factor (BDNF), and glial-cell derived neurotrophic factor (GDNF). [26]

Although the CNS does not exhibit the ensheathed nerve anatomy like the PNS, there is evidence of temporal and spatial alignment of immature glial cells during development that provides a bridge-like structure along with ECM molecules, predominantly laminin; cell adhesion molecules, such as NCAM and L1; and neurotrophic factors. [28, 76, 77] Several studies highlight the importance of organized expression of growth-promoting molecules by glial cells during development. Temporospatial expression of neural cell adhesion molecule (NCAM) produced by neuroepithelial cells aligned to form tunnel-like structures is involved in guidance of optic and olfactory axons, and lack of NCAM functions as an axon-refractory barrier. [78-80] During development of the corpus callosum, there is evidence of an aligned glial bridge-like structure to guide axons across the midline that disappears neonatally. [81] Immature astrocytes oriented perpendicular to corticospinal tract (CST) axons align in longitudinal tiers and participate in axon guidance during rat CST development. [82, 83] Additionally, laminin produced by aligned immature astrocytes serves to guide optic nerve and corpus callosum axons. [76] Mechanically lesioned neuron-astrocyte mouse cortical cocultures treated to prevent glial scarring demonstrated neuron migration and neurite outgrowth with increased astroglial laminin production [84], thus reinforcing the idea that “unreactive” astrocytes generate an environment permissive to growth. Aligned glial/biomatrix bridges developed by culturing neonatal astrocytes on PLA and PLA/PLA-*b*-PEO matrices directed *in vitro* neonatal cerebral cortex neurite outgrowth over the aligned glial cells, thus highlighting importance or temporal and spatial alignment in directing neurite outgrowth. [85]. The glial structures that guide developing

axons in the CNS disappear upon maturation and are not reformed by mature reactive astrocytes following spinal cord injury. Non-native fibroblasts and meningeal cells that migrate in from the periphery following injury may deposit collagen, but no organized deposition of ECM occurs. [9] Finally, incomplete phagocytosis of axon and myelin debris and fluid-filled cystic cavities that form at injury sites severely disrupt the organized structure of the uninjured mature CNS.

Schwann cells are the one-stop-shop for PNS neurons providing them with guidance, ECM molecules, CAMs, and growth factors required for successful regeneration following injury; however, glial cells of the mature CNS play a major role in mediating the secondary injury cascade following injury, and as a result, mature CNS neurons lose the glial support that is evident during CNS development and is required for successful regeneration.

REPORTED EXPERIMENTAL APPROACHES TO REGENERATION

Experimental approaches to regeneration includes pre-clinical *in vitro* and animal models and focus on modification of the non-permissive external environment of the CNS and limited studies into modifying the intrinsic regeneration capability of CNS neurons.

Improvement of Clearance

Clearance of axon and myelin debris occurs rapidly and efficiently in the PNS following injury, in part, because of the rapid infiltration of peripheral macrophages into the lesion site; therefore, several groups have studied transplants of macrophages

activated by exposure to PNS or skin tissue in the injured spinal cord of animal models and have demonstrated partial functional recovery. [86-89] Although this approach is controversial because macrophages are believed to contribute to worsening of damage by the inflammatory cascade [90], clinical trials of autologous transplants are being pursued by two groups: Schwartz and Yoles [91, 92] and Knoller *et al.* in conjunction with Proneuron Biotechnologies (Procord). [93])

Neutralization of the Inhibitory Environment

Neutralization of the inhibitory molecules in myelin and the glial scar for CNS regeneration involves many different approaches. [14, 48, 62, 94]

A monoclonal murine IgM antibody (mAB IN-1) has been shown to block the myelin inhibitory molecule Nogo-A; *in vivo* application in the adult rat CNS resulted in substantial axon sprouting and some long-distance corticospinal regeneration following complete transection of the corticospinal tract, which is significant as no spontaneous regeneration of corticospinal fibers is typically observed. [95] A recombinant, partially humanized IgG version of the IN-1 antibody (rIN-1 Fab) has demonstrated long-distance regeneration of corticospinal axons in adult rats [96], also observed in the marmoset monkey following thoracic lesions treated with mAB IN-1. [97] Clinical trials using anti-Nogo antibodies are in the planning stages in association with Novartis. [98]

Intrathecal administration of NEP1-40 derived from Nogo-66, a competitive antagonist of the Nogo receptor common to all myelin inhibitors, improved corticospinal axon growth and functional recovery following mid-thoracic spinal cord hemisection in

adult rats. [99] An anti-Nogo receptor monoclonal antibody has been shown to promote neurite outgrowth of P3 rat DRG neurons culture on CNS myelin substrates. [100] Biogen Idec Inc. has licensed Nogo receptor-related therapeutics and may pursue clinical trials. [94]

Semaphorins are inhibitory molecules produced at sites of CNS injury and they signal through plexin and neuropilin receptors expressed in neurons. An *in vitro* model of the astrocyte/meningeal cell interface found that meningeal cells expressed NG2, versican, and semaphorins 3A and 3C, and antibody blocking of NG2 and neuropilin 2 but not neuropilin 1 promoted DRG axon growth from astrocytes to meningeal cells. [101] Ephrins expressed on astrocytes have been shown to inhibit regeneration, and adult mice lacking EphA4 exhibited reduced gliosis and regeneration of corticospinal and rubrospinal tracts across the lesion site following spinal cord hemisection, as evidenced by anterograde and retrograde tracing. [102] Astrocyte EphA4 was also blocked by monomeric EphrinA5-Fc to produce longer neurite outgrowth in this study.

Chondroitin sulfate proteoglycans (CSPGs) exist in large quantities in the damaged CNS, particularly the glial scar. [48] Chondroitinase ABC (Ch-ABC) is a bacterial enzyme that catalyzes hydrolysis of chondroitin sulfate GAG chains into dissacharides that diffuse away, thus reducing the inhibitory effects of CSPGs. Administration of Ch-ABC has been shown to induce axonal growth and functional recovery in adult rats [103, 104], as well as promote autonomic motor recovery. [105]

Blocking Rho has the unique potential to overcome inhibition by both myelin and glial scar inhibitory molecules, since their signaling pathways appear to converge on this

downstream effector. Blocking RhoA with C3 transferase (botulinum toxin) enabled regeneration following over-hemisection of the adult mouse spinal cord. [106] In addition to enhancement of regeneration, inactivation of Rho is also believed to offer neuroprotection by protecting cells from apoptosis, and inactivation of Rho kinase may alleviate pain following injury. [107] Cethrin® (BioAxone Therapeutic, Inc.) is a Rho antagonist currently undergoing clinical trials. [98, 108]

Neuronal cyclic adenosine monophosphate (cAMP) is a key player in the intrinsic inability of the CNS to regenerate, perhaps by influencing its ability to overcome inhibition by myelin and glial scar molecules. The pharmaceutical rolipram, originally developed as an anti-depressant, is a phosphodiesterase inhibitor that prevents hydrolysis of cAMP, and it has been shown to prevent the reduction in endogenous cAMP levels in adult rats following spinal cord contusion, and combined with Schwann cell grafts improved axon sparing and myelination. [109] Rolipram delivery in conjunction with implantation of embryonic spinal tissue improved axon growth into the implant and attenuated reactive gliosis. [110]

The application of treatments to block inhibition by the CNS external environment must be approached with great care and designed to only affect injured neurons, as they not only enhance regeneration but also promote significant sprouting and plasticity, which may account for functional recovery. Maladaptive sprouting and growth of non-injured neurons may be an undesirable side effect of these types of treatments. Hyperalgesia is one side effect that has resulted from aberrant sprouting of uninjured small pain fibers in nerve growth factor-treated animal models. [111]

Delivery of Neurotrophic Factors

Neurotrophic factors are key nervous system regulatory proteins that modulate neuronal survival, axonal growth, synaptic plasticity, and neurotransmission. They have also been shown to promote and direct growth cone motility [112]; they exhibit a chemotactic effect for axon guidance, and they aid in sensory nerve growth across the PNS-CNS transition zone. As a result, their role in axon development and regeneration is being studied extensively for application in spinal cord repair [28, 94, 113-115].

The family of neurotrophic factors includes nerve growth factor (NGF), brain-derived neurotrophic factor (BDNF), neurotrophin-3 (NT-3), neurotrophin-4/5 (NT-4/5), ciliary neurotrophic factor (CNTF), glial cell line-derived growth factor (GDNF), and acidic and basic fibroblast growth factor (aFGF, bFGF). Schwann cells produce neurotrophic factors following PNS injury; however, levels following spinal cord injury are almost undetectable. The neural responses promoted by neurotrophic factors are summarized in Table 2.1. [28]

NEURAL RESPONSES PROMOTED	NEUROTROPHIC FACTORS
Motor neuron survival	BDNF, NT-3, NT-4/5, CNTF, GDNF
Motor neuron outgrowth	BDNF, NT-3, NT-4/5, CNTF, GDNF
Sensory neuron survival	NGF, NT-4/5, GDNF
Sensory neuron outgrowth	NGF, BDNF, NT-3
Spinal cord regeneration	NGF, NT-3, CNTF, FGFs
Peripheral nerve regeneration	NGF, NT-3, NT-4/5, CNTF, GDNF, FGFs
Sensory nerve growth across PNS-CNS transitional zone	NGF, NT-3, GDNF, FGFs

Table 2.1 Neural Responses Promoted by Neurotrophic Factors [28]

There is a significant amount of overlap in the responses promoted by neurotrophic factors, and this must be taken into account when considering their use in therapeutic applications. For example, NGF was the first and most widely studied neurotrophic factor and is best known for its essential role during the development of peripheral sensory and sympathetic neurons [116]; however, it has been shown to be clinically useless for regeneration of peripheral nerves because it affects pain-sensitive neurons, resulting in hyperalgesia, or increased sensitivity to pain. [117] NT-3 is useful for regenerating corticospinal axons [77]; however, NT-3 can trigger apoptosis of BDNF-dependent neurons. [118]

Neurotrophins have a very short half-life, are digested in the gastrointestinal tract, and do not pass the blood-brain barrier; as a result, oral or systemic delivery will not promote regeneration of CNS neurons and may result in unwanted side effects due to nonspecific delivery. In addition, there is rapid clearance of drugs injected directly into the spinal cord due to the constant exchange of cerebrospinal fluid (CSF). As a result, delivery methods must be tailored to provide biologically relevant amounts of long-term, localized neurotrophins at the site of injury in order to avoid unwanted side effects. Reviews of reported methods of delivery include direct injection, continuous infusion, *in situ* gene therapy, and transplantation of *ex vivo* genetically engineered cells. [28, 113, 114]

Direct injection to the cerebrospinal fluid (CSF) by means of intracerebroventricular, intraparenchymal, or intrathecal infusion does not provide long-term delivery of growth factors because there is rapid clearance due to the constant

exchange of CSF and does not provide localized delivery. [114] Continuous infusion using an implanted osmotic minipump may be used as a temporary intervention strategy following spinal cord injury or to study the effects of neurotrophins; however, it is not a solution for extended delivery because depleted pumps have to be replaced at 4 weeks, and it also does not provide localized delivery. [119, 120]

In situ gene therapy via vector-mediated expression of neurotrophic factors to the spinal cord has advantages over local or systemic administration. Vectors can be delivered to the spinal cord by single injection, expression can be targeted to lesioned neurons, and vector expression of a neurotrophic factor mimics their physiological production. [114] Two types of vector systems exist: viral vectors and nonviral vectors. Viral vectors include: (1) herpes viral vectors (HSV), (2) adenoviral vectors, (3) adeno-associated viral vectors (AAV), and (4) lentiviral vectors (LV). Nonviral vectors are typically not used for this application due to their inefficiency. Table 2.2 is a summary of research groups studying the viral-mediated vector expression of neurotrophins. AAV and LV vectors do not display detectable inflammatory or cytotoxic responses and may be a good choice for future gene therapy; however, HSV and adenoviral vectors are not suitable because they require immunosuppression and are cytotoxic.

	GROUP	VECTOR	GROWTH FACTOR
1.	Geschwind et al., 1994 [121]	HSV vector	NGF
2.	Zhang et al., 1998 [122]	Adenoviral vector	NT-3
3.	Ruitenberg et al., 1998 [123]	AAV vector	BDNF
4.	Hottinger et al., 2000 [124]	LV vector	GDNF

Table 2.2 Groups Researching *In Situ* Gene Therapy

Ex vivo gene therapy is a combination therapy involving *in vitro* genetic modification of autologous cells to deliver a specific growth factor, followed by transplantation of the cells back into the host. This approach eliminates the risk of immunological rejection and may provide a high concentration of long-term, localized growth factor delivery to a site of injury [113]. Table 2.3 is a summary of research groups studying this method of neurotrophic factor delivery.

	GROUP	CELLS	GROWTH FACTOR
1.	Grill et al., 1997 [125]	Fibroblasts	NT-3
2.	Tuszynski et al., 2002 [126]	Fibroblasts	NGF
3.	Lu et al., 2003 [127]	Neural stem cells	NT-3
4.	Tuszynski et al., 2003 [128]	Fibroblasts	NT-3
5.	Blesch et al., 2004 [129]	Fibroblasts	NT-4/5
6.	Lu et al., 2005 [130]	Marrow stromal cells	BDNF

Table 2.3 Groups Researching *Ex Vivo* Genetically Engineered Cells

Groups 1, 3, and 5 reported partial amelioration of functional deficits by the Basso, Beattie, and Bresnahan (BBB) locomotor rating scale for rats or other functional test methods. Groups 2, 4, and 6 reported extensive axonal growth following cell transplantation. Additional examples of genetically-modified cells used for neurotrophic factor delivery have been reported by Schmidt and Leach. [28] None of the groups reported axon growth beyond the graft, thus demonstrating the need for additional strategies.

Bridging Strategies

The idea of bridging strategies in the CNS arose from the need to restore structure and provide necessary adhesion molecules and growth factors in order to promote regeneration of axons, much in the same way immature CNS glia provide these elements for developing axons and PNS Schwann cells provide these elements for developing and injured PNS neurons. Several approaches are currently under investigation, including transplantation of fetal and embryonic tissue, mechanically-engineered nervous tissue constructs, peripheral nerves, and cells.

Nervous Tissue Transplantation

Neural tissue transplants from human embryos and fetuses have shown promise in promoting CNS regeneration in animal models. Transplants of fetal spinal cord following resection lesions of adult rat spinal cord and contused adult rat and cat spinal cord demonstrated short-distance regeneration into the grafts and attenuation of scar tissue but limited regeneration across the host/graft interface. [131-133] These neural tissue transplants have the potential to not only replace cells but may also provide sources of growth factors, improvement of conduction by remyelination, or neuroprotection. Despite the inherent issues in scale-up as well as the ethical challenges, human fetal spinal cord tissue has been grafted into human patients with syringomyelia in clinical trials. [134, 135]

Mechanically-Engineered Nervous Tissue Constructs

Another unique approach involves the development of transplantable tissue constructs comprised of DRG axons induced to grow by application of mechanical stretch

to the central portion of the axon, thus mimicking the growth of integrated nerves and axon tracts that do not have growth cones and are under mechanical strain during development. [136] Pfister et al. created 5 cm long axon tracts in 8 days, encased them in an 80% collagen hydrogel, and inserted them into a poly(glycolide) (PGA) conduit (Neurotube®). Nervous tissue constructs could be grown at the rate 1 cm/day up to 10 cm in length using this stretch-growth system. Collagen hydrogel-coated 10 mm long constructs were implanted into rats 10 days following modified lateral hemisection injury and were found to survive 4 weeks following implantation and to extend axons into the host spinal cord tissue. [137] This approach not only serves to bridge the injury site but may also circumvent the issue of long-distance regeneration in the inhibitory CNS environment by potentially allowing the creation of new intraspinal connections.

Peripheral Nerve Grafts

In the 1980's, Richardson et al. established that regeneration of CNS axons into autologous peripheral nerve grafts in rats could be accomplished as evidenced by retrograde tracing, although functional recovery was lacking, the axons did not leave the graft, and corticospinal axons did not grow into the graft. [138, 139] These studies reinforced the idea of the permissive regeneration environment of the PNS, and in fact, peripheral nerve contains Schwann cells that aid in phagocytosis, production of ECM and cell adhesion molecules as well as neurotrophic factors, and remyelination following peripheral nerve injury.

Autologous peripheral nerve grafts are typically derived from cutaneous nerves, such as the sural or saphenous nerve, with up to 40 cm available length and 2-3 cm

diameter. [28] It is interesting to note that the sural and saphenous nerves are two of the most vascularized peripheral nerves and are therefore considered extremely suitable for vascularized grafting. [29] Autologous grafts are advantageous because they reduce the risk of immune rejection; however, donor site morbidity is a major drawback, and non-critical sensory nerves must be chosen thus limiting availability. Peripheral nerve allografts are an alternative and have the advantages of large supply and no donor site morbidity; however, there is a risk of disease transmission and immunosuppression is required during the time it takes cells in the allograft to be replaced with host cells. Even so, allografts have been used clinically and may not require long-term immunosuppression. [140]

Autologous intercostal nerves with fibrin glue and acidic fibroblast growth factor (aFGF) were implanted into monkeys after lateral spinal hemisection and demonstrated regeneration of myelinated CNS axons into the graft but not beyond the lesion site. [141] Cheng et al. demonstrated regeneration of corticospinal axons into intercostal nerve implants with fibrin glue, aFGF, and compressive wiring in adult paraplegic rats [142], and extended their studies to one case of peripheral nerve transplant into a human paraplegia patient with a 4-year old ASIA-C injury. [143] The subject received a sural nerve graft with fibrin glue and aFGF. Two and one-half years following the surgery his functional status improved from wheelchair-bound to ambulatory and ASIA-D classification. Although this case included no control subjects and is contradictory, it does suggest that combination therapies may be of real benefit to patients, even those with chronic spinal cord injury.

Cell Transplantation

Several cell types are under investigation for use in bridging strategies, including Schwann cells, olfactory ensheathing cells (OECs), and stem cells. [28, 94, 144, 145]

Schwann Cells

Schwann cells are key players in the success of peripheral nerve regeneration and in the success of CNS regeneration into peripheral nerve grafts, so it is no surprise that grafts of these cells are being pursued as a spinal cord therapy. Richardson et al. documented one of the earliest attempts at bridging a spinal cord injury in the 1980's where regeneration of CNS axons into autologous peripheral nerve grafts in rats was accomplished as evidenced by retrograde tracing. [138, 139] Schwann cell transplantation for CNS repair was a logical next step and has demonstrated varying degrees of axonal regeneration and partial functional recovery in animal models. [94, 145, 146]

These cells also migrate into the injured spinal cord, possibly from the dorsal and ventral roots, upon disruption of the blood-brain barrier and have been found in long-term human spinal cord injuries, indicating that they are able to survive in the human CNS environment as abnormally-organized tumors termed Schwannomas, but in a detrimental manner causing compression of CNS axons. [147] Schwann cells in the PNS provide spatial alignment via linear arrays known as Bands of Büngner; however, Schwann cells do not migrate along CNS white matter tracts, suggesting that they may not provide spatial alignment for CNS axons. [148] Schwann cells may also have the unique ability to aid CNS axons in remyelination following regeneration; however, it has been

demonstrated that the cues for myelination in the CNS and PNS are different, and that nerve growth factor (NGF) promotes myelination by Schwann cells but reduces myelination by oligodendrocytes [149], a factor that warrants further investigation and should be taken into account when designing combination therapies with Schwann cell grafts. Genetic engineering of Schwann cells to alter interactions with migration and myelination cues is a potential way to account for these differences. [146]

Challenges facing Schwann cell grafts include failure to regenerate axons out of the graft, lack of remyelination of axons beyond the injury site, and unfavorable interactions with astrocytes leading to increased inhibitory CSPG production. [146] As a result, several groups are studying *ex vivo* genetic modification of Schwann cells in order to overcome these challenges. Schwann cells genetically modified to secrete upregulated concentrations of NGF were grafted into the midthoracic region of the uninjured adult rat spinal cord and were found to survive for up to one year and to induce robust growth and myelination of neurotrophin-receptive sensory axons; however, it was noted that Schwann cell grafts may enlarge over time, possibly attributable to immortalization of the cells after multiple passages *in vitro*. [150] Expression of neural cell adhesion molecule L1 on Schwann cells and axons correlated with axon-Schwann cell ensheathment, and transduction of Schwann cells to overexpress NGF robustly increased axonal growth, following implantation into adult rat spinal cord injury. [151] Schwann cells genetically modified to secrete upregulated concentrations of BDNF enabled supraspinal axon regeneration across and beyond the transection site in an adult rat model. [152] Genetic

modification may be a viable method of overcoming the inherent challenges in Schwann cell transplantation strategies.

Olfactory Ensheathing Cells

One of the major issues impacting all bridging techniques is that regenerating axons do not want to leave the permissive substrate and reenter the inhibitory CNS environment to reconnect with their target synapses. Olfactory ensheathing cells (OECs) are glial cells of the olfactory system, and the olfactory system has the distinctive capacity to support neurogenesis throughout life [153]. OECs have the unique intrinsic ability to guide and ensheath, but not myelinate, new olfactory receptor axons into the CNS across the normally inhibitory PNS-CNS transition zone [154, 155], and are thought to have the potential to aid regenerating axons in navigating inhibitory environments. Another theory is that OECs aid in preventing an astrocytic response, thus limiting expression of inhibitory CSPGs. [28, 145] OECs are thought to be capable of migrating through glial scar regions, as studies utilizing suspension transplants of OECs enabled regenerating corticospinal axons to cross the lesion site in adult rats [156, 157]; however, a combination of Schwann cells and OECs plus administration of chondroitinase ABC following complete spinal cord transection in adult rats produced improvements in functional scores but no evidence of regeneration of corticospinal or reticulospinal tracts. [158] Major concerns with studies of this cell type include the methods of preparation. [153] Animal studies conducted have used neonatal and adult cells as well as different purification methods, such that the impact of other cell types on results cannot be elucidated. [154] There is also recent controversy as to whether these cells actually

enable axons to regenerate past the lesion site, or if the functional recovery seen is a result of plasticity and neuroprotection, as there is little evidence to support that OEC grafts are able to reestablish functional connections as of yet [159], and migration of injected OECs does not appear to be different than migration of injected bone marrow stromal cells or fibroblasts. [160]

Another caveat of this approach is that centrally-derived autologous cell sources from the olfactory bulb have been used in most animal studies; however, harvest of these cells compromises the host's sense of smell, so peripherally-derived OECs from olfactory endothelium are being explored as a viable alternative. [28] These peripherally-derived cells may not behave the same as the centrally-derived cells and will require further testing. Even with the discrepancies in reported results from animal models, transplantation of human fetal and adult OECs is currently one of the largest human clinical trials, being pursued in China. [161-164]

Embryonic and Adult Stem Cells

Significant loss of neurons and glial cells occurs following spinal cord injury. Pluripotent stem cells are sources for new cells in embryos that are capable of indefinite self-renewal and differentiation into any cell type. In adults, multipotent progenitor cells, also called adult stem cells, are sources for new cells that are capable of differentiation into a limited number of cell types. [94, 165] These cells have the potential to not only bridge the injury site, but may also be able to replace cells that have been lost to injury.

Embryonic stem (ES) cells have the advantage of being a potential indefinite cell source and are being studied extensively for their potential use in spinal cord injury. [140,

166] ES cells from mice were committed to the nervous system lineage by exposure to retinoic acid and transplanted into rats more than 9 days following injury; the transplanted cells differentiated into neurons, astrocytes, and oligodendrocytes and promoted some functional recovery and remyelination, although regeneration has not been demonstrated yet. [167] Major concerns with embryonic stem cells include the ethical debate regarding their use and the long-term immunosuppression that is required following the transplant of foreign cells. Spinal cord injured patients are vulnerable to infection, and long-term immunosuppression in these patients is contraindicated. One method that is being developed to avoid the use of foreign cells is somatic-cell nuclear transfer, which allows the generation of "autologous" embryonic stem cells by replacing the nucleus of a human egg with the nucleus from a somatic cell of the patient, then allowing the embryo to develop to the blastocyst stage from which ES cells can be harvested and grown in culture. [140]

Another source of new cells is the endogenous stem cells in the mature CNS that are capable of differentiating into neurons and glial cells, termed neural progenitor cells (NPCs) [168], but typically only produce oligodendrocytes and astrocytes in the spinal cord. [14, 140, 169] These cells reside around the central canal of the spinal cord. [140] Mouse NPC grafts were found to constitutively secrete several neurotrophins and promoted extensive axon growth in adult rats following dorsal column lesions. [127] Glial cell progenitors are multipotent cells with restricted fates, and include cells capable of differentiating into myelinating Schwann cells in the PNS or oligodendrocytes in the CNS. Transplantation of these cells has been shown to remyelinate axons but has not

demonstrated axonal regeneration. [170] Disadvantages of these cell types is that their populations may also be significantly reduced upon injury to the spinal cord, biopsy is required to obtain this cell source, and it does take time to grow enough cells in the laboratory for transplantation; however, their advantages lie in that they are a true autologous cell source in comparison to ES cells and it may be possible to stimulate their response *in vivo*, thus avoiding transplantation altogether. [94]

The ability of embryonic and endogenous stem cells to proliferate and their multi-potentiality make them ideal candidates for CNS regeneration; however, preventing proliferation of undesirable cell and tissue masses through controlled differentiation is of utmost importance and is a significant factor in designing implantation strategies. [171]

CLINICAL THERAPIES AND TRIALS

Current Clinical Therapies for Spinal Cord Injury

Methylprednisolone sodium succinate (MPSS) was the first and is currently the only treatment for the management of acute spinal cord injury, and has been adopted as the standard of care since 1990 in most of North America [2]; however, no official FDA review of the drug for this indication has been sought and the analysis of the data supporting its use for SCI has been criticized. [172] This steroid drug, when administered within 8 hours of injury, is thought to attenuate the secondary injury cascade and improve functional recovery; however, the National Acute Spinal Cord Injury Studies (NASCIS) II and III only showed modest improvement in patients receiving MPSS, with extensive complications including sepsis, pneumonia, and potential

steroid myopathy. [2, 14, 98]) Although controversy regarding the effectiveness and safety of MPSS remains, establishment of the 8 hour "therapeutic window" by the NASCIS clinical trials led to evaluation of other neuroprotective pharmacological therapies, including GM-1 ganglioside (Maryland and Sygen) and numerous other candidates. [173] Researchers are also investigating the neuroprotective effects of mild hypothermia (about 92°F) for several hours immediately following spinal cord injury. [3] One major issue confounding results from pharmaceutical clinical trials for acute SCI is inconsistency in the use of methylprednisolone in conjunction with the new pharmaceutical agents being tested and lack of control for the use of methylprednisolone in the studies. [2]

The ultimate goal for a spinal cord injured patient is recovery of function, which may result from axonal regeneration, nervous system plasticity, restoration of conduction by remyelination of spared axons, or any combination of these factors. Rehabilitation following spinal cord injury is a clinical therapy that may improve motor recovery of postural and locomotor tasks, such as standing and stepping, by taking advantage of peripheral sensory information that can be used by the spinal cord without involving the brain, thus demonstrating the remarkable plasticity of spinal motor neural circuits to "learn" tasks. [174] Although rehabilitation is not a useful strategy in and of itself to promote axonal regeneration, it has the capacity to improve patient quality of life now, depending upon the type of injury sustained [175], and its potential to limit muscle atrophy may ultimately improve functional recovery from reinnervation of muscle targets by regenerated motor axon tracts.

Standardization of Animal Studies and Clinical Trials

Common animal spinal cord injury models include contusion, transection, compression, ischemic, and combinations of these four. [94] Contusion injuries represent the largest sect of human spinal cord injuries. One major problem with most animal contusion models is that they are applied to the dorsal surface following laminectomy resulting in a posterior compression injury, which standardizes the location and severity of injury; however, most human injuries are the result of ventral impact associated with anterior compression of the vertebrae. [33] Another issue is the contusion device speed is much slower and results in less impact than what is typical for most human injuries. In addition, the compressive force in contusion models is typically removed immediately after injury whereas it may be hours or days before a human injury is decompressed. [108] The Basso, Beattie, and Bresnahan (BBB) locomotor rating scale has been widely accepted as a method to assess locomotor function in rats following spinal cord contusion injury [176]; however, there is no correlation of the BBB scale to the ASIA scale used for human injuries, and differences in innate immune and inflammatory responses to injury compromise the predictive value of findings in rats. [108] Primate models are being explored but their expense is a significant limiting factor. True regeneration is difficult to ascertain in contusion models. Complete transection models allow undeniable determination of regeneration, but these models are not representative of the majority of human injuries nor do they generate the cystic cavitation more commonly seen with contusion injuries. [94]

It has been demonstrated repeatedly that functional improvement does not necessarily correlate to axonal regeneration, and axonal regeneration does not necessarily produce functional improvement. Demonstration of functional regeneration (axonal regeneration with functional recovery) must be validated by several criteria, including anatomical tracing, specific behavioral tests corresponding to the regenerated axon phenotype, electrophysiology to confirm connectivity, and ultimately, subsequent reinjury of the regenerated axons to demonstrate their requirement for functional recovery. [13]

There is a great need for standardization of human clinical trials for spinal cord injury, as is evidenced by several reviews dedicated to discussing issues with past and current human clinical trials. [2, 98, 108, 177] In response to the lack of standardization, the International Campaign for Cures of Spinal Cord Injury Paralysis (ICCP) supported an international panel charged with reviewing the methodology for clinical trials in spinal cord injury, and they have established guidelines for future clinical trials. [178-181]

Worldwide Clinical Trials

As discussed previously, clinical trials investigating implantation of activated autologous macrophages (ProCord®; Proneuron Biotechnologies) and the Rho pathway antagonist, Cethrin® (BioAxone Therapeutic, Inc.) in patients with thoracic and cervical SCI are currently underway. [98, 173] Also, a large-scale clinical trial investigating transplantation of human fetal and adult OECs is currently being pursued in China. [98,

161, 163, 164] Figure 2.8 represents a summary of recent human clinical trials around the world. [98]

TABLE 5. Recent regeneration trials in spinal cord injury

Strategy	Series (ref. no.)	Countries	No. of patients	Neurological results	Other results and comments
Fetal porcine stem cells: into cord	Diacrin study	United States	8		No further recruitment
Autologous activated macrophages: into cord	Procord study, Knoller et al., 2005 (93)	Israel	6	Improvement in some	Phase II trial in progress in 2006
	Schwartz and Yoles, 2005 (138)	Israel, Belgium	14	Improvement in 5 patients	
Neurotrophic factors: intrathecally by pump	CNTF for ALS, Penn et al., 1997 (119)	United States and Canada	4	No improvement	Complications
	BDNF for ALS, Kalra et al., 2003 (87)	United States		Final results not yet reported	Phase III study by Amgen
Peripheral nerve grafts: cord to cord	Cheng et al., 2004 (33)	Taiwan	1		Continuing to recruit
Peripheral nerve grafts: cord to cord	Barros et al., 2003 (8)	Brazil	8	No improvement	
Peripheral nerve grafts: cord to nerve	von Wild and Brunelli, 2003 (173)	Italy	1	Improvement	
Avulsed root inserted into cord: brachial plexus injury	Carlstedt et al., 2000 (26)	Sweden	10	Improvement	
Human olfactory ensheathing glia (fetal and adult): into cord	Huang et al., 2003 (79)	China	171	Improvement	Continuing to recruit
	Feron et al., 2005 (58)	Australia	3		
	Rabinovich et al., 2003 (123)	Russia	15	Improvement	Continuing to recruit
Blood-derived stem cells: ALSI, intrathecal; SCI, intrathecal	Janson et al., 2001 (84)	Portugal, United States, Brazil, Russia			
Schwann cells	Zhu et al.	China	47	Improvement	Continuing to recruit
	Feng et al.	China	9	Improvement	Continuing to recruit
Human fetal spinal cord: syringomyelia	Falci et al., 1997 (53)	Sweden	1		Syrinx smaller
	Wirth et al., 2001 (176)	United States	8	No further deterioration	Syrinx smaller
Rho antagonist	Cethrin study/Bio-Axone	United States, Canada			In progress
Anti-Nogo-A antibody	Novartis study	Europe			Planning stage
Human bone marrow stem cells	Park et al., 2005 (117)	South Korea	5	Improvement	
	Zhang et al.	China	90		
	Bryukhovetskiy	Russia			
	Neuronyx	Czech Republic, United States			
Human embryonic stem cells with oligo differentiation	Keirstead, Wirth	United States			Planning stage
Polyethylene glycol		United States			Planning stage
Electrical stimulation	Shapiro et al., 2005 (140)	United States	10	Some improvement	Continuing to recruit
	Xu, Liu	China	>100	Some improvement	Continuing to recruit

[a] CNTF, ciliary neurotrophic factor; ALS, amyotrophic lateral sclerosis; BDNF, brain-derived neurotrophic factor; SCI, spinal cord injury. All are Phase I studies and are not reported unless indicated.

Figure 2.8 Worldwide Clinical Trials
(Reprinted from Tator 2006 [98])

CONCLUSION

Most of the current approaches in human clinical trials involve either peripheral nerve grafts or cell transplantation. Peripheral nerve grafts face challenges of limited availability and donor site morbidity associated with autografts, and the immune complications inherent to allographic or xenographic transplantation, along with potential complications arising from cell types within peripheral nerve that are foreign to the CNS. Inflammation within the CNS is particularly detrimental and may exacerbate existing injury. Cells are an excellent source of the myriad of factors required for regeneration; however, a major limitation of all cell transplantation approaches is the time required to isolate, purify, genetically modify, and expand suitable autologous cells for transplantation, or the immune complications inherent to allographic or xenographic transplantation. Cells may produce undesirable side effects and do not allow for specific delivery of molecules without genetic modification. Cell transplantation strategies also face the unique challenges of cell survival and migration and do not necessarily address the disorganized structure of the injured CNS; however, current approaches seek to address these challenges by incorporating cells within biomaterial-based scaffolds with channels to improve cell survival, limit migration, and provide guidance for extending axons. [15-17] The next chapter will discuss biomaterial-based bridging strategies in further detail.

CHAPTER THREE

BIOMATERIAL-BASED BRIDGING STRATEGIES

INTRODUCTION

Most of the current approaches in human clinical trials involve either peripheral nerve grafts or cell transplantation; however, biomaterial-based bridging strategies are an alternative approach with a wide range of applications for neural repair. This chapter will briefly review the incorporation of biomaterial scaffolds into cell transplantation approaches in order to improve cell survival, limit migration, and provide guidance to regenerating axons, but will ultimately focus on acellular biomaterial-based bridging strategies with combination therapy for synergistic improvement of neural regeneration.

BIOMATERIALS FOR NEURAL APPLICATIONS

Biomaterials used for bridging strategies may be classified into two main categories: natural materials, including ECM components and other natural polymers; and synthetic polymers . [28, 171].

Natural Materials

Table 3.1 is a summary of natural scaffold materials being investigated for neural applications.

MATERIAL	MOLECULES/SOURCE
ECM proteins	Collagen, fibronectin, laminin,
Proteoglycans	Permissive heparin sulfate proteoglycans (HSPGs) [182]
Glycosaminoglycans	Hyaluronic acid
Fibrinogen/fibrin gels	Blood clotting
Self-assembling peptide scaffolds	Various peptides [183]
Alginate	Brown algae (seaweed, giant kelp)
Agarose	Red algae or seaweed
Chitosan	Chitin/exoskeleton of crustaceans (shrimp, crabs) and insects, bacterial and fungal cell walls
Matrigel™	BD Biosciences

Table 3.1 Natural Polymers used for Neural Scaffolds [28, 171]

Type I collagen and laminin have proven to be useful molecules for spinal cord repair; however, fibronectin has not demonstrated significant promise. [171] Fibronectin in the CNS is associated with macrophages and endothelial cells and increased deposition has been found in active multiple sclerosis lesions [184], so it is not an ideal substrate for CNS repair. Matrigel™ is a commercially available hydrogel material generated from mouse Englebreth-Holm-Swarm (EHS) sarcoma that not only contains basement membrane components such as collagen, laminin, and proteoglycans; but also matrix degrading enzymes, their inhibitors, and growth factors. Alginate hydrogels and alginate hydrogels with fibronectin have been shown to possess less bioactivity than Matrigel in inducing proliferation of cultured cells, maintaining morphology, and inducing DRG neurite outgrowth. [185] Also, alginate is not strictly biodegradable; however, modification by crosslinking with calcium enables dissolution through calcium chelation,

and ultra purified sources of alginate must be used due to cytotoxic impurities present in commercial sources. [171]

Natural polymers are biodegradable because they form hydrogels that are susceptible to enzymatic degradation; however, this also limits their mechanical and design properties and they typically require some type of adhesive (e.g., fibrin glue) to hold them in place. Disadvantages of these materials include a lack of control over degradation rates, potential inconsistencies in material quality between different batches, and potential for microbe or virus contamination. [186] Chitosan purity is of utmost importance for those individuals with shellfish allergy due to the risk of anaphylactic shock.

Synthetic Materials

Synthetic biomaterials are currently under investigation for use in bridging strategies for spinal cord repair because of the ability to customize their chemical and physical properties, including degradation rate, porosity, and mechanical strength. For example, these materials can be designed to be tear resistant for ease in handling and gluing or suturing. Another advantage of synthetic biomaterials is the ability to fabricate them into virtually any design through a variety of polymer processing methods. Table 3.2 shows a summary of synthetic biomaterials being explored for use in nerve regeneration strategies.

POLYMER	ABBREV	DEGRADABLE	COMMENTS
Poly(glycolide)	PGA	Biodegradable	FDA approved
Poly(lactide)	PLA	Biodegradable	FDA approved
Poly(lactide-co-glycolide)	PLGA	Biodegradable	FDA approved
Poly(D,L-lactide)	PLLA	Biodegradable	FDA approved
Poly(caprolactone)	PCL	Biodegradable	
Biodegradable poly(urethane)		Biodegradable	
Poly(organo phosphazene)		Biodegradable	
Poly(ethylene glycol)	PEG	Biodegradable	FDA approved
Polycarbonate		Biodegradable	
Poly(3-hydroxybutyrate)		Biodegradable	
Poly(vinylidene fluoride)	PVDF	Nondegradable	Piezoelectric
Poly(pyrrole)	PPy	Biodegradable	Electrically conducting
Silicone		Nondegradable	FDA approved Inert, impermeable
Expanded Poly(tetrafluoroethylene)	ePTFE (Gore-Tex)	Nondegradable	Inert, impermeable
Poly(2-hydroxyethylmethacrylate)	PHEMA	Nondegradable	
Poly(2-hydroxyethylmethacrylate-co-methylmethacrylate)	PHEMA-MMA	Nondegradable	
Poly[N-(2-hydroxypropyl) methacrylamide	PHPMA	Nondegradable	
Poly(acrylonitrile-co-vinylchloride)	PAN/PVC	Nondegradable	

Table 3.2 Synthetic Polymers used for Neural Scaffolds [28, 171]

Silicone has been studied in research and clinical settings since the early 1960s; silicone and ePTFE are impermeable materials that limit nutrient and waste transport into and out of the scaffold and cell permeation of the scaffold. Although porous nondegradable materials have been developed, nondegradable materials used as implants traditionally pose a high risk of infection and chronic inflammation, and when used for

neural scaffolds, they cause chronic reactive gliosis and compression of regenerated nerves as they remyelinate [187, 188]; therefore, biodegradable materials are preferred. Tunable biodegradation is important not only to ensure that the material remains intact long enough for regeneration of axons through and out of the graft, but also to ensure that the material is sufficiently degraded before remyelination of axons occurs to avoid compressing the newly regenerated nerves.

DESIGN OF NEURAL SCAFFOLDS

Gels and Sponges

Gels and sponges have limited applicability in long-distance spinal cord regeneration therapies and are not suitable to provide guidance to regenerating axons; therefore, they will be briefly discussed. Gels are viscous, cross-linked liquids and are useful for filling small cavities such as cystic cavities formed from contusion injury or small gaps between transected nerves. For example, PEG fusiogens coupled with PEG hydrogels as a tissue adherent have been used to fuse severed nerve endings together to maintain continuity. [189] Sponges are porous structures with slightly higher mechanical strength that can fill a slightly wider defect than gels. *In situ* thermoreversible gelation of agarose gels has been used for simultaneous neurotrophin delivery and conformational repair of an irregular spinal cord defect, and supported adult rat neurite extension into the implant. [190] Collagen impregnated poly-2-hydroxyethyl methacrylate sponges implanted into complete adult spinal cord lesions limited cystic cavitation and enabled axon penetration into the sponge. [191]

Tubes and Fibers

Tubes and fibers are potentially the most appropriate scaffold for long-distance regeneration of axons because of their guidance capabilities. Figure 3.1 demonstrates some of the properties of such devices for nerve guidance that have demonstrated improvement of neurite outgrowth.

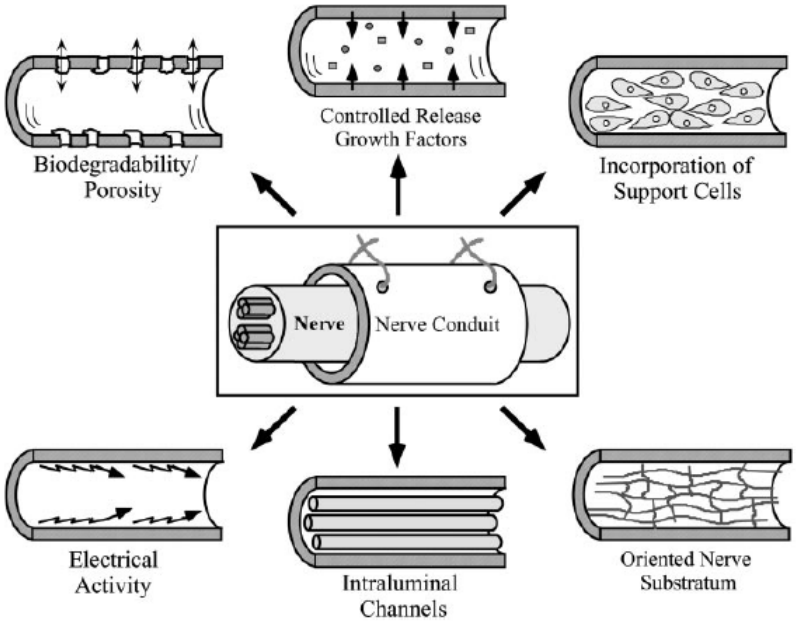

Figure 3.1 Desired Properties of Bridges for Nerve Guidance (Reprinted from Schmidt and Leach [28])

Electrical Activity

Electric fields (EFs) resembling those in the developing and regenerating nervous systems steer growth cones towards the cathode, and recent research is examining the role of galvanotactic mechanisms in neurite outgrowth and the specific signaling molecules involved. Growth cone steering by EFs has been shown to require dynamic

microtubules, microfilaments and regulation of filopodia and lamellipodia by the GTPases Cdc42 and Rac. [192] In bovine corneal epithelial cells, attenuation of Cdc42 signaling abolished galvanotaxis and enhanced contact guidance whereas attenuation of Rho signaling enhanced galvanotaxis and Rho stimulation enhanced contact guidance. [193, 194] These are the same molecules implicated in glial scar and myelin inhibition of neurite outgrowth, and the negative charge of glycosaminoglycans on sulfated proteoglycans may contribute to their inhibitory effect on neurite outgrowth. Cationic biopolymers such as chitosan have demonstrated longer neurite outgrowth than anionic biopolymers such as alginate. [195-197] Polypyrrole (PPy) is an electrically conducting polymer that has been shown to support neurite outgrowth through electrical stimulation of the membrane [198, 199] Poled PLGA tubes implanted into a 1 cm rat sciatic nerve gap demonstrated increased numbers of regenerated and myelinated axons as compared to unpoled tubes 4 weeks postlesion. [200]

Mechanical Properties

Mechanical properties are a somewhat overlooked design element for neural scaffolds, in part because the response of spinal cord tissue to mechanical loading is not well understood; however, recent studies are focused on characterizing the viscoelastic behavior of the spinal cord. [201-204] Although scaffolds must be designed to resist collapse upon implantation, materials that are significantly stiffer than the surrounding tissue may lead to necrosis and inflammation. [205]

Several groups have reported discrepancies in the values of elastic (Young's) modulus of the spinal cord using different measurement methods. The reported modulus

as measured in dogs and cats is estimated to be between 200-600 kPa; however, significant increases in modulus were found to occur quickly after death, making accurate measurement a difficult task. [206] Ozawa et al. reported that the spinal cord gray and white matter have similar moduli of elasticity as measured by the pipette aspiration method in rabbits. The axial direction of gray and white matter, respectively, measured 3.4 ± 1.4 kPa and 3.4 ± 0.9 kPa, the frontal section measured 3 ± 0.3 kPa and 3.5 ± 0.5 kPa, and the sagittal section measured 3.5 ± 0.9 kPa and 2.8 ± 0.4 kPa. [207] This same research group reported that rabbit spinal cord with intact pia mater has an elastic modulus of 2.3 MPa whereas the spinal cord parenchyma elastic modulus is approximately 5 kPa. [208] Bilston and Thibault reported that human spinal cords averaged 1.4MPa with the pia mater intact and 89 kPa with incised pia mater. [203] It is interesting to note that the elastic modulus of human tibial nerves has been reported to be 16 MPa, significantly higher than any of the reported values for the spinal cord. [209]

Although no consensus has been reached regarding the appropriate Young's modulus for neural scaffolds, reports have demonstrated improved adult rat axonal regeneration into poly(2-hydroxyethyl methacrylate-co-methyl methacrylate) [pHEMA-MMA] channels with elastic moduli of 263 kPa and 311 kPa as compared to 177 kPa. [210, 211] Peptide-modified poly(2-hydroxyethyl methacrylate-co-2-aminoethyl methacrylate) [pHEMA-co-AEMA] with elastic modulus of 192 kPa demonstrated chick DRG adhesion and neurite outgrowth comparable to PLL/laminin controls. [212]

Growth cone advance is thought to be mediated by forward propulsion as a result of filopodial contractions [213, 214], and the elastic modulus of scaffolds has been

demonstrated to impact neurite outgrowth. Hydrogels with increasing concentrations of PEG-diacrylate from 50 mg/mL to 200 mg/mL exhibited increasing elastic modulus but little change in ultimate tensile stress. Neurite extension from PC12 cells seeded on these hydrogels with equal concentrations of RGD peptides decreased as the elastic modulus increased, indicating that flexible materials with elastic modulus in the range of approximately 50-200 kPa may be more conducive to neurite outgrowth. [215]

Intraluminal Channels

Entubulation strategies are particularly useful for PNS repair as they mimic the ensheathed structure of the PNS, and they may hold promise for long-distance regeneration in the CNS because of the success of peripheral nerve implants for CNS repair. Degradable, hollow, large diameter conduits were first developed due to the ease of fabrication, but faced challenges of collapse upon implantation. [15, 216] Large diameter conduits also do not accurately mimic nerve architecture, and led to the idea of filling large diameter hollow conduits filled with smaller hollow conduits, not only reduce the susceptibility of collapse but provide more surface area for cell and growth cone attachment. Implantation of poly(2-hydroxyethyl methacrylate-co-methyl methacrylate) [pHEMA-MMA] channels with 4.19±0.04 mm outer diameter encasing 4 smaller tubes with 790±45 μm inner diameter into adult rat complete spinal cord transections at T8 (4 mm gap) improved regeneration of vestibular neurons and showed consistent improvement in locomotor function at 7 and 8 weeks. [210, 211]

In order to design conduits with appropriately sized channels for neural regeneration, consideration of cell and nerve fiber diameters must be taken into account.

Mammalian cells typically range from 10-100 µm in diameter and Table 3.3 shows the diameters of various mammalian nerves. [217]

MYELINATION?	FIBER TYPE	FUNCTION	DIAMETER (µm)
Myelinated	A - α	Proprioception; somatic motor	15-20
Myelinated	A - β	Touch, pressure	5-12
Myelinated	A - γ	Motor to muscle spindles	3-6
Myelinated	A - δ	Pain, temperature, touch	2-5
Myelinated	B - Autonomic	Preganglionic autonomic	<3
Unmyelinated	C - Dorsal root	Pain, reflex responses	0.4-1.2
Unmyelinated	C - Sympathetic	Post ganglionic sympathetics	0.3-1.3

Table 3.3 Mammalian Nerve Fiber Types [217]

Because of the difficulty in fabricating conduits with small diameter linear channels [212, 218, 219], an alternative entubulation approach involves filling guidance channels with filaments to produce small diameter channels to more accurately mimic nerve fiber diameters. Guidance channels developed for PNS repair with 16 PLLA microfilaments within each PLA or silicone tube (1.5 mm inner diameter) were filled with Matrigel, implanted into 14 mm and 18 mm rat sciatic nerve lesions, and at 6 weeks postlesion, improved Schwann cell migration and regenerated nerves across the gap could be seen in all animals with microfilament-filled tubes, as compared to reduced efficiency of nerve formation in tubes without microfilaments. [220] In addition, more axons were demonstrated to penetrate PLA tubes due to the porosity of PLA as compared to nonporous silicone tubes, thus highlighting the importance of nutrient and waste transfer

for neural regeneration. PLA tubes of 1.5 mm diameter filled with PLLA microfilaments of 60-70 µm diameter administered to 6 mm rat dorsal root lesion along with spinal NGF virus injection demonstrated recovery of function to almost normal levels at 7-8 weeks postlesion; cutting the dorsal root through the center of the conduit reversed the recovery, thus demonstrating regeneration through the conduit was responsible for restoration of function. [221]

Poly(acrylonitrile-co-vinyl chloride) [PAN/PVC] hollow fiber membranes (HFMs) with 900 µm inner diameter were filled with polypropylene filaments with smooth inner surface of supracellular size (500 µm to 100 µm), cellular size (30 µm), and subcellular size (5 µm) and were seeded with DRG explants for 7 days; neurite outgrowth on 500 µm filaments was organized into fascicles, and defasciculation and increasingly uniform linear alignment of Schwann cells and neurites was demonstrated as filament size decreased to 5 µm, with corresponding improvement in length of the neurites. [222] HFMs were also developed using PLGA and polyurethane with the incorporation of aligned grooves on the inner surface of the filaments. [223, 224]

Fibers offer an alternative to filament-filled conduits. Poly(l-lactide) (PLA) and polyethylene terephthalate (PET) capillary channel fibers (CCFs) containing eight open grooves with depth of 5-15 µm and width of 10 µm oriented rat skin fibroblast and aortic smooth muscle cell alignment and deposition of ECM proteins within the grooves parallel to groove direction; the alignment and fluid wicking capabilities of these fibers make them a potentially useful scaffold for nerve guidance strategies. [225, 226] In addition,

the size of the fiber grooves is customizable and the variety of groove sizes on each fiber may enable regeneration of multiple motor and sensory axons.

BIOMATERIAL SCAFFOLDS FOR CELL TRANSPLANTATION

Many biomaterial approaches have been investigated to improve Schwann cell survival and limit migration while also improving regeneration. PLGA foam conduits for peripheral nerve repair were created by a low-pressure injection molding technique producing aligned channels with diameters ranging from 60-550 µm; conduits coated with laminin and seeded with Schwann cells were implanted across a rat 7 mm sciatic nerve gap and demonstrated comparable neurite outgrowth to implanted autografts at 6 weeks postlesion. [227] Although this approach may be useful for peripheral nerve repair, there is less evidence supporting its use in CNS repair.

Freeze-dried PLA macroporous scaffolds with channel diameters of 75-200 µm seeded with Schwann cells in fibrin solution were implanted into 4 mm rat transections; Schwann cells underwent apoptosis by 1 week post-implantation and at 6 weeks, myelinated axons were found within the graft but none exited into the caudal spinal cord, probably attributable to the limited survival of the Schwann cells. [17] Xu et al. reported survival of Schwann cells in 3.0 mm long PAN/PVC guidance channels beyond 30 days following implantation into adult rat spinal cord with limited migration for short distances into rostral and caudal host spinal cord; however, limited extension of axons beyond the distal graft-host interface was observed at 90 days. [16] Porous PLGA scaffolds were created by injection molding followed by rapid solvent evaporation with

channel diameters of 450±9 µm and 600±10 µm and were seeded with Schwann œlls suspended in Matrigel; histological analysis of the channels one month after implantation into rat spinal cord injury revealed a centralized core of axons and capillaries surrounded by fibrous tissue and macrophages. [228]

Schwann cells are not native to the CNS and lead to unfavorable interactions with astrocytes leading to increased inhibitory CSPG production and the astroglial response. [146] Although several groups are studying *ex vivo* genetic modification of Schwann cells in order to overcome these challenges, acellular biomaterial-based bridges with combination therapies offers an alternative approach to avoid the immune complications and glial scarring response inherent to PNS glial cell transplantation in the CNS while still delivering the bioactive soluble and adhesive molecules produced by these glial cells. A major advantage of the acellular approach is the ability to provide controlled presentation of bioactive stimuli through controlled release, gene therapy, and recombinant protein immobilization.

ACELLULAR SYNTHETIC BIOMATERIAL BRIDGES

Neurite outgrowth is dependent upon a delicate balance of chemotactic, haptotactic, and contact guidance cues, and careful consideration of specific combinations of molecules must be made depending upon which axon tracts are to be regenerated. [12] Bridges must also be designed to promote axon growth into and through the scaffold via continued availability of active biomolecules, to be selective for

axons while inhibiting attachment of other cells, and to promote axon growth out of the bridge into the inhibitory host environment. [18]

Bioactive Stimuli for Combination Therapies

During PNS development and following injury, Schwann cells increase their synthesis of surface cell adhesion molecules (CAMs), such as NCAM, NgCAM, and L1; they secrete extracellular matrix (ECM) molecules such as collagen, laminin, fibronectin, and tenascin; and they produce and spatially present neurotrophic factors such as nerve growth factor (NGF), neurotrophin 3 (NT-3), neurotrophin 4/5 (NT-4/5), brain-derived neurotrophic factor (BDNF), ciliary neurotrophic factor (CNTF), glial-cell derived neurotrophic factor (GDNF), and acidic and basic fibroblast growth factor (aFGF, bFGF). [26, 28]

Adhesion Molecules

The extracellular matrix (ECM) protein laminin and the L1 neural cell adhesion molecule (NCAM) are of particular interest for spinal cord regeneration strategies because of their significant contributions during CNS development.

Laminin

Laminin is a protein that is abundantly expressed by immature astrocytes in the developing CNS [76] and by Schwann cells in the developing and regenerating PNS [26], making it an attractive candidate for use in combination therapies. Deister et al. demonstrated that laminin concentration had the most impact on neurite extension from explanted dorsal root ganglia cultured within co-gels made from laminin, fibronectin,

collagen I, and hyaluronic acid and that the combinatorial effects were additive rather than synergistic, suggesting that the presence of laminin rather than interactions among the extracellular matrix components is key for neurite outgrowth. [229]

Laminin is a large 900 kDa protein with at least 15 different types in mammals and structurally it is an αβγ trimer, with each trimer containing binding sites for predominantly integrins. Human diseases caused by genetic mutations in laminin proteins give some insight into their importance in proper nervous system development and function. Deficiencies in laminin α2 chains result in abnormal radial sorting of PNS axons to be myelinated by Schwann cells and abnormal myelin thickness and length, resulting in congenital muscular dystrophy (MDC) 1A; CNS white matter tracts in patients with MDC1A also demonstrate abnormal myelination, demonstrating the importance of laminin to CNS oligodendrocytes. [230] In addition, oligodendrocytes in knockout mice lacking the laminin integrin receptor α6β1 have reduced survival rates, and laminin-receptor signalling selectively enhances the survival of mature oligodendrocytes, not oligodendrocyte precursor cells (OPCs); however, Schwann cells lacking the β1 receptor proliferate and survive normally but fail to sort and myelinate axons.[230] Laminin has also been shown to enhance the migration, expansion, differentiation, and elongation of neurites in both mouse and human neural stem cells as compared to poly-L-orthinine, fibronectin, and Matrigel through integrin receptors α3, α6, α7, β1, and β4. [231] Mouse neural stem cells from the ventricular zone express high levels of laminin integrin receptor α6β1. [232]

Peptides are short, linear amino acid sequences that are useful for bridging strategies because of their small size and more specific cell interactions; however, they may not reproduce the bioactivity of the entire protein. [18]. Although laminin is an ideal substrate for many different cell types because it is a ubiquitous constituent of basement membranes, it is this lack of specificity that makes it less than ideal for neural regeneration strategies, in particular because it does not inhibit astrocyte interactions. Laminin contains at least two peptide sequences that are not favorable for astrocyte interactions and bind integrin receptors on neuronal cells: Isoleucine-Lysine-Valine-Alanine-Valine (IKVAV), an α1 chain peptide sequence that promotes adhesion and neurite outgrowth of some neuronal cell types; and Tyrosine-Isoleucine-Glycine-Serine-Arginine (YIGSR), a β1 chain peptide sequence that promotes neuronal attachment but does not necessarily promote neurite outgrowth. [233]

Numerous applications of these laminin peptide sequences have been used to characterize neural cell attachment and neurite outgrowth of cell lines, including pheochromocytoma cells (PC12) that develop properties of sympathetic neurons in the presence of nerve growth factor (NGF) and neuroblastoma tumor cells derived from the sympathetic nervous system, as well as primary chick and rat dorsal root ganglia (DRG) neurons. IKVAV and YIGSR sequences covalently immobilized to fluorinated ethylene propylene (FP) films mediated localized PC12 and NG108-15 neuroblastoma cell attachment and neurite outgrowth to patterned pathways [234, 235]; improved neurite outgrowth, cell adhesion and viability of rat embryonic day 18 hippocampal neurons [236] The neurite outgrowth of chick dorsal root ganglia on expanded

poly(tetrafluoroethylene) fibers was enhanced with IKVAV and YIGSR peptides and the optimal fiber diameter for guidance was 30-50 μm. [237]

Gunn and Turner examined PC12 response to PEG-diacrylate hydrogels with IKVAV and YIGSR peptides and found that neurites extended in response to IKVAV-conjugated gels but only attached without neurite extension to YIGSR-conjugated gels. [215] Copolymerized 2-hydroxylethyl methacrylate (HEMA) and 2-aminoethyl methacrylate (AEMA) gels (P(HEMA-co-AEMA) scaffolds) with covalently bound YIGSR and IKVAV were fabricated in aqueous conditions, thus avoiding organic solvent use, and demonstrated enhanced neural cell adhesion and guided neurite outgrowth of chick dorsal root ganglia neurons. [212]

L1 Neural Cell Adhesion Molecule

L1 is a key player in the overall development of both the CNS and PNS and functions in neuronal adhesion and migration; axon growth, guidance, and fasciculation; as well as target selection, synapse formation, plasticity, survival, and myelination. [238-243] L1 is also expressed by Schwann cells of the peripheral nervous system. [244]

L1 is a 220 kDa vertebrate neural cell adhesion molecule belonging to the L1 subfamily of the immunoglobulin superfamily (IgSF), with members sharing a common structure of six immunoglobulin (Ig) domains followed by three to five fibronectin type III (FNIII) repeats. [245] Genetic deletions or mutations of the L1 gene result in severe, sometimes lethal, neurological deficits in humans and defects in the corticospinal tract and corpus callosum of L1 knockout mice. [246-249] There is also evidence that injury induces reexpression of L1, as three months following complete spinal cord transection in

neonate rats, L1 expression remained substantially increased surrounding the lesion site and L1 was reexpressed on descending fibers of the corticospinal tract above the lesion. [250]

Several *in vitro* and *in vivo* experiments have demonstrated the value of L1 in spinal cord regeneration strategies, in both soluble and substrate-bound forms. Rat cerebellar neurons on PLL extended longer neurites in response to soluble L1-Fc as compared to controls, and the response was inhibited by pretreatment of the neurons with antibodies to L1 or fibroblast growth factor (FGF) receptor. [251] L1 attached to a nitrocellulose membrane stimulated chick tecta and mouse cerebellum neurite outgrowth while inhibiting astrocyte, oligodendrocyte and fibroblast attachment. [252] Reduced L1-Fc immobilized to polystyrene surfaces through Pluronic-pyridyl disulfide (F108-PDS) modification supported significantly higher levels of rat dorsal root ganglia, cerebellar, and hippocampal neurite outgrowth relative to fibronectin and PDL, while inhibiting the attachment of astrocytes, meningeal cells, and fibroblasts. [253] Oliva et al. micropatterned the chimeric protein L1-Fc, consisting of the ectodomain of L1 linked to the Fc fragment of immunoglobulin G (IgG), onto poly-L-lysine coated glass by microcontact printing of bacterial protein A, which binds the Fc fragment, and demonstrated preferential growth of embryonic rat hippocampal axons into the L1-Fc patterned regions. [254] Poly(glycolide) (PGA)-chitosan conduits coated with recombinant L1-Fc implanted into adult rats following optic nerve transection exhibited higher numbers of regenerated fibers and a significant increase in myelination of the

regenerated fibers as compared to PGA-chitosan conduits alone. [255] These studies suggest the usefulness of L1 in both controlled release and immobilized strategies.

Neurotrophic Factors

Neurotrophic factors are key nervous system regulatory proteins that modulate neuronal survival, axonal growth, synaptic plasticity, and neurotransmission. They have also been shown to promote and direct growth cone motility [112]; they exhibit a chemotactic effect for axon guidance, and they aid in sensory nerve growth across the PNS-CNS transition zone. As a result, their role in axon development and regeneration is being studied extensively for application in spinal cord repair [28, 94, 113-115].

Diffusion and Controlled Release from Biomaterials

Porous PLG single and multiple lumen conduits were created utilizing porogen (NaCl) and a gas foaming technique, and NGF was incorporated either by mixing with PLG microspheres prior to gas foaming or by encapsulating into the microspheres; sustained release of NGF from the scaffolds was demonstrated for 42 days and could be controlled by the method of incorporation and polymer molecular weight. [256]

The network crosslinking density of photopolymerized acrylated PLA-b-PEG-b-PLA hydrogels was utilized to control release rates of CNTF, BDNF, and NT-3 with total release times reported as ranging from weeks to several months, and simultaneous delivery of multiple neurotrophins was developed by mixing microspheres of NT-3 encapsulated in poly(lactide-co-glycolide) using a double emulsion technique into the hydrogel solution containing CNTF and photopolymerizing to produce constructs containing NT-3 in the microsphere phase and CNTF in the hydrogel phase; the release

profiles show very rapid release of the neurotrophin in the hydrogel phase and a slow continuous release from the degradable microspheres. [257]

Controlled release of BSA from photopolymerized PEG hydrogels has been demonstrated using the metal chelating ligand iminodiacetic acid (IDA) to reversibly bind BSA in the presence of Cu^{2+} ions as well as protect the protein from free radicals produced during photopolymerization [258, 259]; these methods may be useful for application in controlled release of polyhistidine-tagged neurotrophic factors.

Immobilization to Biomaterials

MacInnis and Campenot [260] reported that a neuronal survival signal can reach the cell bodies unaccompanied by the NGF that initiated it. The discovery that growth factors do not have to be internalized by the cell body in order to promote survival opened the door for research into immobilized growth factors. Neurotrophins have a very short half-life and immobilization is one method to provide a high concentration of long-term, localized growth factor delivery to an injury site by preventing degradation, clearance, or internalization of the neurotrophins.

Kapur and Shoichet [261] immobilized NGF concentration gradients within poly(2-hydroxyethyl-methacrylate) [pHEMA] microporous gels using a modified, commercially-available gradient maker (CBS Scientific, Temecula CA). PHEMA was chosen because its material properties are good for soft tissue engineering, it has been used clinically, and NGF has been stably encapsulated in it for other applications; it was also modified with poly(allyamine) [pAA] to make it cell adhesive. In this research, gradient stability, immobilized NGF bioactivity, and axon extension of

pheochromocytoma (PC12) cells to the immobilized NGF gradients were tested. Their results showed that PC12 cells adhere to the pHEMA-NGF-pAA gels, and respond to immobilized NGF by extending neurites in a manner similar to previous research with soluble NGF. [262, 263] It was observed that PC12 neurites were thicker when cultured on immobilized NGF than when cultured in the presence of soluble NGF.

Review of Combination Therapies

It is likely that combinations of therapies with synergistic effects will be required for long-distance regeneration of axons. Review of combination strategies that have been tested gives some insight into the responses that may be expected from different combinations of growth-promoting stimuli. Combinations of neural cell adhesion molecules L1 and neurofascin and growth and differentiation-5 factor (GDF-5) demonstrated synergistic effects on neurite outgrowth of embryonic chick dorsal root ganglia (DRG) neurons. [264] Chick embryonic DRG cultured in anisotropic three-dimensional (3D) agarose scaffolds with photoimmobilized gradients of laminin exhibited maximal neurite extension as compared to isotropic scaffolds with uniform distribution of laminin [265]; these anisotropic agarose scaffolds with gradients of laminin and nerve growth factor (NGF) exhibited comparable regeneration to peripheral nerve grafts across a 20 mm sciatic nerve gap in rats. [266]. Semipermeable polysulfone tubes with laminin and nerve growth factor (NGF) demonstrated comparable regeneration, myelination, and functional recovery as compared to autologous peripheral

nerve grafts two months after implantation into a 10 mm sciatic nerve gap in adult rats. [267]

CONCLUSION

A synergistic combination of pharmaceutical interventions and therapeutic approaches to spinal cord injury will likely be required to overcome the multitude of factors contributing to CNS regenerative failure and to ultimately achieve functional regeneration. This research is focused on the development of acellular synthethic biomaterial-based bridges because of the flexibility in design and fabrication of scaffold properties coupled with the ability to use different combinations of bioactive adhesive and soluble stimuli suitable for regeneration of a wide variety of neural populations.

CHAPTER FOUR

PROJECT RATIONALE

INTRODUCTION

The human spinal cord is approximately 45 cm long (1.5 ft) with 30 levels, and each spinal level is around 1-2 cm. [14] The most common injury level for a tetraplegic is C5, thus requiring regeneration over 25 levels, or approximately 25-50 cm, for complete restoration of white matter axon tracts. The most common injury level for a paraplegic is T12, requiring regeneration over 10 levels, or approximately 10-20 cm. In 1981, David and Aguayo reported axonal elongation of 3 cm into autologous peripheral nerve "bridges" between the medulla and spinal cord in adult rats. [268] The maximum length to date of CNS regeneration demonstrated in animal models is around 4 cm, with most studies demonstrating only 1-2 cm of regrowth. [154, 269] This fact emphasizes the need for better combinations of therapies with synergistic effects for long-distance regeneration of axons.

RATIONALE FOR BIOACTIVE BIOMATERIAL-BASED APPROACH

The long-term objective of this project is a biomimetic, multi-factorial approach utilizing grooved fibers to restore structure and provide guidance for regenerating axons coupled with bioactive adhesive molecule delivery via immobilization to a hydrogel within the fiber grooves and controlled release of neurotrophic factors from the hydrogel (Figure 4.1).

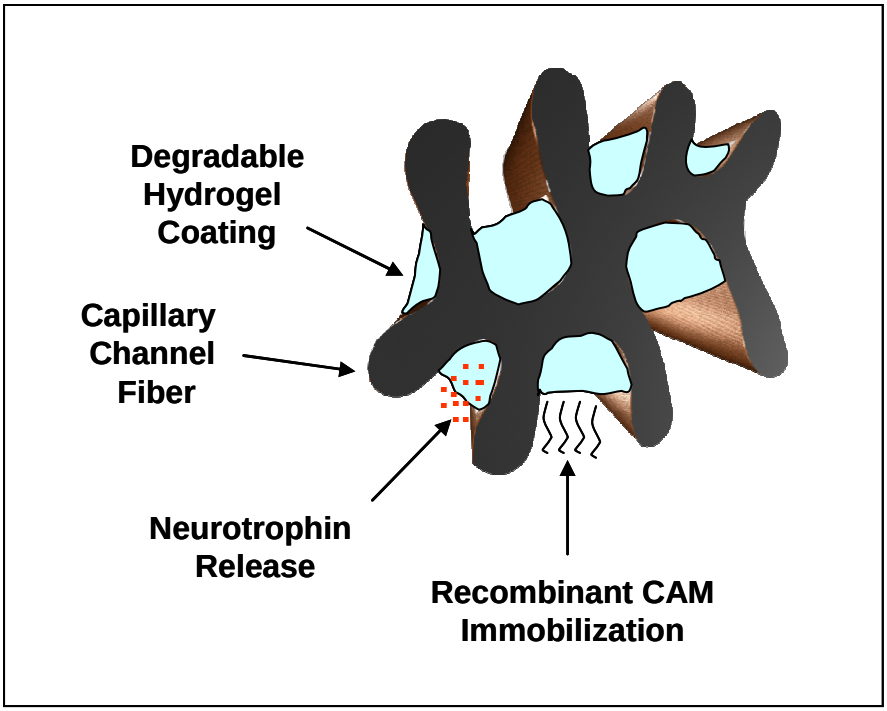

Figure 4.1 Proposed Implant Design

A major obstacle of all implant-based bridging techniques is the invasive nature of implantation and stimulation of the astroglial response; however, a unique advantage of this proposed fiber implant is the possibility to reroute regenerating axons around an existing glial scar through the use of specialized surgical techniques that are currently being used for peripheral nerve grafts [270, 271], and perhaps incorporation of a complementary strategy to modify the inhibitory environment, using Chondroitinase-ABC or Rho antagonist, or to modify growth cone signaling pathways, will minimize the resultant astroglial response from implantation. [272, 273]

Synthetic degradable materials are potentially ideal for neural regeneration strategies, because tunable biodegradation enables the design of an implant that will support axonal regeneration through and out of the graft but degrade prior to axon remyelination to avoid compression of newly regenerated nerves.

Fibers are potentially ideal scaffolds to provide guidance for long-distance regeneration of axons, and the proposed PLA capillary channel fibers (CCFs) contain eight open grooves of adjustable depths and widths and have demonstrated orientation of rat skin fibroblast and aortic smooth muscle cell alignment and deposition of ECM proteins within the grooves parallel to the groove direction. [225, 226]

Bioactivity will be incorporated by delivery of adhesion ligands and neurotrophic factors from a hydrogel coating within the fiber grooves, to mimic the bioactivity that peripheral nerve implants have demonstrated in CNS regeneration. L1 is a particularly attractive candidate for neural regeneration because it is critical for proper nervous system development; genetic deletions or mutations of the L1 gene result in severe, sometimes lethal, neurological deficits in humans, including hypoplasia of the corticospinal tract [248, 249], and injury induces reexpression of L1 in the corticospinal tract. [250] Recombinant human L1 has been shown to be a potent promoter of neurite outgrowth in both soluble and substrate-bound forms, to support selective neuronal adhesion in the presence of astrocytes when coupled to low-protein binding supports, and to function as a neuronal survival factor. [239, 253] The selectivity of neuronal adhesion to L1 in the presence of astrocytes is particulary important, as astrocytes are the key players in nervous system inflammation and mediate the glial scar response. All six

immunoglobulin domains of L1 have been shown to be required for full bioactivity [274]; therefore, based on the increased number and distribution of bioactive regions in L1, selection of an appropriate immobilization chemistry is likely to be critical for full retention of bioactivity.

Neurotrophic factors have a very short half-life, are digested in the gastrointestinal tract, do not pass the blood-brain barrier, and are rapidly cleared from cerebrospinal fluid (CSF); as a result, oral, systemic, or intrathecal delivery will not promote regeneration of CNS neurons and may result in hyperalgesia or other unwanted side effects due to nonspecific delivery. [117] Controlled release of neurotrophins from the proposed implant has the potential to provide biologically relevant amounts of long-term, localized growth factors at the site of injury while avoiding unwanted side effects. NT-3 is an attractive candidate for regeneration of corticospinal tract neurons, a major motor axon tract with limited intrinsic regenerative potential. [77, 118]

RATIONALE FOR HYDROGEL FABRICATION AND PROTEIN IMMOBILIZATION APPROACHES

Tetronic® 904 (T904, BASF) is a tetrafunctional poly(ethylene oxide) – poly(propylene oxide), PEO/PPO, block copolymer that is a nonionic surfactant terminating in primary hydroxyl groups. Selected Pluronics® and Tetronics® are commonly used in contact lens cleaning solutions and mouthwash, and are unique surfactants that are resistant to protein adsorption, have low cytotoxicity, and elicit a reduced immune response. Modified Pluronic® surfactants have been utilized to immobilize histidine-tagged proteins [275], and fibronectin and L1-Fc. [253, 276]

Tetronics® (poloxamines) were chosen over linear Pluronics® (poloxamers) because their four-arm, or star-shaped, structure contains more and shorter side chains as compared to linear block copolymers with similar molecular weight, thus allowing for increased functionality and higher degree of crosslinking with lower polymer concentrations, with single hydrolytically degradable ester bonds at each end. [277] In addition, control over swelling and protein release has been demonstrated with multi-arm PEG acrylates. [278]

Michael addition polymerization using acrylated polymers is an established method of hydrogel fabrication in the absence of ultraviolet (UV) light [278-280] and may also be used in protein immobilization strategies. [281-287] A long-term goal of this project is to polymerize T904-acrylate hydrogels within the capillary channel fiber grooves, and Michael addition polymerization may enable more uniform and complete polymerization within the grooves than is attainable with photopolymerization. The fiber grooves also exhibit capillary-like properties that may be used for uptake of hydrogel solutions. Another long-term goal of this project is controlled release of neurotrophins from the hydrogels, and Michael addition polymerization avoids potential damage to the protein structure from excessive heat that may occur with photopolymerization.

ADVANTAGES OF PROPOSED IMPLANT DESIGN

Biomaterial-based approaches to spinal cord repair are missing from clinical trials in large part because of the limited approval of devices incorporating biomaterials by the U.S. Food and Drug Administration (FDA). Approval of a device with novel materials is costly and requires additional documentation associated with manufacture, quality

control, durability and safety; however, PLA has been FDA-approved and is being studied for neural applications, and Pluronics® and Tetronics® are under investigation for drug delivery applications. [216, 288-290] Entubulation strategies face challenges of channel collapse and obstruction of nerve regeneration, and the difficulty in fabricating conduits with small diameter linear channels [212, 218, 219] led to an alternative entubulation approach of filling guidance channels with filaments to produce small diameter channels. The proposed fiber implant does not require entubulation, and the open channel design allows for unlimited transport of nutrients and waste.

The hydrophobicity of PLA not only negatively impacts cell adhesion to the surface, but also favors protein adsorption that is detrimental to efforts to incorporate bioactivity into biomaterials through covalent protein immobilization. PLA hydrophilicity has been improved through methods such as copolymerization with PEG, which required solvents and high temperatures not suitable for encapsulation of proteins; surface chemical modification via alkali treatment, which increased PLA bulk degradation rate; and plasma treatment, which demonstrated instability of the surface layer. [291] Otsuka et al. demonstrated surface functionalization of PLA via spin coating of acetal-PEG/PLA block copolymers in toluene. [292] Surface coating of PLA with T904-acrylate takes advantage of the hydrophobic interaction of the Tetronic PPO blocks and PLA to enable a functionalized hydrophilic PEG surface that more closely mimics the viscoelastic properties of neural tissue. The simplicity in manufacturing grooved PLA fibers via a melt-spin process (US Patent 1990, 4,954,398), coupled with capillary uptake of a hydrogel coating crosslinked in the absence of solvents and ultraviolet light

via Michael addition, make this a novel approach for application in neural regeneration strategies. In addition, the implant design lends itself to lyophilization, making it suitable for long-term storage. The ability to customize scaffold properties and incorporate different combinations of adhesive stimuli and growth factors, and the simplicity in manufacturing and long-term storage ability, maximizes the potential of this approach to provide readily available, "off-the-shelf" implants for patients with any type of nerve injury.

RESEARCH OBJECTIVES

Because neurotrophic factors are not sufficient for growth cone or cell adhesion to a biologically inert material, this research focused on covalent immobilization of the cell adhesion molecule L1 to acrylated Tetronic® hydrogels for neurite outgrowth with future plans of neurotrophic factor incorporation to further enhance survival and regeneration rates. The objectives of this research were: (1) cloning and expression of a bioactive 140kDa fragment of L1 neural cell adhesion molecule, chosen for its critical role in proper nervous system development and because it has demonstrated selectivity of neuron adhesion in the presence of astrocytes, which play a major role in nervous system inflammation, (2) synthesis and purification of acrylated Tetronic macromers and the development of Michael addition methods for hydrogel crosslinking and protein immobilization, (3) evaluation of hydrogel cytocompatibility, immobilized protein bioactivity, and immobilization efficiency in terms of cell spreading and proliferation using NIH 3T3 fibroblasts and fibronectin because of the well-known RGD-dependent

interaction, to demonstrate the feasibility of this system for neural repair, and (4) assessment of neuronal cell line and primary neuron response to L1, evaluation of the cytocompatibility of T904-acrylate hydrogels with neural cells, and development of immobilization methods for L1.

CHAPTER FIVE

CLONING AND EXPRESSION OF RECOMBINANT L1

INTRODUCTION

L1 is a vertebrate neural cell adhesion molecule belonging to the L1 subfamily of the immunoglobulin superfamily (IgSF), with members sharing a common structure of six immunoglobulin (Ig) domains followed by three to five fibronectin type III (FNIII) repeats. [245] The L1 subfamily is also comprised of the vertebrate members neurofascin, NrCAM and CHL1 and the invertebrate members neuroglian and tractin. [293] L1 is a transmembrane glycoprotein consisting of six Ig domains, five FNIII repeats, a transmembrane region, and a highly conserved cytoplasmic domain. [241, 294, 295] Unglycosylated L1 has a molecular weight of 140-150 kDa, with 21 N-glycosylation sites on the extracellular portion of the protein, resulting in a 200-220 kDa protein depending upon how many residues are glycosylated. [296] L1 also contains two proteolytic cleavage sites: plasmin-mediated cleavage in the third fibronectin repeat resulting in an approximate 140 kDa soluble form of L1, and ectodomain cleavage via the metalloprotease ADAM10 resulting in an approximate 200 kDa soluble form of L1. [297-300] Figure 5.1 depicts the structure of the L1 protein. [241]

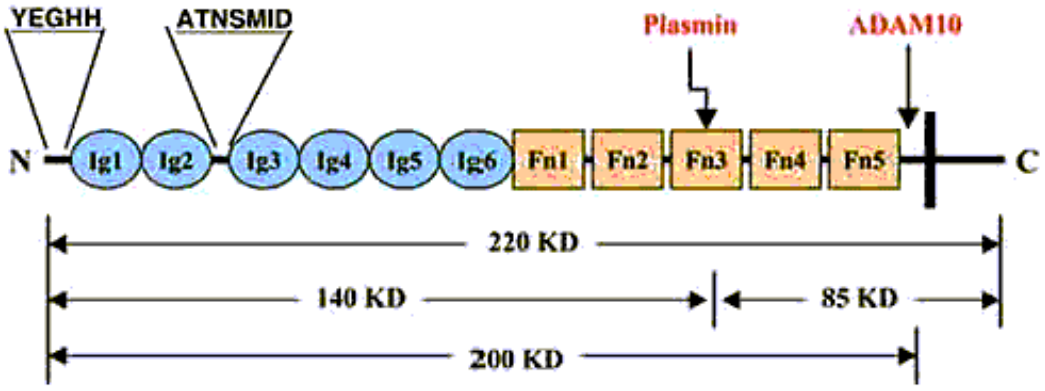

Figure 5.1 Structure of L1
(Reprinted from Haspel and Grumet 2003[241])

L1 is primarily expressed on the surface of neurons and is concentrated in growth cones and axons during development. L1 functions in neuronal adhesion and migration; axon growth, guidance, and fasciculation; as well as target selection, synapse formation, plasticity, survival, and myelination. [238-241] It is also expressed by Schwann cells of the peripheral nervous system, a subclass of leukocytes, intestinal crypt cells, and kidney tubule epithelia [244]; however, L1 expressed by neurons and glia includes an alternatively spliced YEGHH sequence at the N-terminus encoded by exon 2. [301] The 140 and 200 kDa L1 cleavage fragments have been detected in developing rat brain, cerebrospinal fluid (CSF), and the extracellular matrix. [302-304] L1 is capable of interacting with multiple extracellular and intracellular binding partners. The extracellular region may exhibit homophilic binding with L1 on the surface of other cells or soluble L1 or heterophilic binding with other neural cell adhesion molecules, integrins, extracellular matrix constituents (laminin, phosphacan, neurocan), or signaling receptors.

[241, 305] The cytoplasmic region interacts with the actin cytoskeleton via an ankyrin linkage. [306] Homophilic interaction of L1 is closely linked to its ability to induce neurites in culture [305] and the cytoplasmic domain is not required for homophilic adhesion. [307]

Genetic deletions or mutations of the L1 gene result in severe, sometimes lethal, neurological deficits in humans, including X-linked hydrocephalus, mental retardation, aphasia, shuffling gait, adducted thumbs (MASA) syndrome, spastic paraplegia type I, and X-linked mental retardation. [246, 247] L1 mutant mice exhibit defects in the corticospinal tract and corpus callosum. [248, 249] L1 is a key player in the overall development of both the central and peripheral nervous systems, making it an attractive candidate for promoting neural regeneration. L1 expressed ectopically by mouse astrocytes was shown to enhance neurite outgrowth on both astrocyte monolayer cultures and on optic nerve cryosections derived from the transgenic mice; this increase in outgrowth was inhibited by polyclonal L1 antibodies. [308] Purified full-length and recombinant L1 containing the entire extracellular region have been shown to stimulate neurite outgrowth in both soluble and substrate-bound forms. [252, 309] Neurites induced by L1 *in vitro* were 2-3 times longer than those cultured on poly(ethyleneimine), although stronger neurite-promoting activity was shown on laminin. [309]. However, substrate-bound L1 has been shown to selectively support the adhesion of CNS-derived neurons in the presence of astrocytes, meningeal cells, and fibroblasts. [253] Significant axonal regeneration was observed in a hemisection lesion of rat spinal cord two weeks following transplantation of fibroblasts genetically modified to produce L1. [310]

Soluble L1-Fc administered intrathecally to rat spinal cords following contusion injury promoted locomoter recovery. [311]

Production of recombinant L1 has been described in both mammalian and bacterial systems, although bioactive, bacterially-derived L1 is not glycosylated, and there has been debate regarding its mechanism of action. Studies using bacterially-derived L1 have shown that the Ig2 domain is necessary and sufficient for homophilic binding. [312] Studies of mammalian-derived L1 have shown that Ig domains 1-6 reproduce the full biological activity of the entire L1 extracellular region, while Ig domains 1-4 are the minimum regions necessary for homophilic binding. [274] Haspel and Grumet theorized that these differences may be the result of non-authentic homophilic interactions that can be generated in isolated Ig domains as a result of nonnative folding pathways in bacterial systems. [241] Insect-cell expression systems offer several potential advantages for the production of recombinant neural cell adhesion molecules, including generally higher yield relative to mammalian systems and improved posttranslational modification and glycosylation relative to bacterial systems. A recent study described stable expression of the complete L1 extracellular domain and an Ig5-6 fragment in Sf9 cells and demonstrated the neurite outgrowth promoting bioactivity of both proteins using NT2N neurons derived from the NT2 human embryonic carcinoma cell line. [313] The objective of this study was to express the L1 140 KDa physiological cleavage fragment in the baculovirus expression system and to evaluate its neurite outgrowth-promoting bioactivity relative to commercially available mammalian-derived L1-Fc in primary cultures of central nervous system neurons. A C-terminal 6X histidine

tag was incorporated for purification and as a basis for oriented immobilization to biomaterial surfaces for neural regeneration applications.

MATERIALS AND METHODS

Figure 5.2 is a brief summary of the materials and methods used to produce and evaluate the bioactivity of insect-cell derived L1.

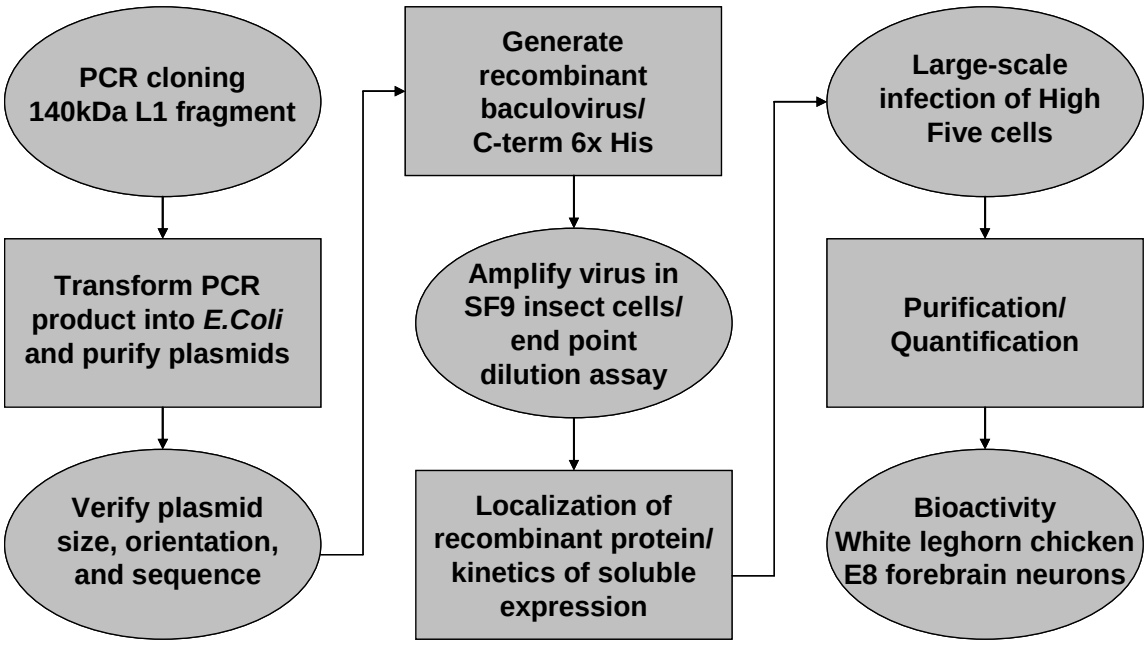

Figure 5.2 Materials and Methods Flowchart

Insect Cell Culture

Sf9 cells (S*podoptera frugiperda*) were purchased from Invitrogen and routinely maintained at 27°C in Sf-900 II Serum-Free Medium (Gibco) supplemented with 25

I.U./mL penicillin and 25 µg/mL streptomycin of penicillin-streptomycin (Mediatech). High Five™ cells (*Trichopulsia ni*) were a gift from Dr. Mark Kindy (MUSC, Charleston, SC) and were routinely maintained at 27°C in Express Five® Serum-Free Medium (Gibco) supplemented with 25 I.U./mL penicillin and 25 µg/mL streptomycin (Mediatech) and 90 µL/mL of 200 mM L-glutamine (Hyclone).

PCR Cloning of the L1 Extracellular Fragment

Freeze-dried *E.coli* containing a plasmid encoding the full-length human L1 open reading frame (ORF) was purchased from ATCC (Clone #65996). The bacteria were thawed and grown overnight in 15 mL tubes at 37°C. Plasmids were purified using the QIAprep® Spin Miniprep Kit (Qiagen). Gene-specific forward (5'-ATG GTC GTG GCG CTG CGG TAC GTG T-3') and reverse (5'-CTT CCT CTG ACT GCC CTC CCT CCA-3') primers were used to amplify an approximately 2500 bp sequence encoding the L1 140 kDa plasmin cleavage fragment by polymerase chain reaction (PCR) using Platinum *Taq* DNA Polymerase High Fidelity (Invitrogen). PCR was performed for 30 cycles (denaturation: 30 seconds, 94ºC; annealing: 25 seconds, 64 ºC; extension: 160 seconds, 68 ºC) with a final 20 minute hold at 68 ºC. The formation of a single product of expected size was confirmed by agarose gel electrophoresis.

Preparation of Entry Clone

The PCR product was ligated by T/A cloning into the pCR®8/GW/TOPO® (Invitrogen) Gateway Entry vector containing a spectinomycin resistance gene and

transformed into One Shot® chemically competent *E.coli* (Invitrogen). The bacteria were plated on LB-spectinomycin (100 µg/mL) agar plates and grown overnight at 37°C. Individual colonies were selected and expanded and plasmids were purified. A clone with appropriate orientation and sequence was identified by DNA sequencing using an ABI 3730 sequencer (DNA laboratory, Arizona State University). The clone sequence was identical to human L1CAM (GenBank accession no. NM_000425) with the exception of a single non-coding base difference at position 855.

Construction of Recombinant Baculovirus

Recombinant baculovirus was generated by an enzyme-catalyzed recombination reaction between the entry vector and BaculoDirect™ C-Term Linear DNA (Invitrogen) containing a C-terminal 6xHis fusion tag and herpes simplex virus thymidine kinase and and *lac*Z genes for negative selection and analysis of viral purity, respectively. A mixture of 100 ng of the pCR®8/GW/TOPO® entry clone, 300 ng of BaculoDirect™ Linear DNA, 4 µL of 5X LR Clonase™ Reaction Buffer, 1 µL of TE Buffer pH 8.0, and 4 µL LR Clonase™ enzyme mix was incubated at 25ºC overnight. After overnight incubation, 2 µL of Proteinase K solution was added to the mixture and incubated at 37ºC for 10 minutes.

Transfection and Amplification of Recombinant Baculovirus

Sf9 cells were plated in 6-well plates (8.0 x10^5 cells/well) and allowed to adhere for one hour at 27ºC. A transfection mixture consisting of 5 µL of the baculovirus

recombination reaction, 200 µL of Grace's Insect Medium, Unsupplemented (Gibco), and 6 µL of Cellfectin® Reagent (Invitrogen) was prepared, mixed, and incubated at room temperature for 45 minutes. The cells were washed with Unsupplemented Grace's Insect Medium, and the transfection mixture was diluted with 800 µL additional medium and added dropwise. After 5 hours incubation at 27ºC, the transfection mixture was removed and replaced with Sf-900 II Serum-Free Medium (Gibco) supplemented with antibiotics and 100 µM ganciclovir. The cells were monitored daily, and the P1 viral stock was collected when late stage infection characteristics were observed (8 days).

P2 viral stock was generated by infecting 8.0 $x10^5$ Sf9 cells/well with 10 µL of P1 viral stock and was collected on day 5. The infected cells were stained for β-galactosidase expression using the β-Galactosidase Enzyme Assay System with Reporter Lysis Buffer (Promega) to confirm the absence of non-recombinant virus. P3 viral stock was generated by infecting 1.0 x 10^7 cells/flask in T-75 flasks with 25 µL of the P2 viral stock and was collected after 96 hours. End-point dilution assay was used to determine viral titer (multiplicity of infection, MOI) of the P3 viral stock, as previously described. [314]

Localization of Recombinant L1 Expression in Insect Cells

Sf9 and High Five™ cells were plated in 6-well plates (1.5 $x10^6$ cells/well) and infected with 11 µL of P3 recombinant baculovirus stock (MOI 0.2). The supernatants were harvested at 48 hours and 72 hours postinfection, complete EDTA-free protease inhibitor added (CPI, Roche, 2.5 µL 7X CPI stock solution per mL supernatant),

centrifuged (3000 x g for 5 mins) to remove cell debris, and immediately frozen at -80 °C. Cells were lysed with RIPA buffer containing CPI at 48 hours and 72 hours postinfection, the lysates centrifuged (3000 x g for 10 mins) to remove cell debris, and immediately frozen at -80 °C. For gel electrophoresis, total protein concentrations of supernatant and lysate samples were determined by BCA assay (Pierce) using BSA standards and sample volumes were adjusted to achieve final protein loading amounts of 30 μg/well supernatant and 3 μg/lane lysate.

Kinetics and MOI Analysis of Recombinant L1

Expression in High Five Cells

High Five™ cells were plated in T-175 flasks (2.73 x10^7 cells/flask) and infected with P3 recombinant baculovirus stock at varying MOI (.002, .02, .2, 2). The supernatant was harvested at 48 hours, 72 hours, and 96 hours postinfection, CPI added, cell debris pelleted (3000 x g for 5 mins), and samples collected for Western Blot analysis (9 μL supernatant + 3 μL 4X reducing buffer) and immediately frozen at -80°C.

SDS-PAGE and Western Blot Analysis

Protein samples were separated by SDS-PAGE on 6% polyacrylamide gels using Tris-glycine buffer under reducing conditions at 100V for 150 minutes. Proteins were then transferred to PVDF membranes at 4°C overnight at 30V. Western blotting was performed using the WesternBreeze® Chromogenic Kit (Invitrogen). Membranes were blocked, incubated with polyclonal goat anti-human L1 primary antibody (R&D

Systems, 1:200 dilution), incubated with rabbit anti-goat IgG alkaline-phosphatase conjugated secondary antibody (Molecular Probes, 1:10,000 dilution), and developed with chromogenic substrate. Western Blots were imaged and analyzed using a GS-700 densitometer and QuantityOne® software (Bio-Rad).

Expression of Recombinant L1 in High Five™ Cells

High Five™ cells were plated in T-175 flasks (2.5 $x10^7$ cells/flask) and infected with recombinant baculovirus at an MOI of 0.2. The supernatant was harvested 72 hours postinfection, CPI added, cell debris pelleted (3000 x g for 5 mins), and supernatant immediately frozen at -80°C.

Protein Purification

The supernatant of infected cells was thawed and dialyzed against 50 mM Na_2HPO_4, 300 mM NaCl buffer, pH 8.0, for 48 hours with one buffer exchange using regenerated cellulose dialysis tubing with a molecular weight cut-off (MWCO) of 6-8 kDa (Fisher). CPI was added immediately prior to dialysis and at the buffer exchange. The dialyzed supernatant was adjusted to 500 mM NaCl, 5 mM imidazole prior to binding. Pre-equilibrated 50% Ni-NTA agarose slurry (Qiagen) was added to the dialyzed supernatant (450 µL equilibrated slurry / 4 flasks), mixed overnight on a shaker plate at 4°C, and transferred to a PolyPrep chromatography column (BioRad). Beads were washed with 4 mL each of 50 mM Na_2HPO_4, 500 mM NaCl, pH 8.0 buffer with increasing imidazole concentrations (0mM, 5mM, 10mM). Bound proteins were then

eluted in three 600 µL fractions using a 50 mM Na_2HPO_4, 500 mM NaCl, 250 mM imidazole, pH 8.0 buffer. The three elutions were combined and a buffer exchange to phosphate buffered saline (PBS) was performed using Zeba desalt columns (Pierce) according to manufacturer's instructions. The purified protein was sterile-filtered through a 0.2 µm syringe filter and stored at 4°C. Samples of the supernatant, wash buffer flow through, and eluted protein were normalized to the original supernatant volume and separated by SDS-PAGE. Gels were silver stained (SilverSNAP® Stain Kit II, Pierce) and imaged using a Kodak Electrophoresis Documentation and Analysis System 120. The yield of purified recombinant L1 was determined by BCA assay (Pierce) using BSA standards.

Bioactivity Assay

Sterile recombinant insect cell-derived L1 and commercial mammalian-derived L1-Fc (R&D Systems) were adsorbed onto 96-well ethylene-oxide sterilized polystyrene plates in 2 µL dots at 25 µg/mL concentration for 1 hour. Control wells were coated with 50 µL of 0.1% poly-l-lysine (PLL) for 1 hour (n=4 wells / group). White leghorn chicken embryonic day 8 forebrain neurons were isolated as previously described [315] and cultured on the adsorbed L1, L1-Fc, and PLL at a density of 30,000 cells/well in Basal Medium Eagle (BME, Gibco) supplemented with 6 mg/mL glucose (Sigma), 1% antibiotic/antimycotic 100X stock solution (Gibco), 10% fetal bovine serum (FBS, Invitrogen), and 2 mM L-glutamine (Hyclone) for 24 hours. Cells were then fixed for 1 hour in 4% paraformaldehyde and stained for actin microfilaments using Alexa Fluor®

594 phalloidin (Molecular Probes, 0.161 µM) and nuclei using DAPI (Molecular Probes, 3 µM). Neurite outgrowth was quantitatively measured from digital fluorescent images using ImagePro software (n=60 neurites / experimental group, comprised of an average of 15 measurements from each of 4 independent wells). Neurite outgrowth data were statistically analyzed by ANOVA using Tukey's method for post-hoc comparisons with $p<0.05$ considered statistically significant.

RESULTS AND DISCUSSION

Efficient expression and purification of bioactive, recombinant L1 is critical for its further investigation and development as a therapeutic molecule for stimulating axonal regeneration following brain and spinal cord injury. Native human L1 contains 6 disulfide bridges in the Ig domains and extensive glycosylation, which accounts for approximately 25% of molecular mass. Baculovirus-mediated insect cell expression offers several potential advantages for recombinant L1 expression, including improved posttranslational processing relative to prokaryotic systems and relatively higher yields as compared to mammalian systems. [316] Physiologically, L1 is expressed as a transmembrane protein that can be proteolytically cleaved to generate two soluble extracellular fragments. The objective of this study was the cloning and baculovirus expression of the 140 kDa extracellular plasmin cleavage product and the evaluation of its bioactivity relative to mammalian-derived L1-Fc containing the entire extracellular region. L1 was expressed with a C-terminal 6X histidine tag for ease of purification and as a basis for oriented immobilization to biomaterial surfaces.

Localization of Recombinant L1 Expression in Insect Cells

L1 contains a 19 amino acid N-terminal signal sequence that targets it for membrane insertion. We hypothesized that a truncated extracellular fragment lacking the transmembrane region would be secreted as a soluble protein. To investigate protein expression and localization, small-scale cultures of Sf9 and High 5 cells were infected with recombinant baculovirus at MOI of 0.2. Western blot analysis using an antibody to human L1 detected immunologically reactive protein in both cell lysates and supernatants derived from both cell lines (Figure 5.3). In both Sf9 and High 5 supernatants, L1 was detected as a distinct single band of approximately 140 kDa (Figure 5.3A), corresponding to the approximate molecular weight of the native human plasmin cleavage fragment. Densitometry analysis of L1 demonstrated an approximate 1.5-2.0 -fold increase in secreted L1 expression in High Five cells relative to Sf9 cells (Figure 5.3B). These results are consistent with previous observations of increased secreted protein expression in High Five cells relative to Sf9 and Sf21 cells, although the level of increase was less than previously reported. [317, 318] Intracellular protein exhibited a broader distribution of molecular weight with a distinct band around 110 kDa and a broad band between 135-150 kDa (Figure 5.3C). These bands observed in the intracellular protein likely correspond to unglycosylated protein immediately following translation (110 kDa) and protein at varying stages of glycosylation (135-150 kDa). Densitometry analysis indicated that intracellular L1 expression was substantially higher in High Five cells at 48 hours, but relatively similar at 72 hours (Figure 5.3D).

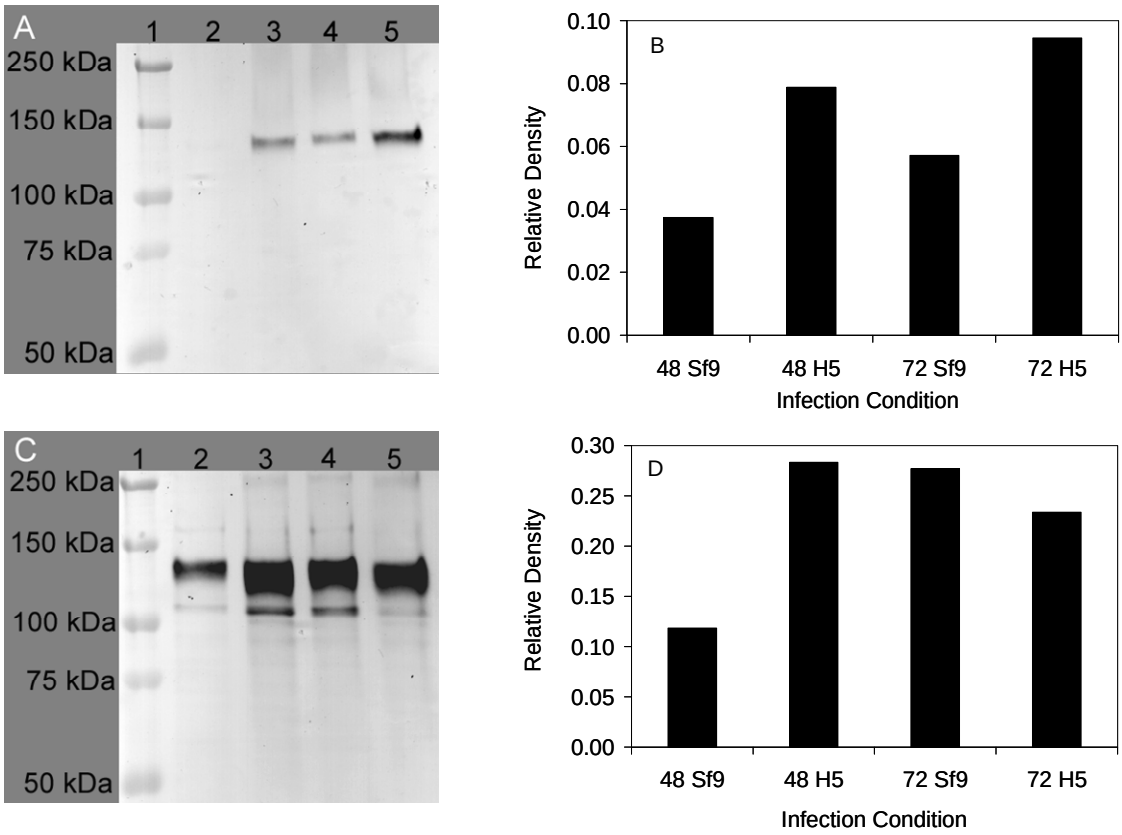

Figure 5.3 Western blot and densitometry analysis of recombinant L1 localization in Sf9 and High Five cells using anti-human L1 polyclonal antibody. Gels were loaded with equal quantities of total protein (supernatants: 30 µg/lane; lysates: 3 µg/lane). Blots are representative of 3 independent experiments. (A) Representative western blot of Sf9 and High Five media supernatants. Lane 1, molecular weight marker; lane 2, 48 hr Sf9 supernatant; lane 3, 48 hr High Five supernatant; lane 4, 72 hr Sf9 supernatant; lane 5, 72 hr High Five supernatant. (B) Comparison of mean relative density of bands of secreted L1. (C) Representative western blot of Sf9 and High Five cell lysates. Lane 1, molecular weight marker; lane 2, 48 hr Sf9 lysate; lane 3, 48 hr High Five lysate; lane 4, 72 hr Sf9 lysate; lane 5, 72 hr High Five lysate. (D) Comparison of mean relative density of bands of intracellular L1.

Kinetics and MOI Analysis of Recombinant L1 Expression in High Five Cells

Following confirmation of L1 expression in insect cells, we investigated optimization of secreted recombinant protein production. High Five cells cultured in T-175 flasks were infected at varying MOI, and the supernatants were sampled and analyzed by Western blotting at varying timepoints postinfection (Figure 5.4A). Secreted protein expression generally increased with increasing MOI and time postinfection, with the exception of 96-hour samples at 2.0 MOI, in which expression decreased relative to the 72-hour time point (Figure 5.4B). Although gel loading was based on equal supernatant volumes to normalize expression levels to initial cell number, total protein analysis demonstrated that all supernatants contained approximately comparable protein levels (30.7 +/- 2.5 μg/sample). Infections at 2.0 MOI resulted in the highest levels of protein production, however, light staining of lower molecular weight bands was consistently observed at all time points, as well as at the 96 hour time point for 0.2 MOI infection. These observations may be attributable to the high density of darkly colored cells observed at 2.0 MOI and the 0.2 MOI 96 hour time point which may be indicative of cell necrosis resulting in the release of intracellular L1 prior to completion of post-translational modification and/or release of proteolytic enzymes. On the basis of providing maximum expression in the absence of lower molecular weight bands, 0.2 MOI with harvest at 72 hours was selected for use in large-scale expression and purification.

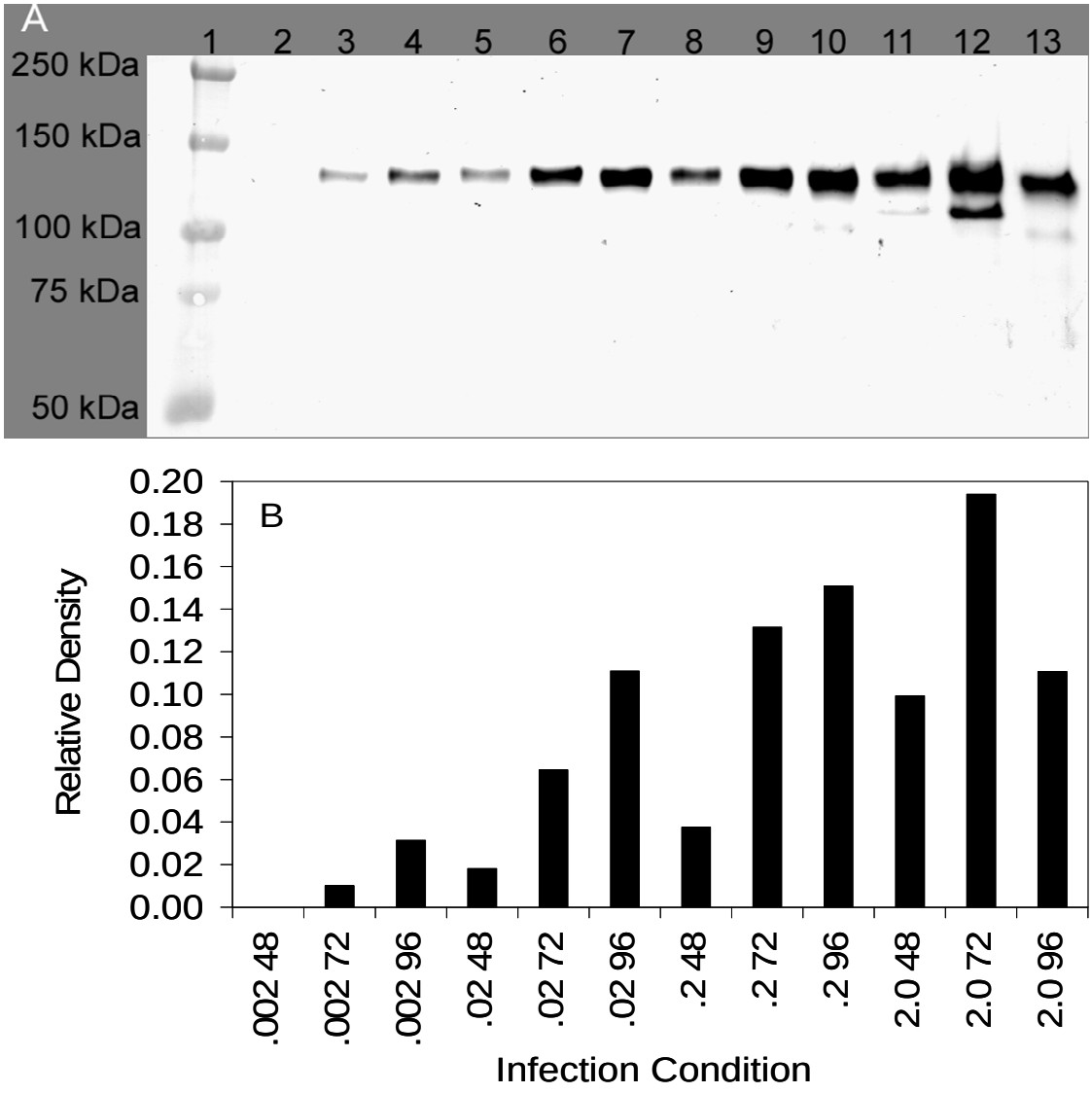

Figure 5.4 Western blot and densitometry analysis of the kinetics of secreted recombinant L1 expression from baculovirus-infected High Five cells using anti-human L1 polyclonal antibody. Gels were loaded with equal total volumes in order to normalize protein to initial cell density. Blot is representative of 3 independent experiments. (A) Representative western blot of secreted L1 at varying infection conditions. Lane 1, molecular weight marker; lane 2, .002 MOI 48 hr; lane 3, .002 MOI 72 hr; lane 4, .002 MOI 96 hr; lane 5, .02 MOI 48 hr; lane 6, .02 MOI 72 hr; lane 7, .02 MOI 96 hr; lane 8, .2 MOI 48 hr; lane 9, .2 MOI 72 hr; lane 10, .2 MOI 96 hr; lane 11, 2 MOI 48 hr; lane 12, 2 MOI 72 hr; lane 13, 2 MOI 96 hr. (B) Comparison of mean relative density of bands of secreted L1 at varying infection conditions.

Purification and Yield of Recombinant L1 in High Five™ Cells

Secreted recombinant L1 was purified from culture supernatants using immobilized metal-affinity chromatography. Due to the presence of disulfide bridges in the Ig domains, all purification procedures were conducted under non-denaturing conditions. Chemically-defined culture medium was used to avoid contamination by serum proteins. Preliminary experiments demonstrated that recombinant protein could not be efficiently recovered directly from culture supernatants (data not shown). Dialysis against 50 mM Na_2HPO_4, 300 mM NaCl buffer, pH 8.0 was performed to increase pH and to remove low molecular weight competing species. The final purification procedure was documented by silver-stained SDS-PAGE (Figure 5.5), revealing a single band of recombinant L1 at approximately 140 kDa.

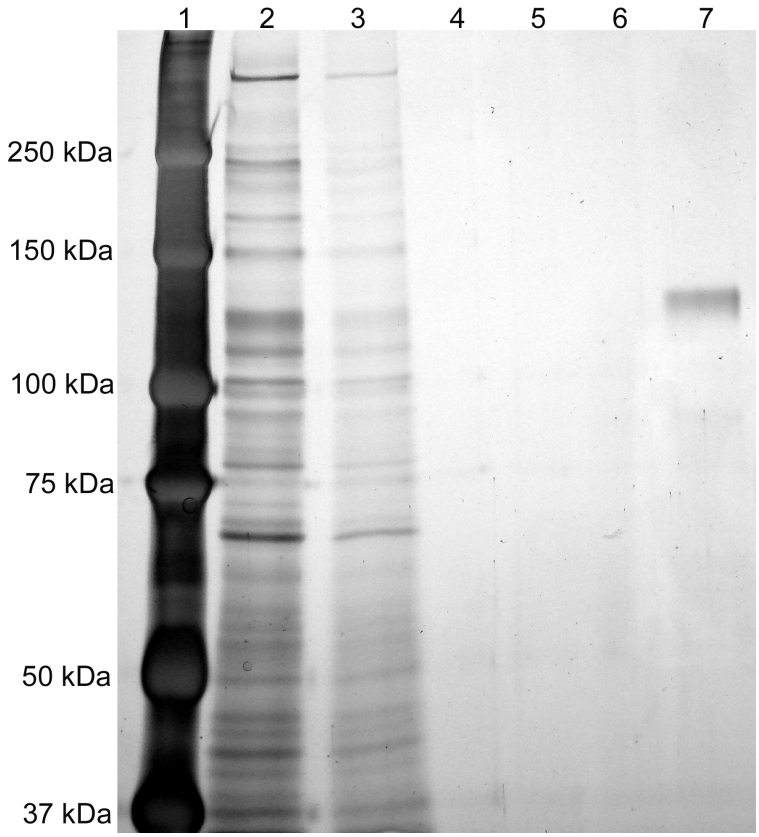

Figure 5.5 Documentation of the purification procedure for secreted recombinant L1 expression from the supernatant of baculovirus-infected High Five cells. Proteins were separated utilizing SDS-PAGE and silver stained. Lane 1, molecular weight marker; lane 2, serum-free supernatant of baculovirus-infected High Five cells; lane 3, flow through; lane 4, 0 mM imidazole buffer wash; lane 5, 5 mM imidazole buffer wash; lane 6, 10 mM imidazole buffer wash; lane 7, combined 250 mM imidazole elutions 1-3. All samples were normalized to the original supernatant volume. Representative of 3 independent experiments.

BCA analysis demonstrated average yield of approximately 250-300 µg per $1x10^8$ High Five cells. Although diversity exists among expression methods and protein structure, this yield is approximately comparable to levels reported for other relatively high molecular weight, highly glycoylated proteins in insect cells. Secreted human xylosyltransferase I (96 kDa) expression levels in High Five cells were reported as 5 mg /

1.0-2.5 x 10^9 cells [319], while intracellular expression levels of DNA (cytosine-C5)-methyltransferase-1 (190 kDa) in Sf9 were reported at 1 mg / 3 x 10^8 cells[320]. Most comparable to our own study, a recent report of stable L1 expression in Sf9 cells using the honeybee melittin secretion signal achieved secreted protein yields of 3 mg / 4 x 10^9 cells for the complete extracellular domain (203 kDa) and 32 mg / 4 x 10^9 cells for the Ig 5-6 fragment (45 kDa). [313] In general, insect cell expression levels are lower than prokaryotic systems and higher than mammalian systems. Expression levels of L1-Fc in HEK 293 cells were reported as 1-5 mg/L, however the cell density was not reported and supernatant was repeatedly collected from stably transfected cells over a 4 week period. [274] Yields of L1 extracellular fragments (30-85 kDa) expressed in *E. Coli* have been reported in the range of 3-5 mg/L. [312, 321]

L1 Functional Bioactivity

As a cell-cell adhesion ligand, the most critical functional activity of L1 during development and as a potential therapeutic molecule is the promotion of axonal growth. Neurite outgrowth from primary central nervous system neurons was evaluated as a functional measure of protein bioactivity. The bioactivity of the secreted insect cell-derived 140 kDa extracellular L1 fragment was compared to mammalian-derived L1-Fc containing the entire extracellular region and poly-l-lysine (PLL), a routine substrate for neuronal cell culture. Chick embryonic forebrain neurons were selected based on their ease of preparation at high yield and purity, allowing clear analysis of neuron-ligand interactions without interference from neuron adhesion and growth on contaminating cell

types. Previous studies have also demonstrated that neurite outgrowth of chick-derived neurons on mammalian L1 occurs through homophilic binding of mammalian L1 and its chick homologue, NgCAM. [305] Both insect cell-derived L1 and mammalian-derived L1-Fc promoted robust neurite outgrowth at 24 hours that was much greater than observed on PLL (Figure 5.6). No neurite outgrowth was observed in blank control wells not coated with L1 or PLL (data not shown), indicating that the observed neurite outgrowth was mediated specifically by the protein/polymer coating applied to the wells. In addition, no neurite outgrowth was observed on intracellular L1 purified from High Five lysates under non-reducing conditions, indicating a lack of bioactivity probably due to incomplete glycosylation of the protein (data not shown).

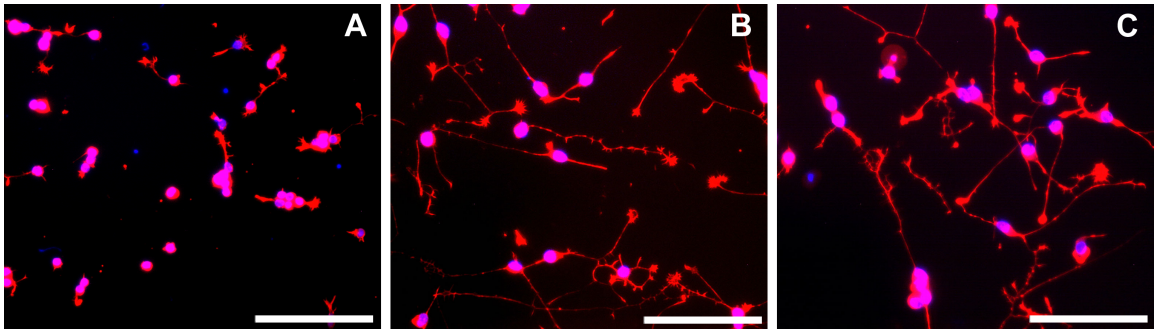

Figure 5.6 Demonstration of L1 bioactivity. Embryonic day 8 chick forebrain neurons cultured on a 96 well polystyrene plate with (A) adsorbed 0.1% PLL, (B) adsorbed mammalian-derived L1-Fc (25 mg/ml), and (C) adsorbed insect cell-derived L1 (25 µg/ml). Cells were cultured 24 hours and then stained for actin (red) and nuclei (blue). Scale bar = 100 µm.

Average measured neurite lengths at 24 hours were 40 µm for PLL, 155 µm for insect cell-derived L1, and 150 µm for mammalian-derived L1-Fc (Figure 4.5). Neurite outgrowth was significantly greater for both insect cell-derived L1 and mammalian-

derived L1-Fc than PLL; however, no statistically significant difference was observed between insect cell-derived L1 and L1-Fc.

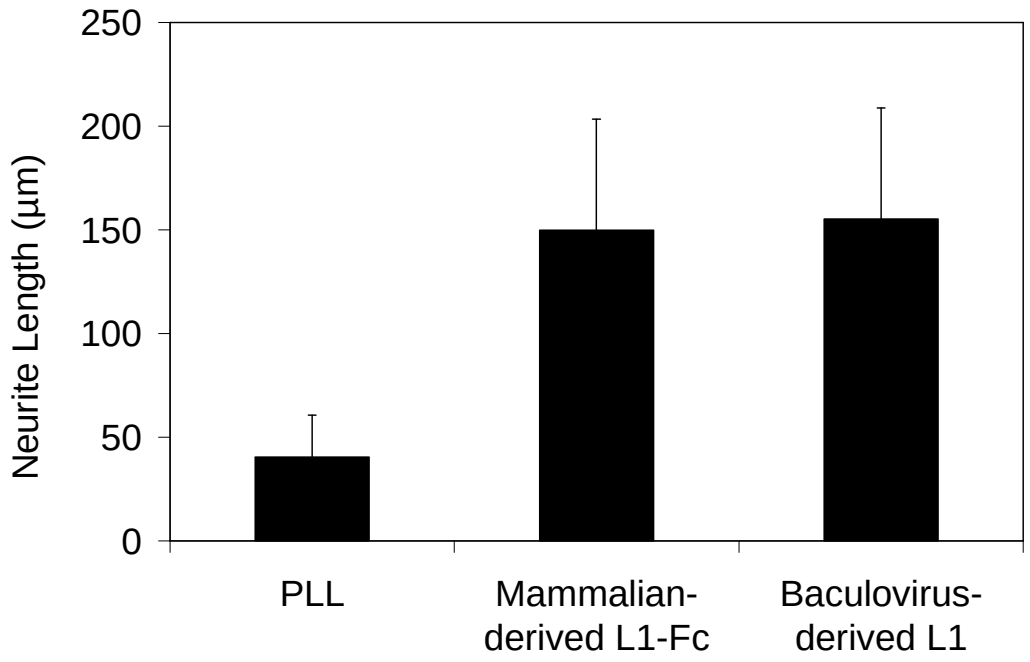

Figure 5.7 Neurite outgrowth on L1. Neurite lengths (mean +/- standard deviation) of embryonic day 8 chick forebrain neurons cultured on a 96 well polystyrene plate with adsorbed 0.1% PLL, adsorbed mammalian-derived L1-Fc (25 µg/ml), and adsorbed insect cell-derived L1 (25 µg/ml).

CONCLUSION

These studies describe the expression of a 140 kDa extracellular fragment of L1 in the baculovirus/insect cell expression system. Recombinant L1 was secreted as a soluble protein into the culture medium and through the incorporation of a C-terminal 6X histidine tag, it could be efficiently recovered at high purity by metal affinity chromatography. Currently, L1 used for experimental studies is primarily expressed as a recombinant Fc-fusion protein in mammalian cells or directly purified from brain lysates

by immunoaffinity chromatography. The baculovirus expression and native purification approaches described here provide an alternative source of recombinant L1 with improved yield and equivalent bioactivity. Continuing studies described in this dissertation examined the immobilization of L1 to biomaterial surfaces and investigated their application in promoting axonal regeneration in the injured nervous system.

CHAPTER SIX

NIH 3T3 RESPONSE TO ACRYLATED TETRONIC®

HYDROGELS WITH IMMOBILIZED FIBRONECTIN

INTRODUCTION

The objectives of these experiments were (1) synthesis and purification of acrylated Tetronic macromers, (2) development of Michael addition methods for hydrogel crosslinking and protein immobilization, and (3) evaluation of hydrogel cytocompatibility, immobilized protein bioactivity, and immobilization efficiency in terms of cell spreading and proliferation using NIH 3T3 fibroblasts and fibronectin.

This work established methods for adding acrylate groups to Tetronic® 904 and fabricating hydrogels using a Michael addition reaction. [322] Michael addition is not only useful for hydrogel fabrication, but may also be used for protein immobilization. Murphy et al. immobilized calmodulin within Peg-tetraacrylate gels via Michael type addition of cysteine thiols to the acrylate groups [281], and Rydholm et al. have demonstrated that pendant thiols on thiol-acrylate polymers may be useful for post-polymerization functionalization. [282] Additionally, peptide acrylation is a well-established method for covalent immobilization of peptides within hydrogels [283-285], and protein acrylation has been used in methods to conjugate antibodies and collagen type I to polymer surfaces [286, 287]

Three methods of protein immobilization to T904-acrylate hydrogels were evaluated (Figure 6.1): (A) Michael type addition of cysteine thiols from encapsulated

reduced protein to acrylate groups within the hydrogel, (B) Michael type addition of cysteine thiols from reduced protein to unreacted pendant acrylate groups on the hydrogel surface, and (C) Michael type addition of acrylated proteins using acrylate-PEG-NHS (N-hydroxysuccinimide) with unreacted pendant thiol groups on the hydrogel surface.

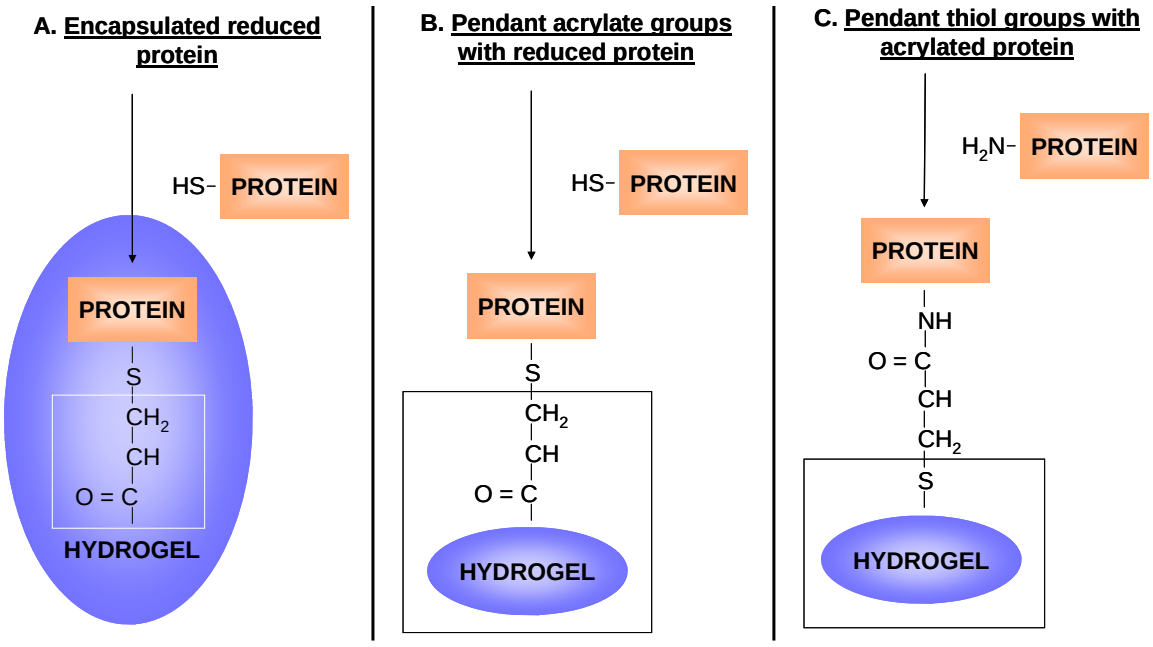

Figure 6.1 Protein Immobilization Methods

NIH 3T3 cells originated from Swiss mouse embryo tissue, and the cell line was established in 1962 by George Todaro and Howard Green at the Department of Pathology in the New York University School of Medicine. [323] These fibroblast cells double every 24 hours and reach a saturation density of approximately 50,000 cells per cm^2, and they are widely used in research laboratories. Fibronectin exists in two main forms: 1) as an insoluble glycoprotein dimer in the ECM, made by fibroblasts, chondrocytes,

endothelial cells, macrophages, as well as certain epithelial cells; and 2) as a soluble disulphide linked dimer found in the plasma, synthesized by hepatocytes. Fibronectin is secreted as a disulfide-bonded dimer of approximate 440 kDa molecular weight, and each subunit contains three types of repeating modules: FN-I, FN-II, and FN-III, with disulfide bonds in FN-1 and FN-II but not FN-III modules. [324, 325] It is widely known that the Arginine-Glycine-Aspartic Acid (RGD) integrin binding tripeptide in the FN-III repeat 10 is an important bioactive site that induces fibroblast attachment to fibronectin via integrin binding [326-328], although there is also evidence of multiple functional synergy sites within the fibronectin protein. [329-332] Fibronectin has free cysteine residues and numerous disulfide bonds that can participate in Michael addition and thiol/disulfide exchange reactions. [333] It also contains multiple lysine residues making it an attractive candidate for acrylation through conjugation to the heterobifunctional PEG derivative, acrylate-PEG-NHS.

MATERIALS AND METHODS

Synthesis and Purification of T904-Acrylate

Figure 6.2 is a schematic of the synthesis of acrylated Tetronic macromers [322], and the protocol is included in Appendix A.

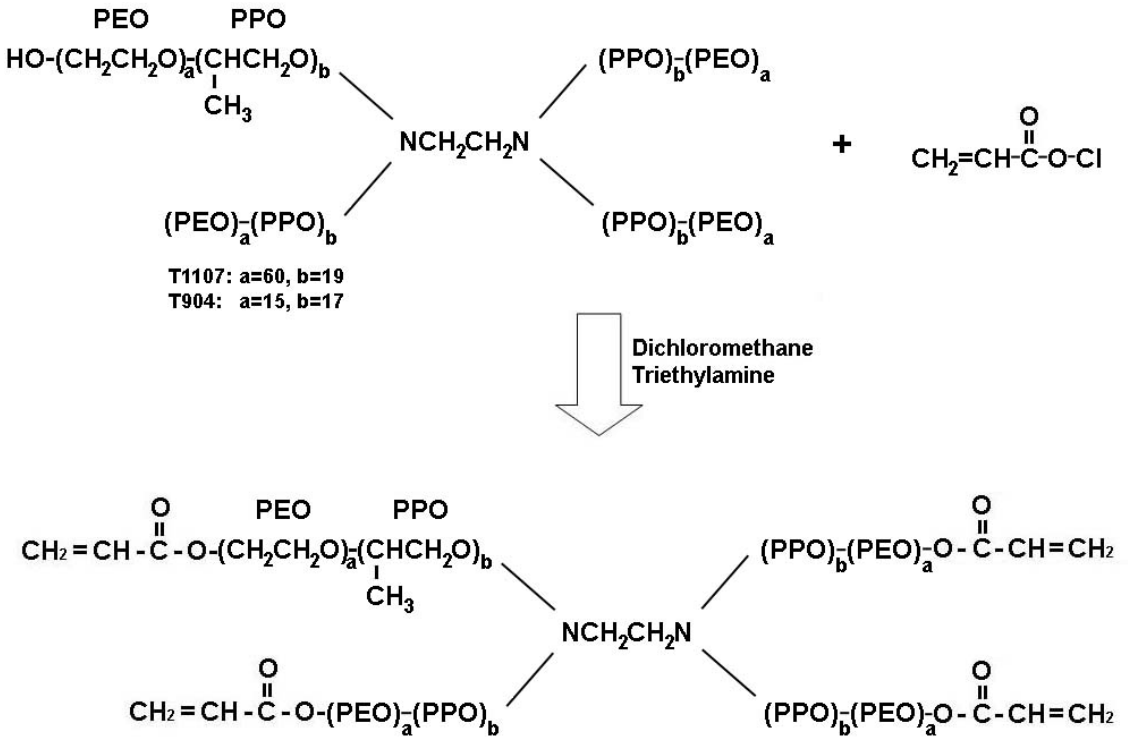

Figure 6.2 Synthesis of Acrylated Tetronic Macromers [322]

Briefly, Tetronic® 904 (MW 6700) was dissolved in toluene, azeotropically distilled, and toluene was removed via solvent evaporation with a rotary evaporator. The T904 was then dissolved in dehydrated dichloromethane and reacted with 4X molar excess triethylamine (TEA) and 8X molar excess acryloyl chloride for 24 hours at 4°C. At the completion of the reaction, the product was filtered, dichloromethane was removed via solvent evaporation, and it was precipitated in a 50/50 ether/hexane mixture. Upon settling of the precipitated product, ether/hexane was decanted and the product was redissolved in dichloromethane, washed with $NaHCO_3$ to neutralize the pH followed by multiple water washes, and water was removed using anhydrous sodium sulfate.

Dichloromethane was removed via solvent evaporation, and the product was precipitated in a 50/50 ether/hexane mixture two times followed by two 100% ether precipitations to ensure removal of all hexane. Upon settling of the precipitated product, ether/hexane was decanted, the product was dried overnight in a cold dessicator on ice under vacuum to remove ether, and ^{1}H-NMR (Brucker 300 MHz, $CDCl_3$) was taken to evaluate the acrylation efficiency. All T904-acrylate products were stored at -20°C protected from light.

NIH 3T3 Cell Culture

NIH 3T3 mouse fibroblasts were purchased from ATCC (American Type Culture Collection) and were routinely maintained 75 cm^2 T-flasks in a humidified chamber at 37°C with 7% CO2 atmosphere in 50/50 Dulbecco's Modified Eagle's Medium and Ham's F-12 with L-glutamine (DMEM/F12 1X, Mediatech) supplemented with 10% v/v bovine growth serum (BGS, Hyclone) and 50 I.U./mL penicillin and 50 µg/mL streptomycin (Mediatech). Culture medium was changed once every two days and cells were passaged weekly. For hydrogel experiments, monolayers of fibroblasts were trypsinized, centrifuged, resuspended, counted in a hemacytometer, and adjusted to the appropriate final concentrations based on pilot studies.

Preparation of T904-Acrylate Solution

T904-acrylate was mixed with 50mM PBS pH 7.4 to make a 28.75% solution (287.5mg T904 + 712.5µL PBS) and was allowed to dissolve overnight with stirring at room temperature protected from light. Because of batch-to-batch inconsistencies in

T904-acrylate pH due to variable efficiency of washing steps during synthesis and because of the dependency of solution pH on temperature, the solution was adjusted to pH 7.2 at room temperature with 6N hydrochloric acid to ensure consistent, appropriate pH for the Michael addition polymerization reaction. Following pH adjustment, the solution was carefully filtered with a 25mm 0.2μm syringe filter (Nalgene) for removal of contaminants and sterilization. The sterile solution was stored at 4°C protected from light, but was brought to room temperature prior to making hydrogels because of its basic pH at colder temperatures.

Preparation of Hydrogels

Prior to making hydrogels, all components were sterilized. Uncharged glass coverslips (Fisher) were UV sterilized for 20 minutes in the cell culture hood. Binder clips, 1mm thick Teflon spacers, vacuum grease, spatulas, and forceps were autoclaved prior to use. All experiments were conducted in the cell culture hood using aseptic technique.

Hydrogel crosslinking via Michael addition reaction was initiated by the addition of dithiothreitol (DTT), as depicted in Figure 6.3.

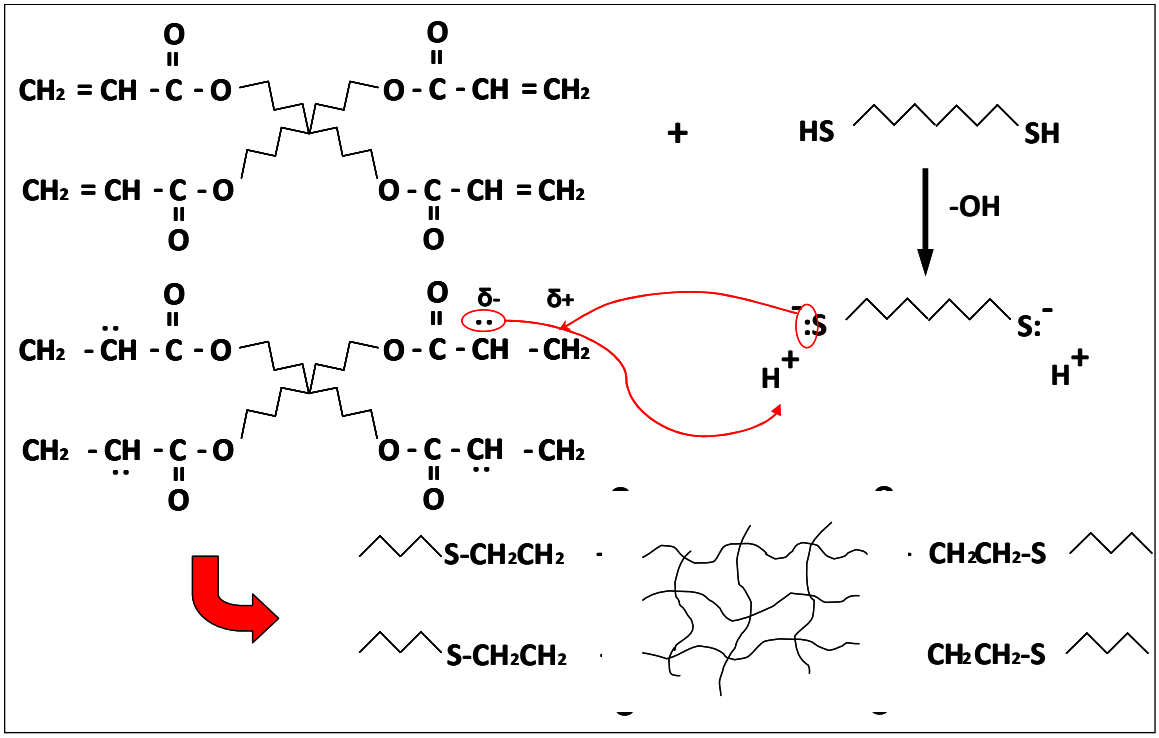

Figure 6.3 Michael Addition Polymerization Scheme [322]

Hydrogels for all conditions tested were fabricated by mixing the 28.75% T904-acrylate solution previously described with 10% v/v fibronectin solution (encapsulated protein) or 50mM PBS solution (surface-immobilized protein) and 10% v/v DTT solution for a final concentration of 23% T904 acrylate (i.e., 80µL T904 acrylate + 10µL of fibronectin/50mM PBS + 10µL DTT = 23% T904-acrylate hydrogel for a 100µL hydrogel).

T904 has a molecular weight of 6700 g/mol. T904-acrylate has an estimated molecular weight of 6916 g/mol and 4 moles of acrylate per mole of T904 acrylate assuming 100% acrylation efficiency. DTT has a molecular weight of 154.26 and 2 moles of thiol per mole of DTT. For encapsulated protein, the DTT concentration

required was calculated based on a 1:1 T904 acrylate:DTT thiol ratio, thus requiring 1.03 mg of DTT per 23 mg of T904 acrylate. For surface-immobilization of acrylated peptide or protein, the DTT concentration required was calculated based on a 1:1.1 T904 acrylate:DTT thiol molar ratio in order to leave unreacted pendant thiols on the hydrogel surface, thus requiring 1.13 mg of DTT per 23 mg of T904 acrylate. For surface-immobilization of reduced protein, the DTT concentration required was calculated based on a 1.1:1 T904 acrylate:DTT thiol molar ratio in order to leave unreacted pendant acrylate groups on the hydrogel surface, thus requiring 0.93 mg of DTT per 23 mg of T904 acrylate. A new DTT stock solution was made for every experiment and was sterilized by filtering through a 13mm 0.2μm syringe-filter (Nalgene).

T904-Acrylate Hydrogels with Surface-Immobilized Reduced Fibronectin

These experiments are based on the immobilization method depicted in Figure 6.1B.

Reduction of Fibronectin

Analysis of GenBank Accession No. P07589, bovine fibronectin (Appendix A) revealed that fibronectin contains 62 cysteines per mol. Fibronectin is a 440 kDa protein, and a 1 mg/mL solution is equivalent to 0.00227 mmol/L concentration of protein. Protein solutions are typically reduced with 1mM to 10 mM DTT. A 2.5 mM DTT solution was used to reduce fibronectin [276], resulting in an approximate 1000 molar excess of DTT to fibronectin, or an approximate 35-molar excess of DTT thiols to fibronectin cysteines. A 10X 25mM stock solution of DTT in 50mM PBS pH 7.4 buffer

was made, 10% by volume was added to the 1mg/mL fibronectin solution for a final 2.5 mM DTT concentration, and reacted for 1 hour at room temperature. Unreacted DTT was removed by column filtration using a PD-10 column and 50mM PBS pH 7.4 buffer followed by analysis of protein concentration via measurement of absorbance at 280nm. Protein samples were kept on ice following filtration and during protein concentration analysis.

Preparation of Hydrogels

PBS and DTT were directly added to room temperature 28.75% T904-acrylate solution, and the gel solution was vortexed briefly, tap-spinned, and 70μL was immediately pipetted directly into 96-well TCPS plate and allowed to polymerize via Michael addition in the dark for 1 hour at room temperature. After 1 hour, reduced fibronectin solution (100μL per well) of 100 μg/mL concentration was added and left for an additional hour at room temperature. Hydrogel crosslinking and fibronectin reduction were coordinated such that reduced fibronectin solution was added to the hydrogels immediately upon completion of reduced fibronectin concentration analysis, to minimize the possibility of disulfide bond reformation. Hydrogels without reduced fibronectin were used as negative controls. Blank 48-well TCPS wells and 96-well bacterial polystyrene wells with 10 μg/mL reduced fibronectin adsorbed overnight were seeded as positive controls for visual confirmation of cell health and bioactivity of reduced protein. Following 1 hour incubation in reduced protein at room temperature, the plate was parafilmed and transferred to 37°C overnight with shaking. The next morning, gels were

rinsed with 200μL of sterile PBS three times and hydrated in 100μL of sterile PBS per well at 37°C until cell seeding.

Cell Seeding

NIH 3T3 cells were seeded at a density of 312.5 cells/mm^2 in DMEM/F12 with L-glutamine supplemented with 10% BGS and 50 I.U./mL penicillin and 50 μg/mL streptomycin and observed at 24 hours post-seeding for attachment and spreading.

T904-Acrylate Hydrogels with Surface-Immobilized Acrylate-PEG-RGD

A pilot study was conducted using stock 10 μmol/mL acrylate-PEG-RGD previously synthesized in our lab using 70μL hydrogels polymerized directly in 96-well TCPS plates.

Immobilization of Acrylate-PEG-RGD

PBS and DTT were directly added to room temperature T904-acrylate solution, and the gel solution was vortexed briefly, tap-spinned, and 70μL was immediately pipetted directly into 96-well TCPS plate and allowed to crosslink via Michael addition at dark for 1 hour at room temperature. After 1 hour, acrylate-PEG-RGD solution (diluted to 1 μmol/mL) was added and left for an additional hour at room temperature. Additional hydrogels were incubated in acrylate-PEG-RGD solution (1 μmol/mL) diluted in a 100X molar excess sodium acrylate solution to determine if this inhibited binding of acrylate-PEG-RGD to the hydrogel surface. Negative control samples included hydrogels without acrylate-PEG-RGD. Positive control samples (for visual confirmation of cell health only)

included blank 96-well TCPS wells and encapsulated fibronectin gels. All conditions used a sample size of n=3 independent gels.

Following 1 hour incubation at room temperature, the plate was parafilmed and transferred to 37°C overnight with shaking. The next morning, gels were rinsed with 200μL of sterile PBS three times and hydrated in 100μL of sterile PBS per well at 37°C until cell seeding.

Cell Seeding

NIH 3T3 cells were seeded at a density of 312.5 cells/mm^2 in DMEM/F12 with L-glutamine supplemented with 10% BGS and 50 I.U./mL penicillin and 50 μg/mL streptomycin.

Cell Staining and Imaging

At 24 hours post-seeding, cells were fixed in 4% paraformaldehyde in PBS for one hour at room temperature, permeabilized with 0.5% Triton X-100 for 2 minutes, and stained for actin filaments with rhodamine phalloidin (Molecular Probes). Hydrogels were carefully removed from the wells and flipped over onto a glass slide for imaging, and digital fluorescent images were obtained using a 10X objective for each condition.

Preparation of Acrylated Fibronectin

Acrylation Reaction

Bovine plasma fibronection (1mg/mL, Sigma-Aldrich) is supplied in 0.5 M NaCl, 0.05 M Tris, pH 7.5. Tris contains primary amines that interfere with fibronectin acrylation using acrylate-PEG-NHS because of competitive binding with the protein

lysine amines; therefore, prior to using the protein solution, a buffer exchange into 50mM PBS, pH 7.4 was performed utilizing 0.5 mL Zeba desalt columns (Pierce) according to the manufacturer's instructions.

Standard reaction conditions for NHS-containing crosslinkers call for 0.1-10 mM concentrations. Fibronectin is a 440 kDa protein, and a 1 mg/mL solution is equivalent to 0.00227 mmol/L concentration of protein. Typically, 2 to 50-fold molar excesses of crosslinker are used for reactions, and the 0.1M concentration of acrylate-PEG-NHS (Nektar, 3450 Da) used for this reaction resulted in a 44 molar excess of crosslinker to fibronectin. A 10X solution of 3.45 mg/mL acrylate-PEG-NHS in anhydrous DMSO was made fresh for each reaction, 10µL of this solution was added to 100 µL of 1mg/mL fibronectin for an organic solvent carryover of 10% final volume in the aqueous reaction, and reacted for 2 hours at room temperature with shaking. At the completion of the reaction, a buffer exchange into 50mM PBS, pH 7.4 was again performed to remove unreacted crosslinker and solvent contamination, and the acrylated protein was stored at 4°C protected from light.

Electrophoresis of Acrylated Fibronectin

Samples of acrylated and non-acrylated fibronectin were immediately collected for SDS-PAGE (sodium dodecyl polyacrylamide gel electrophoresis) analysis (12 µL protein + 4 µL 4X reducing buffer) and immediately frozen at -80°C. Protein samples were separated by SDS-PAGE on a 6% polyacrylamide gel using Tris-glycine buffer under reducing conditions at 100V for 150 minutes. The gel was stained with 0.2% Coomassie Brilliant Blue in Water:Methanol:Acetic Acid with volume ratios 5:4:1 for 45

minutes followed by destaining in Water:Methanol:Acetic Acid with volume ratios 5:4:1 for 3 hours. The gel was imaged using a Kodak Electrophoresis Documentation and Analysis System 120.

T904 Acrylate Hydrogels with Encapsulated and Surface-Immobilized Acrylated Fibronectin

These experiments are based on the immobilization methods depicted in Figure 6.1A and C. Two separate experiments were conducted in order to quantify fibroblast spreading and proliferation in response to hydrogels with encapsulated fibronectin and surface-immobilized acrylated fibronectin (as depicted in the project rationale Figure 4.3A). The dose dependent response of cells to varying concentrations of fibronectin was characterized by analyzing fibroblast spreading at an intermediate time point of 18 hours post-seeding, prior to the typical cell doubling timepoint of 24 hours. A cell proliferation assay was then conducted with protein concentrations chosen based on fibroblast spreading results.

Dose Dependent Response Assay

For hydrogels with encapsulated fibronectin, pilot studies were conducted to determine the optimum timepoint of fibronectin reduction with DTT prior to addition to the T904-acrylate solution (0, 2.5, 5, 10, 15, and 30 minutes) with encapsulated 100μg/mL fibronectin hydrogels. Hydrogels for the dose dependent response assay were made with varying concentrations of encapsulated fibronectin (1.0, 2.5, 5.0, 7.5, 10, 25, 50, 75, 100 μg/mL) with n=3 independent gels per condition. Hydrogels without fibronectin (n=3 independent gels) were used as negative controls. Blank 48-well TCPS wells and 96-well bacterial polystyrene wells with 10 μg/mL reduced fibronectin

adsorbed overnight were seeded as positive controls for visual confirmation of cell health and bioactivity of reduced protein. Fibronectin was mixed with DTT for 5 minutes at room temperature with shaking. This protein/DTT mixture was added to room temperature T904 acrylate solution, the gel solution was vortexed briefly, tap-spinned, and 60μL was immediately pipetted in between two glass slides separated by 1mm Teflon spacers. The hydrogels were allowed to crosslink via Michael addition in the dark for 2 hours at room temperature followed by overnight at 37°C in parafilmed petri dishes with sterile water to provide a humid environment. The next morning, vacuum grease was added to the bottom of 48-well TCPS plates and sterilized under UV light for 20 minutes. The hydrogels were carefully removed from the glass slides by rinsing with sterile PBS and were placed in the wells, gently pressing them down onto the vacuum grease to prevent floating, and hydrated in 1 mL of PBS per well at 37°C until cell seeding.

For hydrogels with surface-immobilized acrylated fibronectin, PBS and DTT were directly added to room temperature T904-acrylate solution, and the gel solution was vortexed briefly, tap-spinned, and 70μL was immediately pipetted directly into 96-well TCPS plate and allowed to crosslink via Michael addition in the dark for 1 hour at room temperature. After 1 hour, acrylated fibronectin solution (100μL per well) of varying concentrations (1.0, 2.5, 5.0, 7.5, 10, 25, 50, 75, 100 μg/mL) was added and left for an additional hour at room temperature, with n=3 independent gels per condition. Negative control samples included hydrogels without acrylated fibronectin (n=3 independent gels) and hydrogels with non-acrylated fibronectin (n=3 independent gels). Blank 96-well TCPS wells were seeded as positive controls for visual confirmation of cell health.

Following 1 hour incubation in acrylated protein at room temperature, the plate was parafilmed and transferred to 37°C overnight with shaking. The next morning, gels were rinsed with 200μL of sterile PBS three times and hydrated in 100μL of sterile PBS per well at 37°C until cell seeding.

NIH 3T3 cells were seeded at a density of 312.5 cells/mm^2 in DMEM/F12 with L-glutamine supplemented with 10% BGS and 50 I.U./mL penicillin and 50 μg/mL streptomycin.

Cell Proliferation Assay

Three timepoints were chosen for cell proliferation analysis: 24 hours (1 day), 72 hours (3 days), and 120 hours (5 days) post seeding. Based on the results of the dose dependent response assay, hydrogels were made with varying concentrations of encapsulated fibronectin (2.5, 5.0, 25, 100 μg/mL) and acrylated fibronectin (7.5, 10, 25, 100 μg/mL) with n=3 independent gels per condition. Negative control samples included hydrogels without encapsulated and acrylated fibronectin (n=3 independent gels) and hydrogels with non-acrylated fibronectin (n=3 independent gels). Blank 96-well TCPS wells were seeded as positive controls for visual confirmation of cell health.

NIH 3T3 cells were seeded at a density of 312.5 cells/mm^2 in DMEM/F12 with L-glutamine supplemented with 10% BGS and 50 I.U./mL penicillin and 50 μg/mL streptomycin. Media was changed daily to maintain an adequate supply of cell nutrients.

Measurement of Fibroblast Spreading

Fibroblast spreading at 18 hours post-seeding was analyzed via measurement of the surface area of the cells. Cells were fixed in 4% paraformaldehyde in PBS for one hour at room temperature, permeabilized with 0.5% Triton X-100 for 2 minutes, and stained for actin filaments with rhodamine phalloidin (Molecular Probes). Hydrogels were carefully removed from the wells and flipped over onto a glass slide for imaging. Twenty digital fluorescent images per well using a 10X objective covering the entire hydrogel surface were recorded for each condition. Cell surface area was quantitatively measured from the digital fluorescent images using ImagePro software (n=21 measurements / experimental group, comprised of an average of 7 measurements from each of 3 independent wells).

DNA Content Analysis

PicoGreen (Molecular Probes) is a fluorescent binding dye and is an established method of characterizing cell proliferation based on DNA content. [284, 334-336] Hydrogel samples were analyzed in triplicate for DNA content at 1, 3, and 5 days to assess cell proliferation. The cell-seeded hydrogels were rinsed with PBS, and fibroblasts were lysed by freeze/thaw of the samples at -80°C three times. Samples were suspended in 2mL of cold 10mM EDTA pH 12.3 solubilization buffer (2mL for encapsulated fibronectin samples, 200μL for acrylated fibronectin samples) as previously described. [337] Following 20 minute incubation at 37°C, the samples were cooled on ice and the pH was neutralized with 1M potassium phosphate pH 4.19 (150μL for encapsulated fibronectin samples, 15μL for acrylated fibronectin samples). Samples were analyzed

according to the manufacturer's instructions using a SpectraMAX Gemini fluorometer (excitation filter at 480 nm and emission filter at 520 nm) based on standard curves derived from serial dilutions of the same cells and their DNA content.

Statistical Analysis

The data was analyzed by ANOVA using Tukey's method for post-hoc comparisons with $p<0.05$ considered statistically significant. All results are expressed as mean ± standard deviation.

RESULTS AND DISCUSSION

Synthesis and Purification of T904-Acrylate

Figure 6.4 depicts the NMR from a typical T904-acrylate product. A 30g reaction typically yielded approximately 15g of final product and ^{1}H-NMR ($CHCl_3$) demonstrated an approximate 83% acrylation efficiency.

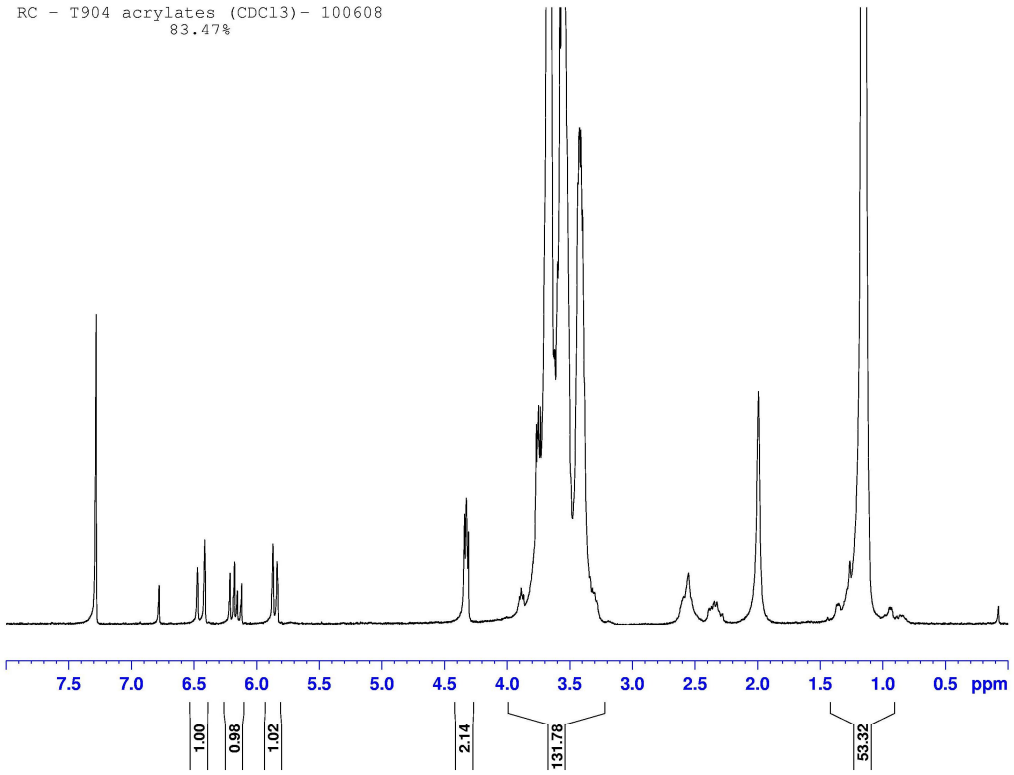

Figure 6.4 Structure and ^{1}H-NMR Spectrum of Acrylated T904 Macromer

NIH 3T3 Response to Surface-Immobilized Reduced Fibronectin

Fibroblasts showed little evidence of attachment and no spreading on hydrogels with reduced fibronectin, comparable to hydrogels with no protein. Positive controls of blank 48-well TCPS and 96-well bacterial polystyrene with 10 μg/mL reduced fibronectin adsorbed overnight demonstrated significant spreading and proliferation of fibroblasts. Acrylate groups are inherently hydrophobic because their CH=CH2 carbonaceous side groups are non-polar and thus do not attract water strongly. We hypothesize that this immobilization technique failed because the inherent

hydrophobicity of the acrylate groups contributes to their retreat within the hydrogel upon application of the hydrophilic reduced fibronectin solution, thus hindering the Michael addition protein conjugation reaction. An alternative explanation is that the filtration method used may not be sufficient to remove all excess DTT, possibly resulting in a reformation of fibronectin disulfide bonds prior to adding the solution to the hydrogels. No further experiments were conducted utilizing reduced fibronectin.

NIH 3T3 Response to Surface-Immobilized Acrylate-PEG-RGD

This pilot study was conducted in order to demonstrate the feasibility of immobilizing acrylated protein to hydrogels through Michael addition reaction by demonstrating cell attachment to an immobilized acrylated peptide, and to prove that the cellular response was, in fact, a result of acrylate binding to unreacted pendant thiols on the hydrogel surface via a competitive binding assay using sodium acrylate. (Figure 6.5) Figure 6.5A depicts significant fibroblast attachment and spreading on hydrogels with immobilized acrylate-PEG-RGD at 24 hours. Figure 6.5B depicts fibroblasts on hydrogels incubated in acrylate-PEG-RGD diluted in 100X molar excess of sodium acrylate, and significant inhibition of cellular response is shown with only slight improvement in fibroblast attachment and spreading over the negative control with no peptide depicted in Figure 6.5C, thus demonstrating that the RGD peptide immobilized by Michael addition is responsible for fibroblast spreading.

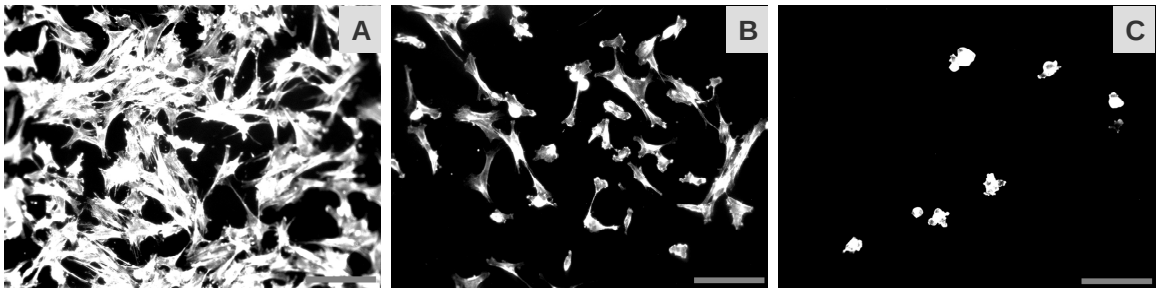

Figure 6.5 Proof of Michael addition surface conjugation of RGD peptide. NIH 3T3 cells cultured on hydrogels with immobilized (A) acrylate-PEG-RGD (1 µM), (B) acrylate-PEG-RGD (1 µM) diluted in 100 molar excess sodium acrylate, and (C) no peptide. Cells were stained for actin with rhodamine phalloidin. Scalebar = 100 µm.

Acrylation of Fibronectin

As stated previously, plasma fibronectin is a disulfide-bonded dimer consisting of a pair of 220 kDa subunits [324, 325]; therefore, a molecular weight marker with an upper limit of 250 kDa could be used with reducing SDS-PAGE for determination of molecular weight. [338] Analysis of GenBank Accession No. P07589, bovine fibronectin (Appendix A) revealed that fibronectin contains 122 lysines per mol, and the acrylate-PEG-NHS used to acrylate fibronectin has a molecular weight of 3450 Da. Conjugation of 1-4 lysines per mol of fibronectin with acrylate-PEG-NHS should result in an estimated 3-13kDa increase in molecular weight. Figure 6.6 demonstrates an approximate 8-10 kDa increase in molecular weight of the acrylated protein as evidenced by lane 2. This data demonstrates successful acrylation of the fibronectin protein.

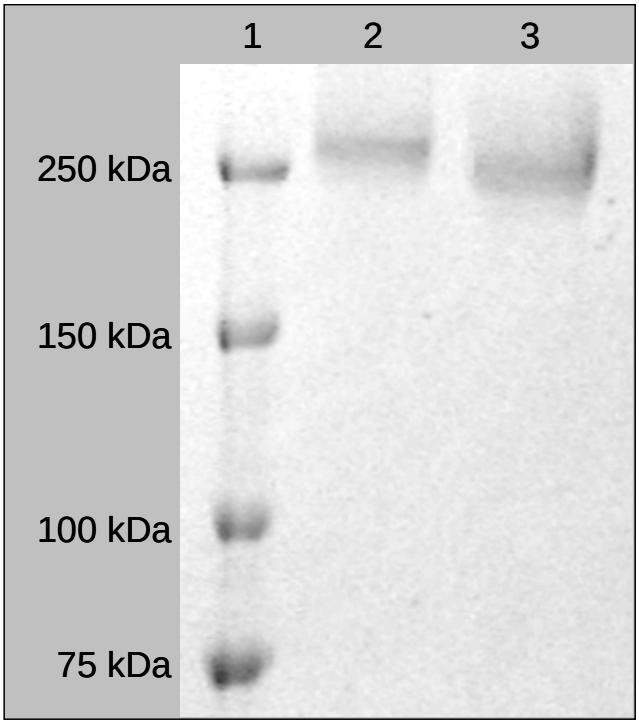

Figure 6.6 Documentation of fibronectin acrylation. Proteins were separated utilizing SDS-PAGE and stained with 0.2% Coomassie Brilliant Blue. Lane 1, molecular weight marker; lane 2, acrylated fibronectin; lane 3, non-acrylated fibronectin. Gels were loaded with equal quantities of total protein (12 µg/lane). Data is representative of three independent experiments.

NIH 3T3 Response to Encapsulated and Surface-Immobilized Acrylated Fibronectin

Dose Dependent Response of Fibroblast Spreading

The purpose of this assay was to determine if fibroblasts display a dose dependent spreading response to hydrogels with varying concentrations of encapsulated and acrylated fibronectin, in order to determine the optimal fibronectin concentrations for cell spreading and to determine conditions for analysis of proliferation rates.

Positive controls of blank 48-well TCPS and 96-well bacterial polystyrene with 10 μg/mL reduced fibronectin adsorbed overnight demonstrated significant spreading and proliferation of fibroblasts. For hydrogels with encapsulated fibronectin, pilot studies were conducted to determine the optimum timepoint of fibronectin reduction with DTT prior to addition to the T904-acrylate solution (0, 2.5, 5, 10, 15, and 30 minutes), and 5 minutes resulted in maximum cell adhesion to hydrogels with encapsulated 100μg/mL fibronectin at 24 hours (data not shown). The 2.5 and 10 minute timepoints resulted in limited cell adhesion at 24 hours and response greatly diminished at the 0, 15, and 30 minute timepoints, most likely a result of limited disulfide bond reduction at the 0 timepoint and reformation of disulfide bonds at the 15 and 30 minute timepoints.

Fibroblast spreading on hydrogels with encapsulated fibronectin is shown in Figure 6.7. The data indicates a plateau beginning at 2.5 μg/mL, and the minimum cell spread area in the plateau region was 2277 μm^2 at 2.5 μg/mL. A statistically significant difference was observed between 25 and 100 μg/mL with a maximum average cell spread area of 3400 μm^2. A statistically significant difference was also observed between 1.0 and 2.5 μg/mL concentrations; however, cell attachment upon visual observation was significantly reduced at 1.0 and 0 μg/mL concentrations, and minimal cell spread areas of 697 μm^2 and 310 μm^2, respectively, were measured.

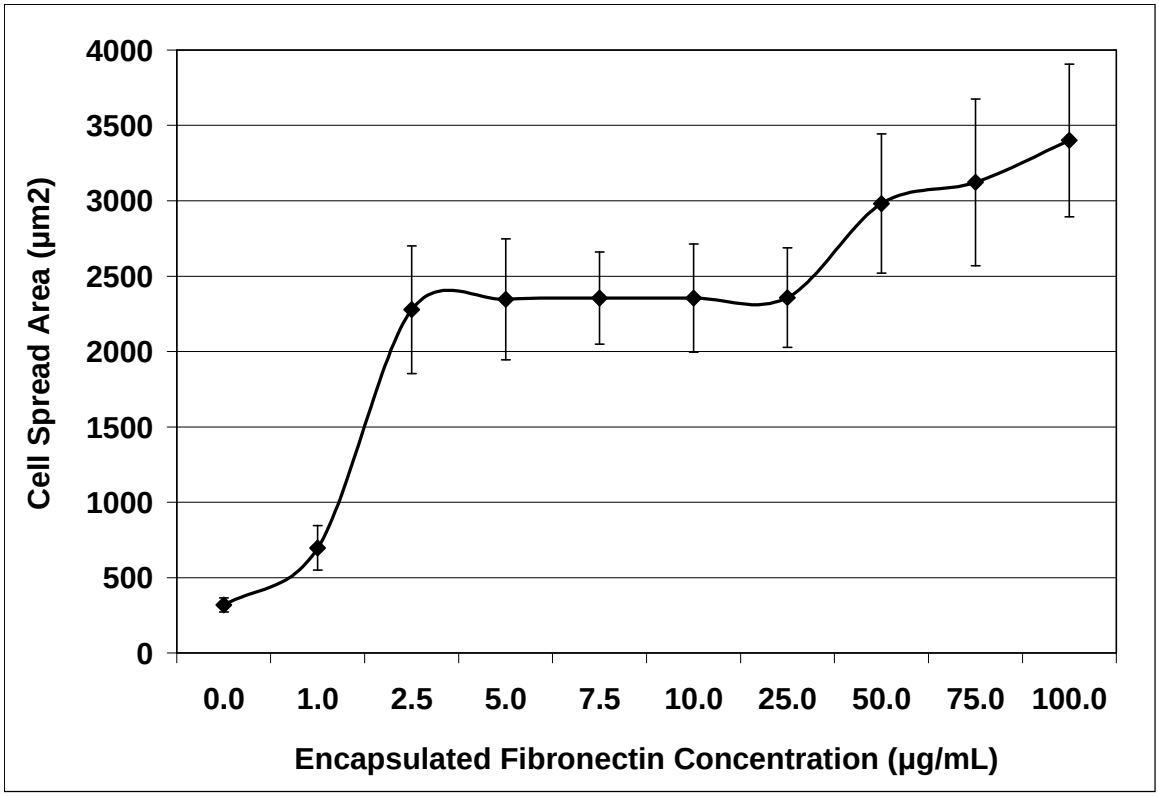

Figure 6.7 Fibroblast spreading on hydrogels with encapsulated fibronectin. Average cell areas (mean +/- standard deviation) of NIH 3T3 cells cultured on hydrogels with encapsulated fibronectin of varying concentrations. Data is representative of three independent experiments.

Figure 6.8 displays the cell spreading on hydrogels with encapsulated fibronectin representative of the average measured area for each condition.

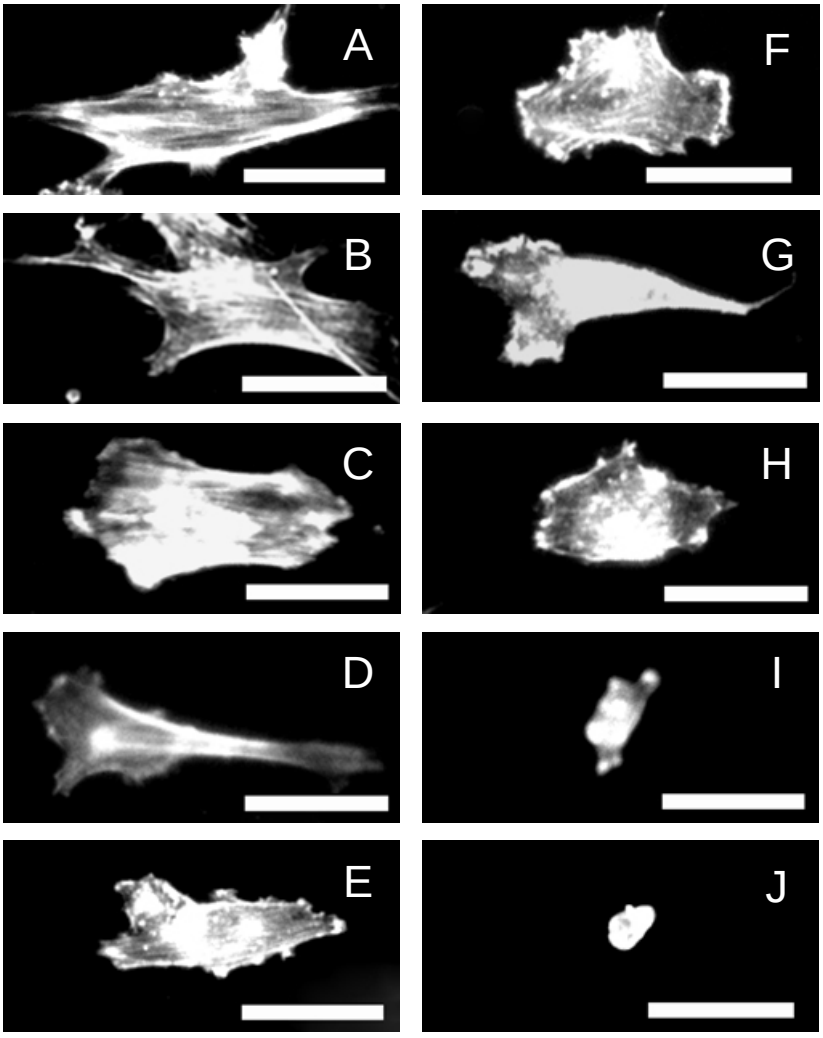

Figure 6.8 Cytoskeletal organization of fibroblasts cultured on hydrogels with varying concentrations of encapsulated fibronectin. (A) 100 µg/mL, (B) 75 µg/mL, (C) 50 µg/mL, (D) 25 µg/mL, (E) 10 µg/mL, (F) 7.5 µg/mL, (G) 5.0 µg/mL, (H) 2.5 µg/mL, (I) 1.0 µg/mL, and (J) 0.0 µg/mL Cells were stained for actin with rhodamine phalloidin. Images are representative of the average cell area for each condition. Scalebar = 50 µm.

Fibroblast spreading on hydrogels with acrylated fibronectin is shown in Figure 6.9. The data indicates an increasing trend of cell spread area in response to increasing fibronectin concentration with a maximum cell spread area of 3423 μm^2 at 100 µg/mL. A

statistically significant difference was observed between 25 and 50 μg/mL. The minimum cell spread area measured was 523 μm^2 at 5.0 μg/mL, which is comparable to the spreading seen on hydrogels with 1.0 μg/mL concentration of encapsulated fibronectin. No measurements were taken below 5.0 μg/mL due to extremely limited cell attachment.

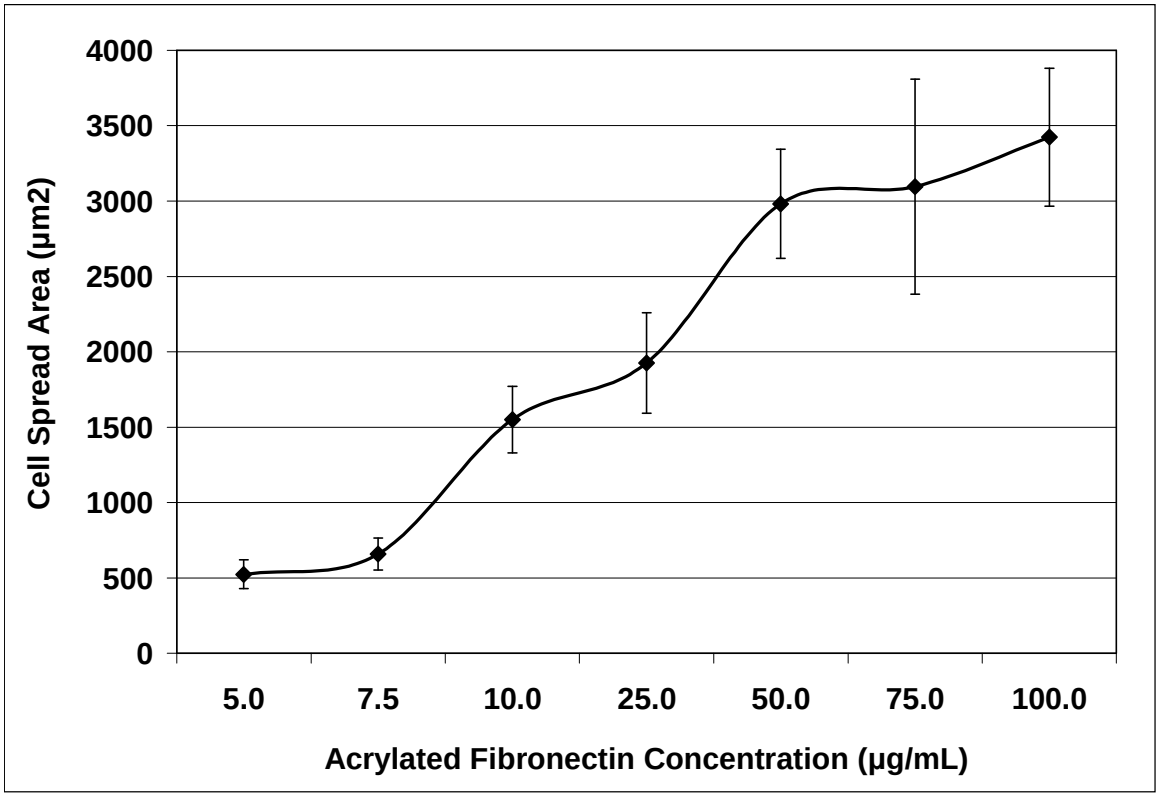

Figure 6.9 Fibroblast spreading on hydrogels with surface-immoblized acrylated fibronectin. Average cell areas (mean +/- standard deviation) of NIH 3T3 cells cultured on hydrogels with acrylated fibronectin of varying concentrations. No hydrogels with acrylated protein concentration below 5 μg/mL were measured due to extremely limited cell attachment and survival. Data is representative of three independent experiments.

Figure 6.10 displays the cell spreading on hydrogels with acrylated fibronectin representative of the average measured area for each condition.

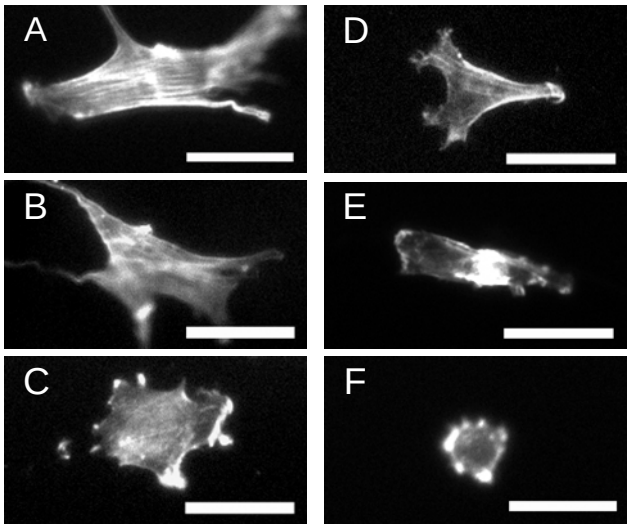

Figure 6.10 Cytoskeletal organization of fibroblasts cultured on hydrogels with varying concentrations of surface-immobilized acrylated fibronectin. (A) 100 μg/mL, (B) 75 μg/mL, (C) 50 μg/mL, (D) 25 μg/mL, (E) 10 μg/mL, and (F) 7.5 μg/mL. Cells were stained for actin with rhodamine phalloidin. Images are representative of the average cell area for each condition. Scalebar = 50 μm.

For both encapsulated and acrylated fibronectin, concentrations of 50, 75, and 100 μg/mL promoted maximum fibroblast spreading, and both methods displayed a maximum cell spread area of approximately 3400 μm^2 with 100 μg/mL of fibronectin. Encapsulated fibronectin supported fibroblast spreading at lower concentrations than acrylated fibronectin; cell spread area of approximately 2000 μm^2 was observed on hydrogels with 2.5 μg/mL of encapsulated fibronectin and 25 μg/mL of acrylated fibronectin.

Prior studies using 100 μg/mL of thiolated fibronectin immobilized to polystyrene surfaces through Pluronic-pyridyl disulfide (F108-PDS) modification demonstrated cell surface areas >8000 μm^2 [339]; therefore, future work may include higher concentrations of fibronectin to determine if increased fibroblast spreading areas are attainable on encapsulated and surface-immobilized acrylated hydrogels.

Fibroblast Proliferation Response

The purpose of this assay was to analyze cell proliferation in response to varying concentrations of encapsulated and acrylated fibronectin over the course of 5 days. Based on the results of the dose-dependent response assay for encapsulated fibronectin, an optimum concentration of 100 μg/mL and three concentrations from the plateau region were chosen based on statistically significant differences in cell spreading: 25 μg/mL, 10 μg/mL, and 2.5 μg/mL. Hydrogels with no encapsulated protein (0 μg/mL) were used as a negative control for comparison. Fibroblast proliferation on encapsulated fibronectin gels is shown in Figure 6.11.

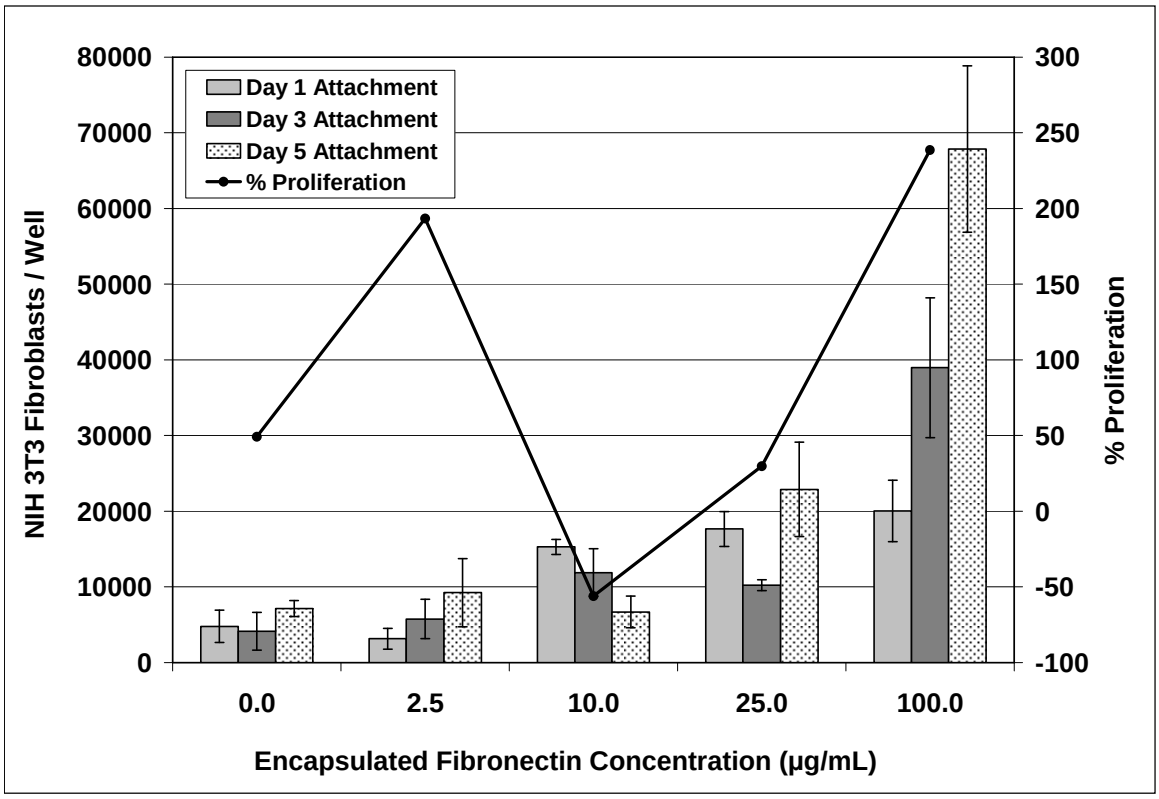

Figure 6.11 Fibroblast proliferation on hydrogels with encapsulated fibronectin of varying concentrations. Cells were seeded at a density of 10,000 cells per well. Error bars represent +/- standard deviation. Data is representative of three independent experiments.

The data indicates significant variability in cell proliferation between 2.5 µg/mL and 25 µg/mL concentrations, which corresponds to the plateau region of fibroblast spreading. Cell attachment at 2.5 µg/mL is comparable to the negative control. Although similar numbers of cells are attached at Day 1 on the 10 µg/mL, 25 µg/mL, and 100 µg/mL conditions, only the 100 µg/mL condition displayed a continual increase in cell proliferation from Day 1 to Day 5.

Hydrogels with 100 μg/mL of encapsulated fibronectin exhibited the maximum average cell spread area of 3400 μm^2 with a 240% increase in proliferation from Day 1 to Day 5. This data is consistent with reports that cell proliferation is improved with increased cell spreading. [339-342] The inconsistency in fibroblast proliferation at fibronectin concentrations below 100 μg/mL may indicate an insufficient amount of surface protein to support cell spreading and cytoskeletal organization, thus demonstrating the importance of optimized surface-ligand densities for cell proliferation. In addition, T904-acrylate hydrogels are hydrolytically degradable, and greater connectivity of fibroblasts on hydrogels with 100 μg/mL fibronectin concentration may have prevented detachment of cells from the degrading hydrogel.

Based on the results of the dose-dependent response assay for acrylated fibronectin, an optimum concentration of 100 μg/mL and three concentrations below optimum were chosen based on statistically significant differences in cell spreading: 25 μg/mL, 10 μg/mL, and 7.5 μg/mL. Hydrogels with no encapsulated protein (0 μg/mL) were included as a negative control for comparison. Fibroblast proliferation on acrylated fibronectin is shown in Figure 6.12. Although significant numbers of fibroblasts were attached at Day 1 on both the 25 μg/mL and 100 μg/mL conditions, the data indicates no cell proliferation occurred for any condition tested.

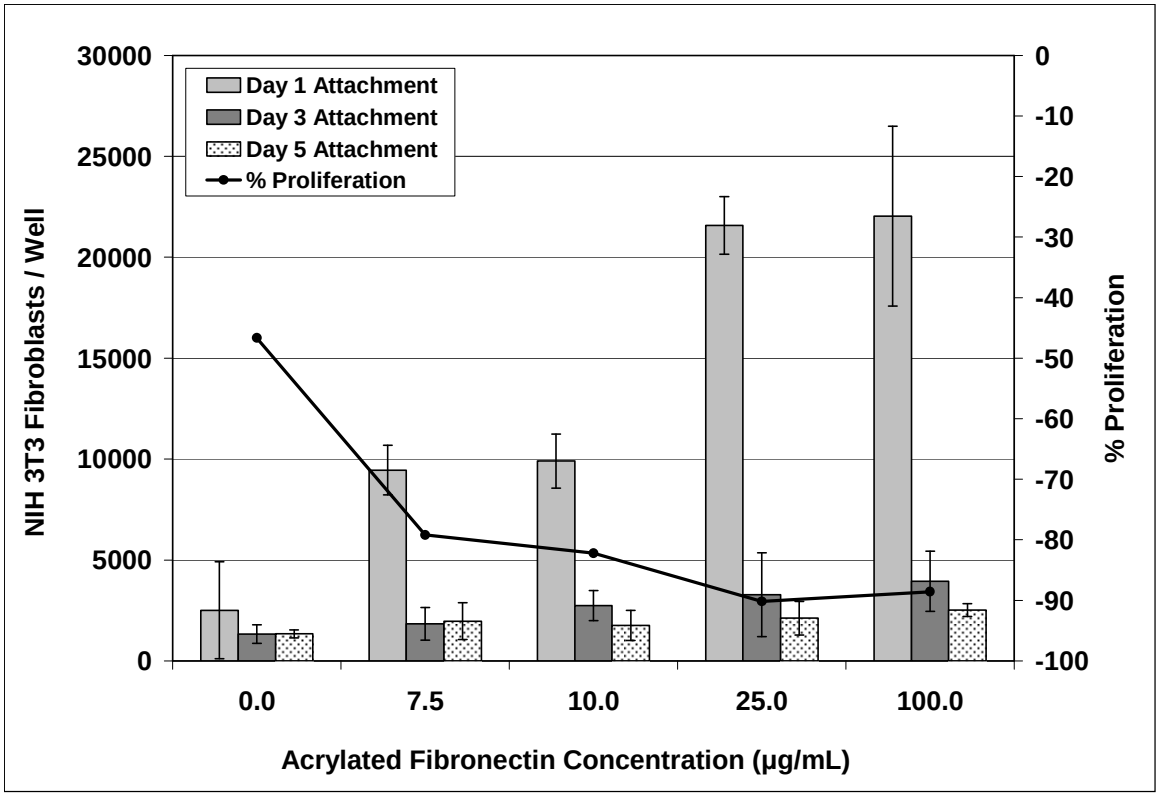

Figure 6.12 Fibroblast proliferation on hydrogels with acrylated fibronectin of varying concentrations. Error bars represent +/- standard deviation. Data is representative of three independent experiments.

This result is in stark contrast to the positive proliferation response observed for the encapsulated fibronectin 100 µg/mL condition at 3 and 5 days. The measured cell areas at 18 hours post-seeding for the 50, 75, and 100 µg/mL conditions are comparable for both encapsulated and acrylated fibronectin, indicating that surface ligand density is high enough to support cell spreading and cytoskeletal organization that is critical to cell proliferation. For both experiments, media was exchanged daily to ensure constant, fresh supply of cell nutrients, so this result is directly correlated to the immobilization strategy used. In a hydrogel with encapsulated fibronectin, hydrolytic degradation may not be

detrimental to cell proliferation because it continually exposes the fibroblasts to fibronectin, and our encapsulated 100 μg/mL fibronectin data supports this theory; however, hydrolytic degradation of T904-acrylate hydrogels with surface-immobilized acrylated fibronectin may result in loss of the surface-conjugated protein layer and inhibition of proliferation.

Another phenomenon was observed in that hydrogels incubated in non-acrylated fibronectin, an anticipated negative control, supported comparable fibroblast proliferation to hydrogels with surface-immobilized acrylated fibronectin (Figure 6.13). Because of the similarity in the lack of support for fibroblast proliferation, we can deduce that this is a surface-mediated phenomena.

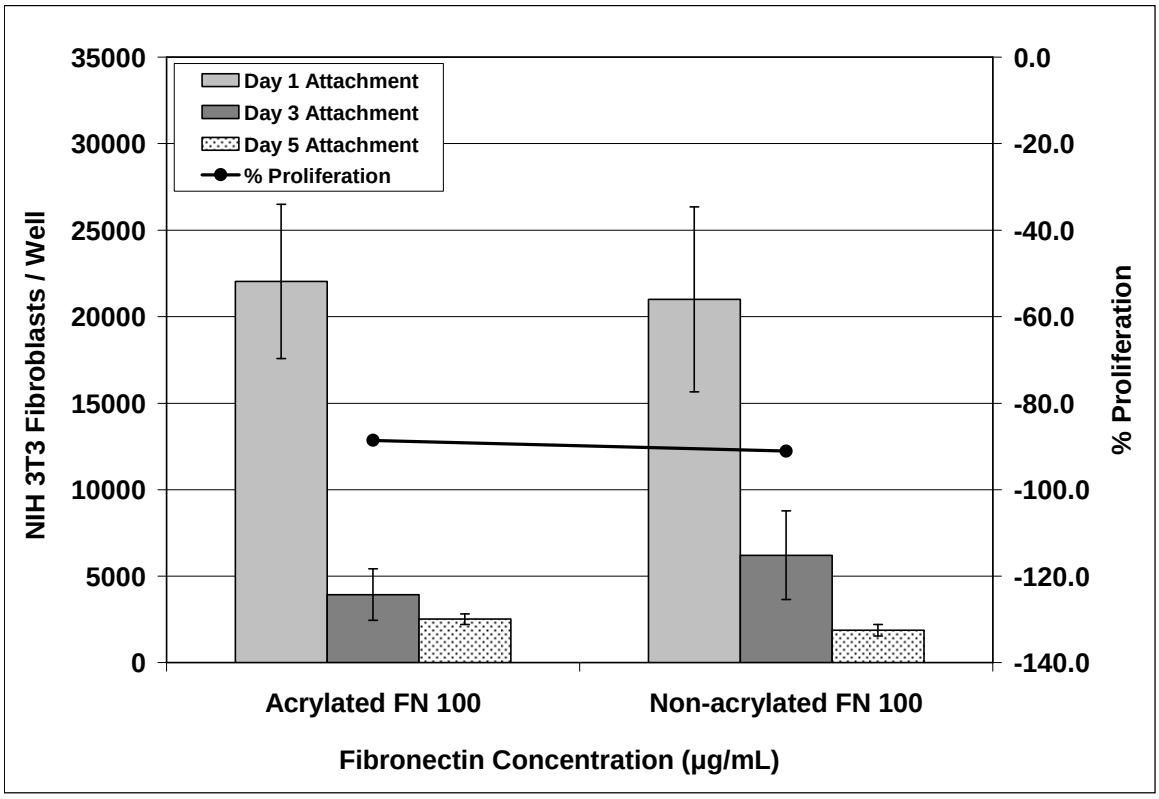

Figure 6.13 Fibroblast proliferation on hydrogels with acrylated and non-acrylated fibronectin of 100 µg/mL concentration. Error bars represent +/- standard deviation. Data is representative of three independent experiments.

The experiment with acrylate-PEG-RGD (Figure 6.4) demonstrated that fibroblast response was inhibited through competitive binding of sodium acrylate, proving the peptide was immobilized through a Michael addition conjugation. Several studies have demonstrated that fibronectin multimer formation occurs *in vitro* via the C-terminal free thiols upon exposure to a thiol reagent [343, 344] and *in vivo* depending upon exposure to metal ions. [345] Another study has shown that homocysteine binding to plasma fibronectin *in vivo* is mediated through thiol-disulfide exchange at the C-terminal

disulfide bonds. [346] We therefore hypothesize that non-acrylated fibronectin is immobilized to our hydrogel surfaces through a thiol-disulfide exchange mediated mechanism. For these experiments, fibronectin solution was added to the gel at an early timepoint of 1 hour post-polymerization, possibly exposing the protein to reactive thiolate species capable of reducing the easily accessible C-terminal disulfide bonds. In order to clarify this phenomena, further experiments with extended gelation times could be conducted to determine if more complete polymerization prior to addition of fibronectin solution will inhibit binding of non-acrylated fibronectin.

CONCLUSION

In conclusion, these studies demonstrated that surface-immobilization of reduced fibronectin to hydrogels with unreacted pendant acrylate groups is not feasible because of the inherent hydrophobicity of acrylate groups. Surface-immobilization of acrylate-PEG-RGD through Michael addition conjugation was demonstrated with a competitive binding assay using sodium acrylate to bind unreacted pendant thiols on the hydrogel surface to prevent RGD immobilization and limit fibroblast spreading and proliferation. NIH 3T3 fibroblasts exhibited maximum cell spreading at 18 hours and proliferation at 5 days on hydrogels with 100 μg/mL fibronectin concentration. Future work may include higher fibronectin concentrations beyond 100 μg/mL to further maximize the cell spreading and proliferation response and to determine if higher protein concentrations will result in more uniform proliferation rates and possibly a second plateau region of fibroblast spreading response. SDS-PAGE analysis demonstrated successful acrylation of the

fibronectin protein. NIH 3T3 fibroblasts seeded on acrylated fibronectin hydrogels displayed a positive dose-dependent spreading response to increasing concentrations of protein; however, long-term proliferation rates were significantly hindered, possibly by the hydrolytic mechanism of hydrogel degradation. In addition, a second potential mechanism of fibronectin conjugation to hydrogel surfaces via thiol-disulfide exchange is theorized, although it is likely that this mechanism will not be effective for proteins with less accessible disulfide bonds. Even with these concerns, the covalent immobilization techniques described are useful for the design of selectively adhesive substrates and may be employed currently to study neural regeneration at early timepoints in a model system to evaluate neuronal cell line and primary neuron response to immobilized neural cell adhesion molecules.

CHAPTER SEVEN

NEURONAL CELL LINE AND PRIMARY NEURON RESPONSE TO ACRYLATED TETRONIC® HYDROGELS WITH IMMOBILIZED L1

INTRODUCTION

The objectives of these experiments were to evaluate the feasibility of using HT22 mouse hippocampal B35 and rat neuroblastoma neuronal cell lines with immobilized L1, to establish primary mammalian neuron dissection protocols, to evaluate the cytocompatibility of acrylic-based Tetronic® hydrogels with primary neurons, and to demonstrate the feasibility of using acrylic-based Tetronic® hydrogels with covalently immobilized L1 for neural applications.

Inherent challenges of primary neuronal cell cultures include animal to animal and developmental age variability and potential glial cell contamination; therefore, two neuronal cells lines, HT22 mouse hippocampal and B35 rat neuroblastoma, were first studied for their ability to respond to immobilized L1 and to differentiate into neuronal phenotypes, in order to establish a model cell line to simulate neuronal response. Both HT22 and B35 cells are typically maintained in media containing 10% serum to promote rapid growth and proliferation; however, a differentiated neuronal phenotype is preferred for these experiments in order to characterize neuronal response. Hippocampal neurons are pyramidal cells, which is also the classification of neurons that are the primary excitation units of the mammalian corticospinal tract. L1 is expressed on regenerating hippocampal axons following injury [347], and neurite outgrowth of primary hippocampal neurons has been demonstrated on adsorbed and immobilized L1-Fc. [253]

HT22 cells are derived from mouse hippocampus, and both primary hippocampal and HT22 cells are typically used in neuronal survival studies. [348] L1 has been described as a survival factor for rat embryonic hippocampal neurons, as evidenced by the prevention of apoptosis when cultured in serum-free media with both soluble and substrate-bound L1 [239]; therefore, it was hypothesized that HT22 cells can attach to immobilized L1 surfaces via homophilic interactions and can be induced to differentiate into a neuronal phenotype in low or serum-free media. B35 cells express low levels of NCAM, primarily the 140 kDa isoform without the variable alternatively spliced exon (VASE) that downregulates neurite outgrowth, and close homologue of L1 (CHL1), but no detectable levels of L1 [349]; however, L1 and NCAM can bind via heterophilic interaction. [241, 350] [351] These cells are normally loosely adherent with round phase-bright cell bodies and short processes, but they have demonstrated the ability to differentiate reversibly and extend long neurites in low serum or with the addition of dibutyryl cAMP [349] ; therefore, it was hypothesized that B35 cells could attach to immobilized L1 surfaces via heterophilic interactions with NCAM and could be induced to differentiate in low or serum-free media.

A protocol for embryonic day 8 chick forebrain dissection was established in Chapter 5. Although chick forebrain neurons are suitable for initial studies, it is preferable to use mammalian-derived cells for future work; therefore, rat postnatal day 7 cerebellar and dorsal root ganglia dissection protocols were established.

Michael addition methods established in the previous chapter were used to fabricate hydrogels and to evaluate immobilization of L1.

MATERIALS AND METHODS

B35 and HT22 Cell Culture

B35 rat neuroblastoma and HT22 mouse hippocampal cells were a generous gift from Dr. Karl Franek (Greenwood Genetics Center) and were routinely maintained in 75 cm^2 T-flasks in a humidified chamber at 37°C with 7% CO2 atmosphere in 50/50 Dulbecco's Modified Eagle's Medium and Ham's F-12 with L-glutamine (DMEM/F12 1X, Mediatech) supplemented with 10% v/v bovine growth serum (BGS, Hyclone) and 50 I.U./mL penicillin and 50 µg/mL streptomycin (Mediatech). Culture medium was changed once every two days and cells were passaged weekly. For experiments, monolayers of cells were trypsinized, centrifuged, resuspended, counted in a hemacytometer, and adjusted to the appropriate final concentrations.

Neuronal Differentiation of HT22 and B35 Cells

96-well bacterial polystyrene plates were sterilized with ethylene-oxide. The laminin and fibronectin extracellular matrix proteins were included as positive controls for cell attachment and as a comparison to L1 for evaluation of neuronal differentiation. Laminin, fibronectin, and L1 were adsorbed overnight at room temperature to bacterial polystyrene plates at 10 µg/mL concentration followed by two sterile PBS rinses. Serum, reduced serum, and serum-free media formulations were tested: (1) DMEM/F12 supplemented with 10% v/v BGS and 50 I.U./mL penicillin and 50 µg/mL streptomycin, (2) DMEM/F12 supplemented with 2% v/v BGS and 50 I.U./mL penicillin and 50 µg/mL streptomycin, and (3) Neurobasal-A (Gibco) supplemented with 2% v/v B27 supplement

(Gibco) and 2mM L-glutamine per manufacturer's guidelines for tumor cell lines, and 50 I.U./mL penicillin and 50 µg/mL streptomycin. For the serum-free media condition, three cell seeding methods were employed: (1) cells were directly seeded in serum-free media, (2) cells were first seeded in 2% serum media for 2 hours followed by replacement with serum-free media to enhance attachment and survival, (3) cells were seeded according to condition 2 with the addition of 20ng/mL nerve growth factor (NGF) to further enhance differentiation into a neuronal phenotype. HT22 and B35 monolayers were trypsinized, centrifuged, resuspended, counted in a hemacytometer, and seeded at a density of 10,000 cells per 96-well. At 24 hours post-seeding, the cells were fixed in 4% paraformaldehyde in PBS for one hour at room temperature and and phase contrast images were obtained with a 20X objective.

Primary Mammalian Neuron Dissection

Postnatal day 7 rat neuron dissection protocols were developed for both cerebellar neurons [253, 352] and dorsal root ganglia (DRG) [353] and are included in Appendices C and D, respectively. Laminin (10 µg/mL) was adsorbed to 96-well bacterial polystyrene plates overnight at room temperature. Cerebellar neurons were seeded at a density of 20,000 cell per 96-well, and DRG were seeded at a density of 10,000 cells per 96-well. After 24 hours, cells were fixed for 1 hour in 4% paraformaldehyde and stained for actin microfilaments using Alexa Fluor® 594 phalloidin (Molecular Probes, 0.161 µM) and digital fluorescent images were obtained.

Cytocompatibility of T904-Acrylate Hydrogels with Primary Neurons

Poly-l-lysine (PLL) was absorbed to 24-well plates in a 0.1% concentration for one hour followed by three water rinses and overnight drying. A 23% T904-acrylate hydrogel solution with a 1:1 acrylate:thiol ratio was prepared as previously described for encapsulated fibronectin hydrogels in Chapter 6. A thin layer of hydrogel solution (10μL) was spread over the surface of two wells coated with PLL and allowed to polymerize via Michael addition for 2 hours at room temperature followed by overnight at 37°C. Adsorbed 0.1% PLL wells were included as positive controls. Primary chick forebrain neurons from embryonic day 8 chicks were dissected and prepared as described in Chapter 5 and were seeded at a density of 80,000 cells per well with no rinsing of the wells prior to seeding. After 24 hours, the cells were fixed in 4% paraformaldehyde in PBS for one hour at room temperature and phase contrast images were obtained with a 10X objective.

T904-Acrylate Hydrogels with Encapsulated L1

These experiments are based on the immobilization method depicted in the Chapter 6 (Figure 6.1A). The response of B35 and primary chick forebrain neurons to 70μg/mL of encapsulated L1 was evaluated using 1mm thick, 30μL hydrogels in 96-well tissue culture polystyrene (TCPS) plates at 24 hours postseeding.

Sterilization of Components Used in Hydrogel Fabrication

Prior to making hydrogels, all components were sterilized. Uncharged glass coverslips (Fisher) were UV sterilized for 20 minutes in the cell culture hood. Binder

clips, 1mm thick Teflon spacers, vacuum grease, spatulas, and forceps were autoclaved prior to use. All experiments were conducted in the cell culture hood using aseptic technique.

Concentration of L1

The L1 protein produced as previously described in Chapter 5 typically displayed a concentration range of 60-160 μg/mL; therefore, the protein was first concentrated to a 700μg/mL concentration in order be able to attain a 70μg/mL encapsulated L1 concentration within the hydrogels. A buffer exchange of six 600μL aliquots of 150 μg/mL L1 protein into 50mM PBS, pH 7.4 with 21% salt concentration was performed utilizing a 5.0 mL Zeba desalt column (Pierce) according to the manufacturer's instructions. The protein was frozen overnight at -80°C, lyophilized, resuspended in 771 μL of sterile water in order to maintain appropriate salt concentration, and stored at 4°C.

Preparation of Hydrogels

A 28.75% T904-acrylate hydrogel solution and a 1:1 acrylate:thiol ratio as described for encapsulated fibronectin hydrogels in Chapter 6 was used for this experiment. L1 was mixed with dithiothreitol (DTT) for 5 minutes at room temperature with shaking. This protein/DTT mixture was added to room temperature T904-acrylate solution, the gel solution was vortexed briefly, tap-spinned, and immediately pipetted in between two glass slides separated by 1mm Teflon spacers. The hydrogels were allowed to crosslink via Michael addition in the dark for 2 hours at room temperature followed by overnight at 37°C in parafilmed petri dishes with sterile water to provide a humid environment. The next morning, vacuum grease was added to the bottom of 96-well

TCPS plates and sterilized under UV light for 20 minutes. The hydrogels were carefully removed from the glass slides by rinsing with sterile PBS and were placed in the wells, gently pressing them down onto the vacuum grease to prevent floating, and hydrated in 100 μL of PBS per well at 37°C until cell seeding. Hydrogels without protein were used as negative controls. Bacterial polystyrene wells with 10 μg/mL L1 and 10 μg/mL reduced L1 adsorbed overnight were used as positive controls for visual confirmation of cell health and bioactivity of reduced protein.

Cell Seeding

B35 cells were seeded at a density of 20,000 cells per 96-well in DMEM/F12 with L-glutamine supplemented with 10% v/v bovine growth serum (Hyclone) and 50 I.U./mL penicillin and 50 μg/mL streptomycin (Mediatech). Medium containing 10% serum was chosen for initial experiments to enhance cell attachment to the hydrogels. Primary chick forebrain cells derived from 8-day old chicks as previously described in Chapter 5 were seeded at a density of 20,000 cells per 96-well based on successful results of this seeding density on 96-well bacterial polystyrene wells with 10 μg/mL L1 adsorbed overnight. Cells were observed at 24 hours post-seeding.

T904-Acrylate Hydrogels with Surface-Immobilized Reduced L1

These experiments are based on the immobilization method depicted in the Chapter 6 (Figure 6.1B). The response of B35 and primary chick forebrain cells to 100μg/mL of surface-immobilized L1 was observed using 70μL hydrogels polymerized directly in 96-well tissue culture polystyrene (TCPS) plates at 24 hours postseeding.

Reduction of L1

Analysis of the amino acid sequence of the 140 kDa cloned fragment of L1 based on GenBank accession no. NM_000425 (Appendix E) revealed that L1 contains 14 cysteines per mol. A 150 μg/mL solution is equivalent to 0.0011 mmol/L concentration of protein. Protein solutions are typically reduced with 1mM to 10 mM DTT. A 2.5 mM DTT solution was used to reduce L1 [276], resulting in an approximate 2273 molar excess of DTT to L1, or an approximate 325-molar excess of DTT thiols to L1 cysteines. A 10X 25mM stock solution of DTT in 50mM PBS pH 7.4 buffer was made, 10% by volume was added to the 1mg/mL fibronectin solution for a final 2.5 mM DTT concentration, and reacted for 1 hour at room temperature. Unreacted DTT was removed by column filtration using a PD-10 column and 50mM PBS pH 7.4 buffer followed by analysis of protein concentration via measurement of absorbance at 280nm. Protein samples were kept on ice following filtration and during protein concentration analysis.

Preparation of Hydrogels

A 28.75% T904-acrylate hydrogel solution and a 1:1.1 acrylate:thiol ratio as described for reduced fibronectin hydrogels in Chapter 6 was used for this experiment. PBS and DTT were directly added to room temperature T904-acrylate solution, and the gel solution was vortexed briefly, tap-spinned, and 70μL was immediately pipetted directly into 96-well TCPS plate and allowed to crosslink via Michael addition in the dark for 1 hour at room temperature. After 1 hour, reduced L1 solution (100μL per well) of 100 μg/mL concentration was added and left for an additional hour at room temperature. Hydrogel crosslinking and L1 reduction were coordinated such that reduced

L1 solution was added to the hydrogels immediately upon completion of reduced L1 concentration analysis, to minimize the possibility of disulfide bond reformation.

Following 1 hour incubation in reduced protein at room temperature, the plate was parafilmed and transferred to 37°C overnight with shaking. The next morning, gels were rinsed with 200μL of sterile PBS three times and hydrated in 100μL of sterile PBS per well at 37°C until cell seeding. Hydrogels without protein were used as negative controls. Bacterial polystyrene wells with 10 μg/mL L1 and 10 μg/mL reduced L1 adsorbed overnight were used as positive controls for visual confirmation of cell health and bioactivity of reduced protein.

Cell Seeding

B35 cells were seeded at a density of 20,000 cells per 96-well in DMEM/F12 with L-glutamine supplemented with 10% v/v bovine growth serum (Hyclone) and 50 I.U./mL penicillin and 50 μg/mL streptomycin (Mediatech). Medium containing 10% serum was chosen for initial experiments to enhance cell attachment to the hydrogels. Primary chick forebrain cells derived from 8-day old chicks as previously described in Chapter 5 were seeded at a density of 20,000 cells per 96-well based on successful results of this seeding density on 96-well bacterial polystyrene wells with 10μg/mL L1 adsorbed overnight. Cells were observed at 24 hours post-seeding.

Preparation of Acrylated L1

These experiments are based on the immobilization method depicted in the Chapter 6 (Figure 6.1C).

Concentration of L1

The L1 protein produced as previously described in Chapter V typically displayed a concentration range of 60-160 μg/mL; therefore, the protein first had to be concentrated to a 1mg/mL concentration in order to prevent hydrolysis of the NHS-ester during acrylation. A buffer exchange of two 1.5mL aliquots of 60 μg/mL L1 protein into 50mM PBS, pH 7.4 with 6% salt concentration was performed utilizing 2.0 mL Zeba desalt columns (Pierce) according to the manufacturer's instructions. The protein was frozen overnight at -80°C, lyophilized, resuspended in 180 μL of sterile water in order to maintain appropriate salt concentration, and stored at 4°C.

Acrylation Reaction

Analysis of the amino acid sequence of the 140 kDa cloned fragment of L1 based on GenBank accession no. NM_000425 (Appendix E) revealed that L1 contains 71 lysines per mol. Standard reaction conditions for NHS-containing crosslinkers call for 0.1-10 mM concentrations. The L1 fragment cloned as described in Chapter V is a 140 kDa protein, and a 1 mg/mL solution is equivalent to 0.0071 mmol/L concentration of protein. Typically, 2 to 50-fold molar excesses of crosslinker are used for reactions, and a 50 molar excess of crosslinker to L1 was used, resulting in a 0.36M concentration of acrylate-PEG-NHS used for this reaction. A 10X solution of 12.4 mg/mL acrylate-PEG-NHS in anhydrous DMSO was made fresh for each reaction, and 10μL of this solution

was added to 100 µL of 1mg/mL L1 for an organic solvent carryover of 10% final volume in the aqueous reaction, and reacted for 2 hours at room temperature with shaking. At the completion of the reaction, a buffer exchange into 50mM PBS pH 7.4 was performed using 0.5 mL Zeba desalt columns (Pierce), according to the manufacturer's instructions, to remove unreacted crosslinker and solvent contamination. The acrylated protein was stored at 4°C protected from light.

Electrophoresis of Acrylated L1

Samples of acrylated and non-acrylated L1 were immediately collected for SDS-PAGE (sodium dodecyl polyacrylamide gel electrophoresis) analysis (3 µL protein diluted in 6 µL PBS + 3 µL 4X reducing buffer) and immediately frozen at -80°C. Protein samples were separated by SDS-PAGE on a 6% polyacrylamide gel using Tris-glycine buffer under reducing conditions at 100V for 150 minutes. The gel was silver stained (SilverSNAP® Stain Kit II, Pierce) and imaged using a Kodak Electrophoresis Documentation and Analysis System 120.

RESULTS AND DISCUSSION

Neuronal Differentiation of HT22 and B35 Cells

Figure 7.1 shows the phase contrast images of HT22 cells on different adsorbed proteins under varying media conditions.

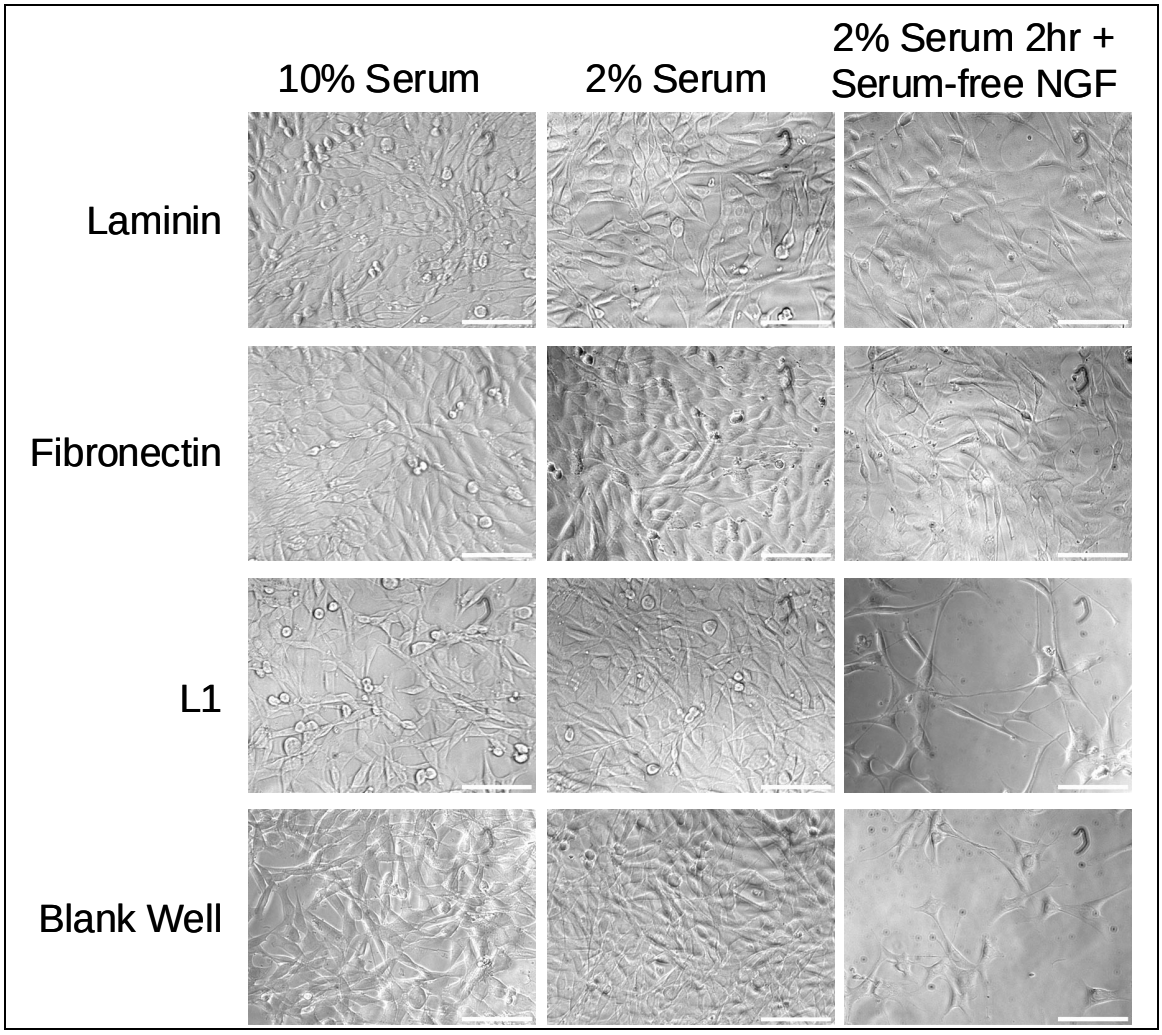

Figure 7.1 Phase contrast images of HT22 mouse hippocampal cells attached to protein-adsorbed wells under varying media conditions. Scalebar = 100 µm.

HT22 cells proliferated extensively on adsorbed laminin and fibronectin under all media conditions tested, and on blank wells under 10% and 2% serum conditions. Slightly less proliferation was observed on adsorbed L1 under 10% and 2% serum conditions. The cells exhibited limited attachment to adsorbed L1 and blank wells when plated directly in serum-free media (data now shown); however, plating in 2% serum media for 2 hours followed by replacement with serum-free media supplemented with

20ng/mL NGF enhanced differentiation into a neuronal phenotype on both adsorbed L1 and blank wells, as evidenced by the arrest of proliferation and the development of pyramidal neuron morphology with neurite outgrowth. Although L1 has been described as a potential survival factor for primary rat embryonic hippocampal neurons in serum-free media [239], its survival role for the HT22 cell line is unknown, and in this experiment, HT22 cells did not attach when cells were plated directly in serum-free media. The similar appearance of the L1 and blank wells for the 2% serum media for 2 hours followed by replacement with serum-free media supplemented with 20ng/mL NGF condition may be attributed to adsorption of media proteins to the hydrophobic bacterial polystyrene surface during the 2 hour incubation in serum media. Because T904-acrylate hydrogels limit protein adsorption, immobilization of L1 to these hydrogels may enable better evaluation of the role of L1 in HT22 attachment and neuronal differentiation.

Figure 7.2 shows the phase contrast images of B35 cells on different adsorbed proteins under varying media conditions.

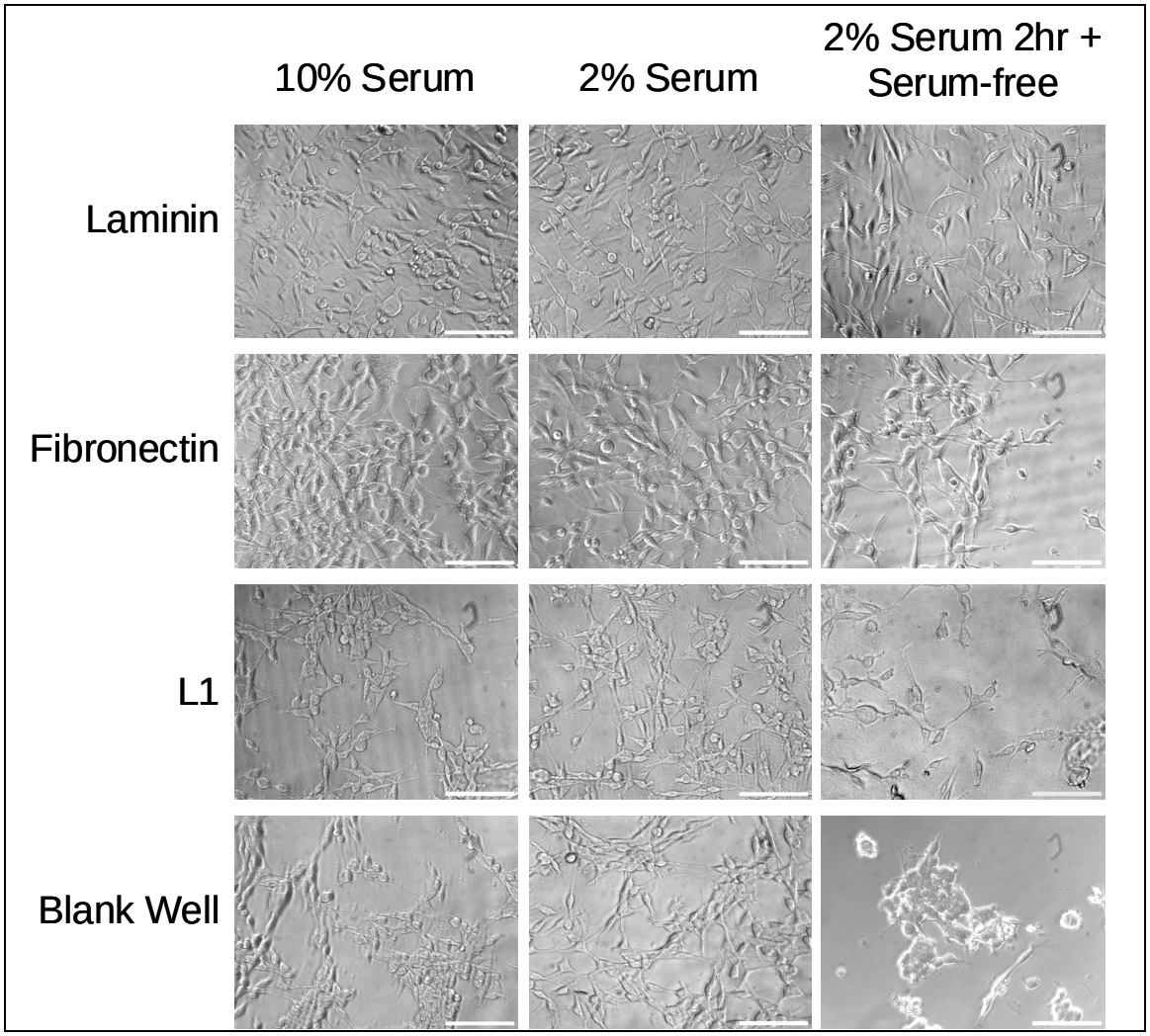

Figure 7.2 Phase contrast images of B35 rat neuroblastoma cells attached to protein-adsorbed wells under varying media conditions. Scalebar = 100 µm.

B35 cells survived and proliferated extensively on adsorbed laminin and fibronectin under serum conditions with slightly less proliferation observed on the 2% serum followed by serum-free media condition. Less proliferation was observed on L1 and blank wells under serum conditions and limited attachment occurred when plated directly in serum-free media (data not shown). When cells were plated in 2% serum for 2 hours followed by serum-free media, arrestment of proliferation occurred on adsorbed L1

and blank wells, but because B35 cells appear to extend neurites even while proliferating, it is difficult to distinguish changes in morphology. No differences were observed with the addition of NGF to serum-free media (data now shown). Although distinct morphological differences are not evident, limited attachment of cells to blank wells in 2% serum for 2 hours followed by serum-free media as compared to L1 indicates that L1 does support attachment of B35 cells. Because T904-acrylate hydrogels limit protein adsorption, immobilization of L1 to these hydrogels may enable better evaluation of the role of L1 in B35 attachment.

Primary Mammalian Neuron Dissection

Primary neurons are sensitive to media osmolalilty; embryonic chick brain has measured approximately 272 mOsm [Bray, 1991 #729] and adult rat brain has measured approximately 307 mOsm. [Bandaranayake, 1978 #730] The measured osmolalities of three of our media formulations are Basal Medium Eagle (BME, 291 mOsm), DMEM/F12 with L-glutamine (322 mOsm), and Neurobasal (224 mOsm). Although both BME and DMEM/F12 are close to the measured osmolality of rat brain, BME was chosen for CNS-derived chick and rat neurons because it does not contain L-glutamine, allowing supplementation at the time of use. L-glutamine is unstable and is rapidly decomposed into ammonia, which is toxic to CNS-derived neurons in concentrations of less than 600μM. [354] [355, 356]

Figure 7.3 shows extensive neurite outgrowth from rat postnatal day 7 cerebellar neurons cultured on laminin. Rat cerebellar neurons also responded favorably to L1 (data not shown).

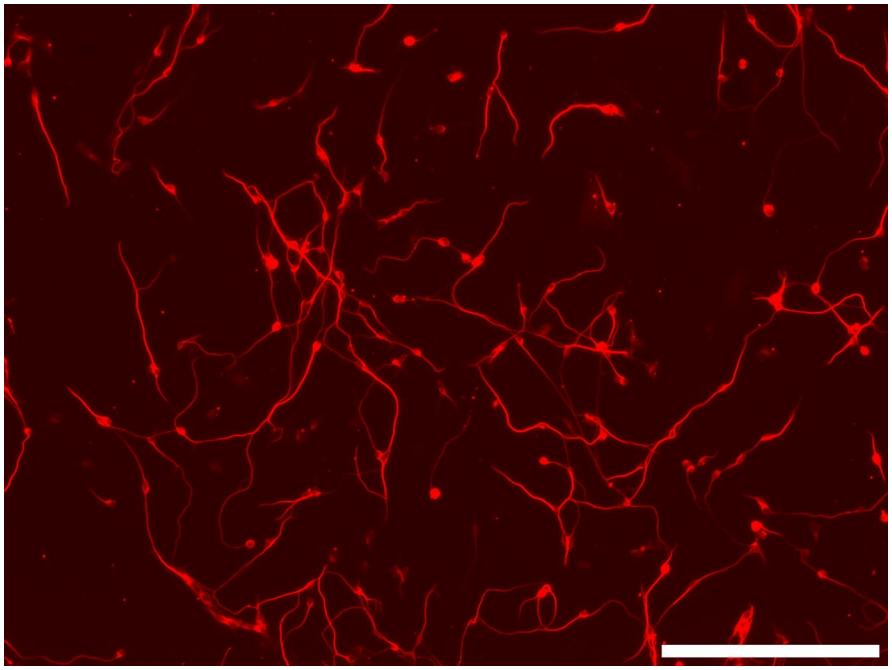

Figure 7.3 Rat postnatal day 7 cerebellar neurons cultured on adsorbed 10 µg/mL laminin. Neurons were cultured 24 hours and then stained for actin (red). Scalebar = 100µm.

Figure 7.4 shows extensive neurite outgrowth and neural networks from rat postnatal day 7 dorsal root ganglia cultured on laminin.

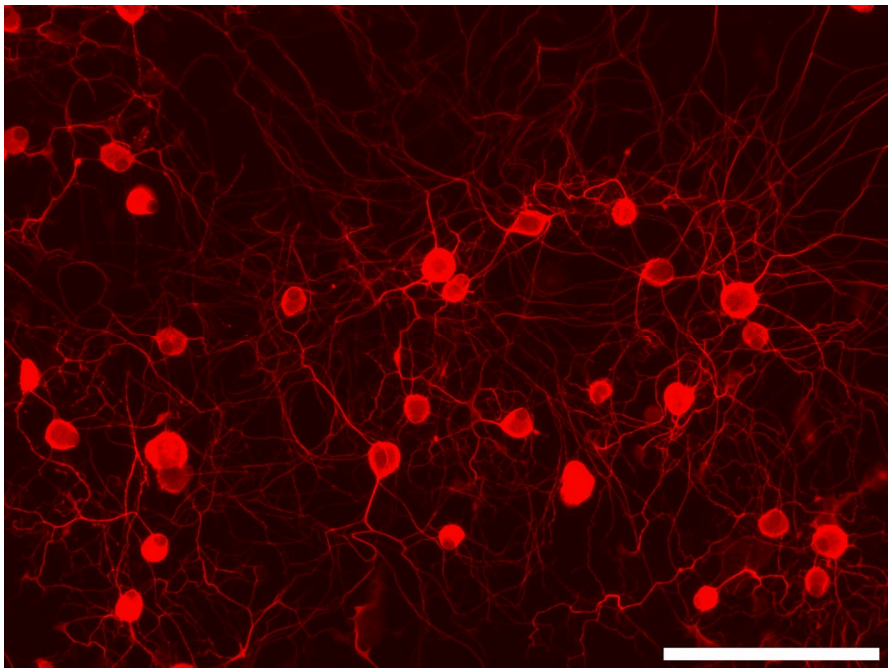

Figure 7.4 Rat postnatal day 7 dorsal root ganglia cultured on adsorbed 10µg/mL laminin. Neurons were cultured 24 hours and then stained for actin (red). Scalebar = 100µm.

Although DRG are a commonly used model to assess neural regeneration, these cells did not attach to adsorbed L1, but did attach to adsorbed fibronectin, on which CNS-derived chick forebrain and rat cerebellar neurons did not attach (data not shown). All primary cells (chick forebrain, rat cerebellar, rat DRG) responded favorably to adsorbed laminin, as expected. In addition, DRG cell bodies are surrounded by satellite Schwann cells that form a discrete anatomical unit. [25] Efforts to remove these contaminating Schwann cells by plating them out on bacterial polystyrene plates prior to DRG cell seeding resulted in incomplete removal of contaminating cells, with resultant Schwann cell proliferation and an inability to ascertain if neurite outgrowth was the result of glial cell support or the cell adhesion molecule. Another approach taken to eliminate glial cell

contamination was to use cytosine arabinoside, a mitotic inhibitor, to prevent the proliferation of Schwann cells; however, the DRG did not survive under these conditions, possibly due to cytotoxicity resulting from noncompetitive antagonism of nerve growth factor (NGF) that is essential for DRG survival. [357, 358] In conclusion, rat postnatal day 7 cerebellar neurons were determined to be the ideal mammalian primary cell model for future work with L1 immobilized to T904-acrylate hydrogels.

Cytocompatibility of T904-Acrylate Hydrogels with Primary Neurons

Figure 7.5 is a phase contrast image of chick forebrain neurons cultured on 0.1% PLL (positive control, 7.5A) and on 0.1% PLL in the presence of a hydrogel (7.5B).

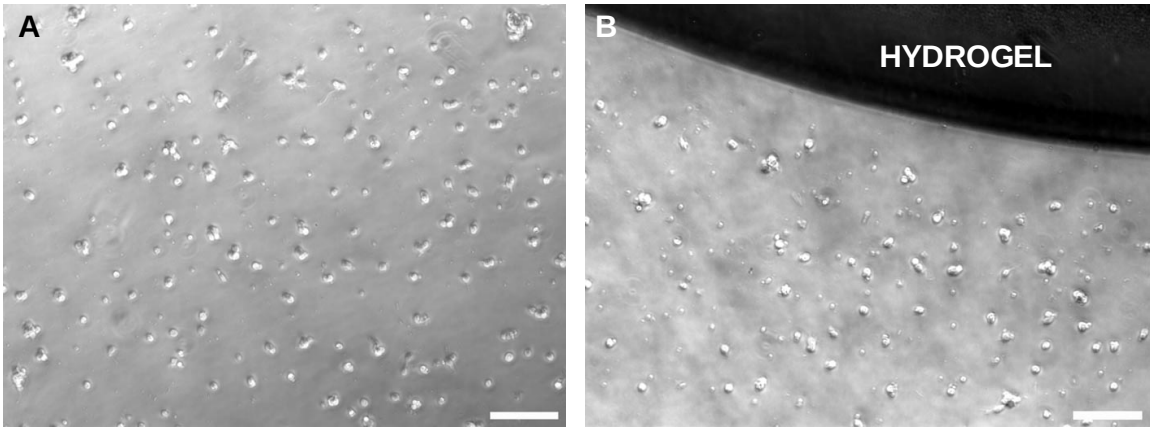

Figure 7.5 Documentation of cytocompatibility. Phase contrast images of chick embryonic day 8 forebrain neurons cultured on (A) 0.1% PLL and (B) 0.1% PLL in the presence of a T904-acrylate hydrogel. Scalebar = 100µm.

The bright, round cell bodies indicate healthy cells with no discernable difference between the positive control and cells exposed to the hydrogel with no rinsing prior to cell seeding.

Neuronal Response to T904-Acrylate Hydrogels with Encapsulated L1

B35 and primary chick forebrain neurons showed little evidence of attachment to hydrogels with encapsulated L1 70μg/mL, comparable to hydrogels with no protein. Positive controls of 96-well bacterial polystyrene wells with 10 μg/mL L1 and 10 μg/mL reduced L1 adsorbed overnight demonstrated significant attachment and proliferation of B35 cells, and significant attachment and neurite outgrowth of primary chick forebrain neurons at 24 hours. This is in stark contrast to the favorable spreading response of NIH 3T3 fibroblasts on encapsulated fibronectin hydrogels of 50, 75, and 100 μg/mL concentrations. NIH 3T3 cell attachment to fibronectin is primarily mediated through RGD, an integrin binding tripeptide in the FN-III repeat; however, Ig domains 1-6 reproduce the full biological activity of the entire L1 extracellular region, while Ig domains 1-4 are the minimum regions necessary for homophilic binding. [274] Ig domains 1-6 are linked by disulfide bonds and these bonds are reduced with DTT prior to encapsulation within the T904-acrylate hydrogels. We therefore hypothesize that the L1 protein loses bioactivity upon encapsulation into T904-acrylate hydrogels via Michael addition because of a change in conformation that occurs when the reduced disulfide bonds of Ig domains 1-6 bind with acrylate groups within the hydrogel. As a result, no further experiments were conducted utilizing encapsulated L1.

Neuronal Response to T904-Acrylate Hydrogels with Surface-Immobilized Reduced L1

B35 and primary chick forebrain neurons showed little evidence of attachment to hydrogels with reduced L1, comparable to hydrogels with no protein. Positive controls of 96-well bacterial polystyrene wells with 10 μg/mL L1 and 10 μg/mL reduced L1 adsorbed overnight demonstrated significant attachment and proliferation of B35 cells, and significant attachment and neurite outgrowth of primary chick forebrain neurons at 24 hours. Acrylate groups are inherently hydrophobic because their CH=CH2 carbonaceous side groups are non-polar and thus do not attract water strongly. We hypothesize that this immobilization technique failed because the inherent hydrophobicity of the acrylate groups contributes to their retreat within the hydrogel upon application of the hydrophilic reduced L1 solution, thus hindering the Michael addition protein conjugation reaction. An alternative explanation is that the filtration method used may not be sufficient to remove all excess DTT, possibly resulting in a reformation of L1 disulfide bonds prior to adding the solution to the hydrogels. As a result, no further experiments were conducted utilizing reduced L1.

Acrylation of L1 For Surface-Immobilization To T904-Acrylate Hydrogels

Analysis of the amino acid sequence of the 140 kDa cloned fragment of L1 based on GenBank accession no. NM_000425 (Appendix E) revealed that L1 contains 71 lysines per mol, and the acrylate-PEG-NHS used to acrylate fibronectin has a molecular weight of 3450 Da. Conjugation of 1-4 lysines per mol of L1 with acrylate-PEG-NHS should result in an estimated 3-13kDa increase in molecular weight. Figure 7.6

demonstrates an approximate 8-10 kDa increase in molecular weight of the acrylated protein as evidenced by lane 3. This data demonstrates successful acrylation of the L1 protein.

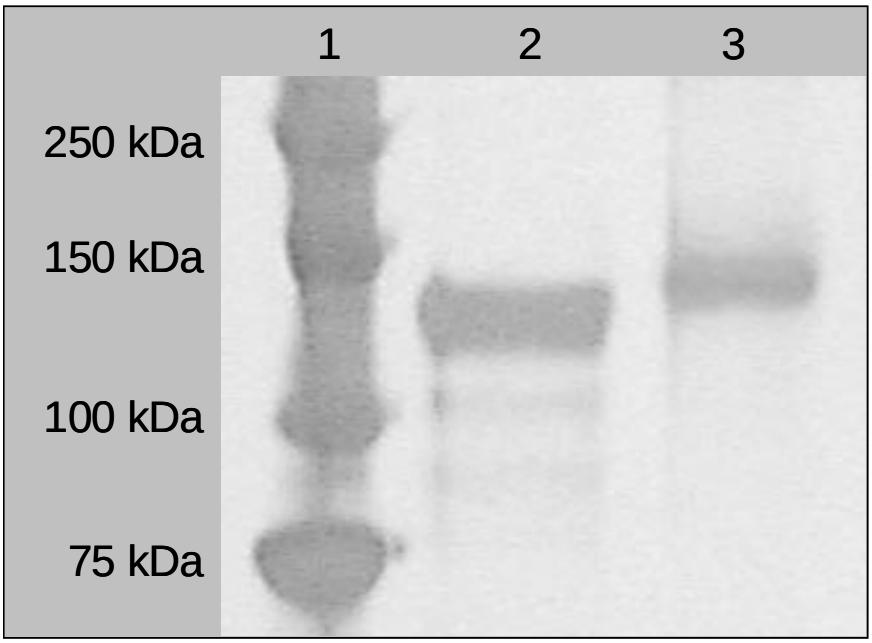

Figure 7.6 Documentation of L1 acrylation. Proteins were separated utilizing SDS-PAGE and stained with Silver Stain (Pierce). Lane 1, molecular weight marker; lane 2, L1; lane 3, acrylated L1. Gels were loaded with equal quantities of total protein (3 µg/lane).

Previous efforts to acrylate lower concentrations of L1 were unsuccessful, likely due to hydrolysis of the NHS-esters.

CONCLUSION

In conclusion, these studies demonstrate that both HT22 and B35 cells may be used to model neuronal cell response to immobilized L1 on a hydrogel surface when cultured in 2% serum for 2 hours followed by serum-free media with and without NGF, respectively. B35 cells display clearer evidence of attachment to L1 and do not require the addition of NGF; however, B35 are loosely adherent and care must be taken when changing media to avoid cell detachment. Mammalian neuron dissection methods for rat postnatal day 7 cerebellar neurons and dorsal root ganglia were developed, but cerebellar neurons were determined to be the ideal primary mammalian neuronal model for future L1 studies. T904-acrylate hydrogels with no rinsing prior to cell seeding were not toxic to primary chick embryonic day 8 forebrain neurons cultured on PLL at 24 hours. These studies also indicate that hydrogels with encapsulated and reduced L1 are not suitable for neural regeneration strategies, possibly due to a conformational change of the protein and hydrophobicity of acrylate groups, respectively. SDS-PAGE analysis demonstrated successful acrylation of the L1 protein, but only when a 1 mg/mL concentration was used; lower concentrations were probably not sufficient to prevent hydrolysis of the NHS-ester during the acrylation reaction. Future work should include further analysis of immobilized acrylated L1 to T904-acrylate hydrogels to study neural regeneration at early timepoints with the conditions described for HT22 or B35 neuronal cell lines and with chick embryonic day 8 and rat postnatal day 7 primary neurons.

CHAPTER EIGHT

CONCLUSION AND RECOMMENDATIONS

CONCLUSION

The first objective of this research was to clone and express a bioactive 140kDa fragment of L1 neural cell adhesion molecule, chosen for its critical role in proper nervous system development and because it has demonstrated selectivity of neuron adhesion in the presence of astrocytes, which play a major role in nervous system inflammation. These studies described the expression of a 140 kDa extracellular fragment of L1 in the baculovirus/insect cell expression system with an average yield of approximately 250-300 µg per $1x10^8$ High Five cells and comparable neurite outgrowth as compared to commercially available mammalian L1-Fc (R&D Systems).

The second objective of this research was to synthesize acrylated Tetronic macromers and develop Michael addition methods for hydrogel crosslinking and protein immobilization, and to evaluate hydrogel cytocompatibility, immobilized protein bioactivity, and immobilization efficiency in terms of cell spreading and proliferation using NIH 3T3 fibroblasts and fibronectin. Using a model cell line with a well known RGD-dependent interaction allowed the demonstration of the feasibility of this system for neural repair. Acrylated Tetronic macromers were synthesized as previously described and typically demonstrated approximately 83% acrylation efficiency. Methods developed for hydrogel crosslinking included using a 1:1 acrylate:thiol ratio for encapsulated protein, a 1.1:1 acrylate:thiol ratio for surface-immobilized reduced protein, and a 1:1.1 acrylate:thiol ratio for surface-immobilized acrylated protein.

Heggli et al. demonstrated functionalization of poly(styrene)-gr-PEG beads with acrylic groups using Michael addition conjugation of cysteine and a 13 amino acid peptide in aqueous solution [359]; however, the studies described in this dissertation demonstrated failure of fibroblast spreading on hydrogels with pendant acrylate groups incubated in reduced fibronectin solution. The failure of cell spreading may be the result of (1) inaccurate acrylate:thiol ratio calculations, (2) limited protein conjugation to the surface, (3) a lack of conjugated protein bioactivity as a result of conformation change due to disulfide bond reduction, or (4) disulfide bond reformation prior to conjugation. The 10% excess acrylate may not be sufficient to leave pendant unreacted acrylate groups on the hydrogel surface because the acrylate:thiol ratio was calculated based on the estimated molecular weight of T904-acrylate. Because our T904-acrylate products typically displayed approximately 83% acrylation efficiency, less acrylate groups may be present than what was assumed for the calculation, resulting in no unreacted pendant acrylate groups within the hydrogels. The acrylate:thiol calculation should be refined to incorporate the acrylation efficiency for a more accurate ratio estimation, and studies using varying percentages of excess acrylate should be conducted to optimize conditions for hydrogel crosslinking and for surface-conjugation of reduced protein. Another potential problem is that acrylate groups are inherently hydrophobic because the CH=CH2 carbonaceous side group is non-polar and thus does not attract water strongly, and incubation of hydrogels with pendant acrylate groups in aqueous fibronectin solution may not favor Michael addition surface-conjugation of reduced protein. An alternative method to coax hydrophobic acrylate groups to the surface by crosslinking hydrogels

between glass slides with a hydrophobic coating, such as Rain-X, may be employed to test this theory; however, polymerization between glass is not translatable to the long-term objective of crosslinking hydrogels within the fiber grooves.

As discussed in Chapter 6, control wells with adsorbed reduced fibronectin on bacterial polystyrene plates did demonstrate fibroblast spreading and proliferation, which could either indicate that disulfide bond reduction did not impact bioactivity of adsorbed fibronectin or that disulfide bonds reformed. Reduced fibronectin was diluted to 100 μg/mL in 50mM PBS pH 7.4, which does not contain divalent cations and is the appropriate buffer for Michael addition conjugation. It is possible that the column filtration performed following fibronectin reduction was not sufficient to remove excess DTT resulting in a reformation of disulfide bonds and possibly conjugation of DTT thiols to hydrogel pendant acrylate groups; an alternative approach to using soluble reducing agents for protein reduction that would eliminate the need for column filtration and reduce the time prior to adding protein solution to the hydrogels is to use an immobilized reducing agent, such as Pierce Immobilized TCEP Disulfide Reducing Gel (Product #77712). An indirect Enzyme-Linked Immunosorbent Assay (ELISA) using an HRP-conjugated anti-fibronectin antibody and a fluorogenic substrate (Pierce QuantaBlu) may be used to test if fibronectin is conjugated to the suface of the hydrogels but will not assay the bioactivity of the immobilized protein. Conjugation of fibronectin thiols to acrylate groups on the hydrogel surface may induce a different protein conformation than adsorption that may interfere with bioactivity even if conjugation is successful; however, the success of encapsulated reduced fibronectin in promoting fibroblast spreading and

proliferation implies that covalent immobilization of reduced fibronectin is not detrimental to bioactivity. There is also evidence that disulfide bond reduction is important to fibronectin's bioactivity *in vivo*. Fibronectin multimer formation occurs *in vitro* via the C-terminal free thiols upon exposure to a thiol reagent [343, 344] and *in vivo* depending upon exposure to metal ions [345], and homocysteine binding to plasma fibronectin *in vivo* is mediated through thiol-disulfide exchange at the C-terminal disulfide bonds.[346] In addition, fibronectin's bioactivity is linked with the RGD tripeptide in the FN-III repeat, which does not contain disulfide bonds. [324, 325]

For both encapsulated and acrylated fibronectin, concentrations of 50, 75, and 100 μg/mL promoted maximum fibroblast spreading, and both methods displayed a maximum cell spread area of approximately 3400 μm^2 with 100 μg/mL of fibronectin. Prior studies using 100 μg/mL of thiolated fibronectin immobilized to polystyrene surfaces through Pluronic-pyridyl disulfide (F108-PDS) modification demonstrated cell surface areas >8000 μm^2 [339]; therefore, future work may include higher concentrations of fibronectin to determine if increased fibroblast spreading areas are attainable on encapsulated and surface-immobilized acrylated fibronectin hydrogels. Encapsulated fibronectin supported fibroblast spreading at lower concentrations than acrylated fibronectin; cell spread area of approximately 2000 μm^2 was observed on hydrogels with 2.5 μg/mL of encapsulated fibronectin and 25 μg/mL of acrylated fibronectin.

Only encapsulated 100 μg/mL fibronectin hydrogels supported fibroblast proliferation at 5 days, indicating that hydrolytic degradation of the hydrogel rapidly erodes the surface layer of conjugated fibronectin, within 48 hours. An alternative

approach for enhanced control of hydrolytic degradation may be activation of the T904 terminal hydroxyl groups with various chloroalkyl chloride chemical intermediaries to generate an acrylamide-terminated Tetronic macromer (Figure 8.1).

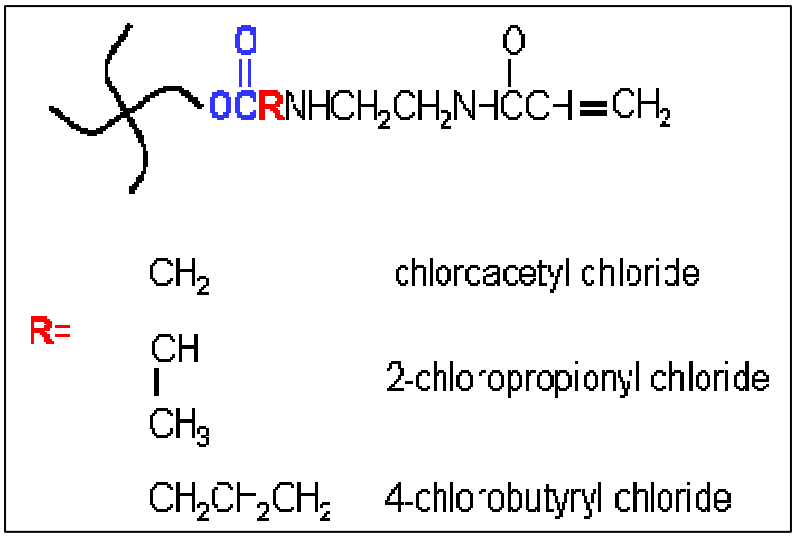

Figure 8.1 Acrylamide-Terminated Tetronic Macromer

The final objective of this research was to assess HT22 and B35 response to L1 in order to establish a model neuronal cell line, to establish methods for primary mammalian neuron culture, to evaluate the cytocompatibility of T904-acrylate hydrogels with primary neurons, and to develop immobilization methods for L1. These studies demonstrated that B35 cells displayed clearer evidence of attachment to L1, but only when cultured in 2% serum for 2 hours followed by serum-free media; however, bacterial polystyrene plates do adsorb protein which may account for the cell attachment observed with both serum media conditions. B35 cells demonstrated a lack of attachment to T904-acrylate hydrogels with no protein when used as negative controls, and immobilization of

L1 to these hydrogels may better enable the elucidation of L1 as a requirement for cell attachment. Dissection protocols were established for both rat postnatal day 7 cerebellar neurons and DRG; however, only cerebellar neurons attached and extended neurites on L1, thus demonstrating their suitability for future studies with mammalian neurons out of the cell types tested. T904-acrylate hydrogels with no rinsing prior to cell seeding were not toxic to primary chick embryonic day 8 forebrain neurons cultured in the presence of the hydrogel with no rinsing on PLL at 24 hours.

These studies demonstrated failure of B35 cell and chick embryonic day 8 forebrain neuron attachment to hydrogels with encapsulated and reduced L1. The proposed mechanisms of failure as discussed for surface-immobilization of reduced fibronectin also apply to surface-immobilization of reduced L1; however, the additional failure of encapsulated L1 indicates a loss of protein bioactivity not demonstrated with encapsulated fibronectin. All six immunoglobulin domains of L1 have been shown to be required for full bioactivity [274], and their quaternary horseshoe structure depicted in Figure 8.2 is important for homophilic binding interactions that are critical for neural applications. Reduction of the L1 protein with DTT breaks the disulfide bonds responsible for this quaternary structure. Although positive controls of adsorbed reduced L1 on bacterial polystyrene demonstrated B35 attachment and proliferation and chick embryonic day 8 neuron attachment and neurite outgrowth, covalent immobilization of reduced L1 appears to effect a loss in bioactivity.

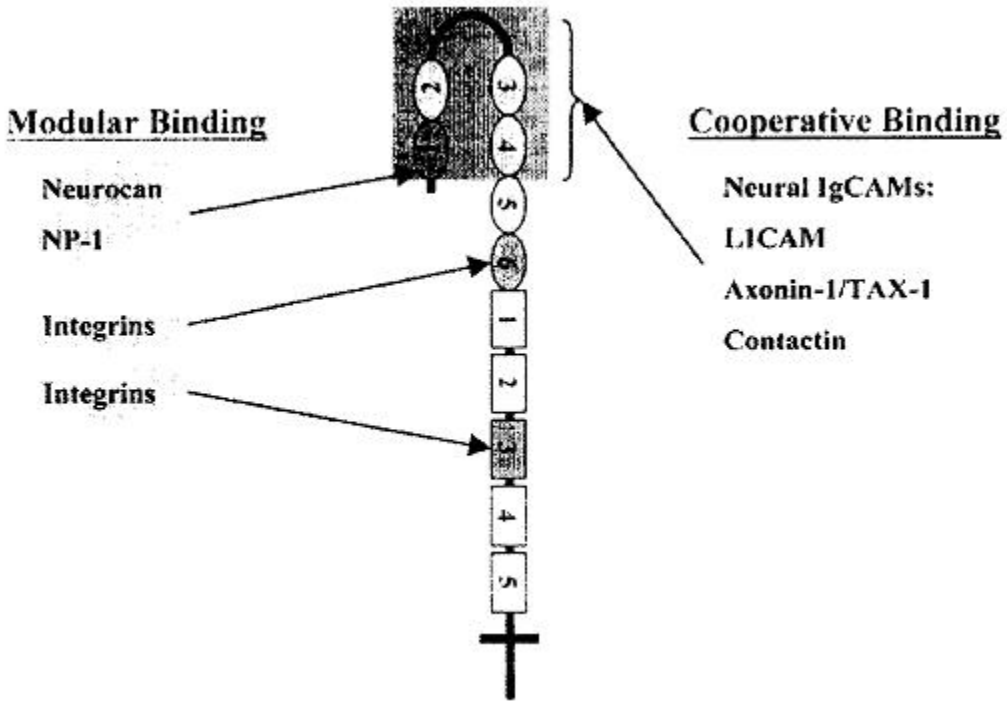

Figure 8.2 Quaternary Structure of L1 Ig Domains
(Reprinted from Haspel and Grumet, 2003 [241])

In addition, these studies demonstrated that a 1mg/mL concentration of L1 was necessary for acrylation of the protein to prevent hydrolysis of the NHS-esters during the acrylation reaction; however, surface conjugation and confirmation of bioactivity is yet unproven. Surface-conjugated acrylated L1 may not be bioactive if the quaternary horseshoe structure is disrupted or if the primary amine at the N-terminus is bound, effectively reversing the orientation of the protein as it appears on the cell surface.

It was stated previously that selection of an appropriate immobilization chemistry is likely to be critical for full retention of L1 bioactivity based on the increased number and distribution of bioactive regions in L1. An alternative approach to test the bioactivity of immobilized L1 in physiologically relevant orientation is encapsulation or surface-

immobilization of NTA-PEG-acrylate previously synthesized in the lab for conjugation to the 6X Histidine tag added to the C-terminus of the insect cell-derived 140 kDa L1 fragment (Figure 8.3).

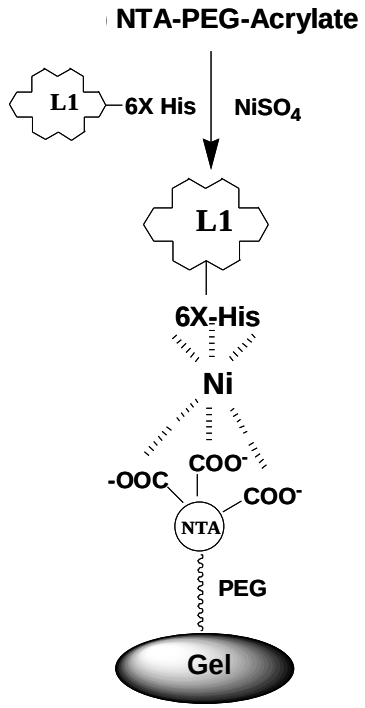

Figure 8.3 Immobilization of L1 through 6X His Tag
(Reprinted from Lee et al., 2007 [360])

Although this method will not overcome the instability of immobilized ligands within or on the surface of T904-acrylate hydrogels, resulting from hydrolytic degradation of the hydrogels and the potential for *in vivo* enzymatic degradation due to the presence of reducing enzymes such as thioredoxins [361], it may be useful for demonstrating the importance of maintaining physiologic protein orientation for

bioactivity. The insect cell-derived 140 kDa L1 fragment also contains a 14 amino acid V5 epitope (-Gly-Lys-Pro-Ile-Pro-Asn-Pro-Leu-Leu-Gly-Leu-Asp-Ser-Thr-) prior to the 6X His tag recognizable by Invitrogen anti-V5 antibody (IgG_{2a}). Another possible immobilization method to maintain physiologic orientation of L1, although with limited clinical applicability, is encapsulation or surface-immobilization of acrylated anti-V5 antibody generated using acrylate-PEG-NHS, to bind to the C-terminus of the L1 protein.

RECOMMENDATIONS

A major limitation of using adherent cultures for protein production is that relatively small amounts of protein may be produced at any given time due to the requirement for large amounts of incubator space. In addition, insect cells require a separate incubator from mammalian cells because they are cultured at 27°C with no CO_2. The insect cell culture system described in Chapter 5 typically yielded 1.8mL of 160 μg/mL concentration of L1 from 4- 175cm^2 T-flasks. These studies have demonstrated the necessity for a 1mg/mL concentration of L1 in order to successfully acrylate the protein. In order to obtain sufficient quantities of protein to continue this research, large-scale transfections will be required. For example, 1mL of 1mg/mL concentration L1 is enough protein to test 100 conditions in 96-well plates using 100μg/mL concentration. To produce 1mL of 1mg/mL will require 6.25mL of 160 μg/mL, or 14 flasks. An alternative approach that may be considered is perfusion bioreators for higher protein production. [362, 363]

Additional considerations for long-term studies include analysis of the appropriate mechanical properties for hydrogels to optimize neurite outgrowth, and the effect of loss of mechanical properties due to hydrogel degradation on neurite outgrowth. Growth cone advance is mediated by a minimum "threshold" value of tension [364], and Gunn et al. demonstrated greatest neurite extension from PC12 cells seeded on PEG-diacrylate hydrogels with an elastic modulus in the range of approximately 50-200 kPa. [215] In this work, only 23% T904-acrylate hydrogels were tested in order to evaluate protein conjugation strategies; however, future studies should be conducted to evaluate the hydrogel mechanical properties over a varying T904-acrylate concentration range in an effort to optimize conditions to provide a synergistic benefit to neurite outgrowth. Analysis of the appropriate mechanical properties for fibers based on spinal cord mechanics is also warranted. Several studies have examined the viscoelastic behavior of the spinal cord. [201-204] In addition, as discussed in Chapter 4, discrepancies exist in the reported values of elastic modulus for the spinal cord and no consensus has been reached regarding the appropriate elastic modulus for neural scaffolds. [203, 206, 208]

A final future consideration is analysis of clearance of acrylate- and acrylamide-terminated Tetronics and PLA breakdown products in the CNS. Total volume of pH 7.33 cerebrospinal fluid is 125-150ml with a turnover rate of 3-4 times per day, or 0.35 ml/min (500 ml/day). [365] Radiolabeled PEG clearance following brain injection has been examined [366], and the potential neurotoxicity of acrylic acid and acrylamide must be assessed. [367] PLA has demonstrated biocompatibility for spinal cord applications

[289], and studies have demonstrated that cerebral spinal fluid (CSF) is capable of buffering and eliminating 3 mM/L increases in lactic acid. [368, 369]

APPENDICES

APPENDIX A

SYNTHESIS OF T904-ACRYLATE WITH TEA, 30g REACTION

Materials/Chemicals

Material/Chemical	Vendor	Part Number	Storage
Tetronic 904	BASF	30085638	Chemical cabinet
Toluene HPLC	Fisher	T290-4	Flammable cabinet
Dichloromethane HPLC	Acros (Fisher)	61005-0040	Flammable cabinet
Ethyl ether anhydrous, BHT stabilized	Fisher	E318-20	Flammable refrigerator in 505
Hexanes HPLC	Fisher	H302-4	Flammable cabinet
Triethylamine (TEA)	Acros (Fisher)	157911000	Chemical cabinet
Acryloyl chloride 96%	Sigma	A24109-500	Flammable refrigerator in 505
Calcium hydride 93% 0-20mm grain	Acros (Fisher)	196791000	Flammable cabinet
Molecular sieves (Grade 514, Type 4A, 8-12 mesh)	Fisher	BP2631-500	Chemical cabinet
Celite fine 500	Fluka (Sigma)	22145	Chemical cabinet
Sodium sulfate anhydrous	Fisher	S421-3	Chemical cabinet
4-Methoxyphenol 99%	Aldrich	M18655	Chemical cabinet

Table A.1: Materials/Chemicals used for Synthesis of T904-Acrylate

Safety

- Wear nitrile gloves when handling organic solvents and triple glove so that total glove thickness is at least 15mil (our gloves are 5mil). If solvent spills on gloves, immediately remove outer glove and replace (solvents - particularly ether, dichloromethane, toluene, hexane - can penetrate nitrile gloves in under 4 minutes). Latex gloves should not be worn to handle solvents as the permeation rate is much quicker (in seconds for dichloromethane).
- Wear lab coat, safety goggles, and nitrile gloves when handling organic solvents and always handle under the chemical fume hood.
- Calcium hydride is extremely reactive and must be handled with care (see page 2).

General Notes

- Parafilm all chemical bottles to prevent moisture penetration.
- Clean rotavap with acetone before and after each use.
- Clean and dry glassware as it is used or there will not be enough for all steps, but allow solvent volatilization under the chemical fume hood first.

Preparation for Synthesis

Make sure all glassware has been cleaned with sodium hydroxide, rinsed at least six times with DI water followed by one acetone rinse, and completely dried in 60°C oven overnight:

- Condenser
- Connector
- Round bottom reaction flasks
- Evaporator trap with inner vapor tube at bottom
- Addition funnel
- Separation funnel
- Buchner funnels
- Filter flasks
- Erlenmeyer flasks
- Glass stopper
- Teflon valves with washers

Glassware used for the reaction and final filter/rotavap/precipitation steps after sodium sulfate wash must be extremely dry and should be dried under vacuum at 100°C for 3 hours and then left to cool under vacuum overnight until use (use vacuum oven).

Make Dehydrated Dichloromethane In Advance

- Typically prepare at least 500mL for each 30g reaction.
- Prepare bottle for dehydrated dichloromethane storage and activated molecular sieves by drying under vacuum at 110°C for 3 hours and then leave to cool under vacuum overnight until use. Activated molecular sieves may be stored under vacuum for one month.
- Cover the bottom of a 1L glass bottle with calcium hydride, add 1L of dichloromethane and mix overnight with stirring. The cap should be closed.
- Filter dehydrated dichloromethane on ice bath using a vacuum-heated and dried Buchner funnel with filter paper and Celite fine 500 into a vacuum-heated and dried 1L filter flask.
- Repeat the previous step using only filter paper to remove any Celite.

- Transfer filtered dehydrated dichloromethane into vacuum-heated and dried 1L amber glass bottle with activated molecular sieves for storage. Dehydrated dichloromethane may be stored for one month.
- **SAFETY NOTE:** Calcium hydride reacts violently with water, acids, lower alcohols, and heat to produce hydrogen gas and caustic calcium hydroxide. The hydrogen gas may be ignited by the heat of the reaction. In the event of fire, use dry chemical, lime or dry sand. DO NOT use water, foam, carbon dioxide, or halon.
- **PROPER DISPOSAL OF CALCIUM HYDRIDE:** Allow solvent to volatilize off the calcium hydride overnight under the chemical fume hood. Dispose of dried calcium hydride in the labeled plastic container that is stored in the flammables cabinet under the hood. Ensure the lid is tightly sealed.

Procedure

ALL STEPS MUST BE PERFORMED UNDER CHEMICAL FUME HOOD!

Day 1 - Azeotropic Distillation and Reaction:

- T904: 30g (MW6700)
- Dehydrated dichloromethane: 300 mL
- 8X Acryloyl chloride: $\frac{8\times\frac{30}{6700}\times 90.51}{1.114}\approx 2.910ml$
- 4X Triethylamine (TEA): $\frac{4\times\frac{30}{6700}\times 101.19}{0.726}\approx 2.496ml$

1. Refer to figure A.1 at the end of this protocol for the azeotropic distillation set-up.
2. Start this early in the morning so the reaction is begun early afternoon in order to allow time for Day 2 steps during the day (reaction needs 24 hours).
3. Use oven dried glassware (condenser, connector, round bottom reaction flask).
4. Weigh T904 with a beaker and dissolve it in 100ml toluene (tare a 150 mL beaker on the balance to measure T904). Allow to dissolve for several minutes while stirring vigorously with spatula.
5. Decant dissolved T904 of **step 2** into the reaction flask. Add an additional 100mL, stir vigorously, and decant into reaction flask. Repeat for a total volume of 300mL.
6. Set up the azeotropic distillation system with magnetic bar inside the flask (parafilm all connections, wrap with glass fibers and foil to insulate, connect water line and drain to condenser and clamp in place using binder clips). Refer to the last page of this protocol for an explanation and diagram of azeotropic distillation.
7. Allow T904 solution to stir for about 10 minutes prior to heating up the oil bath.
8. Heat the reaction flask (hot oil bath) up to 130°C.

9. Boil the flask. As water is removed, it will appear to be cloudy and white in the connector column.
10. The connector column volume is approximately 30mL. Boil off a total of approximately half of the solution volume (150mL). Boil off 120mL, allow the column to fill and reflux for one hour, then stop the distillation and cool down the reaction and remove the final 30mL (approximately 2 hours).
11. Vacuum-evaporate at 90°C to remove the toluene using the evaporator trap with inner vapor tube at bottom.
    a. Use the lower power vacuum pump, 90°C water bath, and maximum rotation (should take approximately 30mins - 1 hr). Add ice on the cooling trap.
12. Dissolve purified T904 in 240ml dehydrated dichloromethane.
13. Set up the reaction batch with stirring system.
14. Pipette TEA to the reaction flask and allow to mix for several minutes with stirring on an ice bath.
15. Cool down the reaction flask for several minutes.
16. Attach the addition funnel to the top of the reaction (parafilm the connection) and add the acryloyl chloride solution in 60ml dehydrated dichloromethane into the addition funnel.
17. Dropwise-add **step 12** solution into the reaction slowly (within 2hrs) using a steady continuous drip. Add ice to ice bath as needed.
18. When all the acryloyl chloride solution has been added, move the reaction system to cold room on 5^{th} floor (put aluminum foil around the reaction flask to protect it from light, grease the fitting, parafilm the closure).
19. Run the reaction with stirring in the cold room for **24 hours**.

Day 2 – Filtration, Ether/Hexane Precipitation:

1. Stop the reaction and filter with filter paper and Celite fine 500 using a Buchner funnel once to remove TEA-HCl. Filter one more time with filter paper without Celite using a Buchner funnel to remove the remaining Celite in the product. Make sure to use dry funnels and filter flasks and use a new funnel/flask for each filtration step. Add solution slowly as it is very viscous and will clog the filter if too much is added too quickly.
2. Add 2 chips of 4-methoxyphenol and allow to dissolve for 5 minutes.
3. Vacuum-evaporate at 30°C to remove the dichloromethane using the evaporator trap with inner vapor tube at bottom.
    a. Use the lower power vacuum pump, 30°C water bath, and maximum rotation (should take approximately 1 hour). Add ice on the cooling trap.
4. Using an Erlenmeyer flask, precipitate in 50/50 ether/hexane. Total volume should be 500mL. Add 250mL of ether to reaction flask and swirl and transfer to Erlenmeyer flask. Then add 250mL of hexanes to reaction flask (to try and remove as much product as possible from the reaction flask) and swirl and transfer to Erlenmeyer flask. Mix with stirring for at least 5 minutes.

5. Remove stir bar, seal Erlenmeyer flask with rubber stopper and wrap with parafilm, cover entire flask in foil and label, and place flask in flammable freezer in 505 at -20°C and allow precipitated product to settle overnight.

Day 3 – pH Neutralizations and Final Precipitations (4 precipitations total):

1. Quickly decant the waste solvent without disturbing the settled product at the bottom.
2. Redissolve the product in 300 mL dichloromethane (does not have to be dehydrated as water will be added during washing steps). Check pH (typically it will be pH 4.0 before starting the wash steps).
3. Transfer the product to the separation funnel. Make sure the Teflon valve has a gasket or it will leak.
4. Wash it with 30ml 10% $NaHCO_3$ once and shake the funnel gently, opening the valve periodically to release the gas. If using different reaction sizes, use 10% of the total volume for washes. Place the funnel back in the ring holder, remove the top, and allow the bicarbonate solution to separate out (water will rise to the top and appear opaque white). Use a piece of rubber hose to "whip" the funnel to encourage separation if needed. Open the valve to pour off the product into a clean, dry beaker, stopping when reaching the separated waste. Remove the waste to a separate beaker.
5. Check the pH of the product and repeat **step 9** until the pH is neutralized (pH 7.0) by pouring the product back into the separation funnel (typically 2 washes).
6. Once product pH is neutralized, add 30ml double-deionized (Millipore) water instead of 10% $NaHCO_3$ and follow the method in **step 9**, to remove sodium bicarbonate. Ensure the pH of the product AND the water waste are neutral, and then do 2 water washes beyond what is required for neutral pH (typically 4-6 total water washes).
7. Add sodium sulfate to the product beaker to dehydrate (approximately 4-6 times) until the solution becomes clear. Add approximately one small weigh boat of sodium sulfate (just enough to cover the bottom of beaker), mix using a spatula for approximately 5 minutes, allow to settle, then pour into another beaker and repeat. Add a very small amount of dichloromethane (not dehydrated) to the waste sodium sulfate to remove any remaining product and add this back to the product. When all the water is removed, the sodium sulfate will become salt-like with individual particles moving instead of slushy and the product will be very clear. The final wash should be in an Erlenmeyer flask so it can be sealed overnight. Dump waste sodium sulfate onto aluminum foil for disposal (allow solvent to evaporate first).
8. Once the solution becomes clear (typically after 4 washes), allow sodium sulfate to settle and filter the product with filter paper using a Buchner funnel to remove sodium sulfate.
9. Decant solution to a new dry round bottom flask.
10. Add 2 chips of 4-methoxyphenol and allow to dissolve for 5 minutes.

11. Vacuum-evaporate at 30°C to remove the dichloromethane using the evaporator trap with inner vapor tube at bottom.
    a. Use the lower power vacuum pump, 30°C water bath, and maximum rotation (should take approximately 1 hour). Add ice on the cooling trap.
12. Using an Erlenmeyer flask, precipitate in 50/50 ether/hexane. Total volume should be 500mL. Add 250mL of ether to reaction flask and swirl and transfer to Erlenmeyer flask. Then add 250mL of hexanes to reaction flask (to try and remove as much product as possible from the reaction flask) and swirl and transfer to Erlenmeyer flask. Mix with stirring for 5 minutes.
13. Remove stir bar, seal Erlenmeyer flask with rubber stopper and wrap with parafilm, cover entire flask in foil and label, and place flask in flammable freezer in 505 at -20°C and allow precipitated product to settle overnight.
14. Quickly decant the waste solvent without disturbing the settled product at the bottom. Dispose of waste solvent in the appropriate waste container.
15. Using an Erlenmeyer flask, precipitate in 100% ether. Total volume should be 500mL. Mix with stirring for 5 minutes.
16. Remove stir bar, seal Erlenmeyer flask with rubber stopper and wrap with parafilm, cover entire flask in foil and label, and place flask in flammable freezer in 505 at -20°C and allow precipitated product to settle overnight. If possible, try to do two precipitations per day (early morning and late evening), but if the product is not settled, leave overnight.
17. Repeat 100% ether precipitations two more times for a total of three (3) 100% ether precipitations.

Final Day – Dry Product and NMR:

1. Set-up a small dessicator with dessicant and place it in a large Styrofoam cooler on ice. Vent the dessicator into the chemical fume hood. Ensure the ice level is below the top of the dessicator to prevent moisture infiltration when opening and closing the dessicator.
2. Allow the dessicator to cool down for at least 30 minutes under vacuum prior to drying any product in it. Ensure vacuum pressure is > 20psi.
3. Tare the balance and weigh a dry large Petri dish and take note of the weight (in order to determine final yield of product).
4. Quickly decant the waste solvent without disturbing the settled product at the bottom. Dispose of waste solvent in the appropriate waste container.
5. Pour the remaining product/solvent mix into the Petri dish for drying. Do not fill Petri dish beyond half full or the product will be forced out of the Petri dish when under vacuum. Dry in multiple steps if necessary, but keep product cold and protected from light (in -20C freezer). Ensure vacuum pressure is > 20psi.
6. Place the Petri dish into the vacuum chamber and dry under vacuum on ice for at least 4 hours (6-8 hours if possible). Replace ice as needed.
7. Once the product is dried and all the ether is removed, weigh the Petri dish and determine the final yield of product.
8. Check NMR of product in chloroform and determine reaction efficiency (25mg product in 1mL chloroform).
9. Store the final dried product in a labeled closed container at -20°C (or cover the Petri dish with foil and label).

Azeotropic Distillation

An azeotropic mixture has a boiling point that does not change when vapor is removed by evaporation. The boiling point may be higher or lower than any of the components of the mixture, e.g. a toluene / water mixture has bp 85.0°C, but bp toluene is 110.6°C and bp water is 100.0°C. Steam distillation is used to separate volatile from non-volatile components and the reduction in boiling point reduces thermal decomposition. For the toluene-water system, below 85°C the two liquid phases coexist. At 85°C the sum of the vapor pressures of water and toluene = one atmosphere, and boiling starts.

In a mixture of toluene and water, boiling occurs at 85°C and both water and toluene are in the vapor that condenses to form two layers. The bottom layer of water has 0.06% toluene dissolved in it. The top layer of toluene has 0.05% water dissolved in it. The relative volumes are 18% water and 82% toluene. The excess toluene flows back into the flask and distils back over with more water. At 85°C, vapor pressure of water = 57.7 kPa and vapor pressure of toluene = 50.6 kPa.

$$\textbf{Weight of water} = \frac{\textbf{molar mass}_{\text{water}}\ \textbf{(g/mol)}}{\textbf{molar mass}_{\text{toluene}}\ \textbf{(g/mol)}} \times \frac{\textbf{Vapor pressure}_{\text{water}}}{\textbf{Vapor pressure}_{\text{toluene}}} = \frac{\mathbf{18}}{\mathbf{82}} \times \frac{\mathbf{57.7}}{\mathbf{50.6}} = \mathbf{0.250... = 25\%}$$

[The most common unit for vapor pressure is the torr. 1 torr = 1 mm Hg (one millimeter of mercury). The international unit for pressure is: 1 pascal = a force of 1 newton per square meter = 10 dyn/cm² = 0.01 mbar= 0.0075 mmHg = 0.00000969 atm= 0.00014 psi.] Be careful! Do experiment in a fume hood because toluene vapor is harmful.

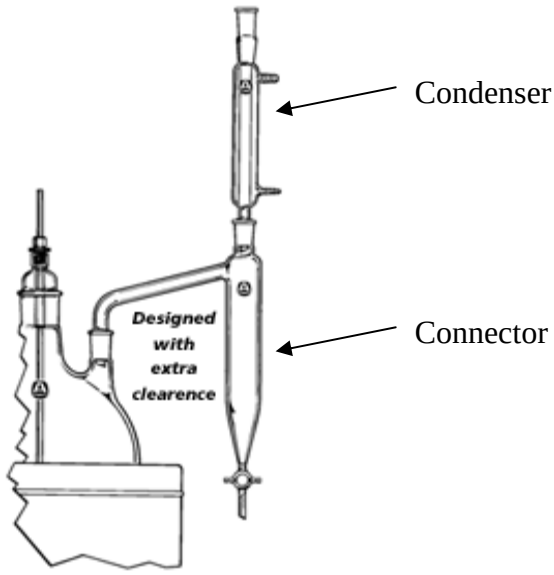

Figure A.1 Azeotropic Distillation Set-Up

NOTE: Designed specifically for azeotropic distillation using solvents lighter than water. The set-up depicted in Figure A.1 uses a Dean-Stark trap that comes standard with a 4mm bore PTFE stopcock. The 12mL and 25mL traps use a 2mm bore stopcocks. We don't use this set-up with the thermometer in a reaction flask. We simply connect the top of a round-bottom reaction flask directly to the connector end and wrap this part with glass fibers and aluminum foil.

APPENDIX B

GENBANK AMINO ACID SEQUENCE FOR BOVINE SERUM FIBRONECTIN

http://www.ncbi.nlm.nih.gov/entrez/viewer.fcgi?db=protein&id=462100

LOCUS P07589 2265 aa linear MAM 10-JUN-2008
DEFINITION Fibronectin (FN).
ACCESSION P07589
VERSION P07589.3 GI:462100
DBSOURCE swissprot: locus FINC_BOVIN, accession P07589;
class: standard.
created: Apr 1, 1988.
sequence updated: Feb 1, 1994.
annotation updated: Jun 10, 2008.
xrefs: K00800.1, AAA30521.2,

L = LYSINE, 122 total
C = CYSTEINE, 64 total

1 qaqqivqpqs pLtvsqskpg Cydngkhyqi nqqwertyLg saLvCtCygg srgfnCeskp
61 epeetCfdky tgntyrvgdt yerpkdsmiw dCtCigagrg risCtianrC heggqsykig
121 dtwrrphetg gymLeCvCLg ngkgewtCkp iaekCfdqaa gtsyvvgetw ekpyqgwmmv
181 dCtCLgegsg ritCtsrnrC ndqdtrtsyr igdtwskkdn rgnLLqCiCt gngrgewkCe
241 rhtsLqttsa gsgsftdvrt aiyqpqphpq pppyghCvtd sgvvysvgmq wLktqgnkqm
301 LCtCLgngvs Cqetavtqty ggnsngepCv Lpftyngktf ysCttegrqd ghLwCsttsn
361 yeqdqkysfC tdhtvLvqtr ggnsngaLCh fpfLynnhny tdCtsegrrd nmkwCgttqn
421 ydadqkfgfC pmaaheeiCt tnegvmyrig dqwdkqhdmg hmmrCtCvgn grgewtCvay
481 sqLrdqCivd gitynvndtf hkrheeghmL nCtCfgqgrg rwkCdpvdqC qdsetrtfyq
541 igdswekyLq gvryqCyCyg rgigewaCqp Lqtypdtsgp vqviitetps qpnshpiqws
601 apesshisky iLrwkpknsp drwkeatipg hLnsytikgL rpgvvyegqL isvqhygqre
661 vtrfdfttts tspavtsntv tgettpLspv vatsesvtei tassfvvswv sasdtvsgfr
721 veyeLseegd epqyLdLpst atsvnipdLL pgrkytvnvy eiseegeqnL iLstsqttap
781 dappdptvdq vddtsivvrw srprapitgy rivyspsveg ssteLnLpet ansvtLsdLq
841 pgvqynitiy aveenqestp vfiqqettgv prsdkvpppr dLqfvevtdv kitimwtppe
901 spvtgyrvdv ipvnLpgehg qrLpvsrntf aevtgLspgv tyhfkvfavn qgreskpLta
961 qqatkLdapt nLqfinetdt tvivtwtppr arivgyrLtv gLtrggqpkq ynvgpaasqy
1021 pLrnLqpgse yavsLvavkg nqqsprvtgv fttLqpLgsi phyntevtet tivitwtpap
1081 rigfkLgvrp sqggeaprev tsesgsivvs gLtpgveyvy tisvLrdgqe rdapivkkvv
1141 tpLspptnLh LeanpdtgvL tvswersttp ditgyrittt ptngqqgysL eevvhadqss
1201 CtfenLspgL eynvsvytvk ddkesvpisd tiipavpppt dLrftnvgpd tmrvtwapps
1261 sieLtnLLvr yspvkneedv aeLsispsdn avvLtnLLpg teyLvsvssv yeqhesipLr
1321 grqktaLdsp sgidfsdita nsftvhwiap ratitgyrir hhpenmggrp redrvppsrn

1381 sitLtnLnpg teyvvsivaL nskeesLpLv gqqstvsdvp rdLeviaatp tsLLiswdap
1441 avtvryyrit ygetggsspv qeftvpgsks tatisgLkpg vdytitvyav tgrgdspass
1501 kpvsinyrte idkpsqmqvt dvqdnsisvr wLpssspvtg yrvttapkng pgpsktktvg
1561 pdqtemtieg Lqptveyvvs vyaqnqnges qpLvqtavtt ipaptnLkft qvtptsLtaq
1621 wtapnvqLtg yrvrvtpkek tgpmkeinLa pdsssvvvsg Lmvatkyevs vyaLkdtLts
1681 rpaqgvvttL envspprrar vtdatettit iswrtkteti tgfqvdaipa ngqtpiqrti
1741 rpdvrsytit gLqpgtdyki hLytLndnar sspvvidast aidapsnLrf LattpnsLLv
1801 swqpprarit gyiikyekpg spprevvprp rpgvteatit gLepgteyti qviaLknnqk
1861 sepLigrkkt deLpqLvtLp hpnLhgpeiL dvpstvqktp fitnpgydtg ngiqLpgtsg
1921 qqpsLgqqmi feehgfrrtt ppttatpvrh rprpyppnvn eeiqighvpr gdvdhhLyph
1981 vvgLnpnast gqeaLsqtti swtpfqesse yiisChpvgi deepLqfrvp gtsasatLtg
2041 Ltrgatynii veavkdqqrq kvreevvtvg nsvdqgLsqp tddsCfdpyt vshyaigeew
2101 erLsdsgfkL sCqCLgfgsg hfrCdsskwC hdngvnykig ekwdrqgeng qmmsCtCLgn
2161 gkgefkCdph eatCyddgkt yhvgeqwqke yLgaiCsCtC fggqrgwrCd nCrrpgaepg
2221 negstahsyn qysqryhqrt ntnvnCpieC fmpLdvqadr edsre

APPENDIX C

RAT POSTNATAL DAY 7 CEREBELLAR NEURON DISSECTION PROTOCOL

Supplies:

- 25mm, 0.2 µm syringe filter (Nalgene 190-2520)
- Sterile 35mm petri dishes (Falcon 353801)
- Sterile 100mm petri dishes (Fisher 08-757-13)
- Sterile 15mL centrifuge tubes (Fisher 05-539-12)
- Sterile 50mL centrifuge tubes (Fisher 05-539-8)
- 3mL syringe with 22G1½ needle (BD309574)
- 96-well plates (Corning 3596)
- Autoclave biohazard bags (Fisher 01-814A)

Dissection Tools:

- Large scissors
- Fine scissors (Fine Science Tools 91500-09)
- Dumont #5 fine forceps Inox – two pair (Fine Science Tools 91150-20)
- Coarse straight forceps
- Styrofoam base covered in foil and sterile needles (any size)

NOTE: Autoclave all dissection tools prior to use.

Materials:

Materials	Part No.	Storage
Gibco Basal Medium Eagle (BME) without L-glutamine	21010-046	+4°C
Fisher Potassium Chloride (KCl)	P217-500	Room Temp.
Acros D(+)-Glucose	41095-5000	Room Temp.
Gibco Fetal Bovine Serum OR Hyclone Fetal Bovine Serum	16140-063 SH30070.02	-20°C
Gibco L-glutamine 200 mM OR Hyclone L-glutamine 200mM (Protect from light)	25030-149 SH30034.02	-20°C
Gibco 100X Antibiotic-Antimycotic 10,000 IU/ml penicillin 10,000 µg/mL streptomycin 25 µg/mL amphotericin B	15240-096	-20°C
Gibco L15 Medium		+4°C
Fisher DNase		-20°C

Table C.1: Materials used for Rat Cerebellar Neuron Dissection

Preparation of Sterile HBSS with 1% Glucose:

HEPES is added to 1X HBSS to replace the buffering action of the missing bicarbonate in order to maintain physiological pH 7.4 in air, so it can be used outside the CO_2 incubator (HBSS is used in this protocol for the dissection and trypsin steps, both of which are done in air).

1L:

- Make 1L of 1X HBSS: add 100mL of 10X HBSS without Ca, Mg, bicarbonate, or phenol red to 900mL of Millipore water with stirring.
- Add 5 mM HEPES (1.3g/L, MW=260.3) to 900mL of 1X HBSS and wait until dissolved.
- Add 10g of glucose and wait until dissolved.
- Add 10 mL (1%) antibiotic/antimycotic.
- Adjust pH to 7.4 with NaOH.
- Bring liquid level up to 1L with 1X HBSS. Verify pH is 7.4.
- Filter-sterilize and store at +4°C.

Preparation of 1.0% Trypsin:

- Dilute 10mL of 2.5% trypsin without Ca, Mg, phenol red in 15mL of sterile HBSS with 1% glucose to make 1.0% trypsin.
- Freeze in 5mL aliquots at -20°C. Store ≤1 year.

OR

Preparation of 1.0% Trypsin/ 0.2% EDTA solution:

- Dissolve 200mg EDTA in 10mL Millipore water (2% w/v) and sterilize with 0.2um syringe filter.
- Add 10mL of 2.5% trypsin without Ca, Mg, phenol red and 2.5mL sterile EDTA solution to 12.5mL of sterile HBSS with 1% glucose to make 1% trypsin-0.2% EDTA.
- Freeze in 5mL aliquots at -20°C. Store ≤1 year.

Preparation of 1.0% Dnase:

- Dilute 40 mg DNase in 4 mL of L15 media for a 10 mg/mL concentration.
- Syringe-filter with 0.2μm syringe filter.
- Freeze in 500μL aliquots at -20°C. Store ≤1 year.

Preparation of Serum Medium:

Base Medium: BME without L-glutamine

- 20 mM potassium chloride (KCl)
- 33 mM glucose
- 10% fetal bovine serum (FBS)
- 50 U/ml penicillin, 50 µg/mL streptomycin, 125 ng/mL antibiotic/antimycotic solution (1:200 dilution)
- 2mM L-glutamine (1:100 dilution)

Instructions:

1. Add media components in the order listed above.
2. Sterile-filter media after adding KCl and glucose using a 25mm, 0.2 µm syringe filter (Nalgene 190-2520).
3. Make stock solution of media without L-glutamine and store at +4°C.
4. Add L-glutamine (2 mM final concentration) immediately prior to use. Use media within 1 week of adding L-glutamine.

To make 10 mL:		To make 50 mL:	
BME	9 mL	BME	45 mL
KCl	15 mg	KCl	75 mg
Glucose	59 mg	Glucose	295 mg
FBS	1 mL	FBS	5 mL
AB/AM	50 µL	AB/AM	250 µL
L-glutamine	100 µL	L-glutamine	500 µL

Preparation for Dissection:

1. Prepare and sterilize media.
2. Ensure dissection tools are autoclaved. If autoclaving is not possible, sterilize tools with 70% ethanol for 30 minutes.
3. UV sterilize the dissection hood for at least 30 minutes prior to dissection.

Dissection:

1. Wipe the styrofoam base covered in foil with 70% ethanol and allow to dry.
2. Carefully pin the rat head to the styrofoam base with two sterile needles through the nose to stabilize the head.
3. Use the large scissors to carefully remove the skin covering the brain.
4. Use the fine scissors to carefully remove the top portion of the brain and expose the cerebellum. Refer to Protocols for Neural Cell Culture (Federoff and Richardson, 3rd edition) Chapter 4, Figure 1. The cerebellum is sausage-shaped and sits directly below the pair of optic lobes.

5. Dissect the cerebellum and carefully remove the meninges and all blood vessels in a 35mm petri dish in ice cold HBSS with glucose.

Dissociation and Plating:

1. Warm L15 and serum media in 37°C incubator with 7% CO_2 for 30 minutes to bring temperature and pH up to physiological levels.
2. Transfer the cleaned cerebellum to a clean 35mm petri dish, add 1 mL of 1% trypsin in HBSS, and mince the cerebellum into small pieces with the fine scissors.
3. Under a sterile cell culture hood, add 100uL 1% DNase and mix gently.
4. Incubate for 15 min in 37ºC water bath.
5. Transfer minced tissue into a sterile 15mL tube, add 3 mL of serum media to deactivate the trypsin, and centrifuge at 1,000 rpm for 5 min.
6. Carefully remove supernatant and add 1 ml fresh media to the cell pellet. Gently resuspend the cells by pipetting up and down a few times, avoiding air bubbles.
7. Gently triturate cells at least 20 times using a 3mL syringe with 22G1½ needle (BD309574). A sterile fire-polished glass pipet may also be used. Avoid air bubbles.
8. Dilute the cell suspension 10-fold in serum media and count the cells using a hemacytometer (typically 7-12 million cells per cerebellum).
9. Plate cells using the serum media. REMINDER: L-glutamine (Gibco or Hyclone, 200 mM) must be added to the media immediately before use: 10 µL L-glutamine to 1 mL media (2mM final concentration)
10. Plating densities of 20,000 cells per 96-well typically provide good results. Corning 3596 96-well plates have a well diameter of 6.4mm and growth area of 0.32 cm^2, so this plating density is equivalent to 62,500 cells/ cm^2.

Conclusion of Dissection:

1. Gently clean all dissection tools immediately with detergent to prevent drying of blood.
2. Wipe the dissection hood with 70% ethanol and UV sterilize for at least 30 minutes.
3. Dispose of all waste in an autoclave biohazard bag, tie the bag shut, and dispose of in the designated freezer.

APPENDIX D

RAT POSTNATAL DAY 7 DORSAL ROOT GANGLIA DISSECTION PROTOCOL

Supplies:

- 25mm, 0.2 µm syringe filter (Nalgene 190-2520)
- Sterile 35mm petri dishes (Falcon 353801)
- Sterile 100mm petri dishes (Fisher 08-757-13)
- Sterile 15mL centrifuge tubes (Fisher 05-539-12)
- Sterile 50mL centrifuge tubes (Fisher 05-539-8)
- 3mL syringe with 22G1½ needle (BD309574)
- 96-well plates (Corning 3596)
- Autoclave biohazard bags (Fisher 01-814A)

Dissection Tools:

- Large scissors
- Fine scissors (Fine Science Tools 91500-09)
- Dumont #5 fine forceps Inox – two pair (Fine Science Tools 91150-20)
- Coarse straight forceps
- Styrofoam base covered in foil and sterile needles (any size)

NOTE: Autoclave all dissection tools prior to use.

Materials:

MATERIAL	VENDOR	PART NUMBER	STORAGE
DMEM-F12 with L-glut	Mediatech	10-090-CV	+4°C
L15 Medium	Gibco		+4°C
BSA (bovine serum albumin)	Sigma	A3059-10G	+4°C
FBS (fetal bovine serum)	Hyclone	SH30070.02HI	-20°C
100X Antibiotic/Antimycotic -10,000 U/mL penicillin G -10,000 ug/mL streptomycin sulfate -25 ug/mL amphotericin	Gibco	15240-096	-20°C
NGF-7S	Invitrogen	13290-010	-20°C
2.5% Trypsin w/o Ca, Mg*, phenol red**	Invitrogen	15090-046	-20°C
EDTA***	Acros	32721-1000	Room Temp.
10X HBSS w/o Ca, Mg*, bicarb, phenol red**	Gibco	14185-052	Room Temp.
Glucose	Sigma	G-7528	Room Temp.
HEPES	Fisher	BP410-500	Room Temp.
Collagenase	Worthington		-20°C
DNAse	Fisher		-20°C

Table D.1: Materials used for Rat Dorsal Root Ganglia Dissection

NOTES:
*Ca^{2+} and Mg^{2+} in the trypsin and the salt solution can cause cells to adhere to each together.
**Phenol red may damage neurons in alkaline pH during the dissection and dissociation steps.
***EDTA (disodium ethylenediamine tetraacetic acid) may be added to trypsin as a chelating agent to bind Ca^{2+} and Mg^{2+} ions that can interfere with the action of trypsin.

Preparation of NGF:
20 µg/mL, 0.1% BSA
- Make 1% BSA solution (10mg in 1mL Millipore water) and sterile filter through 0.2µm syringe filter.
- In laminar flow hood, dissolve 100ug NGF 7S in 4.5 mL DMEM-F12.
- Add 500µL of sterile 1% BSA solution (to make 0.1% final concentration).
- Aliquot into 50µL aliquots (20 µg/mL concentration) and freeze at -20°C. Store ≤1 year.

Preparation of Sterile HBSS with 1% Glucose:

HEPES is added to 1X HBSS to replace the buffering action of the missing bicarbonate in order to maintain physiological pH 7.4 in air, so it can be used outside the CO_2 incubator (HBSS is used in this protocol for the dissection and trypsin steps, both of which are done in air).

1L:

- Make 1L of 1X HBSS: add 100mL of 10X HBSS without Ca, Mg, bicarbonate, or phenol red to 900mL of Millipore water with stirring.
- Add 5 mM HEPES (1.3g/L, MW=260.3) to 900mL of 1X HBSS and wait until dissolved.
- Add 10g of glucose and wait until dissolved.
- Add 10 mL (1%) antibiotic/antimycotic.
- Adjust pH to 7.4 with NaOH.
- Bring liquid level up to 1L with 1X HBSS. Verify pH is 7.4.
- Filter-sterilize and store at +4°C.

Preparation of 1% Trypsin:

- Dilute 10mL of 2.5% trypsin without Ca, Mg, phenol red in 15mL of sterile HBSS with 1% glucose to make 1.0% trypsin.
- Freeze in 5mL aliquots at -20°C. Store ≤1 year.

OR

Preparation of 1% Trypsin/ 0.2% EDTA solution:

- Dissolve 200mg EDTA in 10mL Millipore water (2% w/v) and sterilize with 0.2um syringe filter.
- Add 10mL of 2.5% trypsin without Ca, Mg, phenol red and 2.5mL sterile EDTA solution to 12.5mL of sterile HBSS with 1% glucose to make 1% trypsin-0.2% EDTA.
- Freeze in 5mL aliquots at -20°C. Store ≤1 year.

Preparation of 1.33% Collagenase:

- Dilute 53.2 mg collagenase in 4 mL of L15 media for a 13.3 mg/mL concentration.
- Syringe-filter with 0.2µm syringe filter.
- Freeze in 500µL aliquots at -20°C. Store ≤1 year.

Preparation of 1.0% Dnase:

- Dilute 40 mg DNase in 4 mL of L15 media for a 10 mg/mL concentration.
- Syringe-filter with 0.2µm syringe filter.
- Freeze in 500µL aliquots at -20°C. Store ≤1 year.

Preparation of Serum Medium:

Base Medium: DMEM-F12 with L-glutamine

- 10% FBS (100 μL per mL media)
- 1% antibiotic/antimycotic (10 μL per mL media)
- Add 1μL of NGF (20 μg/mL stock solution) per mL media for 20ng/mL concentration of NGF. Add NGF immediately prior to use.
- Complete culture medium with NGF can be stored at +4°C for up to 5 days.

25mL:

22.5 mL DMEM-F12
2.5 mL FBS
250 μL antibiotic/antimycotic
25 μL NGF (20 μg/mL stock solution)

Preparation for Dissection:

1. Prepare and sterilize media.
2. Ensure dissection tools are autoclaved. If autoclaving is not possible, sterilize tools with 70% ethanol for 30 minutes.
3. UV sterilize the dissection hood for at least 30 minutes prior to dissection.

Dissection Method:

1. Thaw out one 4mL aliquot of trypsin and warm to 37°C in water bath. Use ice-cold sterile HBSS with glucose.
2. Perform dissection in the open dissection hood with microscope.
3. Set-up an autoclave bag for all waste products.
4. Prior to the dissection, pour ice-cold HBSS with glucose into:
    a. 4mL in 100mm petri dish for postnatal rat
    b. 2mL in 35mm petri dish for storage of DRG during dissection
    c. 2mL in 15mL tube (for transfer of DRG from 35mm petri dish)
5. Use the dissection microscope with the under-sided lamp to illuminate the rat.
6. Turn the rat on its side and gently cut along the vertebral column with the large scissors to separate the spinal column.
7. Use the small scissors to cut through the bone on each side of the spinal column and gently separate the two halves to expose the spinal cord.
8. Carefully separate the spinal cord from the bone to expose the DRG.
9. Pluck the DRG from spinal column using fine forceps, and cut the spinal nerves close to the DRG to minimize contamination by nonneuronal cells from nerve sheaths. Transfer the DRG to the separate 35mm petri dish containing cold HBSS with glucose.

10. Transfer DRG from 35mm petri dish to 15mL centrifuge tube with 1mL pipet. The cells may adhere to the plastic tip and petri dish so rinse thoroughly to make sure all tissue is transferred.
11. It should take approximately 15 minutes per rat. Do not take longer than 1 hour to do the dissection (limit time to 1-1/2 hours from start of dissection to plating to minimize cell damage, this includes 30 min dissociation in trypsin).

Dissociation and Plating:

1. Warm L15 and serum media in 37°C incubator with 7% CO_2 for 30 minutes to bring temperature and pH up to physiological levels.
2. In a cell culture hood, allow tissue to settle, remove HBSS, and add 2mL L15 media and 0.5mL of 1.33% collagenase and incubate in 37°C water bath for 30 minutes.
3. Centrifuge cells at 1000 rpm for 5 minutes and discard supernatant.
4. Add 4 mL of DMEM/F12 (no serum), 1mL 1% trypsin in HBSS, and 50µL of 1% DNase, and incubate in 37ºC with 7% CO_2 incubator for 30 minutes.
5. Centrifuge cells at 1000 rpm for 5 minutes and discard supernatant.
6. Add 4 mL of serum medium to deactivate the trypsin, centrifuge again, and discard supernatant.
7. Add 2 mL of warm serum medium and triturate at least 20 times with 3mL syringe with 22G needle (needle diameter is 0.7mm), avoiding air bubbles as this will damage cells. Ensure all tissue is broken up.
8. Add 4mL media and mix gently. Add the 6mL cell suspension to 100mm petri dish and incubate for 2-4 hours in humidified 37°C, 7% CO_2 incubator. Non-neuronal cells should adhere to petri dish and neurons should remain floating or weakly attached.
9. After 2-4 hours, tilt petri dish at 45 degrees and gently wash bottom twice to remove weakly attached neurons, then transfer to 15mL tube.
10. Centrifuge at 1000 rpm for 5 minutes. Ensure there is a pellet, remove media, and resuspend in 200µL warm serum media by triturating 3-4 times gently with 200µL pipet tip.
11. Count cells using hemacytometer (1:2 dilution). Neurons appear rounded and phase-bright whereas non-neuronal cells are darker and irregularly shaped. DRG neuron diameters may be 7µm to 18 µm.
12. Seed approximately twice as many neurons as you think you will need in each 96-well as approximately 30-40% of cells will not attach in the first day of culture and up to 50% are lost after 3 days of culture.
13. Plate cells using the serum media. REMINDER: NGF must be added to the media immediately before use.
14. Plate cells in 100µL media per well. Change media after allowing 2 hours for attachment and add 200µL media per well. **OR** Plate cells in 200µL media and change media the next morning.
15. Incubate in a humidified 37°C, 7% CO_2 incubator.
16. Change media every 2 days.

17. Corning 3596 96-well plates (Fisher 07-200-90) have well diameter of 6.4mm and growth area of 0.32 cm^2, currently seeding 2,000 DRG's per 96-well.

Conclusion of Dissection:

1. Gently clean all dissection tools immediately with detergent to prevent drying of blood.
2. Wipe the dissection hood with 70% ethanol and UV sterilize for at least 30 minutes.
3. Dispose of all waste in an autoclave biohazard bag, tie the bag shut, and dispose of in the designated freezer.

APPENDIX E

PREDICTED AMINO ACID SEQUENCE FOR 140 kDA L1 FRAGMENT

GenBank accession no. NM_000425

L = LYSINE, 71 total
C = CYSTEINE, 14 total

MVVALRYVWPLLLCSPCLLIQIPEEYEGHHVMEPPVITEQSPRRLVVFPT
DDISLKCEASGKPEVQFRWTRDGVHFKPKEELGVTVYQSPHSGSFTITGN
NSNFAQRFQGIYRCFASNKLGTAMSHEIRLMAEGAPKWPKETVKPVEVEE
GESVVLPCNPPPSAEPLRIYWMNSKILHIKQDERVTMGQNGNLYFANVLT
SDNHSDYICHAHFPGTRTIIQKEPIDLRVKATNSMIDRKPRLLFPTNSSS
HLVALQGQPLVLECIAEGFPTPTIKWLRPSGPMPADRVTYQNHNKTLQLL
KVGEEDDGEYRCLAENSLGSARHAYYVTVEAAPYWLHKPQSHLYGPGETA
RLDCQVQGRPQPEVTWRINGIPVEELAKDQKYRIQRGALILSNVQPSDTM
VTQCEARNRHGLLLANAYIYVVQLPAKILTADNQTYMAVQGSTAYLLCKA
FGAPVPSVQWLDEDGTTVLQDERFFPYANGTLGIRDLQANDTGRYFCLAA
NDQNNVTIMANLKVKDATQITQGPRSTIEKKGSRVTFTCQASFDPSLQPS
ITWRGDGRDLQELGDSDKYFIEDGRLVIHSLDYSDQGNYSCVASTELDVV
ESRAQLLVVGSPGPVPRLVLSDLHLLTQSQVRVSWSPAEDHNAPIEKYDI
EFEDKEMAPEKWYSLGKVPGNQTSTTLKLSPYVHYTFRVTAINKYGPGEP
SPVSETVVTPEAAPEKNPVDVKGEGNETTNMVITWKPLRWMDWNAPQVQY
RVQWRPQGTRGPWQEQIVSDPFLVVSNTSTFVPYEIKVQAVNSQGKGPEP
QVTIGYSGEDYPQAIPELEGIEILNSSAVLVKWRPVDLAQVKGHLRGYNV
TYWREGSQRK

REFERENCES

1. Berkowitz, M., *Spinal cord injury : an analysis of medical and social costs*. 1998, New York, N.Y.: Demos. x, 188 p.
2. Sipski, M.L. and D.D. Pearse, *Methylprednisolone and other confounders to spinal cord injury clinical trials.* Nat Clin Pract Neurol, 2006. **2**(8): p. 402-3.
3. Fehlings, M.G. and D.C. Baptiste, *Current status of clinical trials for acute spinal cord injury.* Injury, 2005. **36 Suppl 2**: p. B113-22.
4. Elsberg, C.A., *Dr. Edwin Smith surgical papyrus and the diagnosis and treatment of injuries to the skull and spine 5000 years ago*. 1931. p. 1.
5. Dellon, E.S. and A.L. Dellon, *The first nerve graft, Vulpian, and the nineteenth century neural regeneration controversy.* J Hand Surg Am, 1993. **18**(2): p. 369-72.
6. RamoÌ□n y Cajal, S., et al., *Cajal's degeneration and regeneration of the nervous system*. History of neuroscience ; no. 5. 1991, New York: Oxford University Press. xvi, 769 p.
7. RamoÌ□n y Cajal, S. and R.M. May, *Degeneration & regeneration of the nervous system*. 1928, London: Oxford University Press, Humphrey Milford. 2 v. (xx, 769 p.).
8. Berciano, J., M. Lafarga, and M. Berciano, *Santiago Ramon y Cajal.* Neurologia, 2001. **16**(3): p. 118-21.
9. Tuszynski, M.H. and J.H. Kordower, *CNS regeneration : basic science and clinical advances*. 1999, San Diego: Academic Press. xvi, 678 p., [16] p. of plates.
10. Cai, D., et al., *Neuronal cyclic AMP controls the developmental loss in ability of axons to regenerate.* J Neurosci, 2001. **21**(13): p. 4731-9.
11. Schwab, M.E. and D. Bartholdi, *Degeneration and regeneration of axons in the lesioned spinal cord.* Physiol Rev, 1996. **76**(2): p. 319-70.
12. Deumens, R., G.C. Koopmans, and E.A. Joosten, *Regeneration of descending axon tracts after spinal cord injury.* Prog Neurobiol, 2005. **77**(1-2): p. 57-89.
13. Horner, P.J. and F.H. Gage, *Regenerating the damaged central nervous system.* Nature, 2000. **407**(6807): p. 963-70.
14. Verma, P. and J. Fawcett, *Spinal cord regeneration.* Adv Biochem Eng Biotechnol, 2005. **94**: p. 43-66.
15. Rutkowski, G.E., et al., *Synergistic effects of micropatterned biodegradable conduits and Schwann cells on sciatic nerve regeneration.* J Neural Eng, 2004. **1**(3): p. 151-7.
16. Xu, X.M., et al., *Regrowth of axons into the distal spinal cord through a Schwann-cell-seeded mini-channel implanted into hemisected adult rat spinal cord.* Eur J Neurosci, 1999. **11**(5): p. 1723-40.
17. Hurtado, A., et al., *Poly (D,L-lactic acid) macroporous guidance scaffolds seeded with Schwann cells genetically modified to secrete a bi-functional neurotrophin implanted in the completely transected adult rat thoracic spinal cord.* Biomaterials, 2006. **27**(3): p. 430-42.

18. Geller, H.M. and J.W. Fawcett, *Building a bridge: engineering spinal cord repair.* Exp Neurol, 2002. **174**(2): p. 125-36.
19. Guyton, A.C. and J.E. Hall, *Textbook of medical physiology*. 10th ed. 2000, Philadelphia: Saunders. xxxii, 1064 p.
20. Simons, M. and K. Trajkovic, *Neuron-glia communication in the control of oligodendrocyte function and myelin biogenesis.* J Cell Sci, 2006. **119**(Pt 21): p. 4381-9.
21. Benarroch, E.E., *Neuron-astrocyte interactions: partnership for normal function and disease in the central nervous system.* Mayo Clin Proc, 2005. **80**(10): p. 1326-38.
22. Aloisi, F., *Immune function of microglia.* Glia, 2001. **36**(2): p. 165-79.
23. Chen, Z.J., et al., *Oligodendrocyte precursor cells: reactive cells that inhibit axon growth and regeneration.* J Neurocytol, 2002. **31**(6-7): p. 481-95.
24. Corfas, G., et al., *Mechanisms and roles of axon-Schwann cell interactions.* J Neurosci, 2004. **24**(42): p. 9250-60.
25. Armati, P.J., *The biology of Schwann cells : development, differentiation and immunomodulation*. 2007, Cambridge, UK ; New York: Cambridge University Press. xiii, 249 p., [16] p. of plates.
26. Fu, S.Y. and T. Gordon, *The cellular and molecular basis of peripheral nerve regeneration.* Mol Neurobiol, 1997. **14**(1-2): p. 67-116.
27. Guth, L., *Regeneration in the mammalian peripheral nervous system.* Physiol Rev, 1956. **36**(4): p. 441-78.
28. Schmidt, C.E. and J.B. Leach, *Neural tissue engineering: strategies for repair and regeneration.* Annu Rev Biomed Eng, 2003. **5**: p. 293-347.
29. el-Barrany, W.G., A.G. Marei, and B. Vallee, *Anatomic basis of vascularised nerve grafts: the blood supply of peripheral nerves.* Surg Radiol Anat, 1999. **21**(2): p. 95-102.
30. Brockstein, B., L. Johns, and B.L. Gewertz, *Blood supply to the spinal cord: anatomic and physiologic correlations.* Ann Vasc Surg, 1994. **8**(4): p. 394-9.
31. Waxman, S.G., *Multiple sclerosis as a neuronal disease*. 2005, Amsterdam ; Boston: Elsevier Academic Press. x, 484 p.
32. Thuret, S., L.D. Moon, and F.H. Gage, *Therapeutic interventions after spinal cord injury.* Nat Rev Neurosci, 2006. **7**(8): p. 628-43.
33. Hagg, T. and M. Oudega, *Degenerative and spontaneous regenerative processes after spinal cord injury.* J Neurotrauma, 2006. **23**(3-4): p. 264-80.
34. George, R. and J.W. Griffin, *Delayed macrophage responses and myelin clearance during Wallerian degeneration in the central nervous system: the dorsal radiculotomy model.* Exp Neurol, 1994. **129**(2): p. 225-36.
35. Kruger, S., et al., *Three morphologically distinct types of interface develop between adult host and fetal brain transplants: implications for scar formation in the adult central nervous system.* J Comp Neurol, 1986. **249**(1): p. 103-16.
36. Fitch, M.T., et al., *Cellular and molecular mechanisms of glial scarring and progressive cavitation: in vivo and in vitro analysis of inflammation-induced secondary injury after CNS trauma.* J Neurosci, 1999. **19**(19): p. 8182-98.

37. Faulkner, J.R., et al., *Reactive astrocytes protect tissue and preserve function after spinal cord injury.* J Neurosci, 2004. **24**(9): p. 2143-55.
38. Bush, T.G., et al., *Leukocyte infiltration, neuronal degeneration, and neurite outgrowth after ablation of scar-forming, reactive astrocytes in adult transgenic mice.* Neuron, 1999. **23**(2): p. 297-308.
39. Silver, J. and J.H. Miller, *Regeneration beyond the glial scar.* Nat Rev Neurosci, 2004. **5**(2): p. 146-56.
40. Li, D., P.M. Field, and G. Raisman, *Failure of axon regeneration in postnatal rat entorhinohippocampal slice coculture is due to maturation of the axon, not that of the pathway or target.* Eur J Neurosci, 1995. **7**(6): p. 1164-71.
41. Chen, D.F., S. Jhaveri, and G.E. Schneider, *Intrinsic changes in developing retinal neurons result in regenerative failure of their axons.* Proc Natl Acad Sci U S A, 1995. **92**(16): p. 7287-91.
42. Tseng, G.F., et al., *A time-dependent loss of retrograde transport ability in distally axotomized rubrospinal neurons.* Anat Embryol (Berl), 1995. **191**(3): p. 243-9.
43. Kalil, K. and J.H. Skene, *Elevated synthesis of an axonally transported protein correlates with axon outgrowth in normal and injured pyramidal tracts.* J Neurosci, 1986. **6**(9): p. 2563-70.
44. Fournier, A.E. and L. McKerracher, *Tubulin expression and axonal transport in injured and regenerating neurons in the adult mammalian central nervous system.* Biochem Cell Biol, 1995. **73**(9-10): p. 659-64.
45. Mikucki, S.A. and M.M. Oblinger, *Corticospinal neurons exhibit a novel pattern of cytoskeletal gene expression after injury.* J Neurosci Res, 1991. **30**(1): p. 213-25.
46. Twiss, J.L. and J. van Minnen, *New insights into neuronal regeneration: the role of axonal protein synthesis in pathfinding and axonal extension.* J Neurotrauma, 2006. **23**(3-4): p. 295-308.
47. Verma, P., et al., *Axonal protein synthesis and degradation are necessary for efficient growth cone regeneration.* J Neurosci, 2005. **25**(2): p. 331-42.
48. Fawcett, J.W., *Overcoming inhibition in the damaged spinal cord.* J Neurotrauma, 2006. **23**(3-4): p. 371-83.
49. Qiu, J., et al., *Spinal axon regeneration induced by elevation of cyclic AMP.* Neuron, 2002. **34**(6): p. 895-903.
50. Spencer, T. and M.T. Filbin, *A role for cAMP in regeneration of the adult mammalian CNS.* J Anat, 2004. **204**(1): p. 49-55.
51. Neumann, S., et al., *Regeneration of sensory axons within the injured spinal cord induced by intraganglionic cAMP elevation.* Neuron, 2002. **34**(6): p. 885-93.
52. He, Z. and V. Koprivica, *The Nogo signaling pathway for regeneration block.* Annu Rev Neurosci, 2004. **27**: p. 341-68.
53. McKerracher, L., *Spinal cord repair: strategies to promote axon regeneration.* Neurobiol Dis, 2001. **8**(1): p. 11-8.

54. Neumann, S. and C.J. Woolf, *Regeneration of dorsal column fibers into and beyond the lesion site following adult spinal cord injury.* Neuron, 1999. **23**(1): p. 83-91.
55. Bomze, H.M., et al., *Spinal axon regeneration evoked by replacing two growth cone proteins in adult neurons.* Nat Neurosci, 2001. **4**(1): p. 38-43.
56. Neumann, S., K. Skinner, and A.I. Basbaum, *Sustaining intrinsic growth capacity of adult neurons promotes spinal cord regeneration.* Proc Natl Acad Sci U S A, 2005. **102**(46): p. 16848-52.
57. Barres, B.A., et al., *Does oligodendrocyte survival depend on axons?* Curr Biol, 1993. **3**(8): p. 489-97.
58. Davies, S.J., et al., *Robust regeneration of adult sensory axons in degenerating white matter of the adult rat spinal cord.* J Neurosci, 1999. **19**(14): p. 5810-22.
59. Keirstead, H.S., et al., *Suppression of the onset of myelination extends the permissive period for the functional repair of embryonic spinal cord.* Proc Natl Acad Sci U S A, 1992. **89**(24): p. 11664-8.
60. Pettigrew, D.B. and K.A. Crutcher, *Myelin contributes to the parallel orientation of axonal growth on white matter in vitro.* BMC Neurosci, 2001. **2**: p. 9.
61. Pettigrew, D.B., K.P. Shockley, and K.A. Crutcher, *Disruption of spinal cord white matter and sciatic nerve geometry inhibits axonal growth in vitro in the absence of glial scarring.* BMC Neurosci, 2001. **2**: p. 8.
62. Kwon, B.K., J.F. Borisoff, and W. Tetzlaff, *Molecular targets for therapeutic intervention after spinal cord injury.* Mol Interv, 2002. **2**(4): p. 244-58.
63. Simonen, M., et al., *Systemic deletion of the myelin-associated outgrowth inhibitor Nogo-A improves regenerative and plastic responses after spinal cord injury.* Neuron, 2003. **38**(2): p. 201-11.
64. Kim, J.E., et al., *Axon regeneration in young adult mice lacking Nogo-A/B.* Neuron, 2003. **38**(2): p. 187-99.
65. Domeniconi, M., et al., *Myelin-associated glycoprotein interacts with the Nogo66 receptor to inhibit neurite outgrowth.* Neuron, 2002. **35**(2): p. 283-90.
66. McKerracher, L. and S. David, *Easing the brakes on spinal cord repair.* Nat Med, 2004. **10**(10): p. 1052-3.
67. Domeniconi, M., et al., *MAG induces regulated intramembrane proteolysis of the p75 neurotrophin receptor to inhibit neurite outgrowth.* Neuron, 2005. **46**(6): p. 849-55.
68. Schwab, M.E., *Nogo and axon regeneration.* Curr Opin Neurobiol, 2004. **14**(1): p. 118-24.
69. Schwab, J.M., S.K. Tuli, and V. Failli, *The Nogo receptor complex: confining molecules to molecular mechanisms.* Trends Mol Med, 2006. **12**(7): p. 293-7.
70. GrandPre, T., et al., *Identification of the Nogo inhibitor of axon regeneration as a Reticulon protein.* Nature, 2000. **403**(6768): p. 439-44.
71. Pot, C., et al., *Nogo-A expressed in Schwann cells impairs axonal regeneration after peripheral nerve injury.* J Cell Biol, 2002. **159**(1): p. 29-35.
72. Harrison, R.G., *The outgrowth of the nerve fiber as a mode of protoplasmic movement.* J Exp Zool, 1959. **142**: p. 5-73.

73. Morgenstern, D.A., R.A. Asher, and J.W. Fawcett, *Chondroitin sulphate proteoglycans in the CNS injury response.* Prog Brain Res, 2002. **137**: p. 313-32.
74. Monnier, P.P., et al., *The Rho/ROCK pathway mediates neurite growth-inhibitory activity associated with the chondroitin sulfate proteoglycans of the CNS glial scar.* Mol Cell Neurosci, 2003. **22**(3): p. 319-30.
75. Jacobson, S. and L. Guth, *An Electrophysiological Study of the Early Stages of Peripheral Nerve Regeneration.* Exp Neurol, 1965. **11**: p. 48-60.
76. Liesi, P. and J. Silver, *Is astrocyte laminin involved in axon guidance in the mammalian CNS?* Dev Biol, 1988. **130**(2): p. 774-85.
77. Schnell, L., et al., *Neurotrophin-3 enhances sprouting of corticospinal tract during development and after adult spinal cord lesion.* Nature, 1994. **367**(6459): p. 170-3.
78. Silver, J., M. Poston, and U. Rutishauser, *Axon pathway boundaries in the developing brain. I. Cellular and molecular determinants that separate the optic and olfactory projections.* J Neurosci, 1987. **7**(7): p. 2264-72.
79. Silver, J. and U. Rutishauser, *Guidance of optic axons in vivo by a preformed adhesive pathway on neuroepithelial endfeet.* Dev Biol, 1984. **106**(2): p. 485-99.
80. Silver, J. and R.L. Sidman, *A mechanism for the guidance and topographic patterning of retinal ganglion cell axons.* J Comp Neurol, 1980. **189**(1): p. 101-11.
81. Silver, J., et al., *Axonal guidance during development of the great cerebral commissures: descriptive and experimental studies, in vivo, on the role of preformed glial pathways.* J Comp Neurol, 1982. **210**(1): p. 10-29.
82. Joosten, E.A. and A.A. Gribnau, *Astrocytes and guidance of outgrowing corticospinal tract axons in the rat. An immunocytochemical study using anti-vimentin and anti-glial fibrillary acidic protein.* Neuroscience, 1989. **31**(2): p. 439-52.
83. Hsu, J.Y., S.A. Stein, and X.M. Xu, *Temporal and spatial distribution of growth-associated molecules and astroglial cells in the rat corticospinal tract during development.* J Neurosci Res, 2005. **80**(3): p. 330-40.
84. Costa, S., et al., *Astroglial permissivity for neuritic outgrowth in neuron-astrocyte cocultures depends on regulation of laminin bioavailability.* Glia, 2002. **37**(2): p. 105-13.
85. Deumens, R., et al., *Alignment of glial cells stimulates directional neurite growth of CNS neurons in vitro.* Neuroscience, 2004. **125**(3): p. 591-604.
86. Lazarov-Spiegler, O., et al., *Restricted inflammatory reaction in the CNS: a key impediment to axonal regeneration?* Mol Med Today, 1998. **4**(8): p. 337-42.
87. Rapalino, O., et al., *Implantation of stimulated homologous macrophages results in partial recovery of paraplegic rats.* Nat Med, 1998. **4**(7): p. 814-21.
88. Schwartz, M., et al., *Potential repair of rat spinal cord injuries using stimulated homologous macrophages.* Neurosurgery, 1999. **44**(5): p. 1041-5; discussion 1045-6.
89. Bomstein, Y., et al., *Features of skin-coincubated macrophages that promote recovery from spinal cord injury.* J Neuroimmunol, 2003. **142**(1-2): p. 10-6.

90. Popovich, P.G., et al., *Depletion of hematogenous macrophages promotes partial hindlimb recovery and neuroanatomical repair after experimental spinal cord injury.* Exp Neurol, 1999. **158**(2): p. 351-65.
91. Schwartz, M. and E. Yoles, *Macrophages and dendritic cells treatment of spinal cord injury: from the bench to the clinic.* Acta Neurochir Suppl, 2005. **93**: p. 147-50.
92. Schwartz, M. and E. Yoles, *Immune-based therapy for spinal cord repair: autologous macrophages and beyond.* J Neurotrauma, 2006. **23**(3-4): p. 360-70.
93. Knoller, N., et al., *Clinical experience using incubated autologous macrophages as a treatment for complete spinal cord injury: phase I study results.* J Neurosurg Spine, 2005. **3**(3): p. 173-81.
94. Moon, L. and M.B. Bunge, *From animal models to humans: strategies for promoting CNS axon regeneration and recovery of limb function after spinal cord injury.* J Neurol Phys Ther, 2005. **29**(2): p. 55-69.
95. Schnell, L. and M.E. Schwab, *Axonal regeneration in the rat spinal cord produced by an antibody against myelin-associated neurite growth inhibitors.* Nature, 1990. **343**(6255): p. 269-72.
96. Brosamle, C., et al., *Regeneration of lesioned corticospinal tract fibers in the adult rat induced by a recombinant, humanized IN-1 antibody fragment.* J Neurosci, 2000. **20**(21): p. 8061-8.
97. Fouad, K., I. Klusman, and M.E. Schwab, *Regenerating corticospinal fibers in the Marmoset (Callitrix jacchus) after spinal cord lesion and treatment with the anti-Nogo-A antibody IN-1.* Eur J Neurosci, 2004. **20**(9): p. 2479-82.
98. Tator, C.H., *Review of treatment trials in human spinal cord injury: issues, difficulties, and recommendations.* Neurosurgery, 2006. **59**(5): p. 957-82; discussion 982-7.
99. GrandPre, T., S. Li, and S.M. Strittmatter, *Nogo-66 receptor antagonist peptide promotes axonal regeneration.* Nature, 2002. **417**(6888): p. 547-51.
100. Li, W., et al., *A neutralizing anti-Nogo66 receptor monoclonal antibody reverses inhibition of neurite outgrowth by central nervous system myelin.* J Biol Chem, 2004. **279**(42): p. 43780-8.
101. Shearer, M.C., et al., *The astrocyte/meningeal cell interface is a barrier to neurite outgrowth which can be overcome by manipulation of inhibitory molecules or axonal signalling pathways.* Mol Cell Neurosci, 2003. **24**(4): p. 913-25.
102. Goldshmit, Y., et al., *Axonal regeneration and lack of astrocytic gliosis in EphA4-deficient mice.* J Neurosci, 2004. **24**(45): p. 10064-73.
103. Moon, L.D., et al., *Regeneration of CNS axons back to their target following treatment of adult rat brain with chondroitinase ABC.* Nat Neurosci, 2001. **4**(5): p. 465-6.
104. Bradbury, E.J., et al., *Chondroitinase ABC promotes functional recovery after spinal cord injury.* Nature, 2002. **416**(6881): p. 636-40.
105. Caggiano, A.O., et al., *Chondroitinase ABCI improves locomotion and bladder function following contusion injury of the rat spinal cord.* J Neurotrauma, 2005. **22**(2): p. 226-39.

106. Ellezam, B., et al., *Inactivation of intracellular Rho to stimulate axon growth and regeneration.* Prog Brain Res, 2002. **137**: p. 371-80.
107. McKerracher, L. and H. Higuchi, *Targeting Rho to stimulate repair after spinal cord injury.* J Neurotrauma, 2006. **23**(3-4): p. 309-17.
108. Blight, A.R. and M.H. Tuszynski, *Clinical trials in spinal cord injury.* J Neurotrauma, 2006. **23**(3-4): p. 586-93.
109. Pearse, D.D., et al., *cAMP and Schwann cells promote axonal growth and functional recovery after spinal cord injury.* Nat Med, 2004. **10**(6): p. 610-6.
110. Nikulina, E., et al., *The phosphodiesterase inhibitor rolipram delivered after a spinal cord lesion promotes axonal regeneration and functional recovery.* Proc Natl Acad Sci U S A, 2004. **101**(23): p. 8786-90.
111. Romero, M.I., et al., *Extensive sprouting of sensory afferents and hyperalgesia induced by conditional expression of nerve growth factor in the adult spinal cord.* J Neurosci, 2000. **20**(12): p. 4435-45.
112. Patapoutian, A. and L.F. Reichardt, *Trk receptors: mediators of neurotrophin action.* Curr Opin Neurobiol, 2001. **11**(3): p. 272-80.
113. Jones, L.L., et al., *Neurotrophic factors, cellular bridges and gene therapy for spinal cord injury.* J Physiol, 2001. **533**(Pt 1): p. 83-9.
114. Blits, B., G.J. Boer, and J. Verhaagen, *Pharmacological, cell, and gene therapy strategies to promote spinal cord regeneration.* Cell Transplant, 2002. **11**(6): p. 593-613.
115. Markus, A., T.D. Patel, and W.D. Snider, *Neurotrophic factors and axonal growth.* Curr Opin Neurobiol, 2002. **12**(5): p. 523-31.
116. Miller, F.D. and D.R. Kaplan, *On Trk for retrograde signaling.* Neuron, 2001. **32**(5): p. 767-70.
117. Schwab, M.E., *Repairing the injured spinal cord.* Science, 2002. **295**(5557): p. 1029-31.
118. Giehl, K.M., *Trophic dependencies of rodent corticospinal neurons.* Rev Neurosci, 2001. **12**(1): p. 79-94.
119. Bradbury, E.J., et al., *NT-3, but not BDNF, prevents atrophy and death of axotomized spinal cord projection neurons.* Eur J Neurosci, 1998. **10**(10): p. 3058-68.
120. Shibayama, M., et al., *Neurotrophin-3 prevents death of axotomized Clarke's nucleus neurons in adult rat.* J Comp Neurol, 1998. **390**(1): p. 102-11.
121. Geschwind, M.D., et al., *Transfer of the nerve growth factor gene into cell lines and cultured neurons using a defective herpes simplex virus vector. Transfer of the NGF gene into cells by a HSV-1 vector.* Brain Res Mol Brain Res, 1994. **24**(1-4): p. 327-35.
122. Zhang, Y., et al., *NT-3 delivered by an adenoviral vector induces injured dorsal root axons to regenerate into the spinal cord of adult rats.* J Neurosci Res, 1998. **54**(4): p. 554-62.
123. Ruitenberg, M.J., et al., *Adeno-associated viral vector-mediated gene transfer of brain-derived neurotrophic factor reverses atrophy of rubrospinal neurons*

following both acute and chronic spinal cord injury. Neurobiol Dis, 2004. **15**(2): p. 394-406.
124. Hottinger, A.F., et al., *Complete and long-term rescue of lesioned adult motoneurons by lentiviral-mediated expression of glial cell line-derived neurotrophic factor in the facial nucleus.* J Neurosci, 2000. **20**(15): p. 5587-93.
125. Grill, R., et al., *Cellular delivery of neurotrophin-3 promotes corticospinal axonal growth and partial functional recovery after spinal cord injury.* J Neurosci, 1997. **17**(14): p. 5560-72.
126. Tuszynski, M.H., et al., *Spontaneous and augmented growth of axons in the primate spinal cord: effects of local injury and nerve growth factor-secreting cell grafts.* J Comp Neurol, 2002. **449**(1): p. 88-101.
127. Lu, P., et al., *Neural stem cells constitutively secrete neurotrophic factors and promote extensive host axonal growth after spinal cord injury.* Exp Neurol, 2003. **181**(2): p. 115-29.
128. Tuszynski, M.H., et al., *NT-3 gene delivery elicits growth of chronically injured corticospinal axons and modestly improves functional deficits after chronic scar resection.* Exp Neurol, 2003. **181**(1): p. 47-56.
129. Blesch, A., et al., *Axonal responses to cellularly delivered NT-4/5 after spinal cord injury.* Mol Cell Neurosci, 2004. **27**(2): p. 190-201.
130. Lu, P., L.L. Jones, and M.H. Tuszynski, *BDNF-expressing marrow stromal cells support extensive axonal growth at sites of spinal cord injury.* Exp Neurol, 2005. **191**(2): p. 344-60.
131. Reier, P.J., et al., *Neural tissue transplantation and CNS trauma: anatomical and functional repair of the injured spinal cord.* J Neurotrauma, 1992. **9 Suppl 1**: p. S223-48.
132. Reier, P.J., et al., *Fetal cell grafts into resection and contusion/compression injuries of the rat and cat spinal cord.* Exp Neurol, 1992. **115**(1): p. 177-88.
133. Bregman, B.S., et al., *Recovery of function after spinal cord injury: mechanisms underlying transplant-mediated recovery of function differ after spinal cord injury in newborn and adult rats.* Exp Neurol, 1993. **123**(1): p. 3-16.
134. Thompson, F.J., et al., *Neurophysiological assessment of the feasibility and safety of neural tissue transplantation in patients with syringomyelia.* J Neurotrauma, 2001. **18**(9): p. 931-45.
135. Wirth, E.D., 3rd, et al., *Feasibility and safety of neural tissue transplantation in patients with syringomyelia.* J Neurotrauma, 2001. **18**(9): p. 911-29.
136. Pfister, B.J., et al., *Development of transplantable nervous tissue constructs comprised of stretch-grown axons.* J Neurosci Methods, 2006. **153**(1): p. 95-103.
137. Iwata, A., et al., *Long-term survival and outgrowth of mechanically engineered nervous tissue constructs implanted into spinal cord lesions.* Tissue Eng, 2006. **12**(1): p. 101-10.
138. Richardson, P.M., U.M. McGuinness, and A.J. Aguayo, *Axons from CNS neurons regenerate into PNS grafts.* Nature, 1980. **284**(5753): p. 264-5.

139. Richardson, P.M., U.M. McGuinness, and A.J. Aguayo, *Peripheral nerve autografts to the rat spinal cord: studies with axonal tracing methods.* Brain Res, 1982. **237**(1): p. 147-62.
140. Myckatyn, T.M., S.E. Mackinnon, and J.W. McDonald, *Stem cell transplantation and other novel techniques for promoting recovery from spinal cord injury.* Transpl Immunol, 2004. **12**(3-4): p. 343-58.
141. Levi, A.D., et al., *Peripheral nerve grafts promoting central nervous system regeneration after spinal cord injury in the primate.* J Neurosurg, 2002. **96**(2 Suppl): p. 197-205.
142. Cheng, H., Y. Cao, and L. Olson, *Spinal cord repair in adult paraplegic rats: partial restoration of hind limb function.* Science, 1996. **273**(5274): p. 510-3.
143. Cheng, H., et al., *Spinal cord repair with acidic fibroblast growth factor as a treatment for a patient with chronic paraplegia.* Spine, 2004. **29**(14): p. E284-8.
144. Bunge, M.B., *Bridging areas of injury in the spinal cord.* Neuroscientist, 2001. **7**(4): p. 325-39.
145. Oudega, M. and X.M. Xu, *Schwann cell transplantation for repair of the adult spinal cord.* J Neurotrauma, 2006. **23**(3-4): p. 453-67.
146. Lavdas, A.A., et al., *Schwann cell transplantation for CNS repair.* Curr Med Chem, 2008. **15**(2): p. 151-60.
147. Norenberg, M.D., J. Smith, and A. Marcillo, *The pathology of human spinal cord injury: defining the problems.* J Neurotrauma, 2004. **21**(4): p. 429-40.
148. Baron-Van Evercooren, A., et al., *Cell-cell interactions during the migration of myelin-forming cells transplanted in the demyelinated spinal cord.* Glia, 1996. **16**(2): p. 147-64.
149. Chan, J.R., et al., *NGF controls axonal receptivity to myelination by Schwann cells or oligodendrocytes.* Neuron, 2004. **43**(2): p. 183-91.
150. Tuszynski, M.H., et al., *Grafts of genetically modified Schwann cells to the spinal cord: survival, axon growth, and myelination.* Cell Transplant, 1998. **7**(2): p. 187-96.
151. Weidner, N., et al., *Nerve growth factor-hypersecreting Schwann cell grafts augment and guide spinal cord axonal growth and remyelinate central nervous system axons in a phenotypically appropriate manner that correlates with expression of L1.* J Comp Neurol, 1999. **413**(4): p. 495-506.
152. Menei, P., et al., *Schwann cells genetically modified to secrete human BDNF promote enhanced axonal regrowth across transected adult rat spinal cord.* Eur J Neurosci, 1998. **10**(2): p. 607-21.
153. Barnett, S.C. and J.S. Riddell, *Olfactory ensheathing cells (OECs) and the treatment of CNS injury: advantages and possible caveats.* J Anat, 2004. **204**(1): p. 57-67.
154. Fawcett, J., *Repair of spinal cord injuries: where are we, where are we going?* Spinal Cord, 2002. **40**(12): p. 615-23.
155. Ramer, L.M., M.S. Ramer, and J.D. Steeves, *Setting the stage for functional repair of spinal cord injuries: a cast of thousands.* Spinal Cord, 2005. **43**(3): p. 134-61.

156. Li, Y., P.M. Field, and G. Raisman, *Repair of adult rat corticospinal tract by transplants of olfactory ensheathing cells.* Science, 1997. **277**(5334): p. 2000-2.
157. Li, Y., P.M. Field, and G. Raisman, *Regeneration of adult rat corticospinal axons induced by transplanted olfactory ensheathing cells.* J Neurosci, 1998. **18**(24): p. 10514-24.
158. Fouad, K., et al., *Combining Schwann cell bridges and olfactory-ensheathing glia grafts with chondroitinase promotes locomotor recovery after complete transection of the spinal cord.* J Neurosci, 2005. **25**(5): p. 1169-78.
159. Barnett, S.C. and J.S. Riddell, *Olfactory ensheathing cell transplantation as a strategy for spinal cord repair--what can it achieve?* Nat Clin Pract Neurol, 2007. **3**(3): p. 152-61.
160. Lu, P., et al., *Olfactory ensheathing cells do not exhibit unique migratory or axonal growth-promoting properties after spinal cord injury.* J Neurosci, 2006. **26**(43): p. 11120-30.
161. Huang, H., et al., *Influence factors for functional improvement after olfactory ensheathing cell transplantation for chronic spinal cord injury.* Zhongguo Xiu Fu Chong Jian Wai Ke Za Zhi, 2006. **20**(4): p. 434-8.
162. Huang, H., et al., *Influence of patients' age on functional recovery after transplantation of olfactory ensheathing cells into injured spinal cord injury.* Chin Med J (Engl), 2003. **116**(10): p. 1488-91.
163. Huang, Y.C. and Y.Y. Huang, *Biomaterials and strategies for nerve regeneration.* Artif Organs, 2006. **30**(7): p. 514-22.
164. Dobkin, B.H., A. Curt, and J. Guest, *Cellular transplants in China: observational study from the largest human experiment in chronic spinal cord injury.* Neurorehabil Neural Repair, 2006. **20**(1): p. 5-13.
165. Galvin, K.A. and D.G. Jones, *Adult human neural stem cells for cell-replacement therapies in the central nervous system.* Med J Aust, 2002. **177**(6): p. 316-8.
166. McDonald, J.W., et al., *Repair of the injured spinal cord and the potential of embryonic stem cell transplantation.* J Neurotrauma, 2004. **21**(4): p. 383-93.
167. Liu, S., et al., *Embryonic stem cells differentiate into oligodendrocytes and myelinate in culture and after spinal cord transplantation.* Proc Natl Acad Sci U S A, 2000. **97**(11): p. 6126-31.
168. Kulbatski, I., et al., *Endogenous and exogenous CNS derived stem/progenitor cell approaches for neurotrauma.* Curr Drug Targets, 2005. **6**(1): p. 111-26.
169. Gage, F.H., *Mammalian neural stem cells.* Science, 2000. **287**(5457): p. 1433-8.
170. Brustle, O., et al., *Embryonic stem cell-derived glial precursors: a source of myelinating transplants.* Science, 1999. **285**(5428): p. 754-6.
171. Nomura, H., C.H. Tator, and M.S. Shoichet, *Bioengineered strategies for spinal cord repair.* J Neurotrauma, 2006. **23**(3-4): p. 496-507.
172. Coleman, W.P., et al., *A critical appraisal of the reporting of the National Acute Spinal Cord Injury Studies (II and III) of methylprednisolone in acute spinal cord injury.* J Spinal Disord, 2000. **13**(3): p. 185-99.
173. Baptiste, D.C. and M.G. Fehlings, *Pharmacological approaches to repair the injured spinal cord.* J Neurotrauma, 2006. **23**(3-4): p. 318-34.

174. Edgerton, V.R., et al., *Rehabilitative therapies after spinal cord injury.* J Neurotrauma, 2006. **23**(3-4): p. 560-70.
175. Gittler, M.S., et al., *Spinal cord injury medicine. 3. Rehabilitation outcomes.* Arch Phys Med Rehabil, 2002. **83**(3 Suppl 1): p. S65-71, S90-8.
176. Koopmans, G.C., et al., *The assessment of locomotor function in spinal cord injured rats: the importance of objective analysis of coordination.* J Neurotrauma, 2005. **22**(2): p. 214-25.
177. Anderson, D.K., et al., *Recommended guidelines for studies of human subjects with spinal cord injury.* Spinal Cord, 2005. **43**(8): p. 453-8.
178. Fawcett, J.W., et al., *Guidelines for the conduct of clinical trials for spinal cord injury as developed by the ICCP panel: spontaneous recovery after spinal cord injury and statistical power needed for therapeutic clinical trials.* Spinal Cord, 2007. **45**(3): p. 190-205.
179. Lammertse, D., et al., *Guidelines for the conduct of clinical trials for spinal cord injury as developed by the ICCP panel: clinical trial design.* Spinal Cord, 2007. **45**(3): p. 232-42.
180. Steeves, J.D., et al., *Guidelines for the conduct of clinical trials for spinal cord injury (SCI) as developed by the ICCP panel: clinical trial outcome measures.* Spinal Cord, 2007. **45**(3): p. 206-21.
181. Tuszynski, M.H., et al., *Guidelines for the conduct of clinical trials for spinal cord injury as developed by the ICCP Panel: clinical trial inclusion/exclusion criteria and ethics.* Spinal Cord, 2007. **45**(3): p. 222-31.
182. Kalb, R.G. and S.M. Strittmatter, *Neurobiology of spinal cord injury*. Contemporary neuroscience. 2000, Totowa, N.J.: Humana Press. xvii, 284 p.
183. Holmes, T.C., et al., *Extensive neurite outgrowth and active synapse formation on self-assembling peptide scaffolds.* Proc Natl Acad Sci U S A, 2000. **97**(12): p. 6728-33.
184. Sobel, R.A. and M.E. Mitchell, *Fibronectin in multiple sclerosis lesions.* Am J Pathol, 1989. **135**(1): p. 161-8.
185. Novikova, L.N., et al., *Alginate hydrogel and matrigel as potential cell carriers for neurotransplantation.* J Biomed Mater Res A, 2006. **77**(2): p. 242-52.
186. Lavik, E. and R. Langer, *Tissue engineering: current state and perspectives.* Appl Microbiol Biotechnol, 2004. **65**(1): p. 1-8.
187. Merle, M., et al., *Complications from silicon-polymer intubulation of nerves.* Microsurgery, 1989. **10**(2): p. 130-3.
188. Gibson, K.L., et al., *Comparison of nerve regeneration through different types of neural prostheses.* Microsurgery, 1991. **12**(2): p. 80-5.
189. Lore, A.B., et al., *Rapid induction of functional and morphological continuity between severed ends of mammalian or earthworm myelinated axons.* J Neurosci, 1999. **19**(7): p. 2442-54.
190. Jain, A., et al., *In situ gelling hydrogels for conformal repair of spinal cord defects, and local delivery of BDNF after spinal cord injury*. Biomaterials, 2006. **27**(3): p. 497-504.

191. Giannetti, S., et al., *Acrylic hydrogel implants after spinal cord lesion in the adult rat.* Neurol Res, 2001. **23**(4): p. 405-9.
192. Rajnicek, A.M., L.E. Foubister, and C.D. McCaig, *Growth cone steering by a physiological electric field requires dynamic microtubules, microfilaments and Rac-mediated filopodial asymmetry.* J Cell Sci, 2006. **119**(Pt 9): p. 1736-45.
193. Rajnicek, A.M., L.E. Foubister, and C.D. McCaig, *Prioritising guidance cues: directional migration induced by substratum contours and electrical gradients is controlled by a rho/cdc42 switch.* Dev Biol, 2007. **312**(1): p. 448-60.
194. Rajnicek, A.M., L.E. Foubister, and C.D. McCaig, *Temporally and spatially coordinated roles for Rho, Rac, Cdc42 and their effectors in growth cone guidance by a physiological electric field.* J Cell Sci, 2006. **119**(Pt 9): p. 1723-35.
195. Dillon, G.P., X. Yu, and R.V. Bellamkonda, *The polarity and magnitude of ambient charge influences three-dimensional neurite extension from DRGs.* J Biomed Mater Res, 2000. **51**(3): p. 510-9.
196. Dillon, G.P., et al., *The influence of physical structure and charge on neurite extension in a 3D hydrogel scaffold.* J Biomater Sci Polym Ed, 1998. **9**(10): p. 1049-69.
197. Yu, L.M., K. Kazazian, and M.S. Shoichet, *Peptide surface modification of methacrylamide chitosan for neural tissue engineering applications.* J Biomed Mater Res A, 2007. **82**(1): p. 243-55.
198. Zhang, Z., et al., *Electrically conductive biodegradable polymer composite for nerve regeneration: electricity-stimulated neurite outgrowth and axon regeneration.* Artif Organs, 2007. **31**(1): p. 13-22.
199. Wang, X., et al., *Evaluation of biocompatibility of polypyrrole in vitro and in vivo.* J Biomed Mater Res A, 2004. **68**(3): p. 411-22.
200. Bryan, D.J., et al., *Enhanced peripheral nerve regeneration through a poled bioresorbable poly(lactic-co-glycolic acid) guidance channel.* J Neural Eng, 2004. **1**(2): p. 91-8.
201. Cheng, S., E.C. Clarke, and L.E. Bilston, *Rheological properties of the tissues of the central nervous system: a review.* Med Eng Phys, 2008. **30**(10): p. 1318-37.
202. Clarke, E.C., S. Cheng, and L.E. Bilston, *The mechanical properties of neonatal rat spinal cord in vitro, and comparisons with adult.* J Biomech, 2009. **42**(10): p. 1397-402.
203. Bilston, L.E. and L.E. Thibault, *The mechanical properties of the human cervical spinal cord in vitro.* Ann Biomed Eng, 1996. **24**(1): p. 67-74.
204. Fiford, R.J. and L.E. Bilston, *The mechanical properties of rat spinal cord in vitro.* J Biomech, 2005. **38**(7): p. 1509-15.
205. Peppas, N.A., et al., *Physicochemical foundations and structural design of hydrogels in medicine and biology.* Annu Rev Biomed Eng, 2000. **2**: p. 9-29.
206. Dalton, P.D., L. Flynn, and M.S. Shoichet, *Manufacture of poly(2-hydroxyethyl methacrylate-co-methyl methacrylate) hydrogel tubes for use as nerve guidance channels.* Biomaterials, 2002. **23**(18): p. 3843-51.

207. Ozawa, H., et al., *Comparison of spinal cord gray matter and white matter softness: measurement by pipette aspiration method.* J Neurosurg, 2001. **95**(2 Suppl): p. 221-4.
208. Ozawa, H., et al., *Mechanical properties and function of the spinal pia mater.* J Neurosurg Spine, 2004. **1**(1): p. 122-7.
209. Dumont, C.E. and W. Born, *Stimulation of neurite outgrowth in a human nerve scaffold designed for peripheral nerve reconstruction.* J Biomed Mater Res B Appl Biomater, 2005. **73**(1): p. 194-202.
210. Tsai, E.C., et al., *Synthetic hydrogel guidance channels facilitate regeneration of adult rat brainstem motor axons after complete spinal cord transection.* J Neurotrauma, 2004. **21**(6): p. 789-804.
211. Tsai, E.C., et al., *Matrix inclusion within synthetic hydrogel guidance channels improves specific supraspinal and local axonal regeneration after complete spinal cord transection.* Biomaterials, 2006. **27**(3): p. 519-33.
212. Yu, T.T. and M.S. Shoichet, *Guided cell adhesion and outgrowth in peptide-modified channels for neural tissue engineering.* Biomaterials, 2005. **26**(13): p. 1507-14.
213. Heidemann, S.R., P. Lamoureux, and R.E. Buxbaum, *Growth cone behavior and production of traction force.* J Cell Biol, 1990. **111**(5 Pt 1): p. 1949-57.
214. Lamoureux, P., R.E. Buxbaum, and S.R. Heidemann, *Direct evidence that growth cones pull.* Nature, 1989. **340**(6229): p. 159-62.
215. Gunn, J.W., S.D. Turner, and B.K. Mann, *Adhesive and mechanical properties of hydrogels influence neurite extension.* J Biomed Mater Res A, 2005. **72**(1): p. 91-7.
216. Oudega, M., et al., *Axonal regeneration into Schwann cell grafts within resorbable poly(alpha-hydroxyacid) guidance channels in the adult rat spinal cord.* Biomaterials, 2001. **22**(10): p. 1125-36.
217. Waxman, S.G. and S.G. Waxman, *Clinical neuroanatomy*. 25th ed. 2003, New York: Lange Medical Books/McGraw-Hill, Medical Pub. Division. viii, 389 p.
218. Stokols, S. and M.H. Tuszynski, *The fabrication and characterization of linearly oriented nerve guidance scaffolds for spinal cord injury.* Biomaterials, 2004. **25**(27): p. 5839-46.
219. Stokols, S. and M.H. Tuszynski, *Freeze-dried agarose scaffolds with uniaxial channels stimulate and guide linear axonal growth following spinal cord injury.* Biomaterials, 2006. **27**(3): p. 443-51.
220. Cai, J., et al., *Permeable guidance channels containing microfilament scaffolds enhance axon growth and maturation.* J Biomed Mater Res A, 2005. **75**(2): p. 374-86.
221. Tang, X.Q., et al., *Functional repair after dorsal root rhizotomy using nerve conduits and neurotrophic molecules.* Eur J Neurosci, 2004. **20**(5): p. 1211-8.
222. Wen, X. and P.A. Tresco, *Effect of filament diameter and extracellular matrix molecule precoating on neurite outgrowth and Schwann cell behavior on multifilament entubulation bridging device in vitro.* J Biomed Mater Res A, 2006. **76**(3): p. 626-37.

223. Zhang, N., C. Zhang, and X. Wen, *Fabrication of semipermeable hollow fiber membranes with highly aligned texture for nerve guidance.* J Biomed Mater Res A, 2005. **75**(4): p. 941-9.
224. Wen, X. and P.A. Tresco, *Fabrication and characterization of permeable degradable poly(DL-lactide-co-glycolide) (PLGA) hollow fiber phase inversion membranes for use as nerve tract guidance channels.* Biomaterials, 2006. **27**(20): p. 3800-9.
225. Burg, K.J. and D. Brunson, *A novel use for capillary channel fibers: enhanced engineered tissue systems.* Conf Proc IEEE Eng Med Biol Soc, 2006. **1**: p. 2358-61.
226. Lu, Q., A. Simionescu, and N. Vyavahare, *Novel capillary channel fiber scaffolds for guided tissue engineering.* Acta Biomater, 2005. **1**(6): p. 607-14.
227. Hadlock, T., et al., *A polymer foam conduit seeded with Schwann cells promotes guided peripheral nerve regeneration.* Tissue Eng, 2000. **6**(2): p. 119-27.
228. Moore, M.J., et al., *Multiple-channel scaffolds to promote spinal cord axon regeneration.* Biomaterials, 2006. **27**(3): p. 419-29.
229. Deister, C., S. Aljabari, and C.E. Schmidt, *Effects of collagen 1, fibronectin, laminin and hyaluronic acid concentration in multi-component gels on neurite extension.* J Biomater Sci Polym Ed, 2007. **18**(8): p. 983-97.
230. Colognato, H., C. ffrench-Constant, and M.L. Feltri, *Human diseases reveal novel roles for neural laminins.* Trends Neurosci, 2005. **28**(9): p. 480-6.
231. Flanagan, L.A., et al., *Regulation of human neural precursor cells by laminin and integrins.* J Neurosci Res, 2006. **83**(5): p. 845-56.
232. Lathia, J.D., et al., *Patterns of laminins and integrins in the embryonic ventricular zone of the CNS.* J Comp Neurol, 2007. **505**(6): p. 630-43.
233. Beck, K., I. Hunter, and J. Engel, *Structure and function of laminin: anatomy of a multidomain glycoprotein.* Faseb J, 1990. **4**(2): p. 148-60.
234. Ranieri, J.P., et al., *Spatial control of neuronal cell attachment and differentiation on covalently patterned laminin oligopeptide substrates.* Int J Dev Neurosci, 1994. **12**(8): p. 725-35.
235. Ranieri, J.P., et al., *Neuronal cell attachment to fluorinated ethylene propylene films with covalently immobilized laminin oligopeptides YIGSR and IKVAV. II.* J Biomed Mater Res, 1995. **29**(6): p. 779-85.
236. Tong, Y.W. and M.S. Shoichet, *Enhancing the neuronal interaction on fluoropolymer surfaces with mixed peptides or spacer group linkers.* Biomaterials, 2001. **22**(10): p. 1029-34.
237. Shaw, D. and M.S. Shoichet, *Toward spinal cord injury repair strategies: peptide surface modification of expanded poly(tetrafluoroethylene) fibers for guided neurite outgrowth in vitro.* J Craniofac Surg, 2003. **14**(3): p. 308-16.
238. Burden-Gulley, S.M., M. Pendergast, and V. Lemmon, *The role of cell adhesion molecule L1 in axonal extension, growth cone motility, and signal transduction.* Cell Tissue Res, 1997. **290**(2): p. 415-22.
239. Chen, S., et al., *Prevention of neuronal cell death by neural adhesion molecules L1 and CHL1.* J Neurobiol, 1999. **38**(3): p. 428-39.

240. Chiba, A. and H. Keshishian, *Neuronal pathfinding and recognition: roles of cell adhesion molecules.* Dev Biol, 1996. **180**(2): p. 424-32.
241. Haspel, J. and M. Grumet, *The L1CAM extracellular region: a multi-domain protein with modular and cooperative binding modes.* Front Biosci, 2003. **8**: p. s1210-25.
242. Fercakova, A., *Cell adhesion molecules in the neural development and plasticity.* Bratisl Lek Listy, 2001. **102**(12): p. 552-5.
243. Kiryushko, D., V. Berezin, and E. Bock, *Regulators of neurite outgrowth: role of cell adhesion molecules.* Ann N Y Acad Sci, 2004. **1014**: p. 140-54.
244. Kadmon, G., A.M. Montgomery, and P. Altevogt, *L1 makes immunological progress by expanding its relations.* Dev Immunol, 1998. **6**(3-4): p. 205-13.
245. Hortsch, M., *The L1 family of neural cell adhesion molecules: old proteins performing new tricks.* Neuron, 1996. **17**(4): p. 587-93.
246. Kenwrick, S., M. Jouet, and D. Donnai, *X linked hydrocephalus and MASA syndrome.* J Med Genet, 1996. **33**(1): p. 59-65.
247. Kenwrick, S., A. Watkins, and E. De Angelis, *Neural cell recognition molecule L1: relating biological complexity to human disease mutations.* Hum Mol Genet, 2000. **9**(6): p. 879-86.
248. Cohen, N.R., et al., *Errors in corticospinal axon guidance in mice lacking the neural cell adhesion molecule L1.* Curr Biol, 1998. **8**(1): p. 26-33.
249. Kamiguchi, H., M.L. Hlavin, and V. Lemmon, *Role of L1 in neural development: what the knockouts tell us.* Mol Cell Neurosci, 1998. **12**(1-2): p. 48-55.
250. Kubasak, M.D., et al., *L1 CAM expression is increased surrounding the lesion site in rats with complete spinal cord transection as neonates.* Exp Neurol, 2005. **194**(2): p. 363-75.
251. Doherty, P., E. Williams, and F.S. Walsh, *A soluble chimeric form of the L1 glycoprotein stimulates neurite outgrowth.* Neuron, 1995. **14**(1): p. 57-66.
252. Lagenaur, C. and V. Lemmon, *An L1-like molecule, the 8D9 antigen, is a potent substrate for neurite extension.* Proc Natl Acad Sci U S A, 1987. **84**(21): p. 7753-7.
253. Webb, K., et al., *Substrate-bound human recombinant L1 selectively promotes neuronal attachment and outgrowth in the presence of astrocytes and fibroblasts.* Biomaterials, 2001. **22**(10): p. 1017-28.
254. Oliva, A.A., Jr., et al., *Patterning axonal guidance molecules using a novel strategy for microcontact printing.* Neurochem Res, 2003. **28**(11): p. 1639-48.
255. Xu, G., et al., *Optic nerve regeneration in polyglycolic acid-chitosan conduits coated with recombinant L1-Fc.* Neuroreport, 2004. **15**(14): p. 2167-72.
256. Yang, Y., et al., *Neurotrophin releasing single and multiple lumen nerve conduits.* J Control Release, 2005. **104**(3): p. 433-46.
257. Burdick, J.A., et al., *Stimulation of neurite outgrowth by neurotrophins delivered from degradable hydrogels.* Biomaterials, 2006. **27**(3): p. 452-9.
258. Lin, C.C. and A.T. Metters, *Enhanced protein delivery from photopolymerized hydrogels using a pseudospecific metal chelating ligand.* Pharm Res, 2006. **23**(3): p. 614-22.

259. Lin, C.C. and A.T. Metters, *Metal-chelating affinity hydrogels for sustained protein release.* J Biomed Mater Res A, 2007. **83**(4): p. 954-64.
260. MacInnis, B.L. and R.B. Campenot, *Retrograde support of neuronal survival without retrograde transport of nerve growth factor.* Science, 2002. **295**(5559): p. 1536-9.
261. Kapur, T.A. and M.S. Shoichet, *Immobilized concentration gradients of nerve growth factor guide neurite outgrowth.* J Biomed Mater Res A, 2004. **68**(2): p. 235-43.
262. Cao, X. and M.S. Shoichet, *Defining the concentration gradient of nerve growth factor for guided neurite outgrowth.* Neuroscience, 2001. **103**(3): p. 831-40.
263. Cao, X. and M.S. Shoichet, *Investigating the synergistic effect of combined neurotrophic factor concentration gradients to guide axonal growth.* Neuroscience, 2003. **122**(2): p. 381-9.
264. Niere, M., et al., *Combination of engineered neural cell adhesion molecules and GDF-5 for improved neurite extension in nerve guide concepts.* Biomaterials, 2006. **27**(18): p. 3432-40.
265. Dodla, M.C. and R.V. Bellamkonda, *Anisotropic scaffolds facilitate enhanced neurite extension in vitro.* J Biomed Mater Res A, 2006. **78**(2): p. 213-21.
266. Dodla, M.C. and R.V. Bellamkonda, *Differences between the effect of anisotropic and isotropic laminin and nerve growth factor presenting scaffolds on nerve regeneration across long peripheral nerve gaps.* Biomaterials, 2008. **29**(1): p. 33-46.
267. Yu, X. and R.V. Bellamkonda, *Tissue-engineered scaffolds are effective alternatives to autografts for bridging peripheral nerve gaps.* Tissue Eng, 2003. **9**(3): p. 421-30.
268. David, S. and A.J. Aguayo, *Axonal elongation into peripheral nervous system "bridges" after central nervous system injury in adult rats.* Science, 1981. **214**(4523): p. 931-3.
269. Mohanna, P.N., et al., *A composite poly-hydroxybutyrate-glial growth factor conduit for long nerve gap repairs.* J Anat, 2003. **203**(6): p. 553-65.
270. Dam-Hieu, P., S. Liu, and M. Tadie, *Experimental bypass surgery between the spinal cord and caudal nerve roots for spinal cord injuries.* Neurochirurgie, 2004. **50**(5): p. 500-14.
271. Dam-Hieu, P., et al., *Intraspinal grafting procedures: spinal cord effects induced in the adult rat: a clinical, histopathological, and immunohistochemical study.* Microsurgery, 2006. **26**(7): p. 529-38.
272. Adcock, K.H., et al., *Axon behaviour at Schwann cell - astrocyte boundaries: manipulation of axon signalling pathways and the neural adhesion molecule L1 can enable axons to cross.* Eur J Neurosci, 2004. **20**(6): p. 1425-35.
273. Houle, J.D., et al., *Combining an autologous peripheral nervous system "bridge" and matrix modification by chondroitinase allows robust, functional regeneration beyond a hemisection lesion of the adult rat spinal cord.* J Neurosci, 2006. **26**(28): p. 7405-15.

274. Haspel, J., et al., *Critical and optimal Ig domains for promotion of neurite outgrowth by L1/Ng-CAM.* J Neurobiol, 2000. **42**(3): p. 287-302.
275. Ho, C.-H., et al., *A metal-chelating pluronic for immobilization of histidine-tagged proteins at interfaces: immobilization of firefly luciferase on polystyrene beads.* Langmuir, 1998. **14**: p. 3889-3894.
276. Webb, K., K.D. Caldwell, and P.A. Tresco, *A novel surfactant-based immobilization method for varying substrate-bound fibronectin.* J Biomed Mater Res, 2001. **54**(4): p. 509-18.
277. Cellesi, F., N. Tirelli, and J.A. Hubbell, *Towards a fully-synthetic substitute of alginate: development of a new process using thermal gelation and chemical cross-linking.* Biomaterials, 2004. **25**(21): p. 5115-24.
278. van de Wetering, P., et al., *Poly(ethylene glycol) hydrogels formed by conjugate addition with controllable swelling, degradation, and release of pharmaceutically active proteins.* J Control Release, 2005. **102**(3): p. 619-27.
279. Tirelli, N., et al., *Poly(ethylene glycol) block copolymers.* J Biotechnol, 2002. **90**(1): p. 3-15.
280. Brian D. Mather, K.V., Kevin M. Miller, Timothy E. Long, *Michael addition reactions in macromolecular design for emerging technologies.* Prog. Polym. Sci., 2006. **31**: p. 487–531.
281. Murphy, W.L., et al., *Dynamic hydrogels: translating a protein conformational change into macroscopic motion.* Angew Chem Int Ed Engl, 2007. **46**(17): p. 3066-9.
282. Rydholm, A.E., et al., *Modifying network chemistry in thiol-acrylate photopolymers through postpolymerization functionalization to control cell-material interactions.* J Biomed Mater Res A, 2008. **86**(1): p. 23-30.
283. Hern, D.L. and J.A. Hubbell, *Incorporation of adhesion peptides into nonadhesive hydrogels useful for tissue resurfacing.* J Biomed Mater Res, 1998. **39**(2): p. 266-76.
284. DeLong, S.A., J.J. Moon, and J.L. West, *Covalently immobilized gradients of bFGF on hydrogel scaffolds for directed cell migration.* Biomaterials, 2005. **26**(16): p. 3227-34.
285. Gonzalez, A.L., et al., *Integrin interactions with immobilized peptides in polyethylene glycol diacrylate hydrogels.* Tissue Eng, 2004. **10**(11-12): p. 1775-86.
286. Sebra, R.P., et al., *Controlled polymerization chemistry to graft architectures that influence cell-material interactions.* Acta Biomater, 2007. **3**(2): p. 151-61.
287. Sebra, R.P., et al., *Surface grafted antibodies: controlled architecture permits enhanced antigen detection.* Langmuir, 2005. **21**(24): p. 10907-11.
288. Adams, M.L., A. Lavasanifar, and G.S. Kwon, *Amphiphilic block copolymers for drug delivery.* J Pharm Sci, 2003. **92**(7): p. 1343-55.
289. Gautier, S.E., et al., *Poly(alpha-hydroxyacids) for application in the spinal cord: resorbability and biocompatibility with adult rat Schwann cells and spinal cord.* J Biomed Mater Res, 1998. **42**(4): p. 642-54.

290. Alvarez-Lorenzo, C., et al., *Tetronic micellization, gelation and drug solubilization: Influence of pH and ionic strength.* Eur J Pharm Biopharm, 2007. **66**(2): p. 244-52.
291. Wang, S., W. Cui, and J. Bei, *Bulk and surface modifications of polylactide.* Anal Bioanal Chem, 2005. **381**(3): p. 547-56.
292. Otsuka, H., Y. Nagasaki, and K. Kataoka, *Surface characterization of functionalized polylactide through the coating with heterobifunctional poly(ethylene glycol)/polylactide block copolymers.* Biomacromolecules, 2000. **1**(1): p. 39-48.
293. Hortsch, M., *Structural and functional evolution of the L1 family: are four adhesion molecules better than one?* Mol Cell Neurosci, 2000. **15**(1): p. 1-10.
294. Rathjen, F.G. and M. Schachner, *Immunocytological and biochemical characterization of a new neuronal cell surface component (L1 antigen) which is involved in cell adhesion.* Embo J, 1984. **3**(1): p. 1-10.
295. Moos, M., et al., *Neural adhesion molecule L1 as a member of the immunoglobulin superfamily with binding domains similar to fibronectin.* Nature, 1988. **334**(6184): p. 701-3.
296. Faissner, A., et al., *Biosynthesis and membrane topography of the neural cell adhesion molecule L1.* Embo J, 1985. **4**(12): p. 3105-13.
297. Beer, S., et al., *Metalloproteinase-mediated release of the ectodomain of L1 adhesion molecule.* J Cell Sci, 1999. **112 (Pt 16)**: p. 2667-75.
298. Nayeem, N., et al., *A potential role for the plasmin(ogen) system in the posttranslational cleavage of the neural cell adhesion molecule L1.* J Cell Sci, 1999. **112 (Pt 24)**: p. 4739-49.
299. Silletti, S., et al., *Plasmin-sensitive dibasic sequences in the third fibronectin-like domain of L1-cell adhesion molecule (CAM) facilitate homomultimerization and concomitant integrin recruitment.* J Cell Biol, 2000. **149**(7): p. 1485-502.
300. Mechtersheimer, S., et al., *Ectodomain shedding of L1 adhesion molecule promotes cell migration by autocrine binding to integrins.* J Cell Biol, 2001. **155**(4): p. 661-73.
301. Jacob, J., et al., *L1 mediated homophilic binding and neurite outgrowth are modulated by alternative splicing of exon 2.* J Neurobiol, 2002. **51**(3): p. 177-89.
302. Martini, R. and M. Schachner, *Immunoelectron microscopic localization of neural cell adhesion molecules (L1, N-CAM, and MAG) and their shared carbohydrate epitope and myelin basic protein in developing sciatic nerve.* J Cell Biol, 1986. **103**(6 Pt 1): p. 2439-48.
303. Nybroe, O., A.M. Dalseg, and E. Bock, *A developmental study of soluble L1.* Int J Dev Neurosci, 1990. **8**(3): p. 273-81.
304. Poltorak, M., et al., *Disturbances in cell recognition molecules (N-CAM and L1 antigen) in the CSF of patients with schizophrenia.* Exp Neurol, 1995. **131**(2): p. 266-72.
305. Lemmon, V., K.L. Farr, and C. Lagenaur, *L1-mediated axon outgrowth occurs via a homophilic binding mechanism.* Neuron, 1989. **2**(6): p. 1597-603.

306. Davis, J.Q. and V. Bennett, *Ankyrin binding activity shared by the neurofascin/L1/NrCAM family of nervous system cell adhesion molecules.* J Biol Chem, 1994. **269**(44): p. 27163-6.
307. Wong, E.V., et al., *The cytoplasmic domain of the cell adhesion molecule L1 is not required for homophilic adhesion.* Neurosci Lett, 1995. **200**(3): p. 155-8.
308. Mohajeri, M.H., et al., *Neurite outgrowth on non-permissive substrates in vitro is enhanced by ectopic expression of the neural adhesion molecule L1 by mouse astrocytes.* Eur J Neurosci, 1996. **8**(6): p. 1085-97.
309. Sugawa, M., et al., *Enhancement of neurite outgrowth by the soluble form of human L1 (neural cell adhesion molecule).* Neuroreport, 1997. **8**(14): p. 3157-62.
310. Kobayashi, S., et al., *Grafts of genetically modified fibroblasts expressing neural cell adhesion molecule L1 into transected spinal cord of adult rats.* Neurosci Lett, 1995. **188**(3): p. 191-4.
311. Roonprapunt, C., et al., *Soluble cell adhesion molecule L1-Fc promotes locomotor recovery in rats after spinal cord injury.* J Neurotrauma, 2003. **20**(9): p. 871-82.
312. Zhao, X. and C.H. Siu, *Colocalization of the homophilic binding site and the neuritogenic activity of the cell adhesion molecule L1 to its second Ig-like domain.* J Biol Chem, 1995. **270**(49): p. 29413-21.
313. Gouveia, R.M., et al., *Production and purification of functional truncated soluble forms of human recombinant L1 cell adhesion glycoprotein from Spodoptera frugiperda Sf9 cells.* Protein Expr Purif, 2007. **52**(1): p. 182-93.
314. Summers, M.D. and G.E. Smith, *Determining virus titer by end-point dilution.*, in *A Manual of Methods for Baculovirus Vectors and Insect Cell Culture Procedures*. 1988, Texas Agricultural Experiment Station: College Station. p. 14-16.
315. Heidemann, S.R., et al., *The culture of chick forebrain neurons.* Methods Cell Biol, 2003. **71**: p. 51-65.
316. Altmann, F., et al., *Insect cells as hosts for the expression of recombinant glycoproteins.* Glycoconj J, 1999. **16**(2): p. 109-23.
317. Davis, T.R., et al., *Baculovirus expression of alkaline phosphatase as a reporter gene for evaluation of production, glycosylation and secretion.* Biotechnology (N Y), 1992. **10**(10): p. 1148-50.
318. Davis, T.R., et al., *Comparative recombinant protein production of eight insect cell lines.* In Vitro Cell Dev Biol Anim, 1993. **29A**(5): p. 388-90.
319. Kuhn, J., et al., *High-level expression and purification of human xylosyltransferase I in High Five insect cells as biochemically active form.* Biochem Biophys Res Commun, 2003. **312**(3): p. 537-44.
320. Brank, A.S., D.M. Van Bemmel, and J.K. Christman, *Optimization of baculovirus-mediated expression and purification of hexahistidine-tagged murine DNA (cytosine-C5)-methyltransferase-1 in Spodoptera frugiperda 9 cells.* Protein Expr Purif, 2002. **25**(1): p. 31-40.

321. Appel, F., et al., *Several extracellular domains of the neural cell adhesion molecule L1 are involved in neurite outgrowth and cell body adhesion.* J Neurosci, 1993. **13**(11): p. 4764-75.
322. Cho, E., et al., *Formulation and characterization of Tetronic-based hydrogels as tissue adhesives.* . Acta Biomater., in preparation., 2009.
323. Todaro, G.J. and H. Green, *Quantitative studies of the growth of mouse embryo cells in culture and their development into established lines.* J Cell Biol, 1963. **17**: p. 299-313.
324. Potts, J.R. and I.D. Campbell, *Fibronectin structure and assembly.* Curr Opin Cell Biol, 1994. **6**(5): p. 648-55.
325. Potts, J.R. and I.D. Campbell, *Structure and function of fibronectin modules.* Matrix Biol, 1996. **15**(5): p. 313-20; discussion 321.
326. Albini, A., et al., *Chemotaxis of 3T3 and SV3T3 cells to fibronectin is mediated through the cell-attachment site in fibronectin and a fibronectin cell surface receptor.* J Cell Biol, 1987. **105**(4): p. 1867-72.
327. D'Souza, S.E., M.H. Ginsberg, and E.F. Plow, *Arginyl-glycyl-aspartic acid (RGD): a cell adhesion motif.* Trends Biochem Sci, 1991. **16**(7): p. 246-50.
328. Gee, E.P., D.E. Ingber, and C.M. Stultz, *Fibronectin unfolding revisited: modeling cell traction-mediated unfolding of the tenth type-III repeat.* PLoS ONE, 2008. **3**(6): p. e2373.
329. Clark, R.A., et al., *Fibroblast migration on fibronectin requires three distinct functional domains.* J Invest Dermatol, 2003. **121**(4): p. 695-705.
330. Aota, S., T. Nagai, and K.M. Yamada, *Characterization of regions of fibronectin besides the arginine-glycine-aspartic acid sequence required for adhesive function of the cell-binding domain using site-directed mutagenesis.* J Biol Chem, 1991. **266**(24): p. 15938-43.
331. Sechler, J.L., S.A. Corbett, and J.E. Schwarzbauer, *Modulatory roles for integrin activation and the synergy site of fibronectin during matrix assembly.* Mol Biol Cell, 1997. **8**(12): p. 2563-73.
332. Millard, C.J., et al., *The role of the fibronectin IGD motif in stimulating fibroblast migration.* J Biol Chem, 2007. **282**(49): p. 35530-5.
333. Williams, E.C., et al., *Fibronectin. Effect of disulfide bond reduction on its physical and functional properties.* J Biol Chem, 1983. **258**(9): p. 5911-4.
334. Patel, P.N., et al., *Poly(ethylene glycol) hydrogel system supports preadipocyte viability, adhesion, and proliferation.* Tissue Eng, 2005. **11**(9-10): p. 1498-505.
335. Schmedlen, R.H., K.S. Masters, and J.L. West, *Photocrosslinkable polyvinyl alcohol hydrogels that can be modified with cell adhesion peptides for use in tissue engineering.* Biomaterials, 2002. **23**(22): p. 4325-32.
336. Webb, K., et al., *Cyclic strain increases fibroblast proliferation, matrix accumulation, and elastic modulus of fibroblast-seeded polyurethane constructs.* J Biomech, 2006. **39**(6): p. 1136-44.
337. West, D.C., A. Sattar, and S. Kumar, *A simplified in situ solubilization procedure for the determination of DNA and cell number in tissue cultured mammalian cells.* Anal Biochem, 1985. **147**(2): p. 289-95.

338. Vartio, T. and P. Kuusela, *Disulfide-bonded dimerization of fibronectin in vitro.* Eur J Biochem, 1991. **202**(2): p. 597-604.
339. Webb, K., K. Caldwell, and P.A. Tresco, *Fibronectin immobilized by a novel surface treatment regulates fibroblast attachment and spreading.* Crit Rev Biomed Eng, 2000. **28**(1-2): p. 203-8.
340. Chen, C.S., et al., *Geometric control of cell life and death.* Science, 1997. **276**(5317): p. 1425-8.
341. Mooney, D., et al., *Switching from differentiation to growth in hepatocytes: control by extracellular matrix.* J Cell Physiol, 1992. **151**(3): p. 497-505.
342. Ben-Ze'ev, A., et al., *Cell-cell and cell-matrix interactions differentially regulate the expression of hepatic and cytoskeletal genes in primary cultures of rat hepatocytes.* Proc Natl Acad Sci U S A, 1988. **85**(7): p. 2161-5.
343. Sakai, K., T. Fujii, and T. Hayashi, *Cell-free formation of disulfide-bonded multimer from isolated plasma fibronectin in the presence of a low concentration of SH reagent under a physiological condition.* J Biochem, 1994. **115**(3): p. 415-21.
344. Sakai, K., T. Fujii, and T. Hayashi, *Conformational change precedes the formation of multimeric fibronectin.* J Biochem, 1996. **119**(1): p. 58-62.
345. Vartio, T., *Disulfide-bonded polymerization of plasma fibronectin in the presence of metal ions.* J Biol Chem, 1986. **261**(20): p. 9433-7.
346. Majors, A.K., et al., *Homocysteine binds to human plasma fibronectin and inhibits its interaction with fibrin.* Arterioscler Thromb Vasc Biol, 2002. **22**(8): p. 1354-9.
347. Aubert, I., et al., *Expression of L1 and PSA during sprouting and regeneration in the adult hippocampal formation.* J Comp Neurol, 1998. **399**(1): p. 1-19.
348. Calabrese, E.J., *Dose-response features of neuroprotective agents: an integrative summary.* Crit Rev Toxicol, 2008. **38**(4): p. 253-348.
349. Otey, C.A., M. Boukhelifa, and P. Maness, *B35 neuroblastoma cells: an easily transfected, cultured cell model of central nervous system neurons.* Methods Cell Biol, 2003. **71**: p. 287-304.
350. Kadmon, G., et al., *Functional cooperation between the neural adhesion molecules L1 and N-CAM is carbohydrate dependent.* J Cell Biol, 1990. **110**(1): p. 209-18.
351. Schmid, R.S. and P.F. Maness, *L1 and NCAM adhesion molecules as signaling coreceptors in neuronal migration and process outgrowth.* Curr Opin Neurobiol, 2008.
352. Fedoroff, S. and A. Richardson, *Protocols for neural cell culture*. 3rd ed. 2001, Totowa, N.J.: Humana Press. xxii, 362 p.
353. He, Y. and P.W. Baas, *Growing and working with peripheral neurons.* Methods Cell Biol, 2003. **71**: p. 17-35.
354. Tritsch, G.L. and G.E. Moore, *Spontaneous decomposition of glutamine in cell culture media.* Exp Cell Res, 1962. **28**: p. 360-4.

355. Hassell, T., S. Gleave, and M. Butler, *Growth inhibition in animal cell culture. The effect of lactate and ammonia.* Appl Biochem Biotechnol, 1991. **30**(1): p. 29-41.
356. Felipo, V., et al., *Neurotoxicity of ammonia and glutamate: molecular mechanisms and prevention.* Neurotoxicology, 1998. **19**(4-5): p. 675-81.
357. Martin, D.P., T.L. Wallace, and E.M. Johnson, Jr., *Cytosine arabinoside kills postmitotic neurons in a fashion resembling trophic factor deprivation: evidence that a deoxycytidine-dependent process may be required for nerve growth factor signal transduction.* J Neurosci, 1990. **10**(1): p. 184-93.
358. Wallace, T.L. and E.M. Johnson, Jr., *Cytosine arabinoside kills postmitotic neurons: evidence that deoxycytidine may have a role in neuronal survival that is independent of DNA synthesis.* J Neurosci, 1989. **9**(1): p. 115-24.
359. Heggli, M., et al., *Michael-type addition as a tool for surface functionalization.* Bioconjug Chem, 2003. **14**(5): p. 967-73.
360. Lee, J.S., et al., *Synthesis and characterization of di-functional PEG-based crosslinkers for L1 immobilization*, in *Society for Biomaterials*. 2007: Chicago, IL.
361. Patenaude, A., M.R. Murthy, and M.E. Mirault, *Emerging roles of thioredoxin cycle enzymes in the central nervous system.* Cell Mol Life Sci, 2005. **62**(10): p. 1063-80.
362. Deutschmann, S.M. and V. Jager, *Optimization of the growth conditions of Sf21 insect cells for high-density perfusion culture in stirred-tank bioreactors.* Enzyme Microb Technol, 1994. **16**(6): p. 506-12.
363. Zhang, J., et al., *High-density perfusion culture of insect cells with a biosep ultrasonic filter.* Biotechnol Bioeng, 1998. **59**(3): p. 351-9.
364. Heidemann, S.R. and R.E. Buxbaum, *Mechanical tension as a regulator of axonal development.* Neurotoxicology, 1994. **15**(1): p. 95-107.
365. Kandel, E.R., J.H. Schwartz, and T.M. Jessell, *Principles of neural science*. 4th ed. 2000, New York: McGraw-Hill, Health Professions Division. xli, 1414 p.
366. Cserr, H.F., et al., *Efflux of radiolabeled polyethylene glycols and albumin from rat brain.* Am J Physiol, 1981. **240**(4): p. F319-28.
367. Kohriyama, K., M. Matsuoka, and H. Igisu, *Effects of acrylamide and acrylic acid on creatine kinase activity in the rat brain.* Arch Toxicol, 1994. **68**(1): p. 67-70.
368. Inao, S., et al., *Production and clearance of lactate from brain tissue, cerebrospinal fluid, and serum following experimental brain injury.* J Neurosurg, 1988. **69**(5): p. 736-44.
369. Menzel, M., et al., *Increased inspired oxygen concentration as a factor in improved brain tissue oxygenation and tissue lactate levels after severe human head injury.* J Neurosurg, 1999. **91**(1): p. 1-10.